

# **Synthesis and discovery of the putative cognitive enhancer BRS-015: effect on glutamatergic transmission and synaptic plasticity**

**Blanka Szulc**

**Supervisors: Dr Stephen Hilton and Dr Arnaud Ruiz**

**29/07/2014**

**This research project is submitted in part fulfilment of the requirements for the PhD degree, UCL School of Pharmacy  
Department of Pharmaceutical and Biological Chemistry  
and the Pharmacology Department**

## Abstract

This thesis is concerned with the discovery of a novel heterocyclic compound – BRS-015, its synthesis and an analysis of its effects on excitatory synaptic transmission at a major pathway in the brain. BRS-015 is related to the natural product clausenamamide, which has been shown to facilitate synaptic transmission. As such, clausenamamide and related analogues may possess therapeutic potential as memory enhancing drugs, which are in urgent need of development due to the increasing numbers of patients diagnosed with memory disorders and for which there is no current effective therapy. BRS-015 was synthesized using a novel approach to the core structure of clausenamamide involving an intramolecular acylal cyclisation reaction, which has not previously been reported.

The first section of the thesis opens with a description of the discovery, structure and biological activity of clausenamamide and discussion of previous synthetic strategies adopted by a number of research groups and attempts to classify these into the varying approaches towards the central core of clausenamamide. The second section describes the structure of the rat brain and the types of processes involved in memory formation, as well as the neurophysiological assays used to investigate synaptic transmission and plasticity.

The second group of chapters describes our own approach to the core of clausenamamide and the synthesis of BRS-015, with a detailed discussion of the structural analysis and investigation of the intramolecular acylal cyclisation reaction used during the synthetic process.

The third chapter describes the neurophysiological assays used in our investigations into the effects of BRS-015, which was tested against glutamatergic synaptic transmission and plasticity in acute rat hippocampal slices. BRS-015 was shown to reversibly enhance the amplitude of AMPA receptor mediated EPSCs recorded from CA3 pyramidal neurones and evoked by dentate stimulation. When tested in the presence of selective glutamate receptor antagonists, BRS-015 did not have this powerful enhancing effect on kainate or NMDA receptor mediated EPSCs. In addition, BRS-015 increased the amplitude of glutamate-evoked currents in CA3 pyramidal neurones and did not alter short-term synaptic plasticity but facilitated the induction of mossy fibre LTP, with little effect at associational/commissural synapses. BRS-015 has striking enhancing properties on AMPA receptor mediated synaptic transmission at mossy fibre synapses either by directly interacting with AMPA receptors or via indirect modulation, the mechanisms of which could lead to synapse strengthening.

## Acknowledgements

Firstly I would like to express my sincere thanks to both of my supervisors - Dr Stephen Hilton and Dr Arnaud Ruiz for all of their help, support and advice during my PhD from transitioning through to electrophysiology from chemistry. Your experience and great guidance enabled me achieve success on such a wide-ranging project. Thank you for all your time and in particular your proof-reading of this thesis!

I would secondly like to thank all of my laboratory colleagues in Steve and Arnaud's labs for all their help and support over the years. Special thanks go to Bruno, Georgina, Bhaven, Moussa, Chris, Zenobia, Raiza, Anna and Antonia for all your help, friendship and advice over my time at UCL School of Pharmacy. I would also like to thank the staff in both departments for their friendship and support who are too numerous to mention.

I would like to thank Dr Gary Parkinson for the X-ray structure of the cyclised product and for patiently allowing me to watch him at work. Thank you also to Colin and Mire for your help with NMR and to Emmanuel for mass spectrometry.

Thanks also go to the team in the biological service unit at the School for their help and advice.

I would also like to thank the Leverhulme Trust for generously funding this research, with the provision of a PhD studentship.

Lastly, thanks to all of my family and friends, who are close to my heart who have always been there for me.

## Plagiarism Statement

I, Blanka Szulc, hereby confirm that the work submitted in the thesis is my own. Any ideas submitted in this thesis are my own. Any ideas, quotations, and paraphrasing from other peoples work and publications have been appropriately referenced. I have not violated UCL School of Pharmacy's policy on plagiarism.

Signature .....

Date .....

## Abbreviations

ABSA	<i>p</i> -Acetamidobenzenesulfonyl azide
ACSF	Artificial cerebrospinal fluid
A/C	Associational-commisural fibres
AD	Alzheimer's disease
ADA	5'-Nucleotidase adenosine deaminase
ADHD	Attention deficit hyperactivity disorder
ADME	Absorption, distribution, metabolism, elimination
AGP	$\alpha$ 1-Acid glycoprotein
AMPA	$\alpha$ -Amino-3-hydroxy-5-methyl-4-isoxazolepropionic acid
app	Apparent
BOC	<i>tert</i> -Butoxycarbonyl
br	Broad
Bu	Butyl
°C	Degree Celcius
CAMKII $\alpha$	Calcium/calmodulin-dependent protein kinase II $\alpha$
Cat	Catalytic
CNS	Central nervous system
CREB	cAMP response element-binding protein
d	Doublet
DABCO	Diazabicyclo[2.2.2]octane
DBU	Diazabicyclo[5.4.0]undec-7-ene
DCG-IV	(2 <i>S</i> ,2' <i>R</i> ,3' <i>R</i> )-2-(2',3'-Dicarboxycyclopropyl)glycine
DCM	Dichloromethane
DMAP	4- <i>N,N</i> -Dimethylaminopyridine
DMF	<i>N,N</i> -Dimethylformamide
DMSO	Dimethylsulfoxide
EDTA	Ethylenediaminetetraacetic acid
ee	Enantiomeric excess
EPSCs	Excitatory postsynaptic currents

EPSPs	Excitatory postsynaptic potentials
Et	Ethyl
EtOAc	Ethyl acetate
f-EPSPs	Field excitatory postsynaptic potentials
g	Grammes
GC	Granule cells
GCL	Granule cell layer
h	Hours
HEPES	4-(2-Hydroxyethyl)-1-piperazineethanesulfonic acid
HFS	High frequency stimulation
HPLC	High performance liquid chromatography
IAC	Intramolecular acylal cyclisation
IL-1 $\beta$	Interleukin 1 beta
IR	Infra red
KAR	Kainate receptor
LDA	Lithium diisopropylamide
LTD	Long-term depression
LTP	Long term potentiation
M	Molar
m	Multiplet
<i>m</i> CPBA	<i>meta</i> -Chloroperoxybenzoic acid
Mes	Mesityl
Me	Methyl
MF-LTP	Mossy fibre LTP
mg	Milligrams
mGluRs	Metabotropic glutamate receptors
MFBs	Mossy fibre boutons
MHz	Mega Hertz
mL	Millilitre
ML	Molecular layer
mmol	Millimoles

mp	Melting point
MS	Multiple sclerosis
<i>m/z</i>	Mass to charge ratio
NADPH	Nicotinamide adenine dinucleotide phosphate
NBS	<i>N</i> -Bromosuccinimide
NCS	<i>N</i> -Chlorosuccinimide
NHC	<i>N</i> -Heterocyclic carbene
NMDA	<i>N</i> -Methyl-D-aspartate
NMR	Nuclear magnetic resonance
nOe	Nuclear Overhauser effect
PG	Protecting group
PhTx	Polyamine toxins
PIFA	[Bis(trifluoroacetoxy)iodo]benzene
PPF	Paired pulse facilitation
ppm	Parts per million
PS	Population spike
PTP	Post-tetanic potentiation
q	Quartet
quin	Quintet
R <sub>f</sub>	Retention factor
ROS	Reactive oxygen species
rt	Room temperature
s	Secondary
s	Singlet
SAR	Structure activity relationship
SG	Stratum granulosum
<i>t</i>	Tertiary
t	Triplet
TBDMSCl	<i>tert</i> -Butyldimethylsilyl chloride
TFA	Trifluoroacetic acid
THF	Tetrahydrofuran

TLC	Thin layer chromatography
TMS	Tetramethylsilane
TMSCl	Trimethylsilyl chloride
TMSOTf	Trimethylsilyl trifluoromethanesulfonate
TNF- $\alpha$	Tumor necrosis factor
UV	Ultra violet
$\mu$ L	Microlitre
VDCC	Voltage-dependent calcium channels

# Contents

<b>1.0. Introduction</b> .....	<b>1</b>
<b>1.1. General Introduction</b> .....	<b>2</b>
1.1.1. Memory Deficit Disorders .....	2
1.1.2. Nootropic drugs .....	3
1.1.3. AMPA modulators in a clinical setting .....	9
<b>1.2. Clausenamide</b> .....	<b>11</b>
1.2.1. Mode of action of clausenamide .....	12
1.2.2. Previous synthetic approaches to clausenamide .....	14
<b>1.3. Biological introduction</b> .....	<b>24</b>
<b>1.4. Glutamatergic neurotransmission</b> .....	<b>24</b>
<b>1.5. Ionotropic Glutamate Receptors</b> .....	<b>25</b>
1.5.1. AMPA receptors .....	26
1.5.2. NMDA receptors .....	27
1.5.3. Kainate receptors .....	28
<b>1.6. Anatomy of the hippocampus</b> .....	<b>29</b>
1.6.1. The dentate gyrus .....	30
1.6.2. Hippocampus proper .....	34
<b>1.7. Dentate – CA3 neurotransmission</b> .....	<b>37</b>
1.7.1. Receptors and pharmacology .....	37
1.7.2. Plasticity of giant mossy fibre synapses .....	38
<b>2.0. Project Objectives</b> .....	<b>42</b>
<b>2.1. Synthetic Chemistry</b> .....	<b>43</b>
<b>2.2. Biological objectives</b> .....	<b>47</b>
<b>3.0. Results and Discussion</b> .....	<b>50</b>
<b>3.1. Initial cyclisations</b> .....	<b>50</b>
<b>3.2. Synthetic approach towards clausenamide</b> .....	<b>60</b>
3.2.1. Mechanistic investigation of cyclisation .....	70
<b>4.0. Methodology</b> .....	<b>77</b>
<b>4.1. Hippocampal slice preparation and preservation</b> .....	<b>77</b>
4.1.1. Dissection of the rat brain .....	77
4.1.2. Slice storage and preservation .....	79
4.1.3. Solutions .....	80
<b>5.0. Electrophysiological recordings</b> .....	<b>81</b>
<b>5.1. Extracellular recordings</b> .....	<b>82</b>
<b>5.2. Intracellular recordings: whole-cell patch-clamp</b> .....	<b>84</b>
5.2.1. Voltage-clamp configuration .....	85
5.2.2. Current-clamp configuration .....	86
<b>5.3. Data acquisition and analysis</b> .....	<b>87</b>

---

5.4. Statistics .....	89
5.5. Drugs.....	89
<b>6.0. Electrophysiological profile of BRS-015.....</b>	<b>92</b>
6.1. Effects of BRS-015 on evoked glutamatergic synaptic transmission from the dentate gyrus to CA3 .....	93
6.1.2. Field potential recordings .....	93
<b>6.2. Whole-cell patch-clamp recordings .....</b>	<b>100</b>
6.2.1. Effect of BRS-015 on electrical properties of CA3 pyramidal neurones ....	100
6.2.2. Effect of BRS-015 on dentate-evoked EPSCs.....	102
6.2.3. Dose - response relation: EC <sub>50</sub> .....	103
<b>6.3. Effect of BRS-015 on the paired-pulse ratio and decay-time constant of evoked EPSCs .....</b>	<b>105</b>
<b>6.4. Effect of BRS-15 on pharmacologically isolated EPSCs .....</b>	<b>107</b>
6.4.1. Effect on NMDA receptor-mediated EPSCs .....	108
<b>6.5. Effect on kainate receptor-mediated EPSCs .....</b>	<b>109</b>
<b>6.6. Summary of pharmacological manipulations.....</b>	<b>110</b>
<b>6.7. Effect of BRS-015 on glutamate-evoked currents in CA3 pyramidal neurones.....</b>	<b>111</b>
<b>6.8. Effect of BRS-015 on mossy fibre LTP .....</b>	<b>113</b>
<b>6.9. Effect of single enantiomers of BRS-015 on evoked glutamatergic synaptic transmission from the dentate gyrus to CA3 .....</b>	<b>122</b>
<b>7.0. Toxicity of BRS-015 .....</b>	<b>126</b>
<b>8.0. Discussion and Conclusions .....</b>	<b>130</b>
8.1. The effect of BRS-015 on dentate – CA3 neurotransmission.....	130
8.2. Mechanistic insights into the mode of action of BRS-015.....	131
8.3. Pre- or postsynaptic mechanism of BRS-015? .....	132
8.4. Effect of BRS-015 on synaptic plasticity .....	133
<b>9.0. Conclusions .....</b>	<b>136</b>
<b>10.0. Future Work.....</b>	<b>139</b>
<b>11.0. Experimental .....</b>	<b>143</b>
11.1. General Methods for Synthesis .....	143
<b>12.0. References.....</b>	<b>166</b>

---

## List of Figures

Figure 1: BRS-015 and (±)-clausenamide.....	2
Figure 2: Piracetam-like cognitive enhancers.....	4
Figure 3: Piracetam-like anti-epileptic drugs.....	5
Figure 4: Piracetam-like compounds with unknown efficacy.....	5
Figure 5: Piracetam bound to dimeric GluA2 at three binding sites.....	8
Figure 6: Structures of (-)- and (+)-clausenamide.....	11
Figure 7: Optically active clausenamide stereoisomers .....	12
Figure 8: Structures of piracetam and (-)-clausenamide.....	13
Figure 9: Hippocampal organization of rodent brain and its anatomy.....	31
Figure 10: Timm's staining reveals high zinc level in hippocampal granule cells.....	33
Figure 11: The hippocampal mossy fibre bouton.....	33
Figure 12: Pyrrolidine core containing compounds.....	43
Figure 13: (±)-Clausenamide.....	61
Figure 14: Enamine - energy 29.3681 kcal/mol vs Imine - energy 12.9678 kcal/mol.....	67
Figure 15: <sup>1</sup> H NMR spectrum of the free amine vs. <i>N</i> -chlorinated product.....	68
Figure 16: Relative base pKa's.....	69
Figure 17: X-Ray of compound 166.....	72
Figure 18: The two possible double bond configurations .....	72
Figure 19: Energy confirmations of BRS-015 double bond isomers.....	74
Figure 20: Preparation of transverse hippocampal slices with special cut.....	79
Figure 21: Submersion chamber for hippocampal slices maintenance.....	80
Figure 22: Image showing stage, objectives and recording chamber with stimulus electrode, puff pipette and recording electrode positioned in the tissue.....	83
Figure 23: Cartoon representation of a hippocampal slice showing the experimental approach for mossy fiber f-EPSP recordings.....	84

---

Figure 24: High magnification IR-DIC image of the PCs of the CA3 region.....	86
Figure 25: Schematic of the recording configuration and signal flow.....	88
Figure 26: Analysis of exemplified evoked postsynaptic current with specified parameters for data analysis.....	89
Figure 27: BRS-015 enhances excitatory synaptic transmission from the dentate gyrus to CA3.....	95
Figure 28: Piracetam enhances excitatory synaptic transmission from the dentate gyrus to CA3.....	96
Figure 29: Local application of BRS-015 in stratum lucidum increases the amplitude of dentate-evoked f-EPSPs recorded from CA3.....	98
Figure 30: The enhancing effect of BRS-015 is not accompanied by a change in paired-pulse ratio of f-EPSP amplitude.....	99
Figure 31: BRS-015 does not alter the basic electrical membrane properties of CA3 pyramidal neurones.....	102
Figure 32: BRS-015 facilitates evoked mixed AMPA/KA receptor-mediated EPSCs in CA3 pyramidal neurones.....	103
Figure 33: The effect of BRS-015 on dentate-evoked EPSCs in CA3 pyramidal neurones is concentration-dependent.....	105
Figure 34: Lack of effect of BRS-015 on paired-pulse ratio of mossy fiber-evoked EPSCs.....	107
Figure 35: BRS-015 has no effect on dentate-evoked EPSCs decay-time constant in CA3 pyramidal neurones.....	108
Figure 36: BRS-015 does not affect NMDA receptor-mediated EPSCs in CA3 pyramidal neurones.....	109
Figure 37: No effect of BRS-015 on kainate receptor-mediated EPSCs in CA3 pyramidal neurones.....	110
Figure 38: Bar chart summarising the effect of BRS-015 on pharmacologically isolated EPSCs in CA3 pyramidal neurones.....	111
Figure 39: BRS-015 enhances glutamate-evoked currents in CA3 pyramidal neurones.....	113
Figure 40: Drawing of the experimental design.....	115
Figure 41: BRS-015 lowers the threshold for induction of mossy fibre LTP.....	116

<b>Figure 42: BRS-015 does not alter basal synaptic transmission at A/C fibre – CA3 synapses.....</b>	<b>117</b>
<b>Figure 43: Effect of BRS-015 on mossy fibre LTP in the absence of NMDA receptor blockade.....</b>	<b>118</b>
<b>Figure 44: Comparing the effect of BRS-015 on mossy fibre LTP in the presence or absence of the NMDA receptor antagonist <i>D</i>-AP5.....</b>	<b>119</b>
<b>Figure 45: BRS-015 does not affect synaptic transmission at synapses that undergo mossy fibre LTP.....</b>	<b>120</b>
<b>Figure 46: The effect of (-)-BRS-015 on basal synaptic transmission.....</b>	<b>123</b>
<b>Figure 47: The effect of (+) BRS-015 on basal synaptic transmission.....</b>	<b>124</b>
<b>Figure 48: Schematic diagram showing the possible mechanism by which BRS-015 induces long-lasting enhancement in excitatory synaptic transmission.....</b>	<b>137</b>
<b>Figure 49: Potential analogues development of BRS-015.....</b>	<b>140</b>
<b>Figure 50: Alcohol analogues of BRS-015.....</b>	<b>140</b>

---

### List of Schemes

Scheme 1: Clausenamide cyclisation with LiOH.....	15
Scheme 2: Yakura's approach to clausenamide.....	16
Scheme 3: Formal synthesis of dehydroclausenamide.....	16
Scheme 4: Hartwig and Born synthesis of clausenamide.....	18
Scheme 5: Dai and Huang synthesis of neoclausenamide.....	19
Scheme 6: He's approach to ( $\pm$ )-clausenamide.....	20
Scheme 7: Tellitu and Dominguez's approach to ( $\pm$ )-clausenamide.....	21
Scheme 8: Cappi's approach to (+)-clausenamide.....	22
Scheme 9: Liu and co-workers approach to (-)-clausenamide.....	22
Scheme 10: Zhang's approach to (+)- <i>epi</i> -clausenamide.....	23
Scheme 11: Retrosynthetic approach towards the pyrrolidine core.....	44
Scheme 12: Formation of the oxonium ion and cyclisation.....	45
Scheme 13: Generation of the 5/6-membered ring.....	45
Scheme 14: Cyclisation reactions with Lewis acids.....	46
Scheme 15: Retrosynthetic approach to clausenamide.....	46
Scheme 16: Formation of cyclisation precursors.....	51
Scheme 17: Formation of diacetoxyacetic acid.....	51
Scheme 18: Synthesis of diacetoxyacetyl chloride.....	52
Scheme 19: DMF catalysis of diacetoxyacetyl chloride synthesis.....	52
Scheme 20: Formation of cyclisation precursors 120 and 121.....	53
Scheme 21: Proposed cyclisation outcomes.....	53
Scheme 22: Cyclisation of the enamine.....	54
Scheme 23: Generation of the imine.....	54
Scheme 24: General reaction for formation of cyclisation precursors.....	54
Scheme 25: Formation of the cyclisation precursor and by-product.....	55
Scheme 26: Cyclisation reaction with boron trifluoride dietherate.....	55
Scheme 27: Reformation of the enamine.....	56

---

Scheme 28: Formation of <i>N</i> -cyclohexylidene-1-phenylmethanamine.....	56
Scheme 29: Formation of the cyclohexene cyclisation precursor.....	57
Scheme 30: Formation of the fused six-five membered ring system.....	57
Scheme 31: Pathway to the formation of seven membered ring.....	58
Scheme 32: Cyclisation with the presence of the intermediate acetate.....	58
Scheme 33: Reaction to form Boc protected benzylamine.....	59
Scheme 34: Formation of protected amine with 3-methyl-2-butene substituent.....	59
Scheme 35: Pathway to formation of 5 <i>exo</i> -cyclised product.....	60
Scheme 36: <i>N</i> -methylation of <i>N</i> -Boc phenylalanine.....	61
Scheme 37: Mechanism of trans-esterification.....	62
Scheme 38: <i>N</i> -Boc deprotection.....	63
Scheme 39: Formation of clausenamide cyclisation precursor.....	63
Scheme 40: Mechanism of enamine formation.....	64
Scheme 41: Enamine/ imine tautomerisation.....	65
Scheme 42: Lu and Lewin's enamine stability experiments.....	65
Scheme 43: Enamine formation.....	66
Scheme 44: Enamine/ imine tautomerisation.....	67
Scheme 45: Clausenamide structure generation.....	69
Scheme 46: Cyclisation and formation of BRS-015.....	70
Scheme 47: Mechanism of cyclisation.....	71
Scheme 48: Proposed hydride shift mechanism.....	73
Scheme 49: Formation of the <i>N</i> -H isomer of clausenamide.....	74
Scheme 50: Formation of the <i>N</i> -H cyclisation precursor.....	75
Scheme 51: Cyclisation to give the <i>N</i> -H precursor.....	75
Scheme 52: Potential conformers .....	76
Scheme 53: Synthesis of BRS-015.....	136
Scheme 54: Potential Racemisation of BRS-015.....	139

**List of Tables**

<b>Table 1: Layers of the hippocampus.....</b>	<b>36</b>
<b>Table 2: Optimization of cyclisation reaction using boron trifluoride dietherate..</b>	<b>70</b>
<b>Table 3: Effect of a range of Lewis acids on the yield of cyclisation.....</b>	<b>71</b>
<b>Table 4: The composition of sucrose solution listed.....</b>	<b>81</b>
<b>Table 5: The composition of ACSF solution listed.....</b>	<b>81</b>
<b>Table 6: Results of BRS-015 toxicity screening.....</b>	<b>127</b>

# 1.0. Introduction

## 1.1. General Introduction

This thesis is concerned with the discovery of a novel heterocyclic compound – BRS-015 (**1**) (Figure 1), its synthesis and the analysis of its physiological effects on excitatory synaptic transmission in the brain. BRS-015 is structurally related to the natural product clausenamide (**2**), which has been shown to facilitate synaptic transmission. As such, clausenamide and related analogues may possess therapeutic potential as memory enhancing drugs. BRS-015 (**1**) was synthesized using a novel approach to the core structure of clausenamide (**2**). This thesis therefore opens with a description of clausenamide (**2**) and the synthesis of compounds related to BRS-015 (**1**), to place our research into context for the exploration of its potential as a memory-enhancing compound.

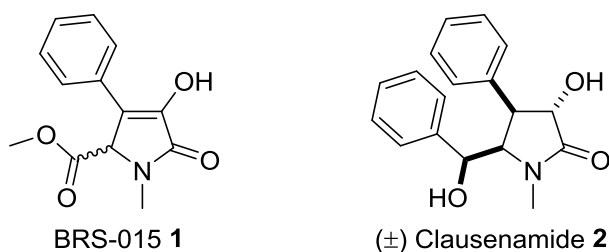


**Figure 1: BRS-015 and (±)-clausenamide**

### 1.1.1. Memory Deficit Disorders

Memory deficit disorders are a broad spectrum of interrelated diseases that are characterised by a decline in cognitive function and a corresponding reduction in both memory formation and recall. Another facet of these disorders is that whilst they can occur at any time in a person's lifetime, they are more strongly correlated with an increase in age (van de Glind *et al.*, 2013). The most prevalent amongst these disorders is dementia with around 800,000 people in the UK affected by this condition. There are approximately one hundred different types of dementia, with Alzheimer's disease (AD) perhaps the most common form, affecting 62% of those living with dementia. Many of those affected have a mixed pattern of dementia, with the second most common type, vascular dementia, also contributing to their condition (<http://www.alzheimers.org.uk>.) One of the key national health challenges associated with this disease, is the changing nature of the demographic profile

of industrialised nations. As the profile shifts towards a more elderly population, there is an associated increase in patients with memory related disorders. To highlight this, the Alzheimer's Society (UK) predicts that the number of people affected by dementia will increase to 1 million by 2021 and 1.7 million by 2051. Furthermore, these figures may be much higher, since many cases of dementia often go undiagnosed (especially in the early stages of dementia). This rise in the number of dementia sufferers is attributed to increasing longevity, due to advances in public health and medical care. For example, there is a sharp increase in the prevalence of dementia with age, while one in twenty-five people aged 70 to 79 has some form of dementia, this rises to one in six people over the age of 80 (<http://www.alzheimers.org.uk>).

At present, there are no medications that have been shown to prevent or cure dementia with one of the main obstacles to creating effective treatments for dementia, being that the disease is still not fully understood. The condition appears to result from a complex interaction of genes, lifestyle factors, and other environmental influences. Without knowing the exact mechanisms that cause damage, especially in AD, it is difficult to target the disease process effectively. A further obstacle is the difficulty of delivering medication across the blood-brain barrier (Marques *et al.*, 2013).

Current medication is used to treat the behavioural and cognitive symptoms of dementia, but has little effect on the underlying pathophysiology. By way of an example, many of the drugs used in clinical practice seek to improve memory deficits by targeting cholinergic neurotransmitter systems and the serotonergic pathway, but less than 10% of patients respond to such treatment.

### **1.1.2. Nootropic drugs**

Nootropic drugs, also known as memory enhancers, smart drugs, and cognitive enhancers, are drugs that improve cognitive function, memory, and concentration. Their action alters the availability and balance of brain neurotransmitters, hormones and enzymes, but the mechanisms by which they improve learning and memory are not fully understood (Froestl *et al.*, 2012). One plausible mode of action is that they strengthen inter-synaptic communication between neurones and brain circuits that are important for

learning and memory. Consistent with this hypothesis, both *in vitro* studies and animal behavior experiments suggest that nootropic drugs facilitate the induction of long-term potentiation (LTP) in the hippocampus, a phenomenon leading to synapse reinforcement, which is thought to underlie memory storage and recall in this brain structure (Giurgea *et al.*, 1983). Hippocampal LTP serves as a cellular model to study synaptic plasticity and its pharmacological enhancement can improve cognitive and memory associated deficits occurring in dementia patients (Bliss *et al.*, 2014). Such an enhancement of LTP can be associated with a lowering of the threshold of its induction, or with its maintenance, which is mechanistically relevant to chemically induced basal neurotransmission (Oh-Nishi *et al.*, 2009).

Thus, one candidate mechanism by which a drug could prove beneficial in treating the progressive decline typical of these disorders would be by either facilitating basal neurotransmission, or secondly by lowering the threshold for LTP induction in the hippocampus, which will be discussed in detail in section 1.7.2.2.

In 2010 Malykh and Sadaie (Malykh and Sadaie, 2010) published a review of piracetam-like drugs, where they divided them into three families, according to their medicinal use: cognitive enhancers, antiepileptic drugs and drugs with unknown clinical efficacy. Piracetam (**3**), oxiracetam (**4**), aniracetam (**5**), pramiracetam (**6**) and phenylpiracetam (**7**) are members of the first group known as cognitive enhancers (Figure 2).

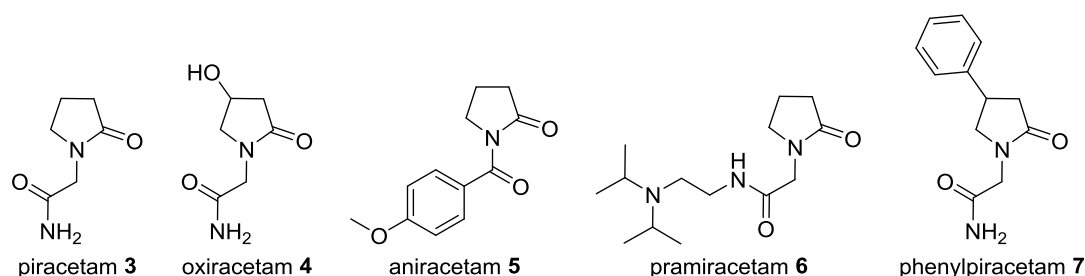


**Figure 2: Piracetam-like cognitive enhancers**

Mechanistically, most have been shown to activate  $\alpha$ -amino-3-hydroxy-5-methyl-D-isoxazole-propionic acid (AMPA) but not kainate (KA) or *N*-methyl-D-

aspartate (NMDA) receptors in neuronal cultures. Their effect on AMPA receptors is proposed to occur *via* an increase in the density of receptor binding sites and elevation of intracellular calcium levels (Copani *et al.*, 1992).

In contrast to the first family of compounds, the second group, comprising levetiracetam (**8**), brivaracetam (**9**) and seletracetam (**10**) (Figure 3), have been shown to inhibit neuronal calcium ion channels, which can explain their antiepileptic properties (Lukyanetz *et al.*, 2002).

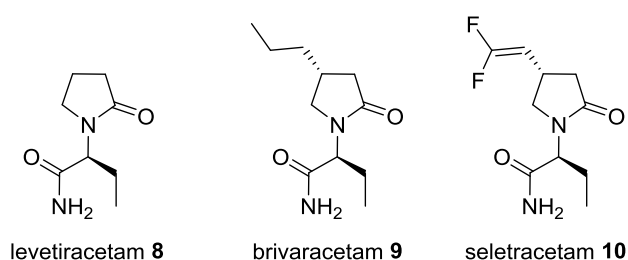


**Figure 3: Piracetam-like anti-epileptic drugs**

Finally, the third group is represented by piracetam derivatives that are mostly in the preclinical stage, or those that have entered the clinical stage and their mode of action is currently under investigational status such as rolipram (**13**) or those that have been taken into patients and failed to reach clinical endpoints such as nefiracetam (**11**) (Figure 4) (Malykh and Sadaie, 2010).

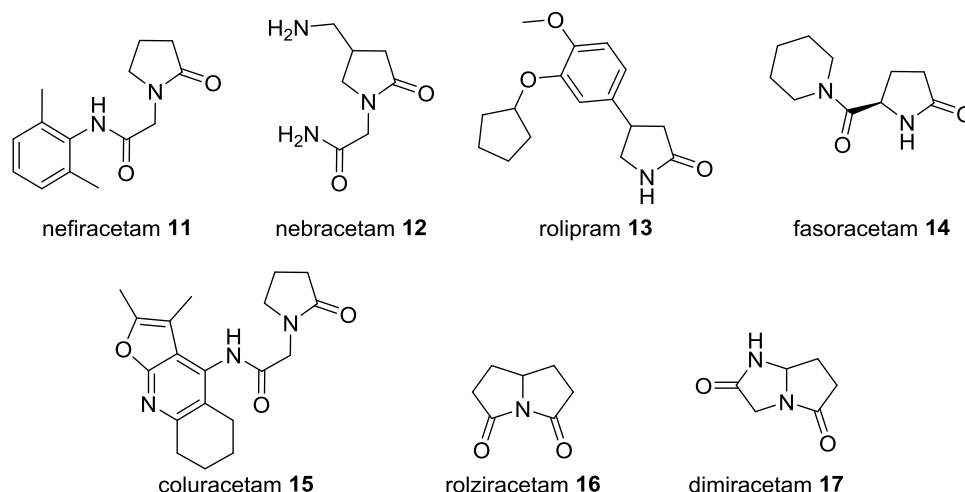


**Figure 4: Piracetam-like compounds with unknown efficacy**

Nootropic drugs are frequently used in the treatment of a very wide spectrum of disorders associated with memory and are often used for the treatment of both

memory and cognition deficits. The largest of this grouping is that of AD but they are also used in the treatment of schizophrenia, stroke, attention deficit hyperactivity disorder (ADHD), aging and epilepsy to name but a few (Froestl et al., 2012, Giurgea et al., 1983).

Despite the fact that piracetam (**3**) (also known as Nootropil) has been used for over 40 years its cognitive enhancing effects have remained ethereal in nature. It was first approved as a nootropic drug in Europe in the 1970's, despite a lack of knowledge as to its exact mechanism. There have been numerous studies carried out in order to investigate its potential in disease models that are associated with memory defects. In 1993 Croisile and others performed a double-blind placebo-controlled, parallel-group study over a one-year period. They used a high dose of piracetam (**3**) (8g/d *per os*) and examined its effects in 33 patients, who had previously presented with slowly progressive memory impairment, which was attributed to probable early onset Alzheimer's disease. The results of their study showed that long-term administration of a high dose of piracetam (**3**) could slow the cognitive deterioration in patients with AD (Croisile *et al.*, 1993).

Further supporting evidence for the nootropic effects of piracetam (**3**) (Figure 2) came from a study where it was demonstrated to be the most effective drug in patients with cognitive deterioration or cerebral ischaemia-induced short-term memory after heart bypass surgery (Uebelhack *et al.*, 2003). Consistent with these results, Holinski's studies further supported the demonstrated cerebroprotective properties of piracetam in patients who underwent heart bypass surgery (Holinski *et al.*, 2008). However, follow-up investigations of the same patient cohort three years later indicated that administration of piracetam prior to an open-heart surgery procedure had no demonstrable preventative effect on post surgical deterioration of cognitive function in older patients (Holinski *et al.*, 2011).

Malykh and Sadaie (Malykh and Sadaie, 2010) carried out meta-analysis of nineteen clinical double blind placebo controlled trials that were performed against the activity of piracetam (**3**) (Figure 2), between 1972 and 2001. Most of the studies were directed towards memory deficit disorders and the results of

the analysis showed that patients treated with piracetam improved by 61% in comparison to 33% in the placebo groups. Adverse effects such as headaches or drowsiness in patients occurred very rarely and were typically mild in nature, clearly highlighting the potential of the racetam family of compounds and piracetam (**3**) (Figure 2) in particular (Batysheva *et al.*, 2009, Fedi *et al.*, 2001, Akhondzadeh *et al.*, 2008). Despite this, piracetam (**3**) (Figure 2) demonstrated no significant improvement in cognitive impairment in patients with Alzheimer's disease, despite its potent neuroprotective and memory enhancing effects on those that had undergone heart bypass surgery.

In piracetam polytherapy with the vasodilator cinnarizine (Fezam), patients with multiple sclerosis (MS) showed improvements in activity and/or mood (Gusev *et al.*, 2008). Fezam has also been used in the treatment of senile macular degeneration and was shown to improve vision significantly (20-80%) in over 76% of patients. The authors proposed that the effects of piracetam were due to improvements in retinal microcirculation (Kiseleva *et al.*, 2005).

Piracetam has also been used in combination therapy in patients with the antipsychotic risperidone. Results from the study demonstrated a synergistic improvement of abnormal behaviour in patients with autistic disorders (Akhondzadeh *et al.*, 2008).

Despite the pluripotent effects reported for piracetam (**3**) (Figure 2), it is known to be a weak positive modulator of AMPA receptors (Copani *et al.*, 1992). Crystallography analysis revealed that piracetam binds to the S1S2 dimer interface of GluA2 (Figure 5). Moreover, it was also shown that it could occupy three binding sites as shown below, where the first binding site (blue) is analogous to the binding site of aniracetam. The second binding site (purple) is analogous to the binding site of cyclothiazide and the third binding site (red), which appears unique to piracetam (Ahmed and Oswald, 2010).

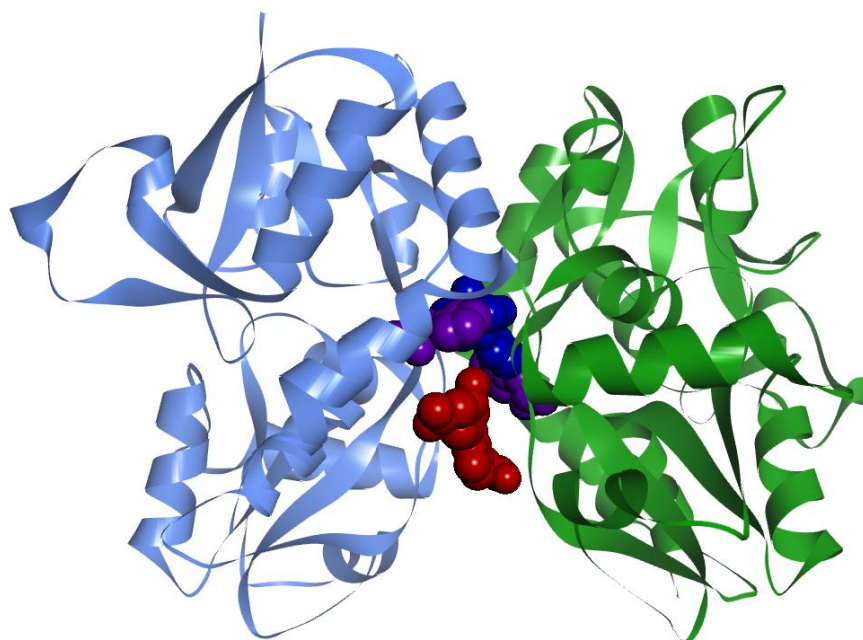


**Figure 5: Piracetam bound to dimeric GluA2 at three binding sites**

However, despite the crystallographic evidence of its binding, the mechanism by which piracetam exerts its nootropic effects remains a matter of conjecture with numerous contrasting studies.

Marisco and others recently demonstrated that in the scopolamine-induced cognition loss animal model, piracetam (**3**) (Figure 2) was shown to decrease the discrimination index in the object recognition task (Marisco *et al.*, 2013). The data that they reported was consistent with previous tests carried out by themselves and others, which described the beneficial effects of piracetam's ability to either prevent or reverse memory impairments induced by scopolamine (Chopin and Briley, 1992, Piercey *et al.*, 1987, Verloes *et al.*, 1988, Lenegre *et al.*, 1988, Schindler, 1989). The exact mechanism by which piracetam achieves this prevention or reversal remains unknown. However, despite the lack of a clear target, Marisco suggested that its effect can be associated with the purinergic system *via* a decrease in oxidative stress and a corresponding maintenance of adenosine triphosphate diphosphohydrolyse (NTPDase), 5'-nucleotidase and adenosine deaminase (ADA)' levels in synaptosomes in the cerebral cortex and hippocampus (Marisco *et al.*, 2013).

In support of this proposed mechanism is the fact that oxidative stress is frequently observed in inflammatory hyperalgesia along with production of associated inflammatory cytokines (Verri *et al.*, 2012). This also correlates with the recently reported analgesic and anti-inflammatory effects of piracetam, further supporting its mechanism of action (Navarro *et al.*, 2013). Piracetam was also shown to reduce the levels of the cytokine tumor necrosis factor (TNF- $\alpha$ ), in a carrageenin-induced model of inflammation, which further forms interleukin 1 beta (IL-1 $\beta$ ). These two cytokines are known to activate nicotinamide adenine dinucleotide phosphate (NADPH) oxidase, which is a catalyst for the generation of reactive oxygen species (ROS). As recently observed by Valencia (Valencia *et al.*, 2013), the hyperactivity of NADPH oxidase was shown to cause a resultant and concomitant increase in oxidative stress and cell death in Huntington's disease, which is also characterised by memory loss symptoms.

### **1.1.3. AMPA modulators in a clinical setting**

One of the key challenges of converting an active compound into a drug is its progression through clinical trials. The area of cognitive enhancers is replete with compounds that have failed to demonstrate a significant improvement over current therapy or obtention of the desired clinical endpoints, which are frequently difficult to both measure and analyse. Therefore the design of any trial has to consider two important elements. The first of these relates to the probability of achieving the desired change in the patient's cognitive function. One mechanism by which a trial can achieve this is by improvement of the cognitive function of patients by counteracting the 'damage' caused by mental decline. However, this positive effect can only be observed when the mental decline equates to a mild intellectual deterioration. In cases of severe mental deterioration, the structural changes of the brain are too complicated, so obtention of the clinical endpoints with a nootropic drug are very challenging. For instance, patients presenting with early signs of dementia are often "good experimental subjects," whereas elderly patients with dementia, depression and variation in cognition arousal can be improved indirectly - *via* the improvement of patient's mood and motivation, classifying them as "poor experimental subjects."

The second concerns the interpretation or achievement of an observed change in the requisite cognitive task. The change has to be measured in a “neutral environment,” meaning that factors that can improve or reduce cognitive performances have to be excluded. For example, the improvement in cognition might be an indirect result of the side effects of a nootropic drug observed in the “experimental subject.” Hakkarainen and Hakamies (Hakkarainen and Hakamies, 1978) have noticed that piracetam caused anxiety, irritability or nervousness, catalysis of arousal and alertness that can trigger or cause indirect effects on cognition (Gainotti *et al.*, 1986).

At present, it is clear that current drug regimens for memory do not effectively treat diseases associated with memory impairment such as Alzheimer’s disease. As such, the search for new treatments continues and in order to develop new therapeutics, researchers including us, frequently take inspiration from nature. One such potential candidate – clausenamide isolated from the Chinese plant *Clausena lansium* has shown good potential for the treatment of neurological disorders, but it is not accessible in sufficient amounts to be developed into a medicine. The following section describes previous synthetic approaches towards this compound and its reported biological activity.

## 1.2. Clausenamide

Clausenamide **2** is a naturally occurring five-membered heterocycle that exists in a racemic form and was first isolated in the early 1980s from the aqueous extracts of the dry leaves of the shrub *Clausena lansium*, the enantiomeric forms of which are shown below (Figure 6). *Clausena lansium* is commonly known as Wampee and is a plant member of the Rutaceae family, occurring in either shrub or tree form with grape-like fruit.

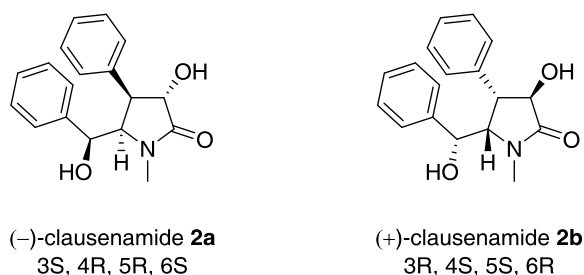


**Figure 6: Structures of (-)- and (+)-clausenamide**

Chinese, Taiwanese and Vietnamese herbalists have used *Clausena lansium* as a folk medicine for thousands of years. Its leaves, seeds and fruit have been used for the treatment of a variety of disorders such as coughs, asthma, ulcers, acute and chronic gastro-intestinal inflammation, acute and chronic viral hepatitis, bronchitis and malaria. Additionally, some coumarins and amides, similar to clausenamide were shown to have pharmacological properties, such as anti-lipid peroxidative and cerebral protective effects, as well as hepatoprotective, hypoglycaemic, anticonvulsant, cardiovascular and antitumor activities (Adebajo *et al.*, 2009, Hartwig and Born, 1987).

This medicinal plant is typically produced in large amounts in the southwest Yunnan province in China. However, only 3.8 grammes of clausenamide are isolated from over 10 kilograms of dried leaves (Hartwig and Born, 1987).

Clausenamide's structure is based on a pyrrolidine ring, with four contiguous chiral centres (C3, C4, C5, C6) leading to 16 possible enantiomers (8 pairs of diastereoisomers) as shown below (Figure 7) (Feng *et al.*, 2009).

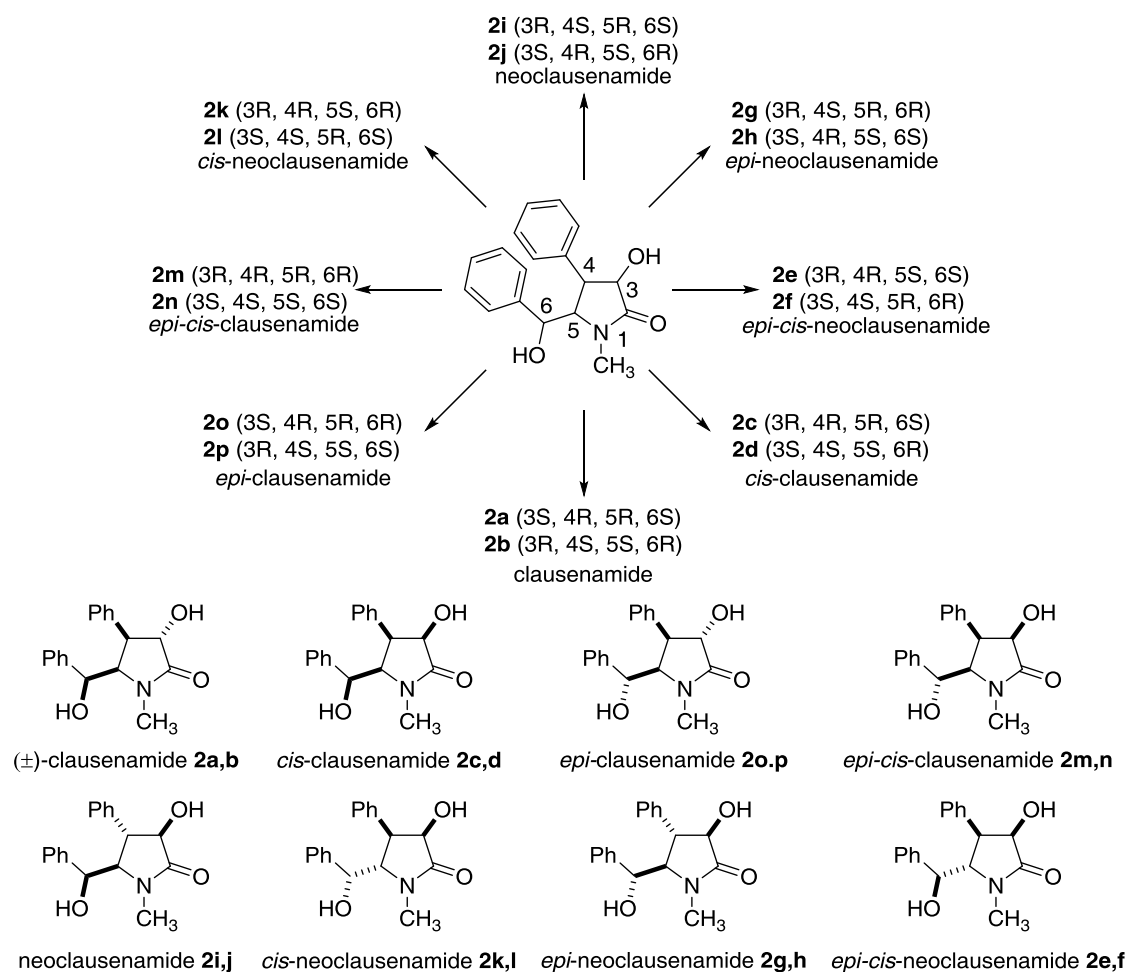


**Figure 7: Optically active clausenamamide stereoisomers (adapted from (Feng *et al.*, 2009)).**

### 1.2.1. Mode of action of clausenamamide

Clausenamamide is isolated as its racemic (+/-) form and as such, there are several issues associated with this for the development of clausenamamide as a potential drug. In the drug development process it is essential to isolate a single enantiomer from the racemate of a drug, as receptors and enzymes have specific stereo-selectivity with one enantiomer having positive effects and the other having either no effect, or deleterious effects as seen from the problems associated with thalidomide use in the 1960s (Kim and Scialli, 2011). In other words, production and analysis of each chiral compound is crucial to obtain a complete ADME (Absorption, Distribution, Metabolism, Elimination) profile as well as establishing the toxicity of each single enantiomer. As a further example, racemic DOPA used for the treatment of Parkinson's disease has been shown

to possess many adverse effects such as nausea, vomiting, anorexia and granulocytopenia (Hutt and Valentová, 2003). However, use of the single enantiomer clearly demonstrated that *L*-DOPA not only reduced those effects, but also enabled the required dose to be lowered to 50% of that of the racemic form. Hence, separation of both enantiomers is crucial in order to ensure that any newly developed drug can be safe and reliable in clinical trials. Despite this, single enantiomers and racemates can sometimes show similar toxicities and pharmacokinetic profiles, so the overall effect of the racemic mixture can sometimes be extrapolated to a single enantiomer (Hutt and Valentová, 2003). Clausenamide has been shown to possess nootropic activity in animal tests and has also been shown to enhance LTP, which is the long-lasting improvement in communication between two neurones, as a result of simultaneous stimulation. Liu and Zhang showed that (-)-clausenamide could potentiate basal synaptic transmission and high frequency stimulation (HFS)-induced LTP on anaesthetised or freely moving rats and increased hippocampal and mossy fibre sprouting (Liu and Zhang, 1998, Xu *et al.*, 2005, Tang and Zhang, 2002, Liu *et al.*, 1999).

Ning and other researches proposed that the facilitating effect on glutamatergic synaptic transmission of (-)-clausenamide in the CA1 region is due to activation of voltage-dependent calcium channels (VDCC) and calcium release which then triggers release of intracellular calcium (from endoplasmic reticulum) and activates the CaMKII $\alpha$ -CREB signal pathway (Ning *et al.*, 2012b, Ning *et al.*, 2012a).

Moreover, (-)-clausenamide was also shown to be 50-100 times more active than the well-known drug piracetam (**3**) (Figure 8) and 5-10 times more active than the racemic form of clausenamide.

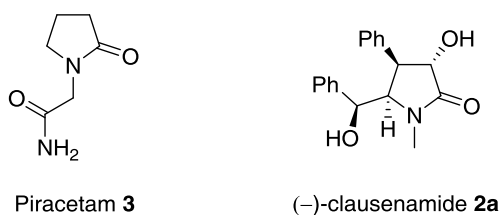


**Figure 8: Structures of piracetam and (-)-clausenamide**

Inspired by this result, Feng and co-workers considered whether clausenamide's nootropic activity might be related to its stereochemistry. They investigated whether there is a correlation between the configuration of the stereoisomers of clausenamide and its associated nootropic activity. To investigate the structure-activity-relationship (SAR), they synthesised all 16 (8 pairs) optically pure stereoisomers of clausenamide starting from the parent compound. They carried out an LTP assay, which indicated that three isomers: **2e**, **2i**, **2p** are more potent in terms of increasing population spike (PS) amplitude than the purported most active enantiomer, (-)-clausenamide. In addition, the corresponding enantiomers **2j**, **2f**, **2o** were shown to be less potent than (-)-clausenamide (Feng *et al.*, 2009).

In order to separate (-)-clausenamide from the naturally occurring racemic mixture, Wang and others carried out high performance liquid chromatographic (HPLC) separation using chiral- $\alpha$ 1-acid glycoprotein (AGP) as the stationary phase. The method used was efficient, universal and enabled ready separation of all the enantiomers of racemic clausenamide (Wang *et al.*, 2010).

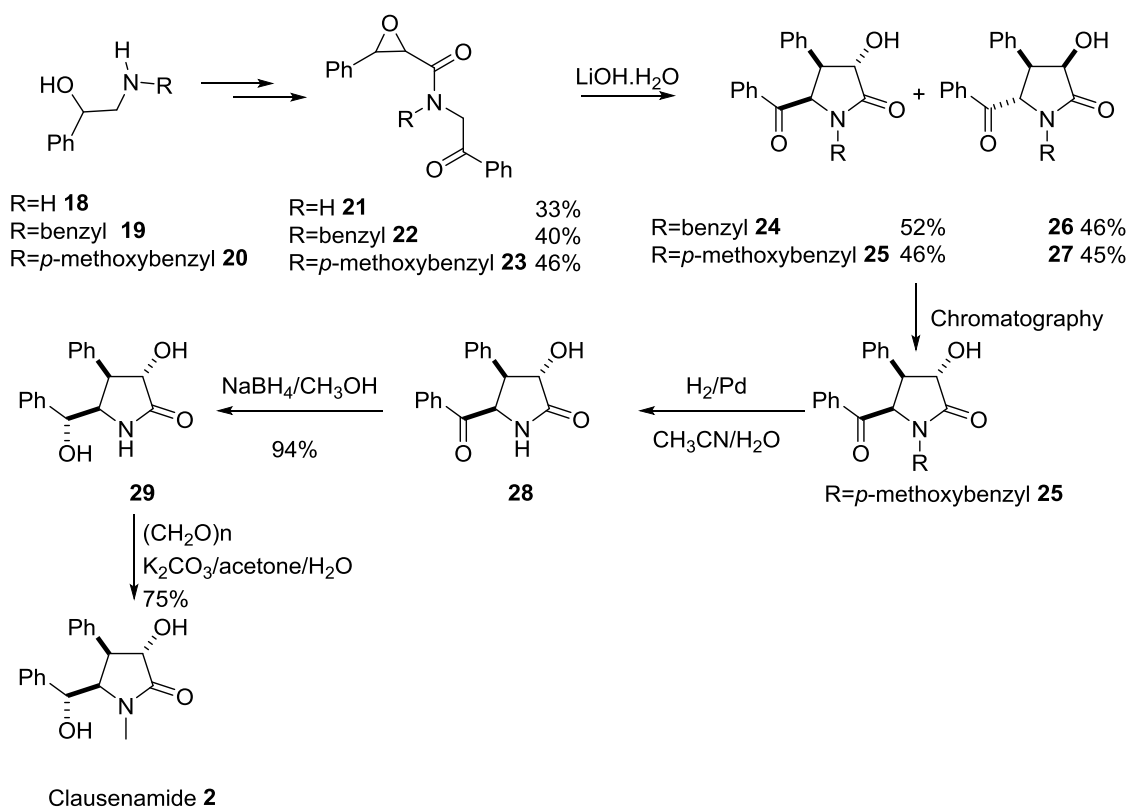
Recent data published by Ning and other researchers confirmed a strong relationship between chirality and modulation of synaptic transmission, as (+)-*epi*-clausenamide (**2p**) but not (-)-*epi*-clausenamide (**2o**) was shown to be more potent than (-)-clausenamide. As suggested, the facilitation of synaptic transmission might be associated with the activation of Synapsin I (Ser 9) (Ning *et al.*, 2012a).

### 1.2.2. Previous synthetic approaches to clausenamide

There have been several reports directed towards the synthesis of clausenamide, all of which utilise different methods and a number of different strategies to synthesise either the pyrrolidine core or the surrounding functionality.

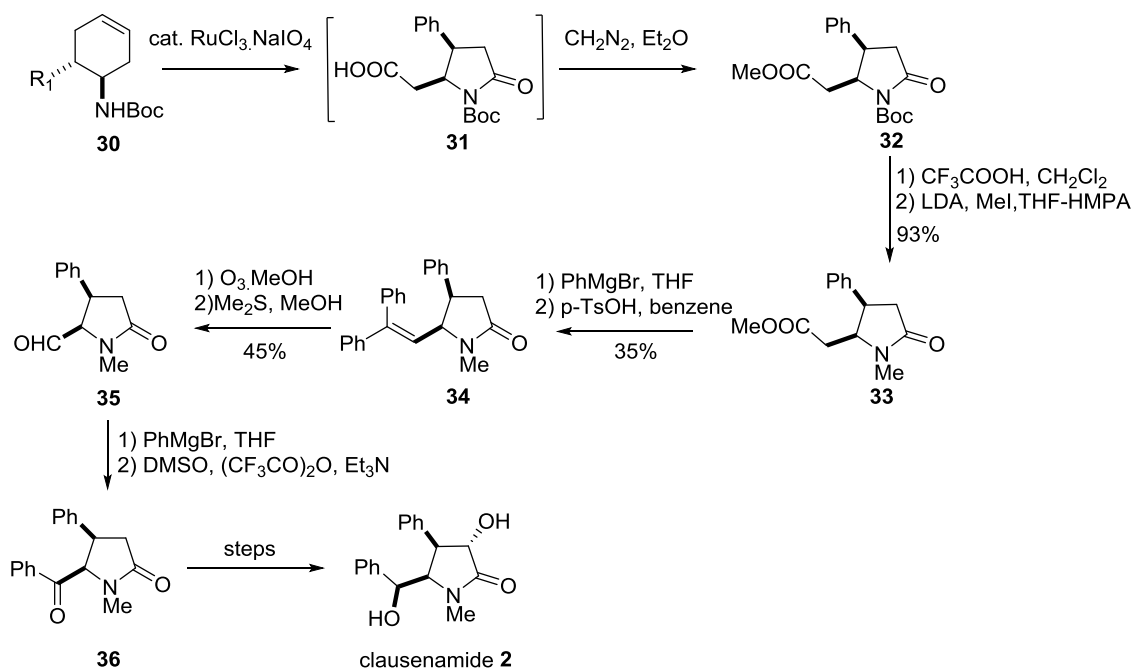
Li and co-workers (Li *et al.*, 2010) synthesised clausenamide **2** in an intramolecular cyclisation from an epoxide precursor **21-23** as outlined below (Scheme 1). Use of lithium hydroxide in a water/methanol mixture led to intramolecular cyclisation to the pyrrolidine core structure **24-27**, but it proved

to be a slow and low yielding complicated method. Finally, elaboration of the cyclised product led to clausenamide **2**, via an eight and six step overall reaction sequence starting from  $\beta$ -phenyl-(*N*-*p*-methoxybenzyl)-ethanol **20** (Scheme 1). Yang and co-workers and Wang and co-workers have also reported an analogous approach towards clausenamide, and related isomers via ring opening of a chiral epoxide (Yang *et al.*, 2009, Wang and Tian, 1996).

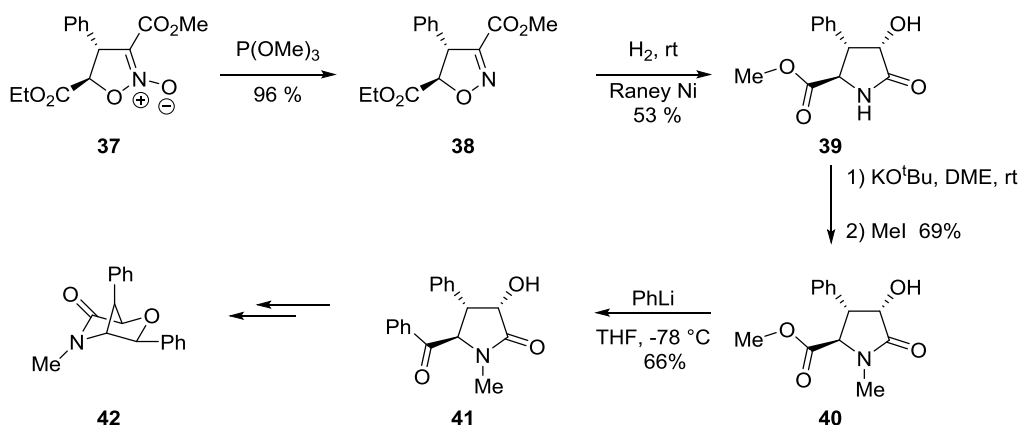


**Scheme 1: Clausenamide cyclisation with LiOH**

Yakura's approach towards the total synthesis of clausenamide involved an oxidative cleavage-lactamization of *trans*-5-substituted 4-acyl or alkyl-aminocyclohexenes. In this approach, *in situ* oxidation of cyclohexene **30** using ruthenium chloride under Sharpless conditions led to the corresponding carboxylic acid **31** that was isolated as its methyl ester **32** in 88% yield. The corresponding *N*-Boc-protected pyrrolidone **32** was deprotected and *N*-methylated with lithium diisopropylamide and methyl iodide to give the *N*-methylpyrrolidone derivative **33**. By use of the Barbier-Wieland degradation procedure, *N*-methylpyrrolidone was subsequently converted into the key intermediate for the synthesis of clausenamide (Scheme 2) (Yakura *et al.*, 1991).

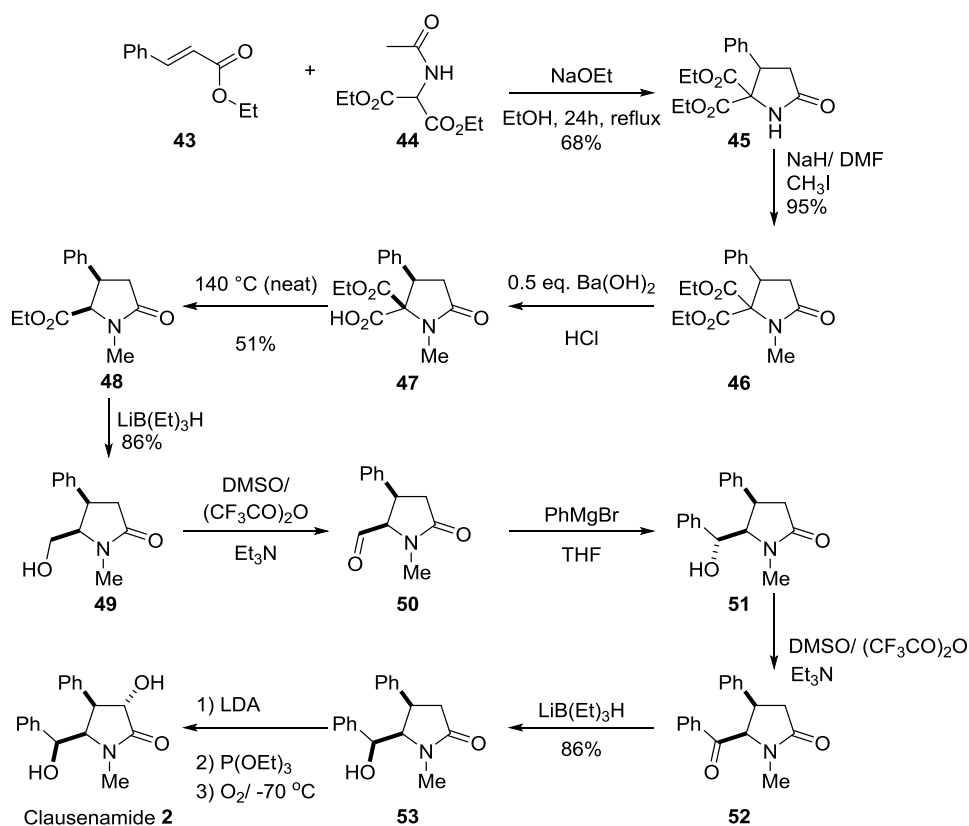


Zhu and others developed an efficient ylide cyclisation for the synthesis of isoxazoline *N*-oxides, which can be used as a precursor in the formal synthesis of dehydroclausenamide. As shown below (Scheme 3), treatment of isoxazoline with Raney Ni under a H<sub>2</sub> atmosphere led to formation of lactam **39**, which is then methylated and reacted with phenyllithium to give phenylketone **41**, which according to literature precedent can be transformed to dehydroclausenamide in a two step process (Scheme 3) (Zhu *et al.*, 2008).



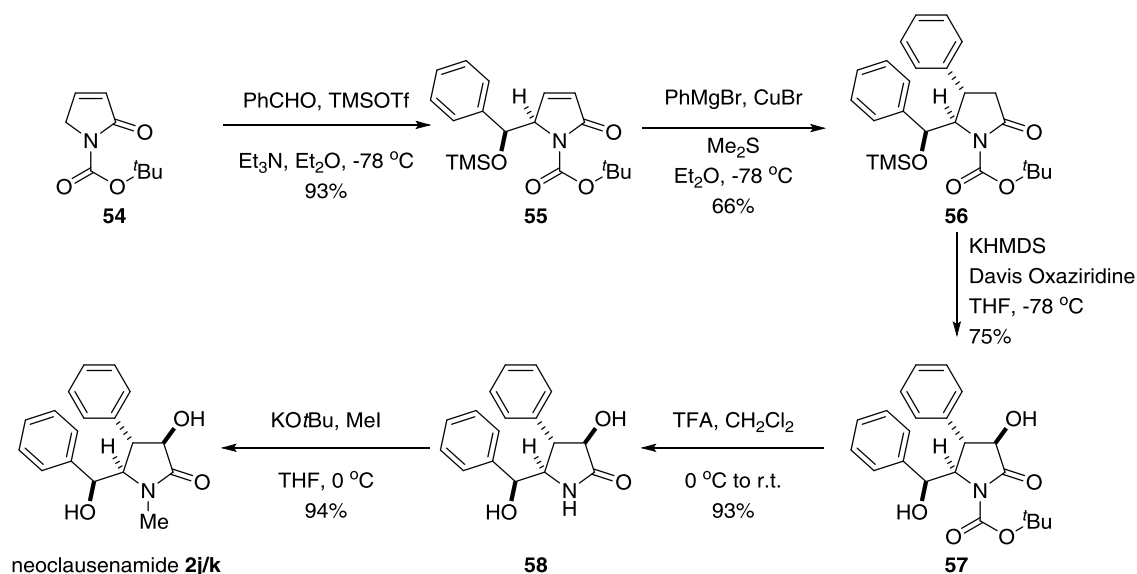
In the diastereoselective total synthesis of clausenamide, Hartwig and Born used ethyl cinnamate **43** and diethyl acetamidomalonate **44** to generate 5,5-bis-(ethoxycarbonyl)-4-phenylbutyrolactam **45** (Hartwig and Born, 1987).

Methylation of pyrrolidinone **45** via deprotonation with sodium hydride and treatment with methyl iodide gave **46** in an impressive 95% yield. Unfortunately, subsequent hydrolysis with barium hydroxide was only partially successful on the ester group located in the *trans*-position to the phenyl group. The resulting acid-ester **47** was then heated with collidine according to literature precedent, to give selectively and exclusively the monocarboxylic ester **48** with 4,5-*cis*-configuration (Abell and Lennon, 1965, Musso, 1968). Under these conditions and in contrast to previous reports; both isomers were formed in around a 1:1 ratio. Alternatively, heating of the acid-ester **47** to 140 °C without solvent improved the ratio to 2:1 in favour of the *cis*-isomer. The *cis*-isomer was then separated by crystallisation and reacted with sterically hindered superhydride (LiB(Et)<sub>3</sub>H) to give exclusively the *cis* alcohol **49**. Swern oxidation of **49** to the aldehyde **50** followed by Grignard addition gave alcohol **51**. This was then reoxidised again under Swern conditions, reduced with superhydride and the alcohol moiety introduced under basic conditions to give clausenamide **2** (Scheme 4) (Hartwig and Born, 1987).



Scheme 4: Hartwig and Born synthesis of clausenamide

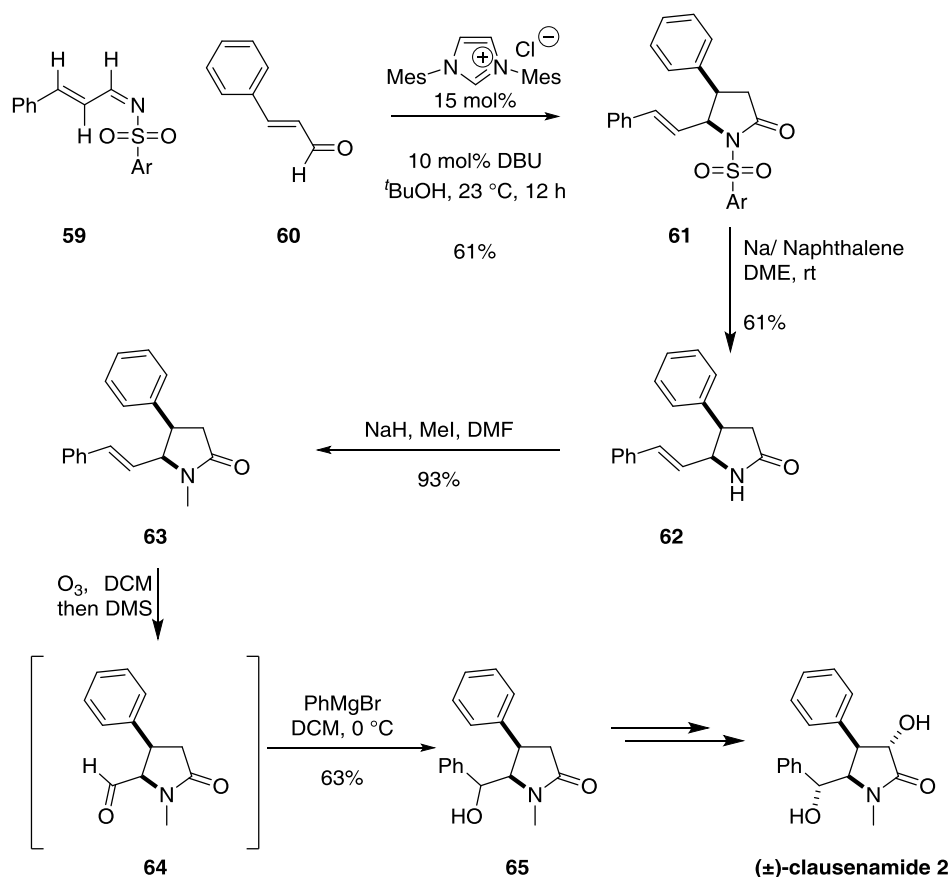
Dai and Huang recently described a novel approach to racemic neoclausenamide **2i,j** starting from *N*-Boc-pyrrol-2-(5*H*)-one **54** using the vinylogous Mukaiyama aldol reaction (Scheme 5) (Dai and Huang, 2012).



**Scheme 5: Dai and Huang synthesis of neoclausenamide**

Reaction of the vinylogous amide **54** with triethylamine and benzaldehyde in the presence of trimethylsilyl trifluoromethanesulfonate (TMSOTf) gave the addition product **55** in excellent yield (93%). Copper catalysed 1-4 Grignard addition of phenylmagnesium bromide led to introduction of the 4-phenyl group *anti* to the secondary alcohol moiety in good yield. Incorporation of the alcohol group at C-2 of the pyrrolidine ring was accomplished *via* use of the Davis Oxaziridine reagent, which led to efficient formation of the bis-alcohol **57** with concomitant deprotection of the tetramethylsilane (TMS) protected alcohol. Finally, deprotection of the pyrrolidinone amide with trifluoroacetic acid (TFA) followed by alkylation with methyl iodide under basic conditions gave racemic neoclausenamide **2i,j** in 94% and 31% overall yield.

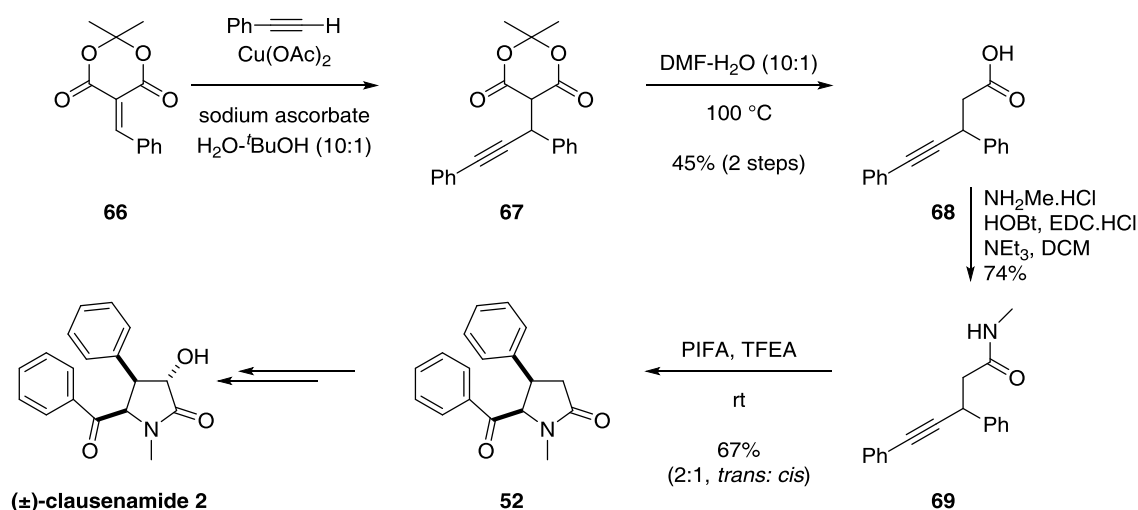
He and Bode recently reported a formal total synthesis of (±)-clausenamide using an *N*-heterocyclic carbene (NHC) approach (He *et al.*, 2012) as shown below (Scheme 6).



**Scheme 6: He's approach to ( $\pm$ )-clausenamide**

Cinnamaldehyde **60** was reacted with *N*-sulfonylimine **59** in the presence of the NHC catalyst to give the lactam **61** in 61% yield as an 8:1 mixture of diastereoisomers. Deprotection and alkylation gave the *N*-methylated product **63** in 60% overall yield as a single isomer after purification. Ozonolysis followed by Grignard addition led to formation of the secondary alcohol **65** in 63% yield. The final two steps to ( $\pm$ )-clausenamide **2** had previously been reported by Hartwig and Born as shown in Scheme 4 (Hartwig and Born, 1987).

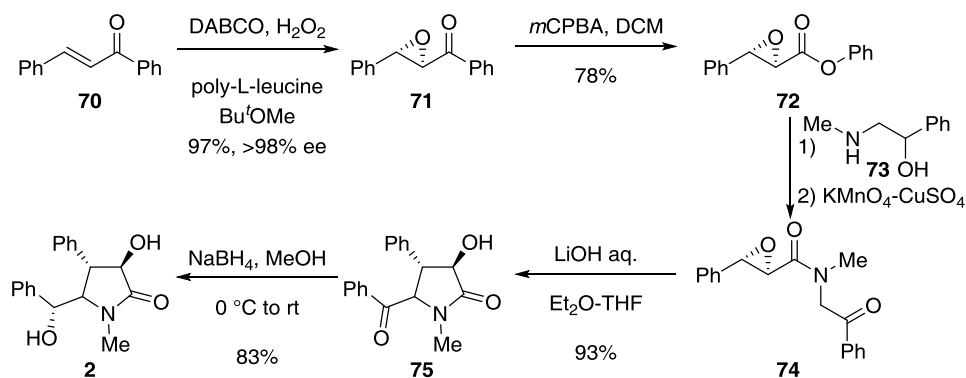
Tellitù and Domínguez developed a novel hypervalent iodine mediated approach to the core structure of clausenamide *via* the use of [bis(trifluoroacetoxy)iodo]benzene (PIFA) as shown in Scheme 7 (Tellitù and Domínguez, 2012).



**Scheme 7: Tellitu and Dominguez's approach to (±)-clausenamide**

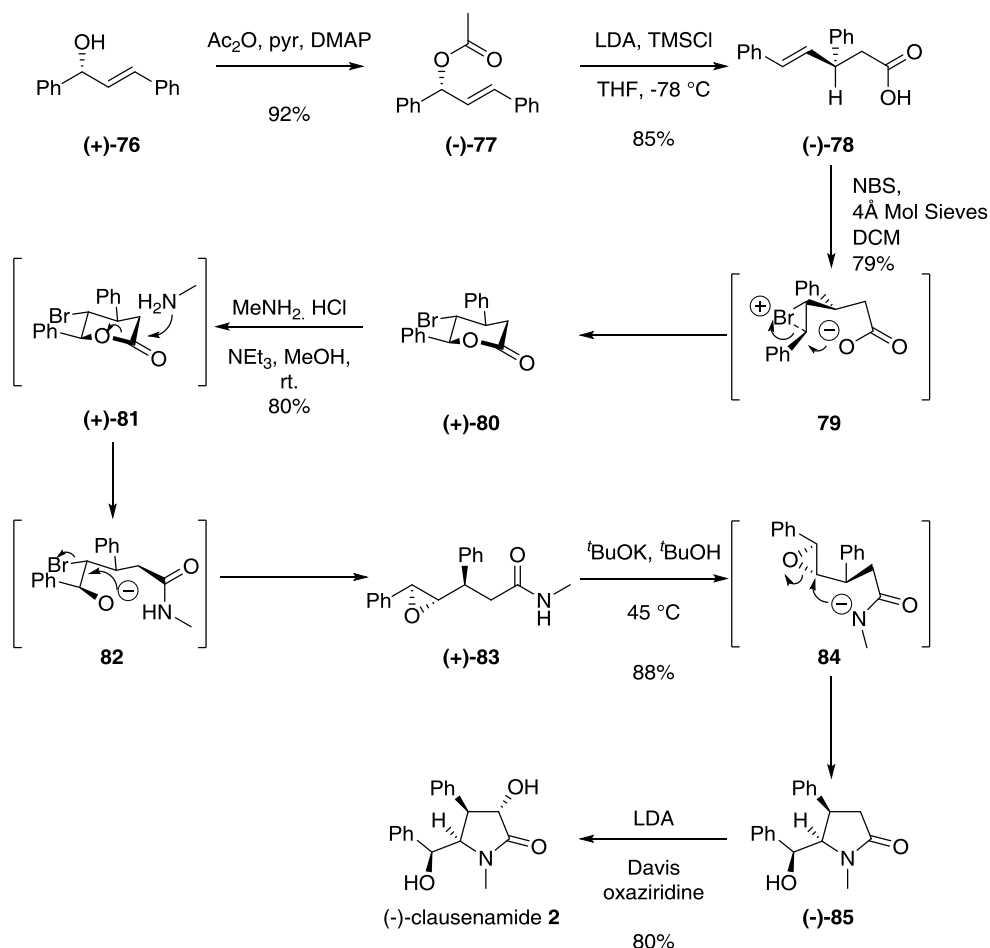
Condensation of Meldrum's acid with benzaldehyde gave adduct **66**, which on reaction with phenylacetylene gave the conjugate adduct **67**. Thermal mediated decarboxylation gave acid **68** in 45% yield over two steps, which was reacted with methylamine under standard coupling conditions to give amide **69** in 74% yield. The key step in the reaction sequence was mediated by PIFA which gave efficient conversion to the pyrrolidinone **52** in 67% yield albeit in a disfavoured 2:1 ratio of *trans*:*cis* isomers. This method was a formal total synthesis as the subsequent steps had previously been reported by Hartwig and Born (Hartwig and Born, 1987).

One of the earliest syntheses of (+)-clausenamide was reported by Cappi and co-workers in their search for the synthetic usefulness of epoxide **71**, which was obtained *via* Juliá-Colonna epoxidation of the chalcone **70** (Scheme 8) (W. Cappi *et al.*, 1998). Reaction of the epoxide with *meta*-chloroperoxybenzoic acid (mCPBA) furnished ester **72** in good yield, which was elaborated to the cyclisation precursor **74** *via* treatment with amine **73** and subsequent oxidation. Cyclisation was carried out under basic conditions, analogous to the method described previously by Li and co-workers (Li *et al.*, 2010). Finally, reduction with sodium borohydride gave (+)-clausenamide **2b** in 40% overall yield.



Scheme 8: Capi's approach to (+)-clausenamide

Liu and co-workers reported a six-step synthesis of (-)-clausenamide **2a** in 2013 involving a novel Ireland-Claisen rearrangement with an overall yield of 34% and >98% enantiomeric excess (ee) (Liu *et al.*, 2013) as shown (Scheme 9).

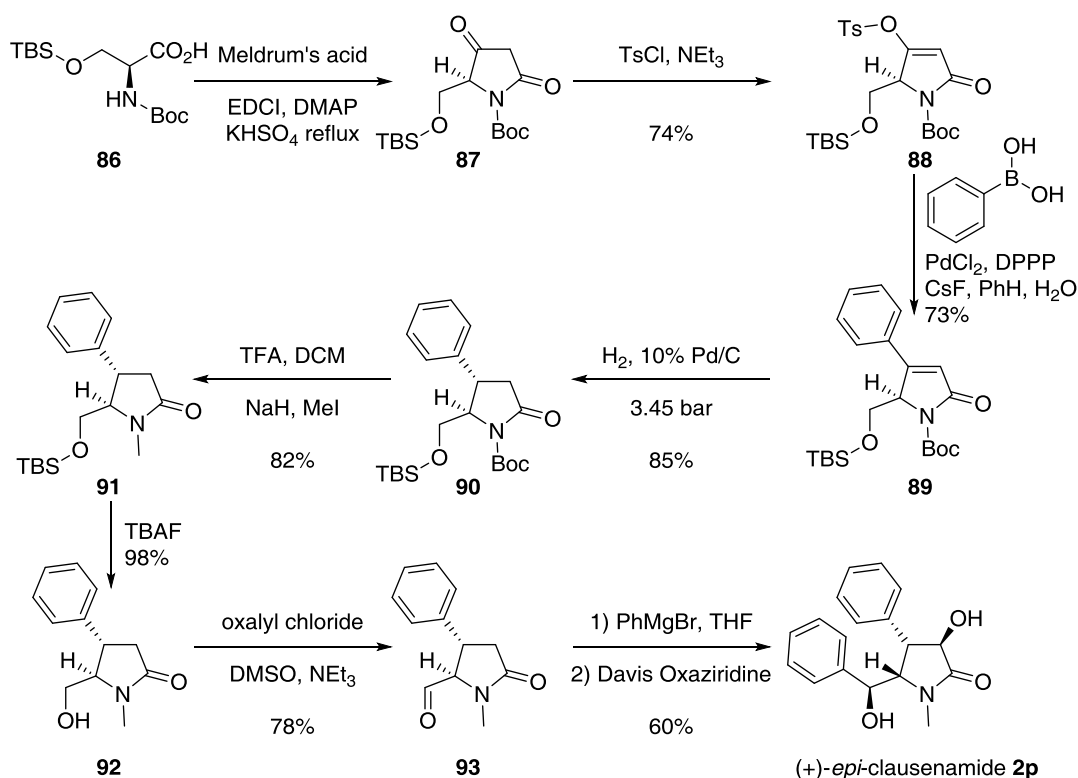


Scheme 9: Liu and co-workers approach to (-)-clausenamide

The starting alcohol **76** was prepared from the racemate by kinetic resolution under standard Sharpless asymmetric epoxidation conditions and then acylated

with acetic anhydride. Subsequent Ireland-Claisen rearrangement *via* treatment with excess lithium diisopropylamide (LDA) and trimethylsilyl chloride (TMSCl) gave the *S*-configured **78** in 85% yield. *N*-Bromosuccinimide (NBS) mediated bromolactonisation led to efficient formation of the lactone **80** in 88% yield. Reaction of **80** with methylamine gave the ring opened product **81**, which on treatment with base gave (-)-3-deoxy-clausenamide **85** in 88% yield. Finally treatment with LDA and Davis oxaziridine gave (-)-clausenamide **2a** in 80% yield.

As a result of the potent induction of LTP displayed by (+)-*epi*-clausenamide **2p** compared to (-)-clausenamide **2a**, Zhang and co-workers developed a novel enantioselective approach starting from protected *L*-serine (**86**) (Scheme 10) (Zhang *et al.*, 2012).



Condensation of the serine derivative **86** with Meldrum's acid gave the  $\beta$ -keto lactam **87**, which was converted to its tosylate enolate **88** in 74% yield. Suzuki-Miyaura coupling led to efficient incorporation of the aryl subunit to give **89**, which was then reduced using catalytic palladium on carbon at elevated pressure. Deprotection and alkylation with methyl iodide led to introduction of

the *N*-methyl group to give **91** in 82% yield. Finally deprotection of the silylated alcohol **91**, followed by oxidation, Grignard addition and treatment with Davis oxaziridine gave (+)-*epi*-clausenamide **2p** in the first reported enantioselective synthesis of this key compound.

As outlined above, the various synthetic strategies towards clausenamide (**2**) nearly all involve linear methodology with modest to poor yields. The key steps in most approaches are limited by their need to synthesise the correct stereochemistry of the final and intermediate product. As such, they are limited in their applicability towards the synthesis of clausenamide and various derivatives.

### 1.3. Biological introduction

At present, the pharmaceutical market suffers from a lack of provision of available drugs to treat disorders associated with memory impairment such as Alzheimer's or Parkinson's disease. The pyrrolidin-2-one family of cognition-enhancers, such as piracetam **3** have been studied over a number of decades and there are several members of this nootropic family that are in use in a number of countries as neuroprotective agents after stroke, to control cognition impairment and to cure epilepsy (Malykh and Sadaie, 2010). In order to find new potent molecules, robust neurophysiological assays are required to demonstrate the mechanism of action at a molecular level.

### 1.4. Glutamatergic neurotransmission

Fast communication in the central nervous system (CNS) implies that individual neurones propagate spikes down their axon where synapses with other neurones are formed. When such activity reaches the axon terminal, the neurotransmitter packaged into the presynaptic neurone is released; it then diffuses and binds to receptors localised on the membrane of the postsynaptic neurone allowing the passage of information. Such receptors are also present on axon terminals in the presynaptic neurone itself, where they modulate both the excitability and the capacity to release neurotransmitters. For fast ionotropic transmission at most excitatory synapses in the brain, glutamate is the main excitatory neurotransmitter (Storm-Mathisen *et al.*, 1983) and acts on AMPA, kainate and NMDA receptors (Bellocchio *et al.*, 2000, Takamori *et al.*, 2000, Kullmann, 2007). AMPA and NMDA receptors are mostly colocalized in the postsynaptic membrane (Bekkers and Stevens, 1989) (McBain and Dingledine, 1992) whilst kainate receptors can be distributed both pre- and post-synaptically (Huettnner, 2003, Lerma and Marques, 2013). Glutamate also activates metabotropic glutamate receptors (mGluRs), which are G-protein coupled receptors that indirectly affect neuronal excitability by modulation of other conductances, e.g. K<sup>+</sup> channels.

Several electrophysiological techniques that have been used to study the intrinsic electrical properties of peripheral and central neurones as well as the biophysical and pharmacological profile of neurotransmitter receptors found at

excitatory and inhibitory synapses and are described below (Neher and Sakmann, 1992). In the late 1930s Cole and Curtis (Cole and Curtis, 1939) invented the voltage-clamp technique, which enabled an analysis of membrane currents underlying changes in cellular excitability by holding the membrane potential at a fixed value, e.g. -70 mV. In the late 1970s Neher and Sakmann (Neher and Sakmann, 1976, Hamill et al., 1981) introduced the patch-clamp technique, which extended the reach of the voltage-clamp technique to be able to resolve single channel currents activated by neurotransmitters (ligand-gated ion channels and receptors) or by changes in membrane voltage (voltage-operated ion channels). This technique first applied to invertebrate preparations (Gola and Romey, 1970), required optimization when applied to mammalian brain slices because in order to obtain a really high electrical resolution, a high resistance between the recording electrode and the cell membrane is required (defined as giga ohm seal or 'gigaseal'). Edwards and others (Edwards *et al.*, 1989) invented a visualization method for neurones in thin brain slices based on differential infrared videomicroscopy. This approach enables identification of single neurones and some of their processes whilst permitting simultaneous recording from them under visual control.

The following section provides a general overview of the different types of ionotropic receptors activated by glutamate.

### **1.5. Ionotropic Glutamate Receptors**

Excitatory synapses express AMPA, NMDA and less commonly kainate receptors, all of which can be activated by the release of glutamate following invasion of the terminal by the presynaptic action potential. AMPA and kainate receptors mediate the initial electrophysiological response to glutamate, whereas NMDA receptors are responsible for a slower and longer phase of neurotransmission. Neurotransmission is then terminated by glutamate diffusion and clearance mechanisms as well as receptor mechanisms.

### 1.5.1. AMPA receptors

Fast excitatory postsynaptic currents (EPSCs) are mostly mediated by AMPA receptors. AMPARs are heteromers composed of four subunits GluA1-4 forming an ion channel permeable to  $\text{Na}^+$ ,  $\text{K}^+$  and for some,  $\text{Ca}^{2+}$ . All subunits of AMPAR are expressed in the hippocampus: GluA1 and GluA2 mainly in principal cells and interneurons, whereas GluA3 occurs at lower levels and GluA4 occurs only in embryonic and early postnatal principal cells (Keinanen *et al.*, 1990). AMPARs have fast kinetics and high opening probability, and their activation, deactivation and desensitization occurs within milliseconds. Dynamic changes in subunit composition are reflected in the biophysical properties of AMPARs. For instance, the presence of the GluA1 subunit is necessary for calcium permeability and as such, the corresponding synaptic plasticity. For example, cerebellar stellate cells exhibit a form of synaptic plasticity that is dependant of incorporation of GluA1 or GluA2 subunits during high frequency stimulation (Liu and Cull-Candy, 2002). AMPARs containing GluA2 will have a reduced  $\text{Ca}^{2+}$  permeability as well as channel conductance and prolonged decay kinetics of synaptic current (Cull-Candy *et al.*, 2006). Moreover, incorporation of the GluA2 subunit will abolish any physiologically occurring block by endogenous polyamines at GluA1-enriched AMPARs (Rozov and Burnashev, 1999, Savtchouk and Liu, 2011). It is therefore clear that the sensitivity of evoked EPSCs to polyamine toxins (e.g. phillanthotoxin) or intracellular polyamines can be used to establish calcium-permeability of AMPARs. Noteworthy is the presence of two pools of AMPARs: functional pools and reserve pools. Functional pools of AMPARs are present on the synaptic surface, whereas reserve pools exist either intracellularly (driven by endo- and exocytosis) or at the extrasynaptic surface membrane (regulated by lateral diffusion). Importantly, AMPARs endure an activity-dependent recycling process between the two pools mentioned above, thus providing a mechanism for the strengthening of synaptic transmission in hippocampal pyramidal neurons. (Kullmann, 2007).

### 1.5.2. NMDA receptors

To date, three families of NMDA receptor subunits have been identified: GluN1, GluN2A-D and GluN3A-B. (Paoletti and Neyton, 2007) NMDAR are permeable to  $\text{Ca}^{2+}$ ,  $\text{Na}^{+}$  and  $\text{K}^{+}$  (Ascher and Nowak, 1988). Before the separation into three glutamatergic ionotropic receptors, a division of NMDA and so called 'non-NMDA' receptors existed. Indeed, NMDAR show many distinctive properties amongst other ionotropic glutamate receptors. Firstly, NMDAR mediated signals have characteristic slow kinetics (hundreds of milliseconds) due to slow glutamate unbinding. Secondly, NMDAR channels are highly permeable to  $\text{Ca}^{2+}$  and their opening probability and gating is subunit specific (Gielen *et al.*, 2009). Thirdly, their ion channels can be subjected to a voltage-dependant block by  $\text{Mg}^{2+}$  (Mayer *et al.*, 1984, Nowak *et al.*, 1984). At the resting membrane potential (more negative than -50 mV), NMDARs are blocked by  $\text{Mg}^{2+}$ , which is relieved by a sufficient membrane depolarisation of the membrane (for example caused by strong activation of AMPAR), displaying a characteristic outward rectification in the I-V relationship of NMDAR-mediated currents (Ascher and Nowak, 1988). Lastly, NMDAR channels require not only glutamate as a co-activator but also either a molecule of either glycine or *D*-serine (Kew *et al.*, 2000).

NMDARs contain many regulatory binding sites to which a number of small molecules can bind, either in an agonistic or antagonistic manner. Such diverse pharmacology is important, as many neuropsychiatric disorders are linked to both the hyperactivation and hypofunction of NMDARs (Paoletti *et al.*, 2013). Moreover, NMDA receptors play an important role in synaptic plasticity, for instance the induction of long-term potentiation (LTP) in CA1 region of the hippocampus and NMDA receptor-dependent metaplasticity at mossy fiber-CA3 synapses.

NMDARs have been proposed to act as 'coincidence detectors', implying that sufficient depolarization of the postsynaptic membrane removes the  $\text{Mg}^{2+}$  block, allowing  $\text{Ca}^{2+}$  fluxes into the cell. This calcium influx triggers various forms of synaptic plasticity, including long-term potentiation, which results from the activation of calcium-dependent signal transduction cascades that cause trafficking of AMPA receptors into the synapse, thus strengthening synaptic

signalling (Swanson, 2009, Huganir and Nicoll, 2013). NMDA receptors are the switch that triggers LTP, which is expressed and maintained by the presence of an increased number of active AMPA receptors at the potentiated synapse (Malenka and Bear, 2004).

### 1.5.3. Kainate receptors

Kainate receptors are built from multimeric assemblies of GluK1-3 and GluK4,5 subunits (Kumar et al., 2011, Mayer, 2005). GluK1-3 and GluK5 subunits are expressed in the CA3 region of the hippocampus, striatum and the inner layer of the cortex, whereas GluK4 is distributed exclusively in the hippocampus. A large fraction of high-affinity kainate binding sites are localised in the stratum lucidum where mossy fibre synapses are formed (Foster *et al.*, 1981). Kainate receptors possess similar pharmacology to AMPA receptors and as mentioned previously they have been combined into the 'non-NMDA receptors' family (Lerma, 2003). The measurement of native kainate currents in the hippocampus became possible with the discovery of the selective AMPA receptor antagonists GYKI 52466 and 53655 (Donevan and Rogawski, 1993). Activation of postsynaptic kainate receptors results in the generation of small and slow EPSCs in CA3 pyramidal neurones, whose amplitude represents only 10% of the total peak current generated by AMPA receptor activation (Vignes and Collingridge, 1997). However postsynaptic kainate receptors have much slower deactivation kinetics when compared to AMPAR (Barberis *et al.*, 2008) and enhance spike discharge probability *via* GluK5-mediated metabotropic mechanisms (Sachidhanandam *et al.*, 2009).

KAR also mediate presynaptic effects at hippocampal mossy fibre synapses where they modulate local excitability and neurotransmitter release from boutons (Schmitz et al., 2000, Kullmann, 2001). As such, presynaptic kainate receptors are important in short-term plastic properties such as frequency-dependent facilitation of excitatory synaptic transmission (Schmitz *et al.*, 2001) and longer forms of plasticity including LTP (Bortolotto *et al.*, 2005). KARs may also play a role in the maturation of mossy fibre synapses during development (Marchal and Mulle, 2004).

To summarize, pre- and postsynaptic actions of KARs allow coordinated spike transmission between presynaptic terminals and postsynaptic neurones.

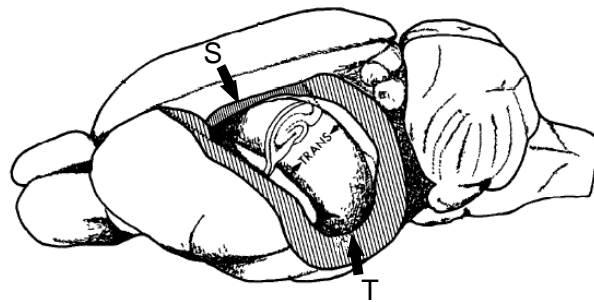
The electrophysiological study presented here was conducted in acute hippocampal slices from young adult rats. Below are presented some anatomical and physiological features of this region of the brain involved in learning, memory and spatial navigation tasks.

### **1.6. Anatomy of the hippocampus**

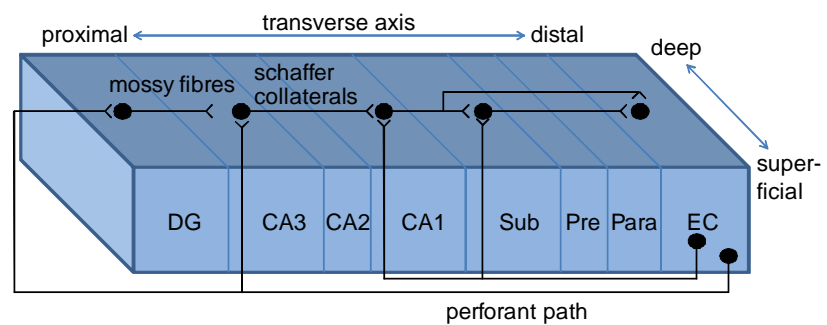
The hippocampus is a structure within the limbic system that displays a highly organized laminar distribution. The hippocampus plays a central role in both learning and memory and as such, has been widely reported and studied in the literature. The rat hippocampus differs markedly from that of the human brain, appearing as an elongated C-shaped structure with its long axis spanning rostro-dorsally from the septal nuclei near the midline of the brain through to caudo-ventrally behind the thalamus of the temporal lobe (Amaral and Witter, 1989). The long axis is also known as the septotemporal axis, whereas the transverse axis spans the width of the hippocampal formation as shown in Figure 9A.

The term “hippocampal formation” refers to six regions which are functionally connected in a uni- or bi-directional fashion: the dentate gyrus, regions of the *Cornus Amoni* (also termed the hippocampus) consisting of CA3, CA2 and CA1, the subiculum, the presubiculum, the parasubiculum and the entorhinal cortex (EC). The classic tri-synaptic hippocampal circuit is as follows: neurones located in the entorhinal cortex give rise to axons that project to the dentate gyrus. This projection is called the perforant pathway and it has two components: the medial and lateral perforant paths (Steward and Scoville, 1976). Moreover, it is unidirectional as the dentate gyrus does not project back to the entorhinal cortex. The mossy fibre pathway starts in the principal cells pertaining to the dentate gyrus or granule cells, which synapse onto CA3 pyramidal neurones *via* mossy fibre axons. The axons of CA3 pyramidal neurones or Schaffer collaterals then project to CA1 cells. The pattern of connectivity then becomes much more complicated as the CA1 region projects both to neurones in the subiculum and the entorhinal cortex.

A



B



C

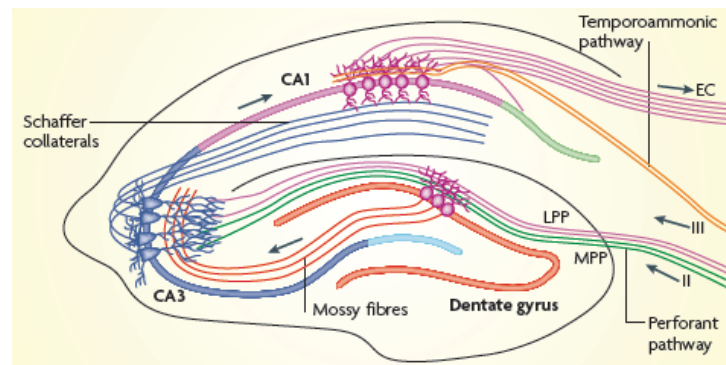


**Figure 9: Hippocampal organization of rodent brain and its anatomy** **A:** Anatomy of the rodent hippocampus with highlighted location of hippocampal formation (drawing adapted from (Amaral and Witter, 1989)). The septotemporal axis extends from the septal nuclei (S) towards the thalamus of the temporal lobe (T). **B:** The connectivity within rodent hippocampal formation (diagram adapted from (Andersen P, 2007a)). **C:** Illustration of the trisynaptic loop (Deng *et al.*, 2010).

### 1.6.1. The dentate gyrus

The dentate gyrus is a highly organised structure, which is comprised of three layers, with the closest to the hippocampal fissure being the relatively cell-free molecular layer (ML), the second known as the granule cell layer (GCL), also referred to as stratum granulosum (SG) and thirdly the polymorph layer, which

is also referred to as the hilus, where pyramidal basket cells, mossy cells and other interneurons reside (Amaral *et al.*, 2007). The GCL is packed with its principal cells- granule cells (GC) in a characteristic “U” or “V” shape and together with the ML is referred to as the *fascia dentata*.

#### 1.6.1.1. Dentate granule cells

There are approximately 1 million compactly packed GCs within the rat dentate gyrus (West *et al.*, 1991). GCs have small (10-18  $\mu\text{m}$ ) elliptical cell bodies that are arranged four to six cells thick in the GCL and a characteristic cone-shaped spiny dendritic trees, with all the branches directed superficially toward the ML (Claiborne *et al.*, 1990). GCs receive the main neocortical input from layer II neurones of the entorhinal cortex (minor input also comes from layer V, VI) *via* the perforant path (Figure 9C). GCs dendrites form characteristic trunks that span all the ML, where they receive synaptic connections from various sources depending on the location. As such, the outer and medial part of the ML receives input from the lateral and medial perforant pathway respectively; whereas the inner part receives its input from commissural/associational fibres. GCs only project to the CA3 region of the hippocampus. This exclusive projection is called the mossy fibre pathway (Blackstad *et al.*, 1970, Claiborne *et al.*, 1986). It is highly enriched in ionic zinc packaged with glutamate into presynaptic vesicles and can be visualised by processing hippocampal tissue with Timm’s staining (Figure 10).

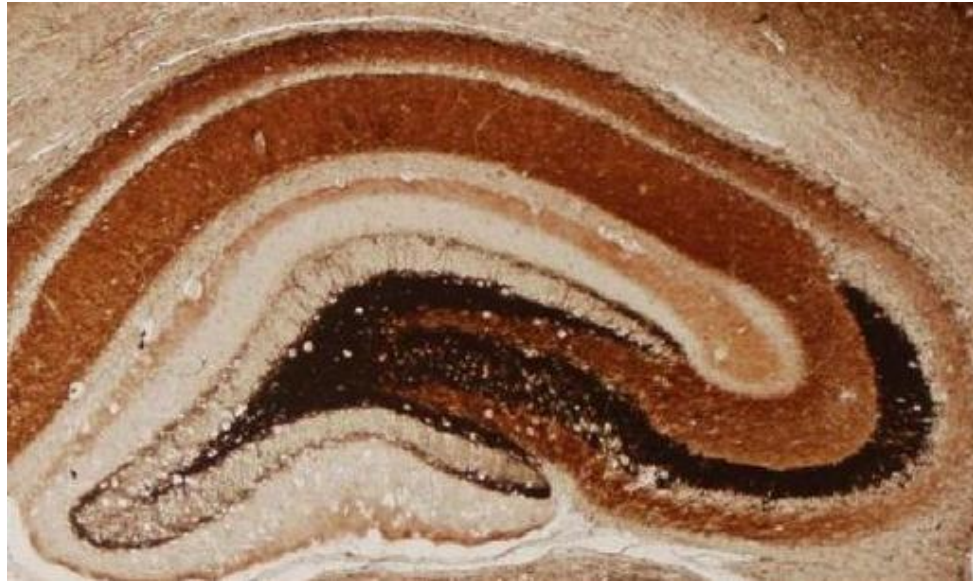


**Figure 10: Timm's staining reveals high zinc level in hippocampal granule cells**

Mossy fibres form giant synapses with a specialised spine or 'thorny excrescence' present in proximal dendrites of CA3 pyramidal cells (Figure 11).

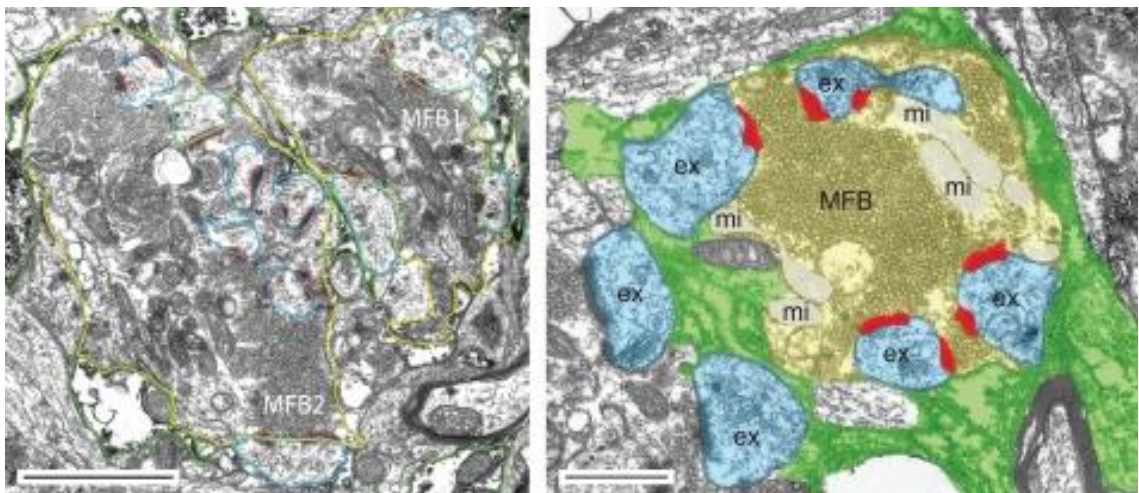


**Figure 11: The hippocampal mossy fibre bouton.** Low power electron microscopic images of mossy fibre boutons taken from an adult rat with the contour of spiny excrescences on the left highlighted in blue (scale bar: 2.5  $\mu\text{m}$ ) and magnified on the right (scale bar: 1  $\mu\text{m}$ ). Images taken from Rollenhagen and Lubke (Rollenhagen and Lubke, 2010).

However, their main targets are interneurons in the hilus and CA3 (Acsady *et al.*, 1998). For each GC, there is typically one mossy fibre that extends to the CA3 region. Mossy fibres innervate their main excitatory targets only sparsely with  $\sim 50$  synapses per CA3 cell (Amaral *et al.*, 1990). However within the hilus,

mossy fibres have been shown to branch extensively (Claiborne *et al.*, 1986). The axonal plexus of mossy fibres is refined to the hilus, although some fibres occasionally enter the GCL and terminate onto proximal dendrites of BCs. Recurrent excitation of GC dendrites by mossy fibre collaterals is observed very rarely in rodents compared to GCs in monkeys which extend basal dendrites into the hilus and are therefore innervated by mossy fibres more frequently (Austin and Buckmaster, 2004). Although mossy fibre projections are confined to the hilus and the SL in CA3 at their transverse axis, mossy fibres can travel up to 400 µm in their septotemporal plane (Acsady *et al.*, 1998).

Cajal (Cajal, 1909) recognized early in their studies of the mossy fibre system, that the terminals of mossy fibres are unique, as these axons possess more than one terminal. Electron microscopy studies have shown that mossy fibres possess three morphologically different terminals: the large mossy fibre boutons (MFBs), filopodial extensions of the mossy fibre terminals and small *en passant* synaptic varicosities (Claiborne *et al.*, 1986). MFBs terminate onto CA3 pyramidal cells within the SL, but are also present, albeit slightly smaller in size, within the hilus where they terminate onto mossy cell dendrites. Interestingly, the small varicosities considerably outnumber MFBs (160-200 small varicosities versus ~20 MFBs) and synapse onto dendrites of local interneurons within the SL or the hilus, showing that the main postsynaptic target of mossy fibres are in fact inhibitory cells (Acsady *et al.*, 1998). Using electron microscopy, the authors showed that the nature of the GABAergic postsynaptic targets was diverse, with some postsynaptic cells immunoreactive to parvalbumin, calretinin as well as the neuropeptide substance P. Using MFB – interneurone paired recordings, Szabadics and Soltesz (Szabadics and Soltesz, 2009) showed that mossy fibres targeted parvalbumin positive BCs and regular spiking BCs, as well as ivy cells and septum projecting spiny SL cells.

Mossy fibres are also immunoreactive for neuromodulators such as dynorphin and, as mentioned, Zn<sup>2+</sup>. Furthermore, mossy fibres show intense immunoreactivity for GABA (Sandler and Smith, 1991) and have also been reported to contain the GABA synthetic enzyme glutamate decarboxylase GAD67 (Schwarzer and Sperk, 1995). The finding that GABA can be released

at rat mossy fibre synapses following seizure-like activity raised the possibility that GABA release was only associated to a pathological condition (Gutierrez, 2000). However, the first electrophysiological evidence that GABA can be released from a subset of MFBs in normal animals came from studies in guinea-pig slices, and later in rats (Walker et al., 2001, Walker et al., 2002, Uchigashima et al., 2007). Studies in neonatal rats additionally showed mono-synaptic GABAergic signalling at the mossy fibre synapse in young animals (Bergersen et al., 2003, Safiulina et al., 2006). The subcellular distribution of  $Zn^{2+}$  and GABA immunogold particles have also been described (Ruiz *et al.*, 2004).

### 1.6.2. Hippocampus proper

It was De Garengeot's pioneering research into the structures of the brain who first coined the term for this region due to its similarity in shape to a ram's horn (Garengeot, 1742). He therefore named the hippocampus "*Cornu ammonis*" ("Ammon's horn") after the Egyptian god Amun Kneph, whose symbol was a ram (Andersen P, 2007a). Following De Garengeot's pioneering studies, the term - cornu ammonis to describe the hippocampus is no longer used, but remains the terminology of Lorente de Nó who described the subdivision of the hippocampus into three regions: CA1, CA2 and CA3, maintaining the link with the original name given by De Garengeot. Within the CA3 region five further layers can be distinguished (Figure 9). Their basic characterization is summarized below (Table 1).

Name of layer	Cellular neurophysiology
<b>Stratum lacunosum-moleculare</b>	<ul style="list-style-type: none"> <li>• Termination point of EC fibres</li> <li>• Contains interneurones</li> </ul>
<b>Stratum radiatum</b>	<b>Suprapyramidal region</b> <ul style="list-style-type: none"> <li>• CA3 to CA3 associational connections;</li> <li>• CA3 to CA1 Schaffer collateral connections;</li> <li>• Contains interneurones</li> </ul>
<b>Stratum lucidum</b>	<ul style="list-style-type: none"> <li>• Mossy fibres</li> <li>• Acellular</li> </ul>
<b>Stratum pyramidale</b>	<ul style="list-style-type: none"> <li>• pyramidal neurones</li> </ul>
<b>Stratum oriens</b>	<b>Infrapyramidale region</b> <ul style="list-style-type: none"> <li>• CA3 to CA3 associational connections;</li> <li>• CA3 to CA1 Schaffer collateral connections;</li> <li>• Contains interneurones.</li> </ul>

**Table 1: Layers of the hippocampus**

Each individual layer contains principal cells that are glutamatergic and interneurones that release GABA.

#### **1.6.2.1. Pyramidal cells**

The principal cellular layer is known as the pyramidal cell layer or *stratum pyramidale* and is packed with pyramidal neurones, usually three to six cells deep. PCs have shorter basal and longer apical dendrites that pervade the stratum oriens and hippocampal fissure respectively. The location of PCs within the hippocampus determines their size as well as their contribution in numerous synaptic pathways. By way of example, CA3 PCs are larger than those found in the CA1 region (Andersen P, 2007b).

#### **1.6.2.2. CA3 pyramidal cells**

The cellular body of PCs in the CA3 region varies greatly in size, with the smallest (20 µm in diameter) occupying the limbs of the DG and the largest (30

$\mu\text{m}$  in diameter), which can be found in the distal region (Ishizuka *et al.*, 1995). Similarly to the cell body region pattern, Ishizuka and others (Ishizuka *et al.*, 1995) found that dendritic length in the rat hippocampus fluctuated between 8-10 mm to 16-18 mm, depending on the proximity to the dentate gyrus and CA1 respectively. The apical dendrites of CA3 pyramidal cells span the stratum lucidum, stratum radiatum and stratum lacunosum-moleculare, making diverse synaptic connections as listed above (Table 1). Depending on the location of the soma of PCs, the distribution of their dendritic trees is also shown to vary. Basal and apical dendrites of CA3 PCs located in the limb region of CA3 receive a great number of mossy fibre connections from GCs and very little or few connections from the EC. Among pyramidal neurones in the hippocampus, only CA3 pyramidal neurones receive a mossy fibre input, thus electrophysiological recording presented in this thesis will be obtained from these. Noteworthy, CA3 pyramidal neurones project to other CA3 cells and this projection is called the associational/commissural pathway, depending if it is on the same (associational) or opposite (commissural) side of the brain (Ishizuka *et al.*, 1990).

#### **1.6.2.3. CA1 and CA2 pyramidal cells**

The CA1 region displays more anatomical homogeneity than that found in the CA3 region. Cell bodies of CA1 PCs are on average 15  $\mu\text{m}$  in diameter, whereas their average dendritic length is between 12-13 mm (Ishizuka *et al.*, 1995). Basal dendrites span the stratum oriens layer whereas apical dendrites occupy the stratum radiatum and stratum lacunosum-moleculare both in a conical fashion. CA1 pyramidal neurones receive excitatory synaptic inputs from axons of CA3 pyramidal neurones (Schaffer collaterals) and NMDA-dependant and long term potentiation at these CA3-CA1 synapses has been extensively studied (Bliss and Collingridge, 2013). Pyramidal cells, with size-like CA3 PCs are found in the CA2 region (Ishizuka *et al.*, 1995). Recently, Kohara and others discovered that CA2 pyramidal cells receive monosynaptic inputs from DG cells *via* longitudinal projection (Kohara *et al.*, 2014). Interestingly, CA2 pyramidal neurones proved to be more resistant to cell death caused by epilepsy when compared with other pyramidal neurones (Corsellis and Bruton, 1983).

## 1.7. Dentate – CA3 neurotransmission

### 1.7.1. Receptors and pharmacology

Dentate – CA3 transmission is initiated by action potentials in granule cells whose discharge at basal rates is less than 0.5 Hz triggering  $\text{Ca}^{2+}$  influx through various types of voltage-gated calcium channels (VGCCs) (Jung and McNaughton, 1993). Granule cells to CA3 synapses act as ‘conditional detonators.’ The term ‘conditional’ relates to the fact that in response to a single action potential, postsynaptic targets have a very low discharge probability *in vivo* (Henze *et al.*, 2002). Moreover, another *in vivo* study in awake rats showed that granule cells fire at low frequency and preferentially in bursts. As such, low frequency of spiking combined with a high proportion of bursts should lead to the maximum facilitation at mossy fibre synapses (Pernia-Andrade and Jonas, 2014). Transmission at mossy fibre synapses is regulated by several neurotransmitters and neuromodulators. In addition, mossy fibre synaptic transmission is regulated by various metabotropic glutamate receptors localized both on pre- and postsynaptic mossy fibre bouton membranes (Henze *et al.*, 2000). Immunohistochemical studies have also revealed groups II and III mGluRs in large mossy fibre boutons (Shigemoto *et al.*, 1997) consistent with the effect of group II mGluR agonists such as (2S,2'R,3'R)-2-(2',3'-dicarboxycyclopropyl)glycine (DCG-IV), which block transmission at mossy fibre synapses in both rats and guinea pigs (Kamiya *et al.*, 1996, Yoshino *et al.*, 1996). Other studies have shown that activation of mGluRs at mossy fibre synapses by endogenous glutamate is followed by inhibition of glutamate release (Vogt and Nicoll, 1999). At mossy fibre synapses onto stratum lucidum inhibitory interneurons, both calcium-permeable (CP) and calcium-impermeable (CI) AMPA receptors can be found (Toth and McBain, 1998), whereas mossy fibre synapses onto CA3 pyramidal cell contain only CI-AMPA receptors (Toth *et al.*, 2000). Finally, in a recent study (Berg *et al.*, 2013), it was shown that the majority of subunits are found at the postsynaptic site with GluN1, GluN2B,D and GluN3B exceptionally having a presynaptic locus.

The relative large size of giant MFBs (~ 4-10  $\mu\text{m}$ ) enables direct patch-clamping of the terminal and thus the study of presynaptic action potential modulation by

voltage-activated channels including presynaptic Na<sup>+</sup> channels (Engel and Jonas, 2005) and Ca<sup>2+</sup> channels (Geiger and Jonas, 2000, Bischofberger *et al.*, 2006). Mossy fibre bouton recordings have also shed light on the role of presynaptic ionotropic receptors such as GABA<sub>A</sub> receptors or glycine receptors (Ruiz and Kullmann, 2012). It was shown that P/Q-type and N-type VGCCs are mainly expressed at the bouton membrane to ensure the efficient and precisely timed Ca<sup>2+</sup> influx at MFBs (Bischofberger *et al.*, 2002, Li *et al.*, 2007, Alle *et al.*, 2011). Other than Ca<sup>2+</sup> channels, inactivation of a voltage-gated K<sup>+</sup> conductance such as that mediated by Kv1.1 prolongs the action potential duration by up to 3-fold during high frequency stimulation. Such activity-dependent prolongation of the presynaptic AP waveform causes an increase of Ca<sup>2+</sup> influx in mossy fibre boutons, which in turn enhances neurotransmitter release (Geiger and Jonas, 2000).

### **1.7.2. Plasticity of giant mossy fibre synapses**

Hippocampal mossy fibre synapses onto CA3 pyramidal cells represent a highly unique excitatory pathway at CNS synapses with pronounced short-term facilitation and an NMDA-receptor independent presynaptic mechanism of LTP. Mossy fibre synapses also undergo a form of long-term depression (LTD), which is independent of NMDARs, mGluRs or cannabinoid receptors activation (Lei *et al.*, 2003).

#### **1.7.2.1. Short term plasticity**

It has been postulated that mossy fibre synapses act as “conditional detonators” (Henze *et al.*, 2002). Activation of mossy fibre synapses *in vivo* can trigger action potentials in postsynaptic targets in response to a brief train of presynaptic activity (>40 Hz). Mossy fibre synapses express two unique forms of short-term plasticity that facilitate temporal signal integration in CA3 pyramidal neurones: paired-pulse facilitation and frequency dependent facilitation. These two forms of plasticity enhance synaptic transmission enormously and can generate spikes in CA3 cells when modest increases in presynaptic frequency firing occur, even at relatively low frequencies. MF-CA3 synapses exhibit very high levels of paired pulse facilitation (PPF)- a phenomenon in which excitatory postsynaptic potentials (EPSPs) evoked by an

impulse are increased when that impulse closely follows a prior impulse (Salin 1996). In addition, a specific property of mossy fibre-CA3 synapses is the ability to undergo frequency-dependant facilitation, meaning that modest increases of presynaptic activity cause large increments in the amplitude of postsynaptic responses, thus leading to a growth in synaptic strength. The mechanisms responsible for this unusual property of dentate-CA3 transmission are not fully elucidated. Residual  $\text{Ca}^{2+}$  levels in the presynaptic terminal as well as  $\text{Ca}^{2+}$  released from intracellular calcium stores are reported to play a role (Liang et al., 2002, Scott and Rusakov, 2006, Lauri et al., 2003). Other mechanisms, dependent on  $\text{Ca}^{2+}$ /calmodulin protein kinase II activity, have also been reported. In contrast, associational-commissural synapses show little or no degree of facilitation (Salin *et al.*, 1996). Finally, the partial occlusion of frequency-dependent facilitation by the induction of LTP suggests a mechanistic link between short- and long-term potentiation at mossy fibre synapses.

#### 1.7.2.2. Long term plasticity

Hebb's postulate (Hebb, 1949) describes the basis of strengthening synaptic plasticity as a result of presynaptic stimulation of the postsynaptic cell. Such an enhancement in signal transmission between two neurones can cause a long lasting change in synaptic plasticity called long term potentiation. Repetitive stimulation induces synaptic plasticity in Schaffer collateral-CA1 and MF-CA3 synapses. In contrast to LTP at Schaffer collateral-CA1 synapses, LTP at MF-CA3 synapses has been found to be NMDA-receptor independent (Harris and Cotman, 1986). There is evidence for the involvement of presynaptic  $\text{Ca}^{2+}$ -induced  $\text{Ca}^{2+}$  release (Lauri *et al.*, 2003) and that mGluR as well as ionotropic receptors, including  $\text{GABA}_A$  and kainate receptors, have a modulatory role on LTP but are not essential for its induction (Schmitz *et al.*, 2003, Ruiz *et al.*, 2010). Two forms of NMDAR-independent mossy fibre LTP are determined by the nature of the stimulus induction paradigm. The first one is non-Hebbian in nature and exclusively dependant on changes in the presynaptic membrane potential and presynaptic firing rate. The second implies that mossy fibre LTP induction is Hebbian and requires both pre- and postsynaptic activity. Thus, the nature of mossy fibre LTP is defined by the type of protocol used for the induction. As such, low lasting high frequency stimulation L-HFS (3x100 Hz for 1 s) protocol

induces LTP despite postsynaptic hyperpolarization, whereas brief high frequency stimulation B-HFS (8x100 Hz for 0.1 s) requires depolarization of CA3 pyramidal neurones and presynaptic activation of mossy fibres (Henze *et al.*, 2000). Yeckel and others showed that postsynaptic calcium elevation enables the induction of mossy fibre LTP, despite the protocol used (Yeckel *et al.*, 1999). In case of L-HFS induced LTP, it is associated with postsynaptic release of calcium from intracellular stores, whilst the B-HFS induced form of mossy fibre LTP is concerted *via* the calcium influx *via* L-type calcium channels by postsynaptic depolarization (Kapur *et al.*, 1998, Yeckel *et al.*, 1999). Other studies have shown that (Huang *et al.*, 1994, Yeckel *et al.*, 1999) mossy fibre LTP is linked to cAMP-signalling cascades, whereas the presynaptic (L-HFS protocol) or postsynaptic (B-HFS protocol)  $Ca^{2+}$  influx activates a cAMP cascade pre- or post-synaptically respectively (Henze *et al.*, 2000). The involvement of KAR in the induction of mossy fibre LTP has been investigated across pharmacological and mouse knockout studies. Again, their effect has been a subject of disagreement, but as summarized by Nicoll and Schmitz KAR are generally not essential for the induction of mossy fibre LTP (Nicoll and Schmitz, 2005). Contrary to its induction, expression of LTP is more unified and dominated by a presynaptic mechanism *via* an increase in the probability of neurotransmitter release (Zalutsky and Nicoll, 1990, Nicoll and Malenka, 1995, Tong *et al.*, 1996). Recently, Wiera and co-workers (Wiera *et al.*, 2013) suggested that LTP expression in MF-CA3 synapse could be tuned by the activity of MMP-9, a member of the metalloproteinase family. Interestingly, a recent study indicates the existence of NMDAR-dependent metaplasticity at mossy fibre synapses, in which NMDARs act as a switch to generate LTP, which is expressed and maintained by the presence of an increased number of active AMPA receptors at potentiated synapses (Rebola *et al.*, 2011).

## **2.0. Project Objectives**

## 2.0. Project Objectives

Diseases associated with memory impairment affect an increasing number of patients as a result of the increasing age profile of many societies. As such, there is an urgent and pressing need to develop new therapeutics to improve and ultimately restore patients' cognitive function. Current medicines have shown limited therapeutic effect and this research was designed to address this deficit. In this project we elected to take inspiration from Nature, where a small molecule natural product – clausenamide (**2**), was shown to have potent neuroprotective and memory enhancing effects. Clausenamide (**2**) contains four contiguous chiral centers and despite the work of Feng and co-workers (Feng *et al.*, 2009) into the determination of which enantiomer is most active, the search for synthetically tractable analogues remains a viable challenge due to the difficulty in obtaining sufficient amounts of the parent compound and the relatively complicated and generally low yielding syntheses in the literature.

The overall aim of this research is therefore to develop novel synthetic methodology to access the core structure of clausenamide and to investigate the effects of our synthetic analogues in neuronal slices to develop a small molecule that could enhance or restore memory to meet the challenge of our ageing society. Clausenamide (**2**) and its related congener - kainic acid (**94**) are potent small molecules that can regulate synaptic function and as such, have key implications in a range of CNS disorders. Heterocycles related to these compounds, have therefore frequently been used as synthetic building blocks in approaches towards both natural products and related analogues and are of significant importance to the pharmaceutical industry. Examples of molecules from this class of compound are outlined below (Figure 12).

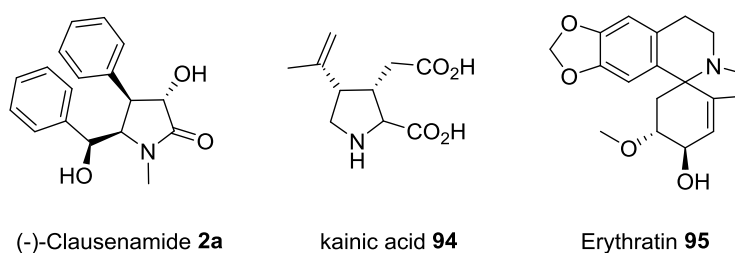


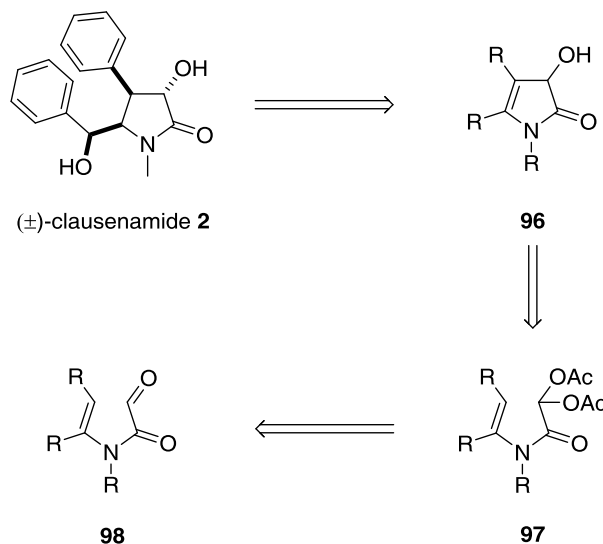
**Figure 12: Pyrrolidine core containing compounds**

As a result of the synthetic diversity and potent biological activities of these molecules, there have been numerous reported approaches towards the core structures. Despite these, most rely on linear synthetic methodology resulting in numerous steps rendering them unattractive for the generation of small molecular libraries. Tandem or domino synthetic processes using a modular approach are accordingly highly attractive, as they reduce the overall number of linear steps and result in the formation of several bonds in one transformation.

## 2.1. Synthetic Chemistry

As stated above, we intend to synthesise the core structure of clausenamide (**2**), but we envisage that any synthetic approach to its synthetic core should be flexible enough in order to synthesise structurally related analogues such as kainic acid as part of a longer-term program.

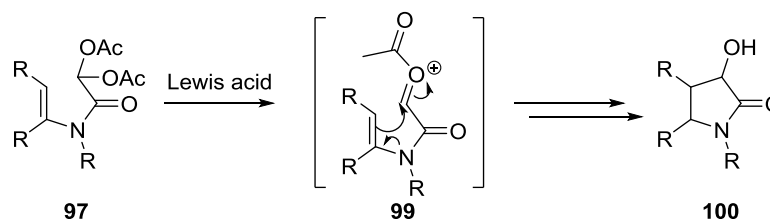
As outlined in the introduction there have been a number of approaches towards the formation of clausenamide but most require harsh conditions for their syntheses. Our retrosynthetic approach towards formation of the 5-membered pyrrolidine core of clausenamide **2** is outlined below (Scheme 11).



**Scheme 11: Retrosynthetic approach towards the pyrrolidine core**

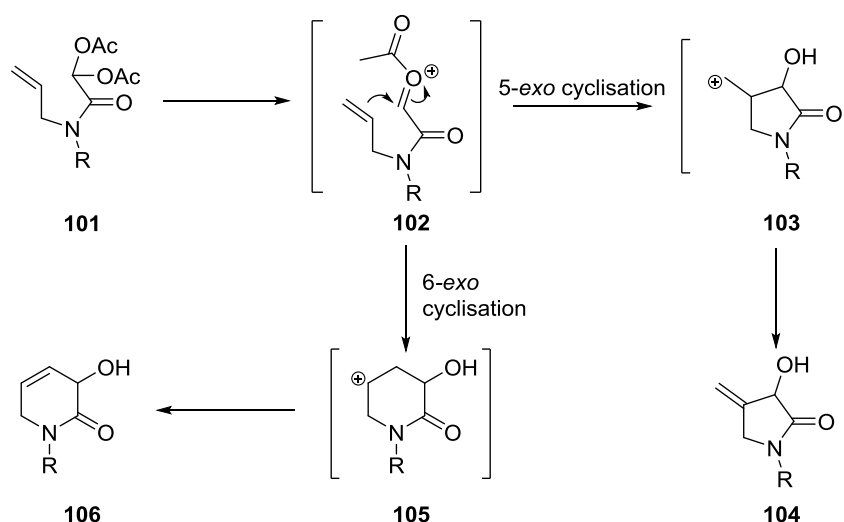
We envisage that the key C3-C4 carbon-carbon bond of the pyrrolidine ring can be formed *via* an ene-type intramolecular Acylal Cyclisation reaction (IAC), where the electron-rich enamine part of the molecule reacts with the electron deficient glyoxamide synthon. There are few reports in the literature on

protected glyoxals, but a recent report on the synthesis of epidithiodiketopiperazines outlined the utility of diacetoxyacetyl chloride as a synthon for glyoxylic acid chloride. The aldehyde is protected as its more stable form of an acylal. Accordingly we anticipated that reaction of the acylal **98** with a Lewis acid should lead to formation of an oxonium ion **99**, which will react with the enamine already present in the molecule leading to cyclisation to form the pyrrolidine ring **100** (Scheme 12).



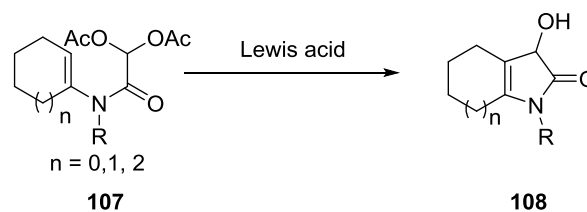
**Scheme 12: Formation of the oxonium ion and cyclisation**

In order to explore the synthetic scope of the reaction, we intend to initially carry out a number of cyclisation reactions with the structurally simple alkene **101** with a range of Lewis acids and proton sources to determine the requisite conditions for cyclisation. It is anticipated that this precursor will potentially generate the 6-membered piperidinone ring **106** as the intermediate secondary carbocation **105** is more stable than the primary **103** (Scheme 13).



**Scheme 13: Generation of the 5/6-membered ring**

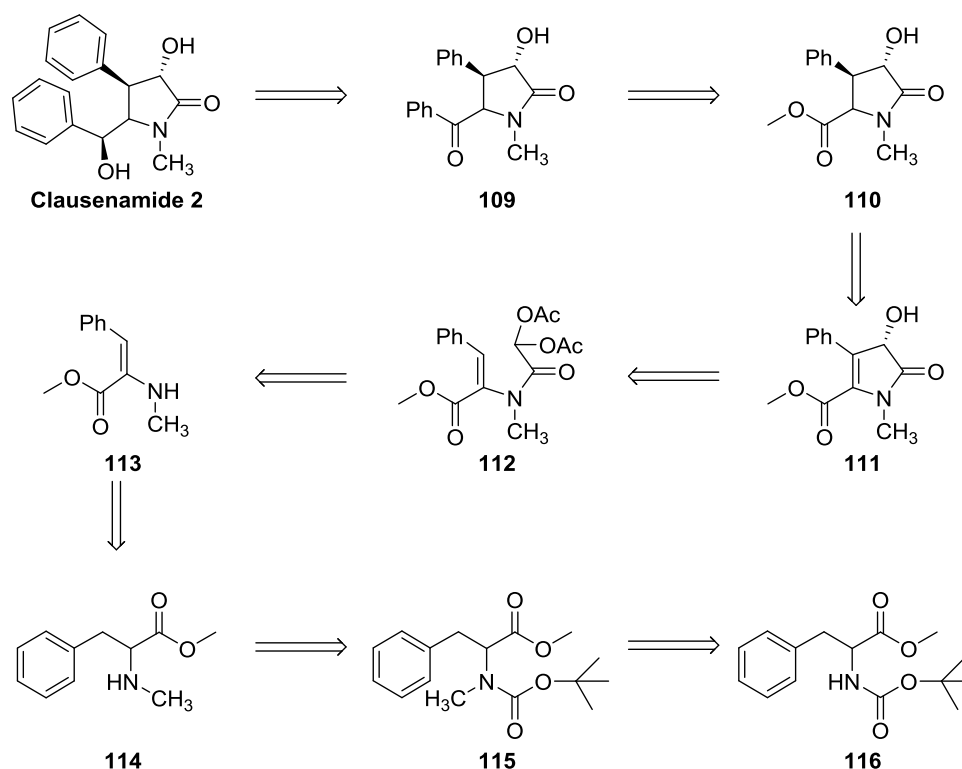
Once we have determined which Lewis acid to employ in the cyclisation reactions, we will extend the cyclisation reaction towards specific formation of the pyrrolidinone ring **108** starting from the enamide **107** (Scheme 14)



**Scheme 14: Cyclisation reactions with Lewis acids**

The cyclisation precursor enamides can readily be obtained *via* reaction of the enamine with diacetoxyacetyl chloride. We anticipate that the enamines themselves will be synthesised *via* condensation of an amine with the corresponding ketone under Dean-Stark water removal conditions.

Following the successful outcome of the cyclisation reactions, we intend to apply the knowledge that we have gained in an approach towards the synthesis of the natural product clausenamide. Our retrosynthetic approach to this is outlined below (Scheme 15).



**Scheme 15: Retrosynthetic approach to clausenamide**

It will be necessary to synthesise the phenylalanine derived dehydroamino acid **113** in order to synthesise our desired cyclisation precursor. However, this should readily be achieved *via* *N*-halogenation and elimination as per the work by (Lu and Lewin, 1998). Reduction of the double bond in **111**, will enable us to achieve a formal total synthesis of clausenamide **2** as the subsequent steps have previously been reported.

## 2.2. Biological Objectives

In order to investigate the biological activity of the synthetic compounds that will be synthesised from the first phase of this research program, their effects on synaptic transmission and plasticity will be explored using electrophysiology. In order to achieve this goal, an investigation of their effects in acute rat hippocampal slices as per previous endeavours by other researchers in this field will be conducted, who have investigated a number of AMPA modulators in this manner.

Key to progressing any compound towards further investigation is its activity. We intend to look for an enhancement of synaptic transmission and plasticity from our analogues, as (-)-clausenamide has been shown to have such an enhancing effect. However, in order to demonstrate this and to obtain a more in-depth analysis of activity and elucidation of the hitherto unqualified mechanism of action, we will perform the following sequence of experiments with our analogues.

One of the key weaknesses with the research that has been carried out on clausenamide and its enantiomers has been the lack of a clearly described mechanistic target. In order to try to elucidate this and to provide a more in-depth analysis, we will explore basal synaptic transmission at a major hippocampal input in the brain to determine whether the enhancing effects of compounds related to clausenamide occur *via* a pre- or post-synaptic mechanism. To achieve this, we will focus on mossy fibre to CA3 synapses as they are one of the major inputs into the hippocampus and can provide information with regard to the mechanism of action of our compounds at the synaptic level.

In the first instance, we intend to explore whether our compounds have any activity on mossy fibre to CA3 synapses by investigating evoked postsynaptic responses. Once compounds have shown activity, we will compare their effect against the well known memory enhancing compound – piracetam, in order to have a standard against which to compare. We will focus on piracetam as our major comparator as it has been the mainstay of memory deficit disorder

treatments for over 50 years and most studies compare the activities of new compounds against this key cornerstone of treatment.

Following demonstration of an enhancing effect, compounds will be investigated for their exact mechanism of action at the synaptic level. We will focus on the three main receptors – NMDA, AMPA and kainate and *via* a combination of stimulation and chemical blocking agents, explore the exact target of our compounds. We will also focus on whether our molecules work *via* a pre- or postsynaptic mechanism.

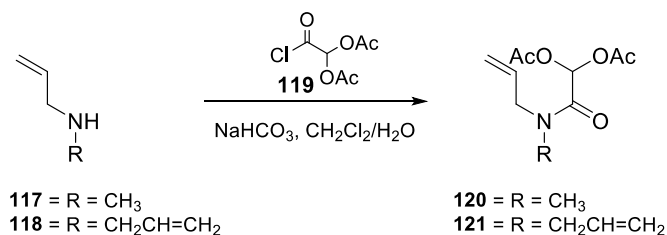
As part of our research focuses on potential chiral analogues of clausenamidine, we will also explore the activity of each enantiomer if time permits.

## **3.0. Results and Discussion**

### 3.0. Results and Discussion

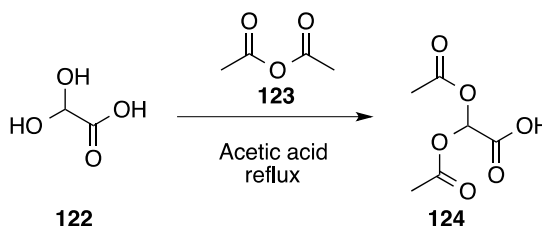
#### 3.1. Initial cyclisations

As outlined in the objectives, we decided to first investigate the effects of a number of acids on the cyclisation of *N*-allyldiacetoxglyoxamides to determine the requisite conditions for cyclisation. To this end, we decided to synthesise precursors **120** and **121** via reaction of commercially available amines **117** and **118** with diacetoxyl chloride **119** under Schotten-Bauman conditions (Scheme 16).



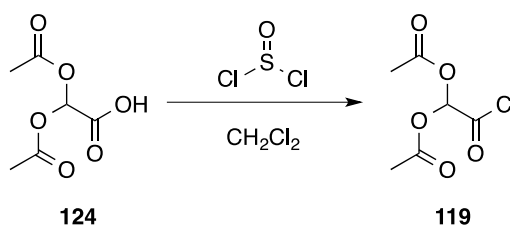
#### Scheme 16: Formation of cyclisation precursors

However this necessitated synthesis of the non-commercially available acid chloride **119** as a key component in our reactions. As such, we required sufficient amounts of diacetoxyl chloride **119** in order to allow us to investigate the proposed cyclisation reactions. The published two-step synthetic route to diacetoxyl chloride **119** involved reaction of acetic anhydride **123** with acetic acid and glyoxylic acid monohydrate **122** at 150 °C (Scheme 17) to give intermediate **124**.



#### Scheme 17: Formation of diacetoxyl chloride

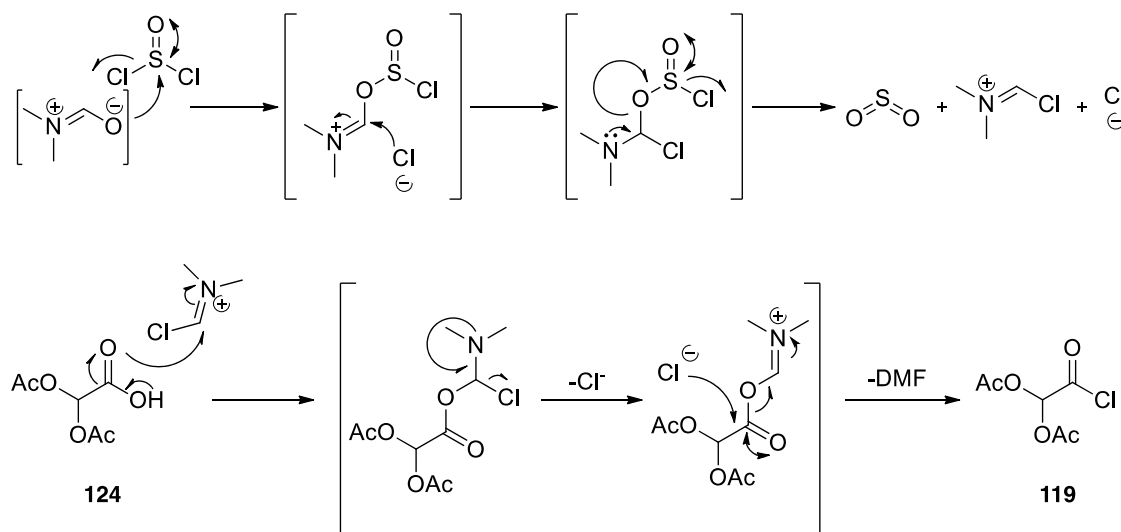
The second step requires addition of thionyl chloride to the crude compound, whereupon the reaction is heated under reflux and the product thus obtained, purified by distillation (Scheme 18).



**Scheme 18: Synthesis of diacetoxyacetyl chloride**

However, in our hands, diacetoxyacetyl chloride **119** could only be obtained in low yield (<23%) and furthermore, analysis of the crude material prior to distillation showed that considerable amounts of intermediate **124** were still present.

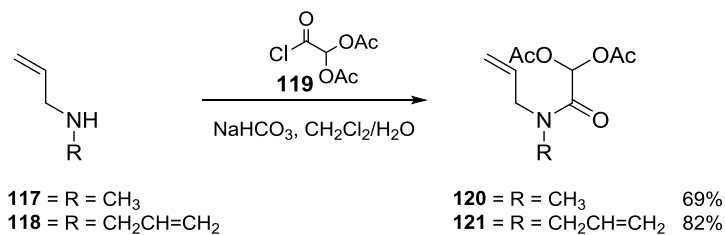
In order to improve the yield and to convert more of the starting material to the acid chloride, we added dimethylformamide as a reaction catalyst, which can promote the reaction towards completion as shown below (Scheme 19).



**Scheme 19: DMF catalysis of diacetoxyacetyl chloride synthesis**

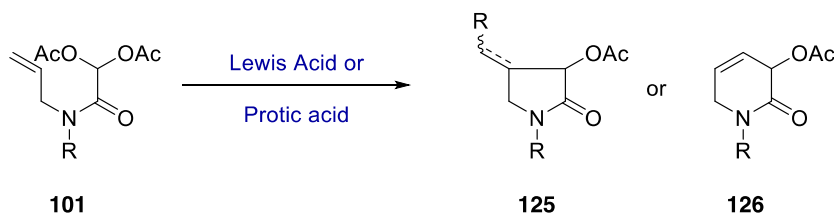
The reaction was monitored by  $^1\text{H}$  NMR spectroscopy to ensure complete conversion to the acid chloride and once complete, distillation of the crude mixture led to the required diacetoxyacetyl chloride **119** in a much improved yield of 75% (Scheme 19).

Following obtention of the acid chloride **119**, precursors **120** and **121** were obtained in 69% and 82% yield respectively following reaction of amines **117** and **118** with diacetoxyacetyl chloride **119** (Scheme 20).



### Scheme 20: Formation of cyclisation precursors 120 and 121

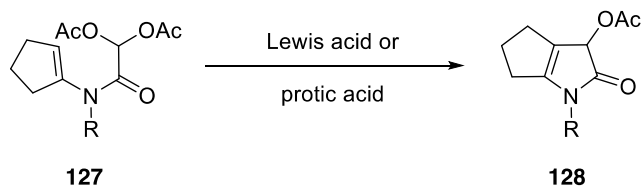
With both cyclisation precursors **120** and **121** in hand, we next turned our attention towards the intramolecular cyclisation reactions. As the acylal's were stable even on prolonged heating, we decided to investigate the effects of addition of a range of acid sources to these compounds to determine the degree of cyclisation (Scheme 21).



### Scheme 21: Proposed cyclisation outcomes

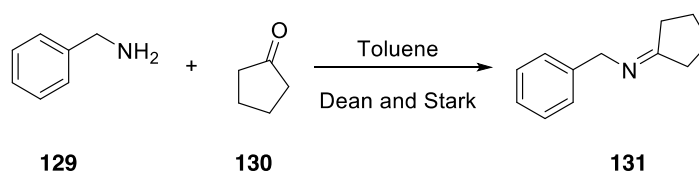
Initial experiments were carried out with varying amounts of trifluoroacetic acid in dichloromethane as a solvent both at room temperature and at reflux. Surprisingly, we observed that the acylal precursors proved to be relatively stable species and in all cases, starting material was recovered. Indeed, only on prolonged heating (>72 hours) could any loss of starting material be observed. Accordingly we next investigated the effect of hydrobromic acid and hydrochloric acid in a range of solvents such as dichloromethane, water and methanol. Such attempts led to the degradation of the starting material with unidentifiable complex product mixtures being observed in all cases.

As a result of the complex product mixtures observed, it was evident that to gain useful insight into the requisite conditions, we required an alternative cyclisation precursor that would provide unambiguous information. We then, turned our attention towards the following cyclopentenyl cyclisation precursor **127**. We anticipated that cyclisation of the enamine would lead to formation of the pyrrolidinone ring **128** (Scheme 22).



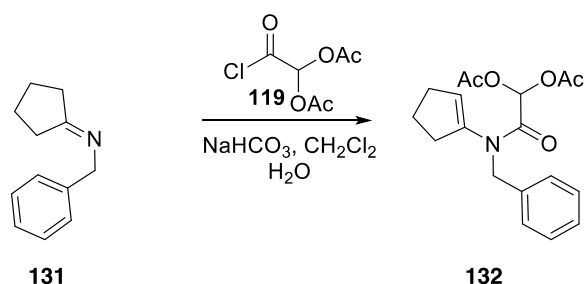
**Scheme 22: Cyclisation of the enamine**

In order to synthesise the precursor **127** we decided to first generate the imine/enamine **131** *via* condensation of benzylamine **129** with cyclopentanone **130** under Dean-Stark water removal conditions (Scheme 23). Due to the unstable nature of the imine/enamine **131**, we decided to react it with diacetoxyacetyl chloride **119** without further purification or characterisation.



**Scheme 23: Generation of the imine**

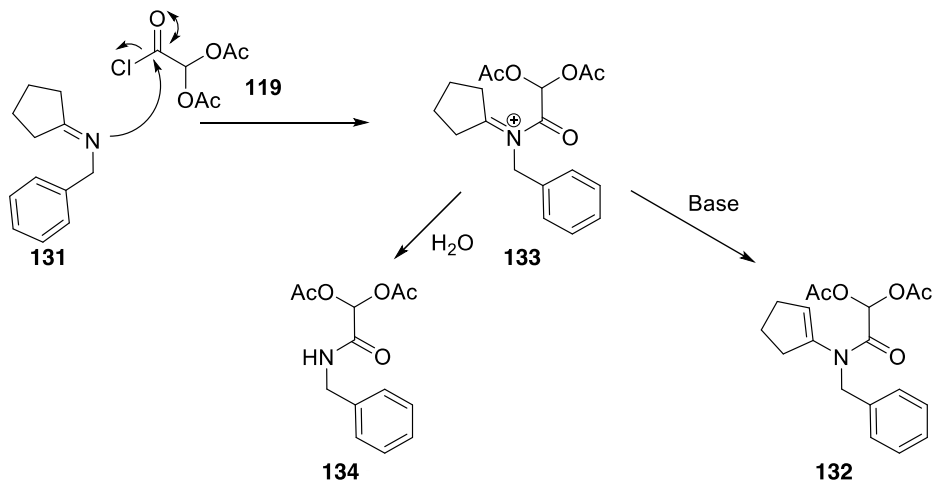
Reaction of the intermediate imine **131** with diacetoxyacetyl chloride **119**, under Schotten-Bauman conditions using a biphasic mixture of water and dichloromethane (DCM) in the presence of sodium bicarbonate gave the cyclisation precursor **132** in a reasonable yield of 46% (Scheme 24).



**Scheme 24: General reaction for formation of cyclisation precursors**

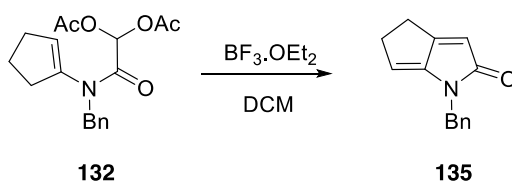
This reaction occurs *via* nucleophilic attack of the amine on the carbonyl of diacetoxyacetyl chloride **119**. The amine breaks the oxygen double bond, leading to loss of chloride and reformation of the carbonyl (Scheme 25). However, in using the Schotten-Bauman conditions, water can also act as a

nucleophile and can therefore lead to isolation of the by-product **134**. The yield of the two products is presumably a reflection of the rate of reaction and relative ratio between the imine and enamine intermediate.



**Scheme 25: Formation of the cyclisation precursor and by-product**

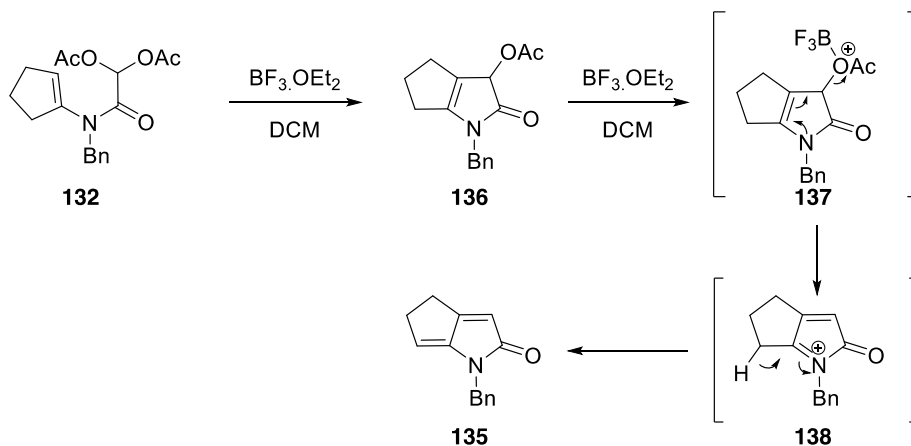
Following purification by column chromatography and verification of the structure, we next turned our attention to cyclisation of the substrate **132**. Due to the implied failure of the preceding use of protic acids, we decided to first investigate the use of Lewis acids in the cyclisation. As Lewis acid, we chose boron trifluoride diethyl etherate due to its utility in a plethora of reported cyclisation reactions and its mild nature (Scheme 26).



**Scheme 26: Cyclisation reaction with boron trifluoride dietherate**

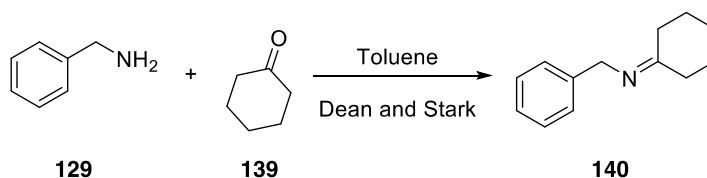
Cyclisation precursor **132** was reacted with boron trifluoride dietherate in dichloromethane at reflux for 6 hours. However, on analysis of the crude  $^1\text{H}$  NMR spectrum following work-up we were surprised to observe that the final product wasn't the acetate that we had predicted, but was instead diene **135**, which was obtained in 67% yield.

Presumably on reformation of the enamine **136** after initial cyclisation and further exposure to Lewis acid, the acetate is again activated and eliminated to give the intermediate iminium ion **137**, which loses a proton to generate the observed product **135** (Scheme 27).



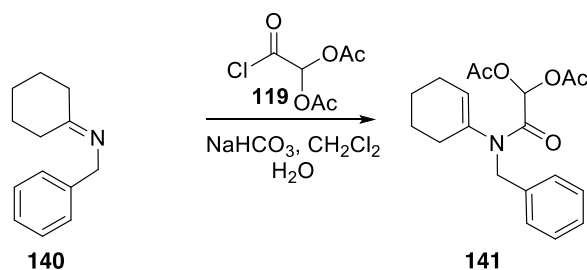
**Scheme 27: Reformation of the enamine**

As a result of this unusual reaction, we decided to determine if the same reaction would occur with six or seven membered ring precursors. We centered our attentions on six membered rings as they are important molecular building blocks for more complex molecules. The reactions utilized the same procedure as the previous reaction. Therefore to obtain the six membered ring attached to the amine we reacted benzylamine **129** with cyclohexanone **139** in order to generate the analogous *N*-cyclohexylidene-1-phenylmethanamine **140** (Scheme 28).



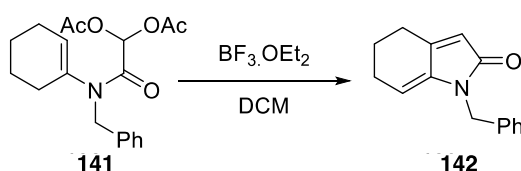
**Scheme 28: Formation of *N*-cyclohexylidene-1-phenylmethanamine**

Formation of the cyclisation precursor 2-(benzyl(cyclohexenyl)amino)-2-oxoethane-1,1-diyl diacetate **141** proceed smoothly under the Schotten-Bauman conditions used previously (Scheme 29).



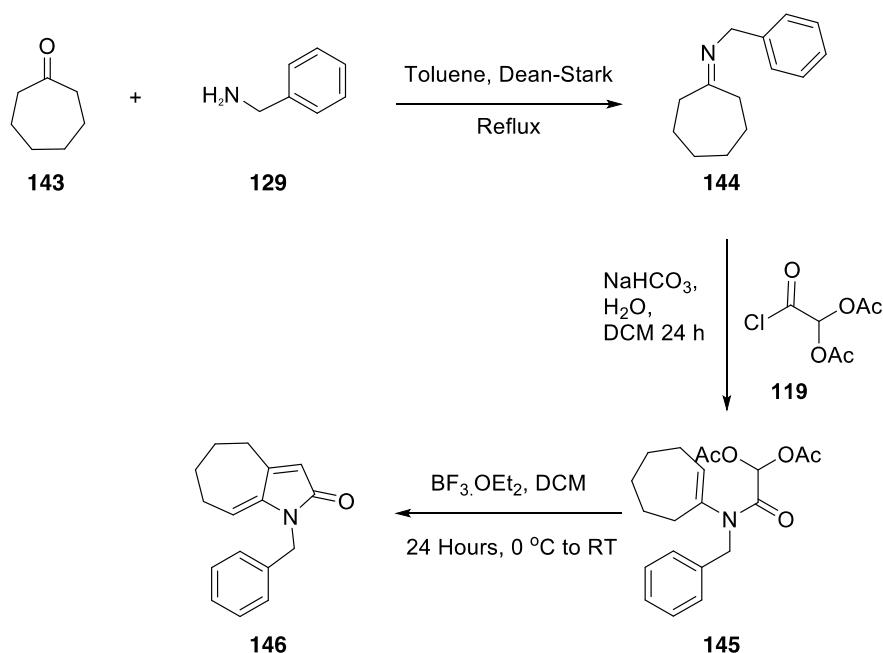
### Scheme 29: Formation of the cyclohexene cyclisation precursor

Cyclisation of **141** was important as it could correlate with the previous cyclisation outcome observed for the pentenyl precursor **132** which had led to formation of the conjugated dienone **135** (Scheme 30). Following purification, pleasingly the <sup>1</sup>H NMR spectrum confirmed the presence of the desired molecule **142** in 38% yield.



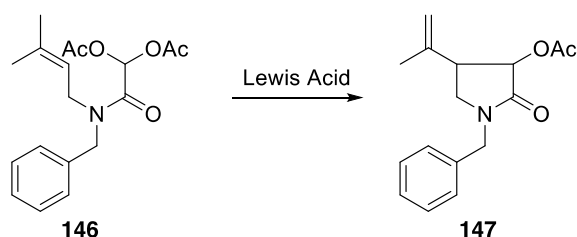
### Scheme 30: Formation of the fused six-five membered ring system

The same approach was taken in the formation of the seven membered ring building block, with analogous synthetic steps to obtain precursor **142**. Due to the ease of elimination, we conducted the final cyclisation reaction at room temperature to try to obtain the intermediate alcohol, but still obtained the diene **146** in 31% yield (Scheme 31).



**Scheme 31: Pathway to the formation of seven membered ring**

Due to the reactive nature of the enamines in the above cyclisations, we decided to synthesise a cyclisation precursor that would not lead to elimination of the intermediate acetate. The planned cyclisation precursor is outlined below (Scheme 32).



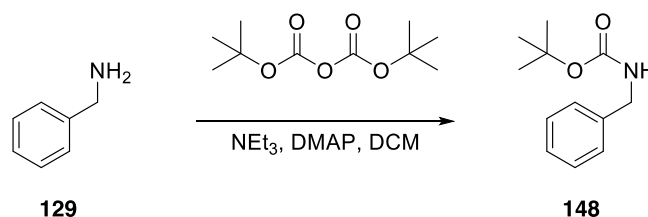
**Scheme 32: Cyclisation with the presence of the intermediate acetate**

Thus on cyclisation we should obtain the exclusive 5-exo cyclised product **147** with reduced possibility of elimination of the second acetate group. The molecule is reminiscent of our initial precursor, with the one difference being the presence of the two methyl groups on the alkene. This will therefore obviate formation of the piperidine ring and give exclusive formation of the pyrrolidine ring.

In order to obtain the precursor **147**, we needed to synthesise *N*-benzyl-3-methylbut-2-en-1-amine. However benzylamine **126** is a less nucleophilic

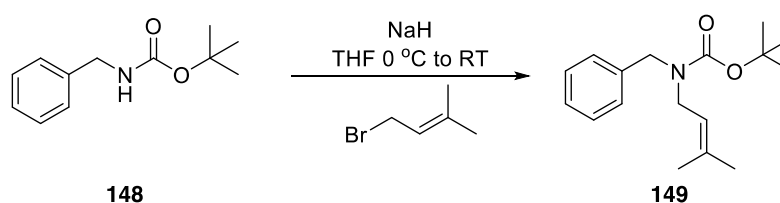
species than the corresponding secondary amine and as such, simple alkylation with the corresponding bromide would have led to complex mixtures of alkylated amines.

Thus it was first necessary to protect benzylamine **126** with di-*tert*-butyl dicarbonate thereby facilitating facile single alkylation with 1-bromo-3-methyl-2-butene to reduce the formation of complex mixtures (Scheme 33).



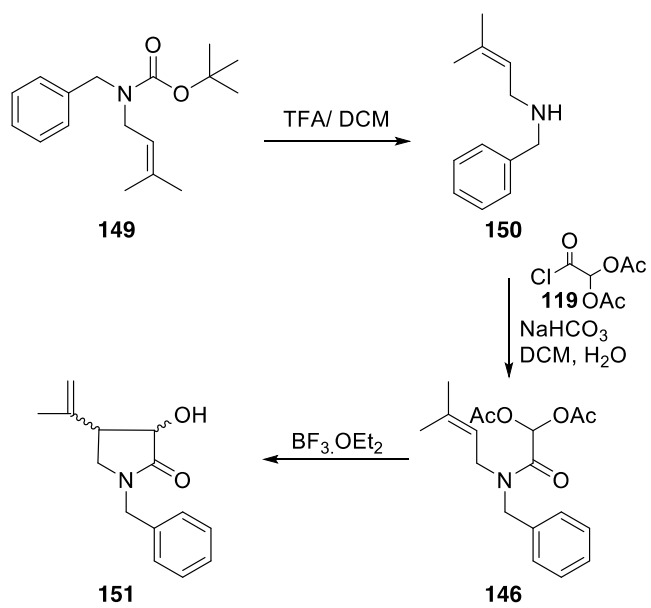
**Scheme 33: Reaction to form Boc protected benzylamine**

The reaction is possible solely with triethylamine and di-*tert*-butyl dicarbonate in DCM. However, the reaction proceeds slowly. Therefore addition of the nucleophilic catalyst 4-*N,N*-dimethylaminopyridine (DMAP) results in an increase of the rate of reaction due to formation of the more reactive acylating species. Finally reaction of protected benzylamine **148** with 1-bromo-3-methyl-2-butene gave **149** in 49% yield (Scheme 34).



**Scheme 34: Formation of protected amine with 3-methyl-2-butene substituent**

Efficient deprotection with trifluoroacetic acid in dichloromethane gave amine **150** as the free base in excellent yield after basic work-up. Amine **150** was acylated under Schotten-Bauman conditions to provide the diacetoxy amide **146** in 62% yield. However, cyclisation *via* addition of the Lewis acid boron trifluoride diethyl etherate gave an inseparable mixture of diastereoisomers in 93% yield (Scheme 35) but still provided proof that the original concept was successful.



**Scheme 35: Pathway to formation of 5-exo-cyclised product**

### 3.2. Synthetic approach towards clausenamide

Following the successful testing of the intramolecular acyl cyclisations we next turned our attention towards the synthesis of the natural product clausenamide. To demonstrate the potential of this methodology, we decided to attempt the synthesis of clausenamide **2** as it contains the hydroxypyrrolidinone architecture that would be ideal to exemplify our methodology (Figure 13).

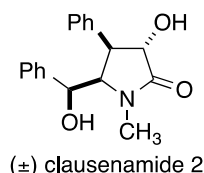
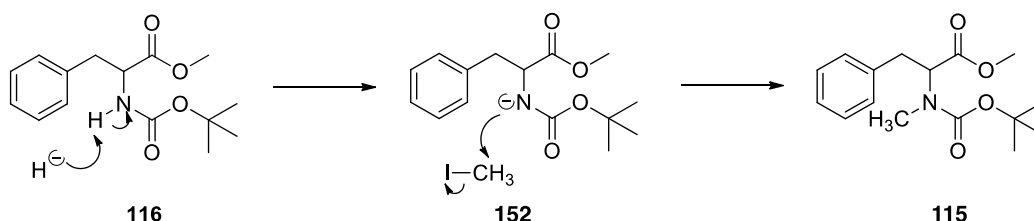


**Figure 13: (±)-Clausenamide**

The first step in our synthetic sequence towards clausenamide as outlined in the project objectives, was to introduce a methyl group on the nitrogen atom of previously Boc protected phenylalanine as outlined below (Scheme 36).

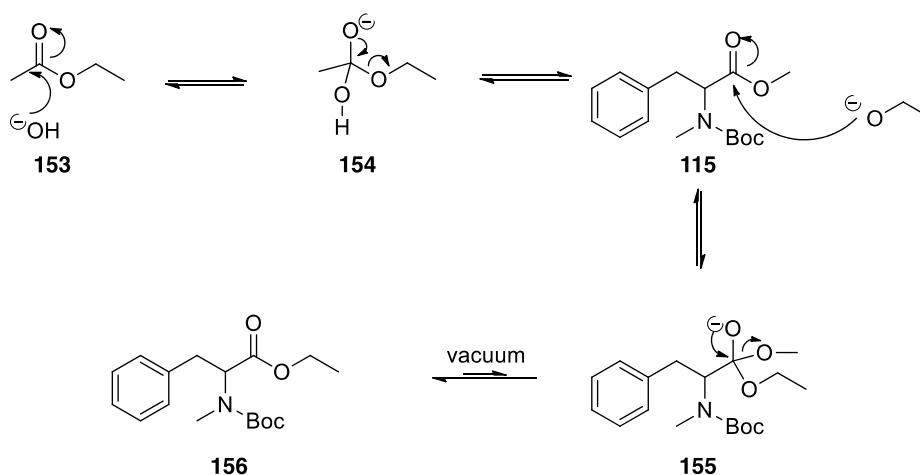


**Scheme 36: N-methylation of N-Boc phenylalanine**

*N*-Methylation of amino acid derivatives using sodium hydride and methyl iodide in DMF has been reported by Benoiton and others (Benoiton *et al.*, 1971). By using MeI/NaH with a Leucine derivative in an 8:3:1 molar ratio in the presence of DMF at 80 °C they achieved the desired methylated product in 96% yield. Following their procedure we synthesised the methylated phenylalanine derivative **115** in 78% by using 3:1:1 MeI/NaH/Boc-Phe molar ratio in DMF at room temperature on a 1 gramme scale. Contrary to Benoiton and co-workers we achieved improved results of nitrogen alkylation by addition of sodium hydride prior to methyl iodide addition.

However, one key drawback was that when scaling up the reaction, (10 gramme scale of SM) we encountered problems with the formation of a mixture

of methyl and ethyl ester of *N*-methylated phenylalanine (Scheme 37). When a large amount of sodium hydride is used in the reaction, our initial use of saturated aqueous ammonium chloride as a quenching agent was not ideal. After quenching, the mixture was not sufficiently acidic and some sodium hydride may have remained and led to the formation of aqueous sodium hydroxide which in turn could react with ethyl acetate leading to sodium ethoxide. This may account for the *trans*-esterification that we observed in the reaction (Scheme 37).



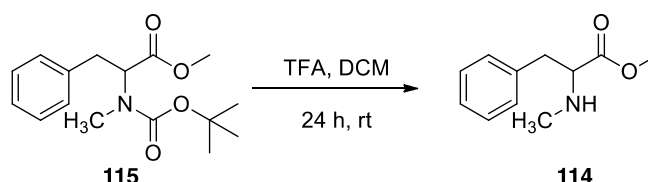
### Scheme 37: Mechanism of *trans*-esterification

Unfortunately the  $R_f$  values of both the methyl and ethyl *N*-methylated ester of phenylalanine were equal and hence separation by flash column chromatography was next to impossible. In order to overcome this, we attempted further *trans*-esterification of our mixture by performing repeated reactions with 10% HCl in MeOH in order to produce the methyl ester exclusively.

Due to the problems with this, it was clearly crucial to find an alternative quenching agent, which would neutralize the reaction mixture and avoid the risk of ethyl ester formation. In the end, we discovered that use of phosphonate buffer appeared optimum, as the quenched reaction mixture was pH neutral with no ethyl/methyl ester mixture observed. Pleasingly, with the use of phosphonate buffer at pH 7, the removal of DMF proved to be quicker and less complicated, which made the process of purification much easier. We were also

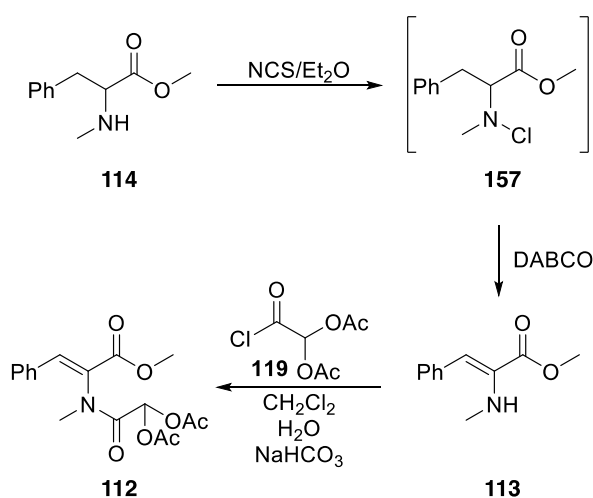
able to improve the yield of the reaction and obtained the desired product in 81% yield on a larger scale.

With the methylated product in hand the next step in the synthesis was removal of the BOC protecting group to liberate the free amine. To achieve this, we treated the BOC protected compound **115** with TFA in dichloromethane and after neutralization, obtained the amine **114** in 98% yield (Scheme 38).



**Scheme 38: N-Boc deprotection**

In the next step in our synthetic sequence, we needed to dehydrate *N*-methylphenylalanine methyl ester **114**. To achieve this, we first needed to *N*-chlorinate the nitrogen atom and eliminate HCl *via* addition of an organic soluble base. We elected to carry this out in a one-pot procedure, where the resulting enamine would be acylated with diacetoxyacetyl chloride **119**, due to the unstable nature of the enamine. As such, the crude enamine **113** thus obtained was acylated under Schotten-Bauman conditions to provide the diacetoxy amide **112** in poor yield over three transformations (Scheme 39). We now had the desired fully protected cyclisation precursor in good yield as an inseparable mixture of *E*- and *Z*-isomers.

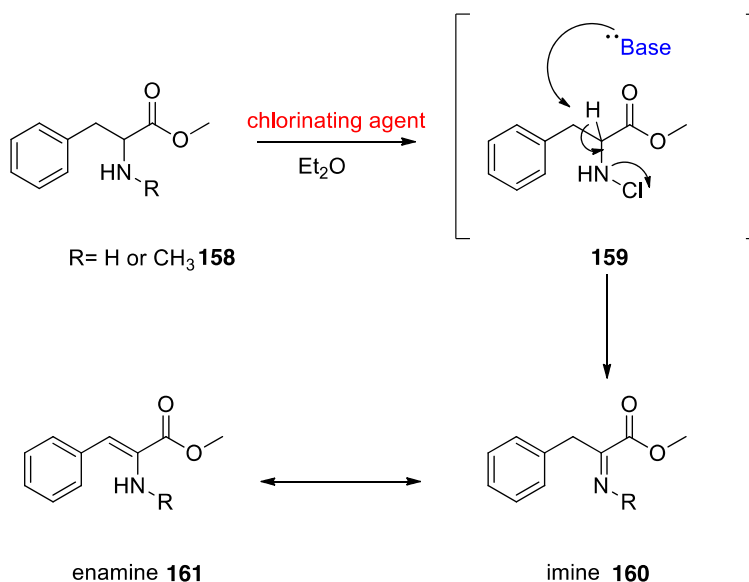


**Scheme 39: Formation of clausenamide cyclisation precursor**

However, one key drawback with this method, was the fact that the yields obtained were consistently low and only seemed to work on a larger scale. As such we decided to investigate this reaction further in order to try to increase the yield.

As shown above (Scheme 39), the deprotected product **114** was first treated with NCS and cautiously monitored in the dark. As only one proton was available on the nitrogen atom, only monchlorination was possible, which allowed us to add the chlorinating agent in a single addition. Chlorination of the amine analogue **158** needed to be monitored more carefully and as such, NCS was added portionwise over two hours. The resulting light sensitive *N*-chloro- $\alpha$ -amino acid ester **159** was then reacted with DABCO to give the dehydroamino acid ester **160** and HCl as a side product. The enamine product of this elimination **161** was sensitive to air, rapidly decolouring and was therefore not stable.

It is known that enamines exist in equilibrium with their tautomeric imine counterparts and the reaction outcome is clearly dependant on the equilibrium between these two key species as shown below (Scheme 40).

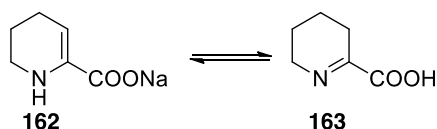


**Scheme 40: Mechanism of enamine formation**

Enamine-imine tautomerization has been a subject of interest in the literature (Erker et al., 1995, Lu and Lewin, 1998), with a special focus on the conditions

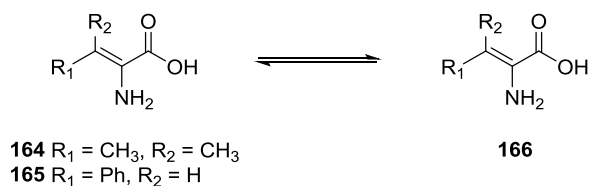
that influence its equilibrium. It has been shown that tertiary enamines, with regard to the imine, are more stable than primary and secondary ones. Nevertheless, it is possible to gain extra stabilization of those less stable systems *via* appropriate substitution at the  $\beta$ -carbon. Solvents have been shown to play an important role as well. Polar solvents favour the enamine tautomer form, in other words they favour enamization.

In the literature there are some examples of enamine/imine tautomerism in  $\alpha,\beta$ -unsaturated- $\alpha$ -amino acids. A study of dehydropipecolinic acid was conducted by Lu and Lewin (Lu and Lewin, 1998), where they showed that this compound exists as its enamine form **162** when isolated as a sodium salt and as its imine form **163** when extracted as hydrochloride salt (Scheme 41).



**Scheme 41: Enamine/ imine tautomerisation**

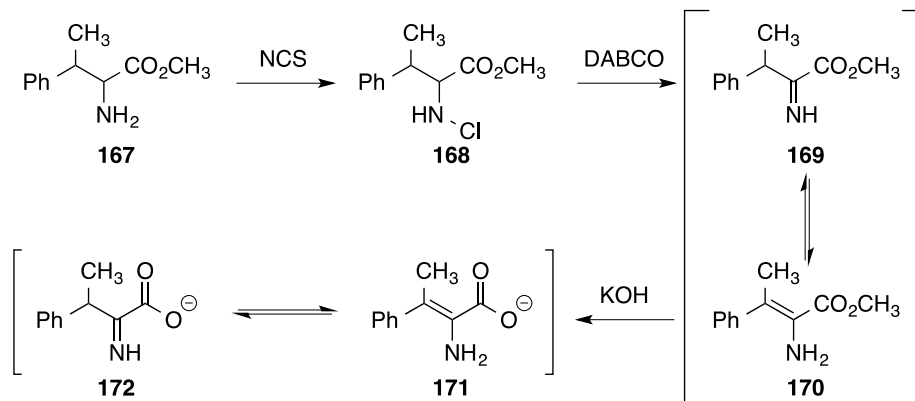
It was also reported by Lu and Lewin, that dehydropipecolinic acid possesses a long lifetime when diluted in solution at pH=7. However, the nature of its tautomer was not indicated. Lu and Lewin also synthesised the sodium and lithium carboxylate salts of dehydropipecolinic acid **162**, dehydrovaline **164** and dehydrophenylalanine **165** by using the same elimination conditions as we used during the synthesis of compound **114** (Scheme 42).



**Scheme 42: Lu and Lewin's enamine stability experiments**

As outlined below, both  $\alpha,\beta$ -unsaturated- $\alpha$ -amino acids were converted to the corresponding methyl or ethyl ester and subsequently treated with NCS and cautiously monitored. The resulting light sensitive *N*-chloro- $\alpha$ -amino acid ester **168** was reacted with DABCO or DBU to afford unsaturated ester **169** and HCl as by- product. Further hydrolysis of the unsaturated ester with either lithium

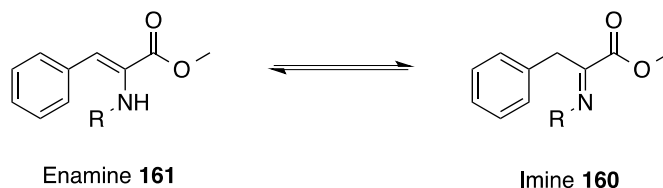
hydroxide in aqueous tetrahydrofuran or sodium hydroxide in aqueous dioxane led to the lithium or sodium carboxylate salts **171** (Scheme 43).



**Scheme 43: Enamine formation**

They reported that the unstable product could be stored intact at low temperatures (below 20 °C) in the presence of radical scavengers for up to few weeks. The proton NMR spectra of both compounds indicated that they exist in their enamine forms **171** only. The nuclear Overhauser effect (nOe) on the vinyl resonance ( $\delta$  6.48 ppm), resulting from an effect of the ester methyl group resonance ( $\delta$  3.86 ppm), defined the *Z* configuration of the phenyl ring to the carboxyl groups. In contrast, the cyclic unsaturated ester occurred as a 1:1 mixture of imine and enamine tautomers in  $\text{CDCl}_3$ . When an aqueous solution of the sodium salts of **172** and **171** was used, the enamine form was favourable in both, but gave rise to an equimolar mixture of *Z* and *E* isomers of the imine form in **165**. They also reported an interesting effect of the solvent, where in dimethylsulfoxide (DMSO), the sodium salt gave 67% formation of its enamine form (in 1:1 *Z*:*E* isomers mixture) and 60% of its imine form when  $\text{D}_2\text{O}$  was used. In summary of their work, they demonstrated that the enamine tautomers of  $\alpha,\beta$ -unsaturated- $\alpha$ -amino acids (dehydrophenylalanine) are more stable than their corresponding imine form and equienergetic in the cyclic dehydropipecolate ester. Although, in basic aqueous media, the imine tautomers are the ones that are more stable forms, but only in cases where the double bond is not stabilized by any extended conjugation (Lu and Lewin, 1998). However, this clearly does not correlate to the low yield (~48%) that we observed in our acylation reaction and therefore the key question, is why does

this occur and what is the equilibrium between the two conformers **161** and **160** as shown below (Scheme 44).



**Scheme 44: Enamine/ imine tautomerisation**

When looking at bond strength, the imine form **160** is more stable than the corresponding enamine **161**, because the C=N bond is stronger than the C=C bond. In our case when the amine analogue was used as the starting material, the enamine form **161** should be favoured, due to stability gained by conjugation *via*  $\pi$  orbital overlap from the aryl group through to the ester carbonyl. In theory, we should expect the same situation for the *N*-methyl analogue. As stated by Tong and others: “The conjugation of the enamine is controlled by changes in the electronic and steric effects of the substituent.” (Tong *et al.*, 2012). Therefore, it is possible that the *N*-methyl-imine is not as stable as the enamine due to steric occlusion of the methyl with the aromatic ring. This would possibly be an explanation for the low yields obtained after acylation of our crude dehydrogenated product (Figure 14) (Erker *et al.*, 1995).



**Figure 14: Enamine - energy 29.3681 kcal/mol vs Imine - energy 12.9678 kcal/mol**

We also decided to look at whether our chlorination step was linked to the low yield of the reaction. Initial attempts at chlorination of **114** had focused on the use of NCS in the presence of diethyl ether. However, we needed to filter succinimide before addition of DABCO, which therefore exposed the reaction mixture to air and increased the risk of hydrolysis. In order to overcome this, we decided to use liquid *tert*-butyl hypochlorite as chlorinating agent. It was the cheapest and the safest option for the chlorination, as *tert*-butyl hypochlorite

was generated *in situ* from *tert*-butanol and commercial hypochlorite. Household bleach could also be used, but only one that possessed low amounts of detergents and surfactants, as they produced large amounts of soap in the reaction, making extraction of *tert*-butyl hypochlorite next to impossible.

Successful chlorination of the amine **114** could be observed from the  $^1\text{H}$  NMR spectrum after two hours of stirring the reaction mixture in the dark. As shown below (Figure 15), the *N*-methyl group is clearly shifted from 2.35 ppm to 3.00 ppm when chlorinated, indicative of attachment of the electronegative chlorine atom.

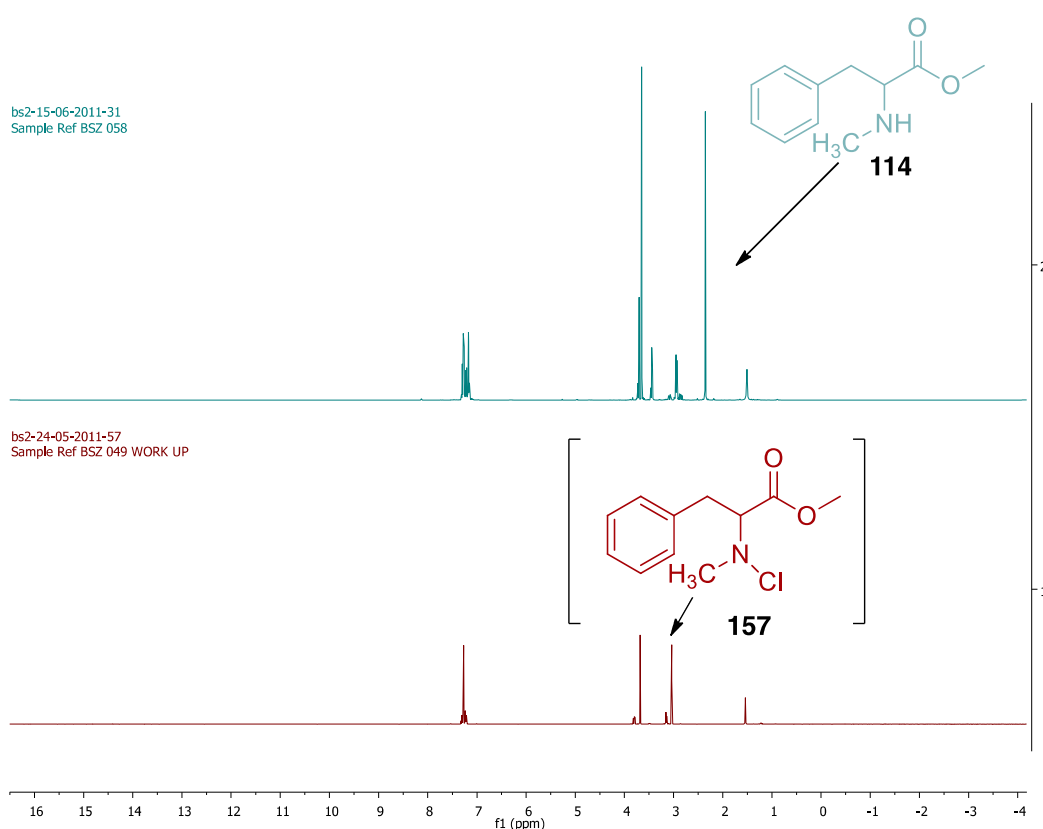


**Figure 15:**  $^1\text{H}$  NMR spectrum of the free amine vs. *N*-chlorinated product

Having established the requisite chlorination conditions we next turned our attention to the elimination step. We screened a number of different non-nucleophilic bases, as it was crucial to use a strong base, but at the same time a poor nucleophile so that no nucleophilic substitution would occur. The ones of high basicity such as: potassium *tert*-butoxide, lithium *bis*-(trimethylsilyl)-amide proved to be harsh, as degradation of the starting material was clearly observed

by TLC. Use of amine's of moderate basicity such as triethylamine or *N,N*-diisopropylethylamine failed, as only the non dehydrogenated product was attained. We next screened sterically hindered mild bases such as 2,6-lutidine, DBU and DABCO. Among these, DABCO (pKa = 8.7) gave the desired product in a shorter time and with better yields than 2,6-lutidine, where starting material was recovered. DBU proved to be too strong a base, as again, degradation of starting material was observed. This correlated with the strength of basicity as shown below (Figure 16).

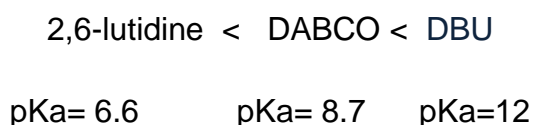
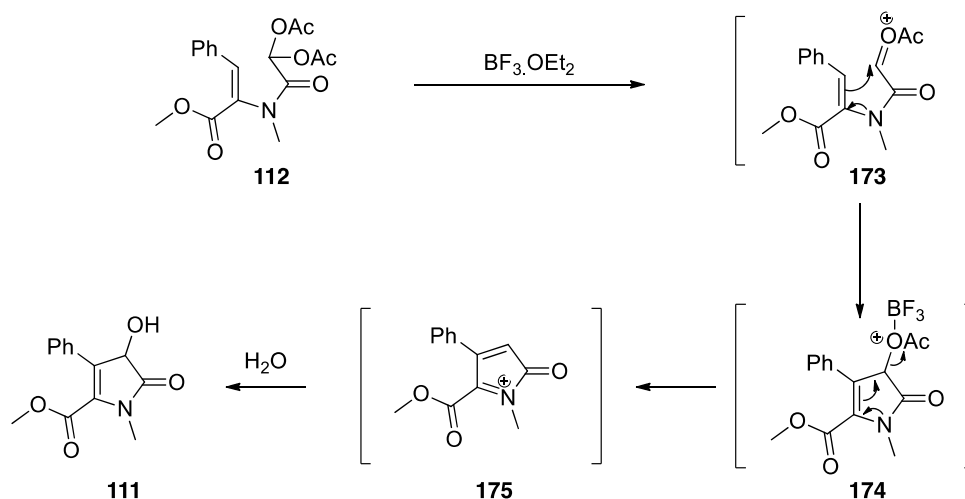


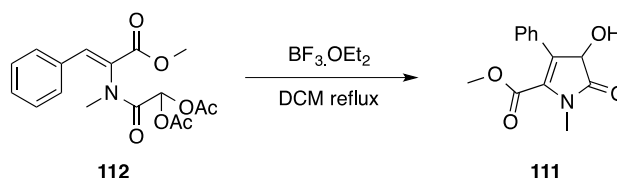
**Figure 16: Relative base pKa's**

As outlined above, Lewis acid mediated cyclisation of a number of enamines had led to elimination of the acetate with formation of the corresponding diene. As such, we believed that our approach towards clausenamide should obviate this problem, as there is no  $\beta$ -hydrogen to facilitate formation of the diene and on aqueous work-up we anticipated that we would generate the core structure of clausenamide (Scheme 45).



**Scheme 45: Clausenamide structure generation**

Having established that intramolecular cyclisation occurs by use of boron trifluoride diethyl etherate as a Lewis acid in dichloromethane, we decided to carry out the same reaction with our cyclisation precursor **112** (Scheme 46).



**Scheme 46: Cyclisation and formation of BRS-015**

To our delight, we successfully obtained the core structure of clausenamidine in 58% yield. We next turned our attention to the improvement of the yield of this reaction. Due to the relatively low boiling point of DCM we decided to use different solvents with higher boiling points as outlined below (Table 2).

<b>BF<sub>3</sub>.Et<sub>2</sub>O (equiv.)</b>	<b>Solvent</b>	<b>Reaction Temp. (°C)</b>	<b>Yield</b>	<b>Time (hrs)</b>
2	DCM	40	58%	12 (reflux)
2	DCE	60	62%	6 (reflux)
20	neat	126	70%	3 (reflux)
20	neat	-	72%	36 (r.t.)

**Table 2: Optimization of cyclisation reaction using boron trifluoride dietherate**

We were pleased to observe that by using neat boron trifluoride diethyl etherate we improved the yield and shortened the time of reaction, as the core structure of clausenamidine could be obtained in 70% yield in just 3 hours at reflux.

We next carried out the cyclisation with neat boron trifluoride diethyl etherate at room temperature for 36 hours and surprisingly produced the desired product in 72% yield.

As we observed that Lewis acid-mediated cyclisation leads to the formation of the core structure of clausenamidine, we decided to carry out screening of a number of other Lewis acids to try to improve the yield of the reaction.

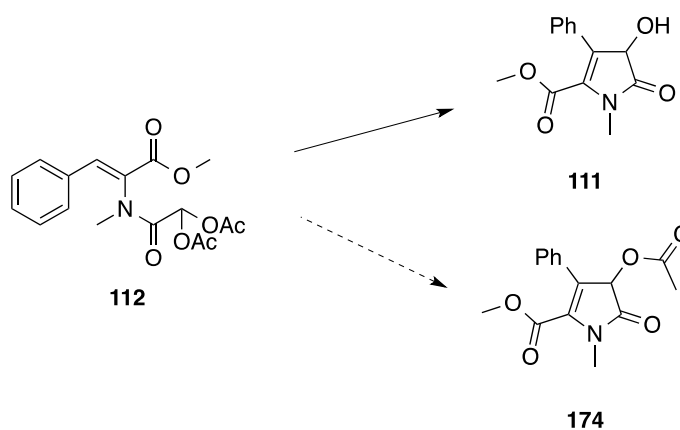
We screened alternative conditions for cyclisation of **112** using different Lewis acids. The reactions were performed under reflux for 2 hours, using two equivalents of each Lewis acid. Using the same conditions, Lewis acids screening was carried out for **112**, giving comparable yields and the results of our studies are outlined in the following table (Table 3).

Lewis acid	Yield
BF <sub>3</sub> .Et <sub>2</sub> O	70%
CF <sub>3</sub> SO <sub>3</sub> Si(CH <sub>3</sub> ) <sub>3</sub>	40%
AlCl <sub>3</sub>	21%
SnCl <sub>4</sub>	32%
TiCl <sub>4</sub>	47%
FeCl <sub>3</sub> .6H <sub>2</sub> O	52%
FeCl <sub>3</sub>	43%
InCl <sub>3</sub>	60%
(CF <sub>3</sub> SO <sub>3</sub> ) <sub>2</sub> Zn	66%

**Table 3: Effect of a range of Lewis acids on the yield of cyclisation**

### 3.2.1. Mechanistic investigation of cyclisation

Whilst the IAC reaction had led to the core structure of clausenamides, the formation of the alcohol as the major product was somewhat surprising as we had predicted that the acetate **174** would be preferred. It is therefore probable that further activation of the acetate **174** with Lewis acid, occurs leading to elimination to give the conjugated enamine **175** that reacts with water on work-up to give the corresponding alcohol **111** (Scheme 45 and 47).



**Scheme 47: Mechanism of cyclisation**

We were also intrigued by the nature of the double bond formation in terms of the reaction mechanism. It was hard to determine the double bond location by <sup>1</sup>H NMR or <sup>13</sup>C NMR experiments or by infra-red spectroscopy. The final

structure was therefore determined by X-ray crystallographic analysis as outlined below (Figure 17).

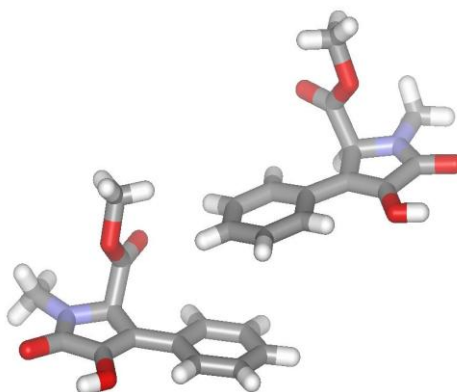


**Figure 17: X-Ray structure of compound 166**

What is clear from the X-ray, is that our predicted compound **111** has not formed, but instead, it is the compound where the double bond has shifted into conjugation **176** (Figure 18).

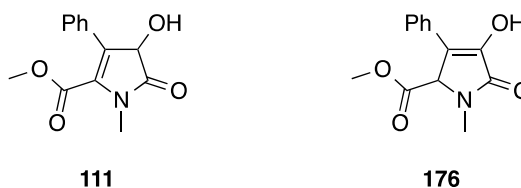
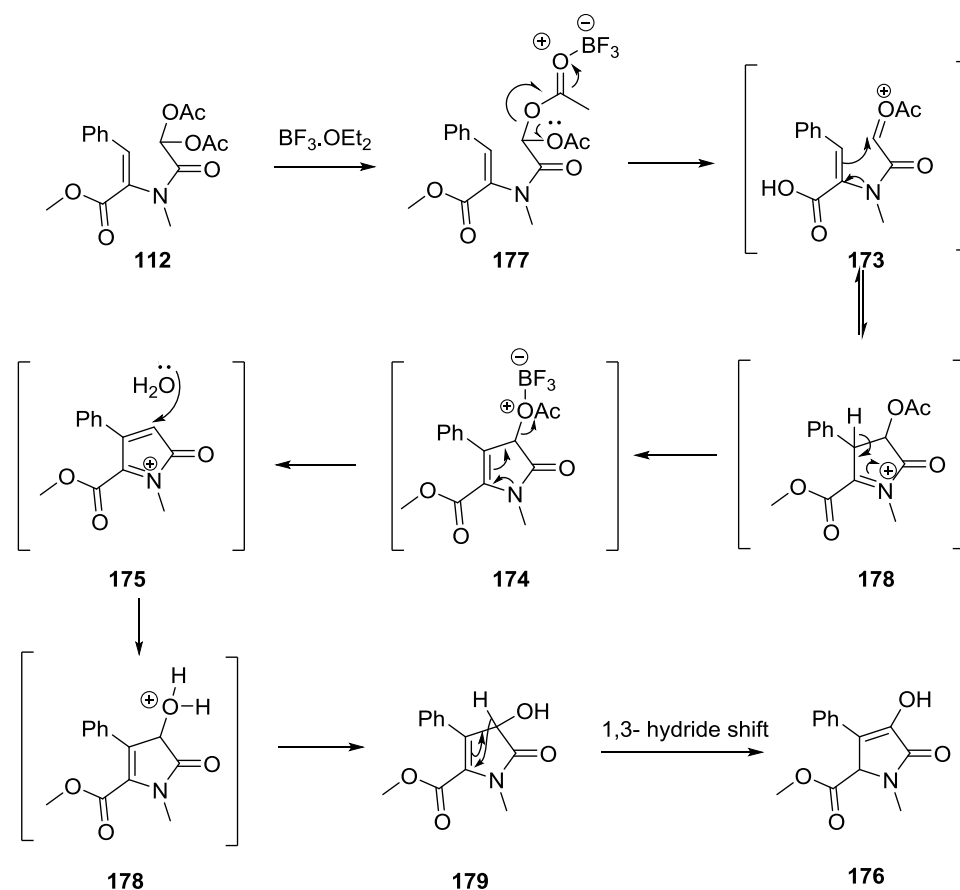


**Figure 18: The two possible double bond configurations**

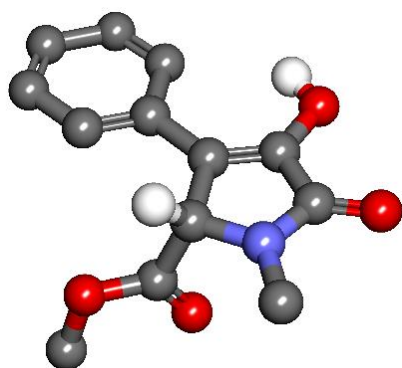
We were surprised that compound **111** was not generated as we initially thought but **176**. One possible explanation is that a 1,3-hydride shift of the proton attached to the carbon as hydroxyl group occurs as shown below (Scheme 48).



**Scheme 48: Proposed hydride shift mechanism**

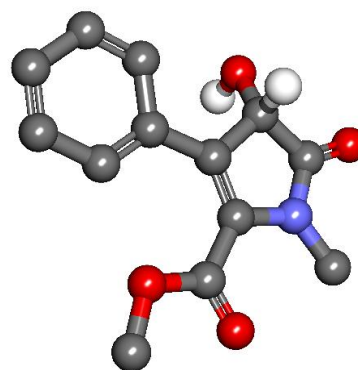
In order to understand the nature of the molecule and to look at the potential of why a 1,3-hydride shift might occur as a possible mechanism, we elected to look at the total energy of each conformer as outlined below (Figure 19). We envisaged that it must be due to the stability of both possible products with one possessing higher energy than the other.

On calculating and comparing the energies of both products, we were pleased to observe that the total energy of **176** is five times less than the energy of **111**, clearly indicating that **176** is much more stable and so consequently would be favoured.



Compound 176

Total energy 8.4760 kcal/mol

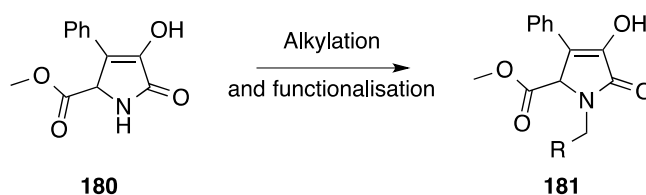


Compound 111

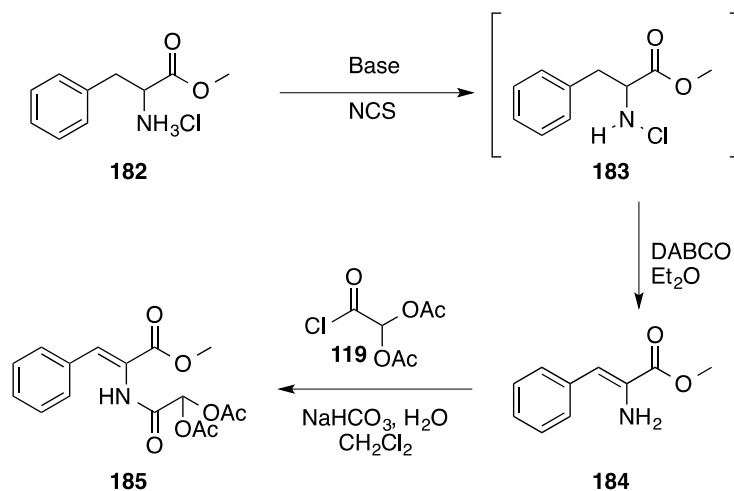
Total energy 40.4550 kcal/mol

Figure 19: Energy confirmations of BRS-015 double bond isomers

Following the successful obtention of the core structure of clausenamide, we were mindful of the need to be able to vary the structure around the central core. Compounds based on piracetam (**3**) that have progressed to the clinic or been taken forward to clinical trial have had varying degrees of substitution on the nitrogen atom. As such, we elected to look at the synthesis of the *N*-unsubstituted compound **180** as shown below. We envisaged that alkylation as per previous researchers, would enable us to access a wide array of *N*-substituted derivatives **181** (Scheme 49).

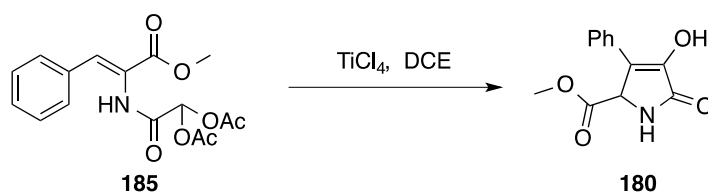
Scheme 49: Formation of the *N*-H isomer of clausenamide

In order to synthesise the *N*-H precursor **185**, we first formed the free base of phenylalanine methyl ester and treated it with *N*-chlorosuccinimide in the dark as per our previous synthesis of the core structure of clausenamide. Unlike the synthesis of the *N*-methyl precursor (Scheme 39), we were mindful of the fact that over-chlorination of the nitrogen atom could occur, due to two potential sites for chlorination. As such, we decided to use NCS instead of *tert*-butylhypochlorite in this instance (Scheme 50).



**Scheme 50: Formation of the *N*-H cyclisation precursor**

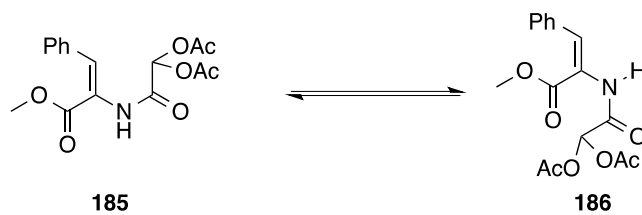
As shown above, the *N*-chloro compound **183** was treated with DABCO to promote elimination and tautomerisation to the enamine **184**. Surprisingly, the enamine **184** proved remarkably stable and could be isolated and purified by column chromatography in 26% yield. Enamine **184** was subsequently alkylated with diacetoxyacetyl chloride **119** under Schotten-Bauman conditions to give the *N*-H precursor **185** in good yield (74%). As per our investigations with the *N*-methyl precursor, we elected to carry out the cyclisation with a range of Lewis acids. Surprisingly in this instance, boron trifluoride did not lead to formation of the cyclized product, and instead necessitated treatment with a stronger Lewis acid and higher temperatures. As such, treatment of **185** with titanium tetrachloride in 1,2-dichloroethane gave the cyclized product **180** in 52% yield as shown below (Scheme 51).



**Scheme 51: Cyclisation to give the *N*-H precursor**

The requirement for more forcing conditions was surprising as we had anticipated that the *N*-H precursor would cyclise in an analogous fashion to its *N*-methylated congener. Its apparent stability may in part be due to the absence

of the *N*-methyl substituent, which places the diacetate and enamine in close proximity for cyclisation as shown below (Scheme 52).



**Scheme 52: Potential conformers**

With the obtention of the desired cyclised derivatives, the focus of the project moved towards the analysis of their physiological effects.

## 4.0. Methodology

## 4.0. Methodology

### 4.1. Hippocampal slice preparation and preservation

All animal procedures strictly followed University College London (UCL) Research Ethics Committee regulations. Sprague–Dawley rats (Harlan Laboratories Ltd, Oxon, UK) aged 21–40 days were killed by an overdose of sodium pentobarbital injected intraperitoneally ( $100 \text{ mg kg}^{-1}$ ) and rapidly decapitated in accordance with the UK Animals (Scientific Procedures) Act, 1986.

#### 4.1.1. Dissection of the rat brain

Sprague Dawley rats were killed by decapitation and the skull was exposed by a skin incision. Using scissors, the skull was cut along the midline starting from the foramen magnum, followed by two cuts in the medio-lateral direction at the cerebellum to facilitate the opening of the skull and exposure of the brain. Using a spatula, the brain was scooped out of the skull by cutting the cranial nerves and quickly submerged into an oxygenated ice-cold sucrose solution.

The brain was placed on a filter paper inside a Petri dish and *via* the use of a blade; the brain was trimmed in the coronal plane removing the olfactory bulbs and the cerebellum. By cutting along the midline, the two hemispheres were separated and placed onto the medial side with the lateral side facing up. An additional angled cut at approximately  $90^\circ$  (“magic cut”) was made along the dorsal sides of the hemisphere for mossy fibre recordings. (Bischofberger *et al*, 2006). Using the spatula, the hemispheres were glued onto their dorsal sides on a stage angled  $15\text{--}30^\circ$ , transferred into a buffer tray and submerged with ice-cold sucrose solution.  $300 \mu\text{m}$  thick transverse slices of the dorsal hippocampus were obtained using a Vibratome (Figure 20) (Leica VT 1200S, Leica Biosystems, Nussloch GmbH, Nussloch, Germany). Throughout the cutting process, the hemispheres were constantly oxygenated with  $95\% \text{O}_2/5\% \text{CO}_2$ .

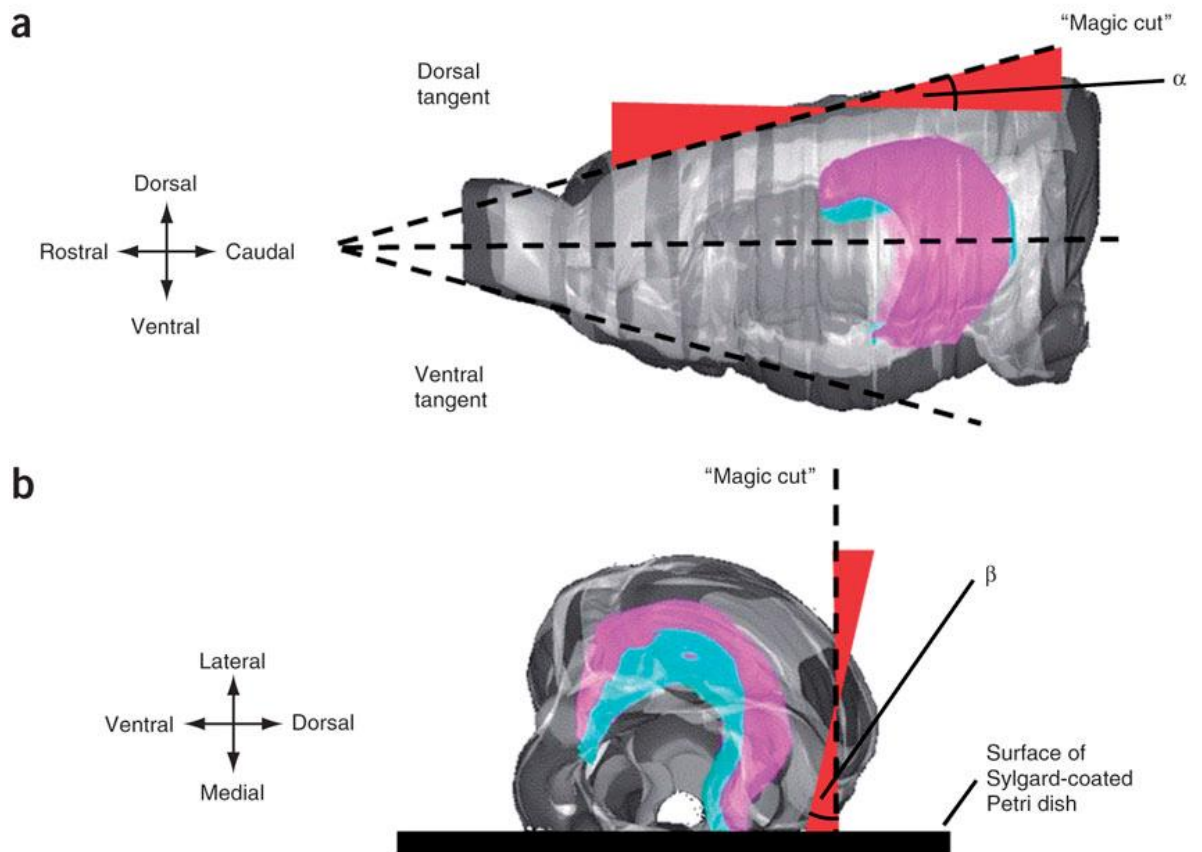


**Figure 20: Preparation of transverse hippocampal slices with special cut. A, B:** Computer reconstruction of the adult rat brain showing the hippocampal formation (pink CA1 and CA3 areas, blue DG) **A:** Two hemispheres of the brain orientated in the exact position, as when removed from the skull; **B:** One hemisphere of the brain, orientated as after the cut along the midline and a 90° turn onto the medial side. Taken from (Bischofberger *et al.*, 2006).

#### 4.1.2. Slice storage and preservation

Transverse hippocampal slices thus obtained, were incubated at 35 °C for 30 min in the sucrose solution and thereafter maintained at room temperature (22 °C) until required. All slices were stored in a bespoke submersion chamber (pictured) filled with sucrose solution and perfused with 95% O<sub>2</sub>/5% CO<sub>2</sub> (Figure 21).



**Figure 21: Submersion chamber for hippocampal slices maintenance:** Picture of the custom-made submersion chamber showing the nylon mesh that holds the brain slices, filled with sucrose solution and oxygenated with 95% O<sub>2</sub>/ 5% CO<sub>2</sub> through a plastic tube to reduce solution turbulence.

### 4.1.3. Solutions

The composition of the sucrose solution used for dissection and slice storage is presented below (Table 4) as well as that used for the artificial cerebrospinal fluid (ACSF) for perfusion during electrophysiological recordings shown below (Table 5).

Substance	Concentration (mM)
Sucrose	75
<i>D</i> -Glucose	10
NaCl	87
NaHCO <sub>3</sub>	25
KCl	2.5
NaH <sub>2</sub> PO <sub>4</sub>	1.25
MgCl <sub>2</sub>	7
CaCl <sub>2</sub>	0.5

**Table 4: The composition of sucrose solution listed**

Substance	Concentration (mM)
<i>D</i> -Glucose	25
NaCl	125
NaHCO <sub>3</sub>	25
KCl	2.5
NaH <sub>2</sub> PO <sub>4</sub>	1.25
MgCl <sub>2</sub>	2
CaCl <sub>2</sub>	4

**Table 5: The composition of ACSF solution listed**

The osmolarity of both solutions was adjusted to ~ 320 mOsmol/L and the pH to 7.4 prior to use.

## 5.0. Electrophysiological recordings

After one-hour incubation, individual slices were transferred to a recording chamber that was continuously perfused with oxygenated ACSF and held by nylon strings attached to a platinum wire. The gravity-driven perfusion rate was set to 2 ml/min. Glass electrodes were pulled from borosilicate capillaries (outer diameter of 1.50 mm and inner diameter of 0.86 mm purchased from Harvard Apparatus Ltd., Edenbridge, UK) with a Flaming/Brown micropipette puller (Model P-97, Sutter Instruments Co., California, USA). Heat settings were adjusted so that pipettes had resistances ranging between from 3 to 6 M $\Omega$ .

Hippocampal slices were visualised with an Olympus BX 51WI microscope (Olympus Europa Holding GmbH, Hamburg, Germany) which was connected to a KPM-3 Hitachi infrared (IR) video camera. Stimulus electrodes (bipolar tungsten electrodes purchased from FHC Inc. Bowdoin, Maine, USA) were positioned under a low magnification (10 x) objective (Olympus), while for patch-clamp experiments, neurones were visualised under IR-differential interference contrast (DIC) imaging with a water-immersion high-magnification (60 x) objective (Olympus) and a fourfold magnification changer (Luigs & Neumann GmbH, Ratingen, Germany). For local application, a picospritzer (Picospritzer III, Intracel, Unit 4, Shepreth, Herts, UK) was connected to a pipette holder designed for pressure application (Figure 22).

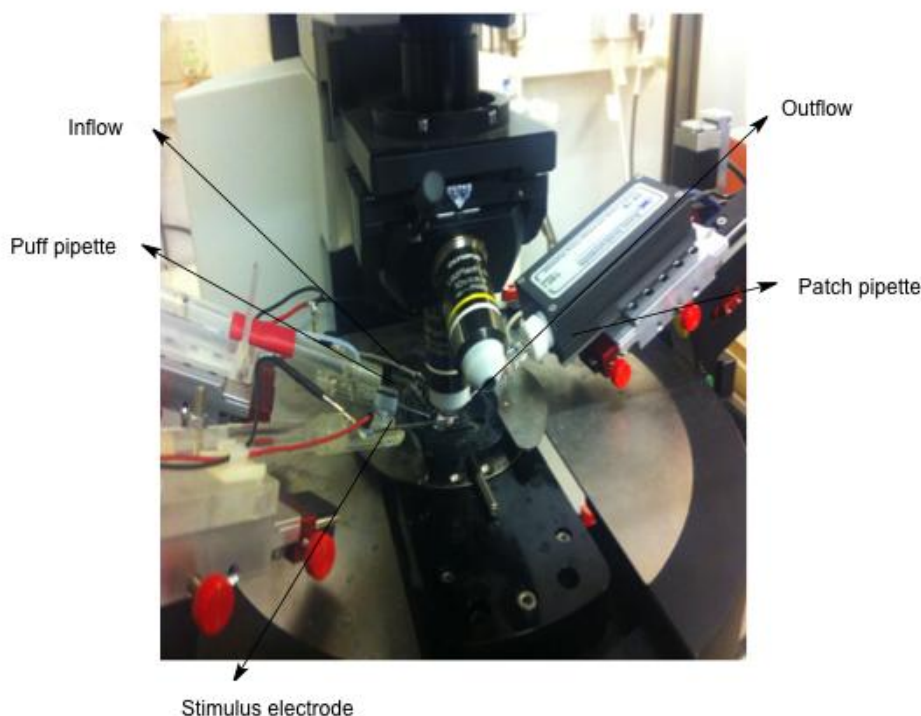


**Figure 22: Image showing stage, objectives and recording chamber with stimulus electrode, puff pipette and recording electrode positioned in the tissue.**

To study the effects of BRS-015 and its analogues, various electrophysiological recordings were performed in acute hippocampal slices. These were divided into extracellular recordings or recordings of evoked field excitatory postsynaptic potentials (f-EPSPs) and patch clamp recordings, where there is direct access to the intracellular compartment of individual neurones, hence enabling a measurement of the trans-membrane potential as well as the input resistance, cell capacitance and firing properties.

### **5.1. Extracellular recordings**

The measurement of extracellular recordings is a less challenging method when compared with whole-cell recordings because it does not rely on the formation of a giga-seal onto individual neurones. As such, this recording configuration does not enable the detection of changes in the electrical properties of individual neurones (e.g. input resistance,  $R_{in}$ ) or fine alterations of neuronal

firing properties in response to application of a drug or a modulator of synaptic transmission. However, it provides a rapid method with which to explore the effects of a drug on a group of neurones. Local f-EPSPs are generated by bulk activation of excitatory synapses resulting in the movement of positive charges through glutamate receptors in postsynaptic neurones. This creates current sinks (and sources) that can be detected as negative (downward) deflections when recording from the extracellular space. An intracellular electrode positioned at the soma would on the other hand measure a depolarisation, i.e. a positive-going waveform or excitatory postsynaptic potential (EPSP).

MF f-EPSPs (MF-EPSPs) were evoked every 10 seconds using paired electrical stimuli (inter-stimulus interval: 20 ms; constant current, 0.3 – 1.5  $\mu$ A, 50  $\mu$ sec) and recorded with an ACSF-filled glass pipette ( $\sim$ 3 M $\Omega$ ) placed within the CA3 stratum lucidum as shown in the schematic below (Figure 23).

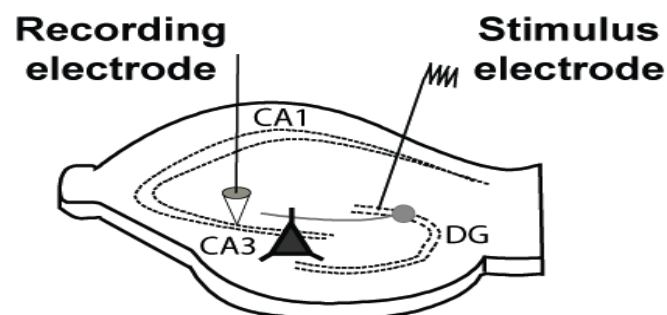


**Figure 23: Cartoon representation of a hippocampal slice showing the experimental approach for mossy fibre f-EPSP recordings:** Stimulus and recording electrodes positioned in DG and SL of CA3, respectively.

Extracellular electrical stimulation in the dentate gyrus can lead to the activation of three potential different pathways (Henze *et al.*, 2000) besides the monosynaptic, orthodromic mossy fibre- CA3 input, including:

- Anti-orthodromic pathway *via* MF collaterals in the hilus;

- Antidromic pathway *via* hilar projecting associational collaterals of CA3 pyramidal neurones;
- Polysynaptic pathway, where a strong stimulation causes firing of CA3 pyramidal neurones, thus synaptic activation of other CA3 pyramidal neurones.

Therefore, to ensure that DG stimuli activated monosynaptic mossy fibre-CA3 inputs, three criteria need to be met:

1. EPSPs had to have a large degree of paired-pulse facilitation (PPF > 200%) (Salin *et al.*, 1996);
2. EPSPs needed to show a large amplitude increase upon a modest increase in stimulus frequency (e.g. 0.1 Hz to 1 Hz);
3. The application of DCG-IV (1  $\mu$ M) at the end of each recording depressed MF-EPSPs > 70% (Kamiya and Ozawa, 2000, Barnes *et al.*, 2010).

To study the effect of BRS-015 on mossy fibre LTP, two different stimulus paradigms were used. Firstly, we designed a protocol where sub-threshold tetanic stimulation (100 Hz for 1 second) in the dentate gyrus only elicited a typical post-tetanic potentiation (PTP). Secondly, we used a classic induction protocol of long-term potentiation (3 times 100 Hz for 1 second, every 10 seconds), where sustained LTP (>20 minutes) was formed after initial PTP. A second stimulus electrode was placed in the distal stratum radiatum in order to activate associational commissural fibres as a control pathway.

## **5.2. Intracellular recordings: whole-cell patch-clamp**

Whole-cell recordings were obtained from CA3 pyramidal neurones imaged with infra-red videomicroscopy (Figure 24)

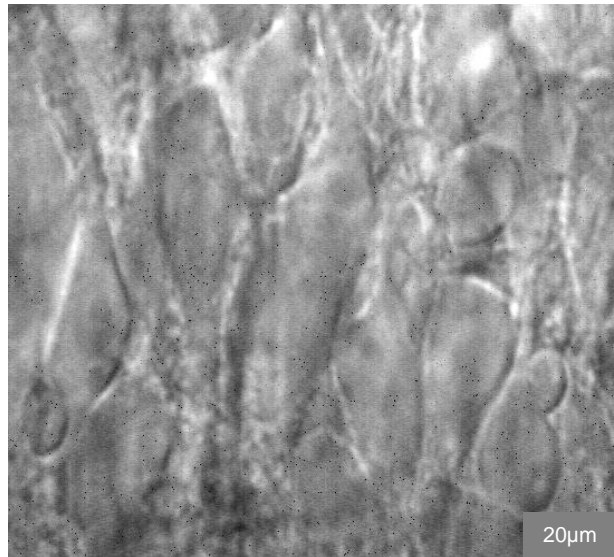


**Figure 24: High magnification IR-DIC image of the PCs of the CA3 region**

### 5.2.1. Voltage-clamp configuration

For voltage-clamp recordings in which cells were held at  $V_{holding} = -70\text{mV}$ , electrodes were filled with a cesium chloride based internal solution containing: 120 mM CsCl, 5 mM QX314 Br, 8 mM NaCl, 0.2 mM  $\text{MgCl}_2$ , 10 mM HEPES, 2 mM EGTA, 2 mM MgATP and 0.3 mM  $\text{Na}_3\text{GTP}$ . The osmolarity and pH of intracellular solutions were adjusted to  $\sim 310\text{ mOsmol/L}$  and 7.2 respectively.

A bipolar tungstene electrode was positioned in the stratum granulosum for activation of granule cells and mossy fibres. Excitatory postsynaptic currents evoked by dentate gyrus stimulation ( $20\ \mu\text{s}$ ;  $20 - 100\ \mu\text{V}$ ) were only analyzed if currents were reversibly depressed  $> 80\%$  by superfusion of DCG-IV ( $1\ \mu\text{M}$ ) at the end of each experiment, consistent with the selective sensitivity of mossy fibre synapses. The access resistance, monitored throughout the experiments by a voltage step was  $< 20\ \text{M}\Omega$  and results were discarded if it changed by more than 20%. The liquid junction potential was not corrected. EPSCs were filtered at 2 kHz (internal 4-pole low-pass Bessel filter), and sampled at 10 kHz. Single shock electric pulses were delivered every 10 sec (0.1 Hz).  $\text{GABA}_A$  and  $\text{GABA}_B$  receptors were routinely blocked by picrotoxin ( $50\ \mu\text{M}$ ) and CGP-52432 ( $10\ \mu\text{M}$ ). To record KAR-EPSCs, the selective AMPARs antagonist GYKI-53655 ( $50\ \mu\text{M}$ ) and the NMDA receptor antagonist *D*-AP5 ( $50\ \mu\text{M}$ ) were included in the

recording solution. NMDA-EPSCs were recorded in the presence of NBQX (20  $\mu$ M) while voltage-clamping pyramidal neurones at +40 mV.

EPSCs, evoked when holding CA3 pyramidal cells at -70 mV, were fully abolished by addition of 6-cyano-7-nitroquinoxaline-2,3-dione (CNQX; 50  $\mu$ M) or 2,3-dihydroxy-6-nitro-7-sulfamoyl-benzo[f]quinoxaline-2,3-dione (NBQX; 20  $\mu$ M), confirming that they were mediated by AMPA and kainate receptors.

For glutamate puffs, glutamate (100 mM in ACSF) was applied at 5-20 psi (10-50 ms). Puffs were applied every 60 seconds to allow for glutamate clearance. The puff electrode was positioned at the border of SL and SR, 100  $\mu$ m away from the soma of the recorded CA3 pyramidal cell and along its apical dendrite.

### 5.2.2. Current-clamp configuration

To examine how a drug or compound alters the electrical properties of a given neurone, it is necessary to characterize the current – voltage (I–V) relation in response to hyperpolarizing and depolarizing current steps and to determine the threshold for action potential (AP) generation, as well as the mean firing rate. Current-clamp recordings from individual CA3 pyramidal neurones were carried-out to examine the effect of BRS-015 on intrinsic membrane properties of CA3 pyramidal neurones, including the membrane potential, input resistance and the mean firing frequency. The pipette solution for current-clamp recordings contained: 135 mM K- gluconate, 5 mM KCl, 1 mM CaCl<sub>2</sub>, 5 mM EGTA-Na, 10 mM HEPES, 10 mM glucose, 5 mM MgATP, and 0.4 mM Na<sub>3</sub>GTP.

### 5.3. Data acquisition and analysis

Recordings were obtained using an Axopatch 200B amplifier (Axon Instruments, Union City, USA) that fed analog data to an A/D converter. The resulting data were collected and analysed with custom-built routines in the LabVIEW environment (version 8) using National Instruments drivers and was stored on a personal computer (Figure 25).

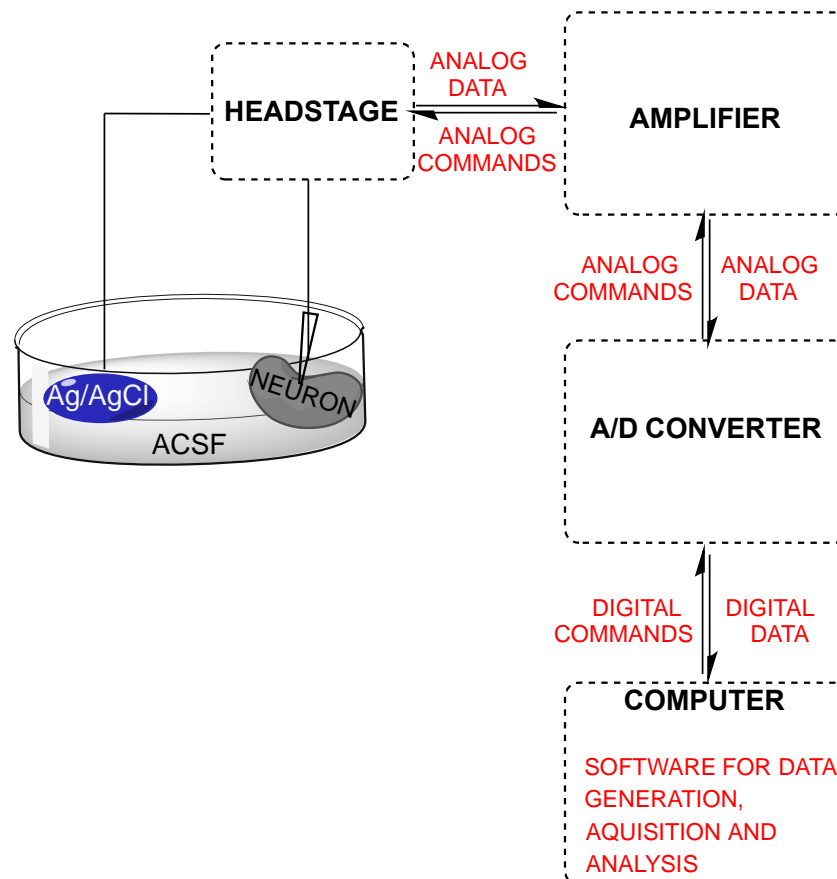


**Figure 25: Schematic of the recording configuration and signal flow. A:** The cartoon shows the connection between the headstage, amplifier, A/D converter and the personal computer used for data storage and analysis.

For each recording, EPSC amplitude was normalised to pre-BRS-015 level, and the overall change in amplitude for 'n' neurones was determined by averaging normalised amplitudes and expressed as a percentage. PSC traces of representative examples were typically averages of between 3 and 10 individual traces.

The PPR was determined by dividing the peak amplitude of the second EPSC to that of the first EPSC using a paired-stimulus protocol (inter-stimulus interval, 50 ms) (Figure 26).

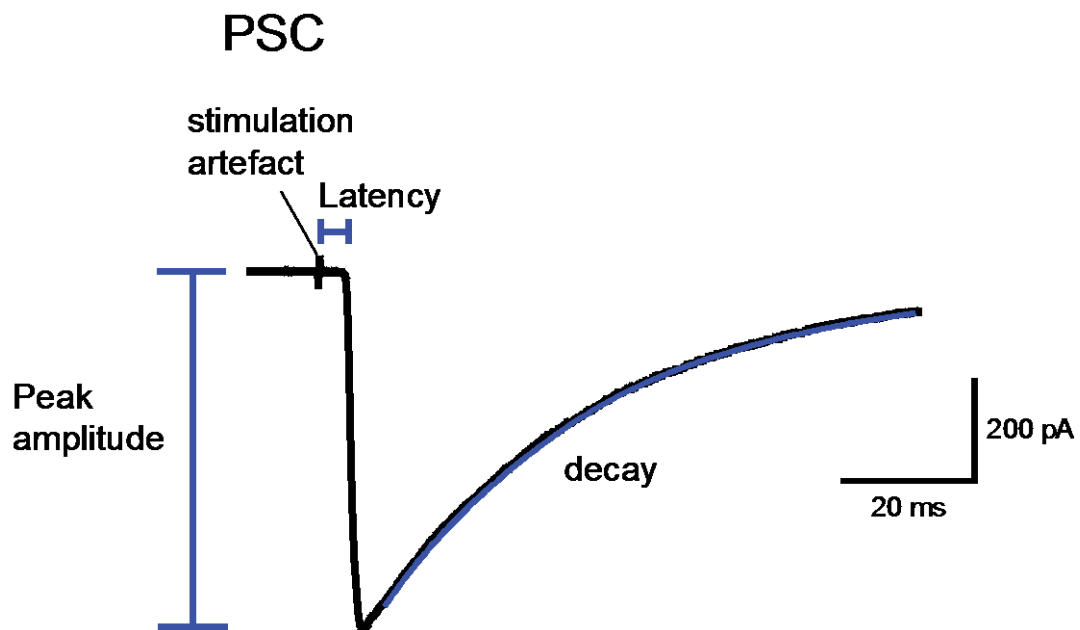


**Figure 26: Analysis of exemplified evoked postsynaptic current with specified parameters for data analysis**

Analysis of the decay kinetics was carried out by fitting trace averages with a single exponential using Matlab R2010a (TheMathWorks, version 7.10).

I-V relationships from CA3 pyramidal neurones were obtained with no constant current injection, by applying a series of hyperpolarizing and depolarizing steps (-120 pA to +100 pA; 500 ms). For each cell, the input resistance was calculated by fitting the linear portion of the I-V relation at hyperpolarized potentials. The slope of the I-V relation yielded the input resistance. The mean firing frequency was calculated by dividing the number of action potentials by the duration of a supra-threshold current step of increasing intensity that did not inactivate  $\text{Na}^+$  channels (20 to 100 pA, 500 ms). The rheobase current was defined as the minimum injected current (20 – 60 pA) that triggered action potentials in the recorded neurone.

## 5.4. Statistics

All data are given as mean  $\pm$  standard error of the mean (SEM). Statistical significance between means was calculated by using paired Student's *t*-test, except in Figure 44 where an unpaired *t*-test was applied. Data were significant if  $P < 0.05$ . In all figures, error bars indicated  $\pm$  SEM. Averaged traces, used as representative examples, include 3-10 individual responses.

## 5.5. Drugs

*D*-(-)-2-Amino-5-phosphonopentanoic acid (*D*-APV), a competitive NMDA receptor antagonist, was obtained from Abcam Biochemicals (Cambridge, UK) and diluted to 50  $\mu$ M.

Compound BRS-015 was prepared in DMSO at a stock concentration of 50 mM.

3-[[[(3,4-Dichlorophenyl)methyl]amino]propyl] diethoxymethylphosphinic acid (CGP-52432), a selective GABA<sub>B</sub> antagonist, was purchased from Tocris Bioscience (Bristol, UK) and diluted to a final concentration of 10  $\mu$ M.

6-Cyano-7-nitroquinoxaline-2,3-dione (CNQX), a potent AMPA/kainate receptor antagonist, was bought from Tocris Bioscience (Bristol, UK) and diluted to a final concentration of 50  $\mu$ M.

(2*S*,2'*R*,3'*R*)-2-(2',3'-Dicarboxycyclopropyl)glycine (DCG-IV), a selective agonist on presynaptic mGluR<sub>2/3</sub> was obtained from Tocris Bioscience, (Bristol, UK) and prepared at final concentration of 1  $\mu$ M.

Picrotoxin, a noncompetitive GABA<sub>A</sub> receptor antagonist, was purchased from Abcam Biochemicals (Cambridge, UK) and prepared in DMSO for use at a final concentration of 50  $\mu$ M.

Glutamate was purchased from Abcam Biochemicals (Cambridge, UK) and diluted to 100 mM.

1-(4-Aminophenyl)-3-methylcarbonyl-4-methyl-3,4-dihydro-7,8-methylenedioxy-5*H*-2,3-benzodiazepine hydrochloride (GYKI 53655), a non-competitive AMPA and kainate receptor antagonist, was obtained from Abcam Biochemicals

(Cambridge, UK) and prepared in water for use at a final concentration of 50  $\mu\text{M}$ .

2,3-Dioxo-6-nitro-1,2,3,4-tetrahydrobenzo[*f*]quinoxaline-7-sulfonamide (NBQX), a potent AMPA receptor antagonist, was bought from Tocris Bioscience (Bristol, UK) and diluted to a final concentration of 20  $\mu\text{M}$ .

## **6.0. Electrophysiological profile of BRS-015**

## 6.0. Electrophysiological profile of BRS-015

This section describes the neuropharmacological properties of compound BRS-015 as a modulator of excitatory synaptic transmission at a major hippocampal synapse. Several electrophysiological techniques were used to analyse the profile of compound BRS-015 at a major central synapse, including extracellular field potential recordings and whole-cell recordings in different configurations. Afferent mossy fibre axons were activated by electrical stimuli delivered in the stratum granulosum and postsynaptic recordings were made from CA3 pyramidal neurones. An initial characterisation of the acute effects of BRS-015 was first undertaken using both extracellular recordings and whole-cell voltage-clamp recordings. This led to the establishment of the relation between the concentration of BRS-015 in brain tissue and the degree of modulation of evoked EPSCs in pyramidal neurones. Finally, a pharmacological screen was performed using selective antagonists at common receptors found at central synapses to search for a putative target *via* which BRS-015 modulated synaptic transmission.

## 6.1. Effects of BRS-015 on evoked glutamatergic synaptic transmission from the dentate gyrus to CA3

### 6.1.2. Field potential recordings

Extracellular recordings were first chosen to assess the acute effect of compound BRS-015 on excitatory synaptic transmission in a CA3 neuronal population. A bipolar tungsten electrode was positioned in the supra-granular blade of the dentate gyrus to activate mossy fibres and a recording pipette filled with ACSF was implanted in the stratum lucidum in the CA3 sub-region to record evoked f-EPSPs. Electrical stimuli were applied every 20 seconds when searching for typical mossy fibre responses. In order to identify mossy fibre inputs, several stringent criteria were applied when maximizing the position of stimulus and recording electrodes: 1) a measurable latency (peak 8-10 msec) of the response onset that is compatible with afferent mossy fibre activation at room temperature (Derrick *et al.*, 1991), 2) pronounced facilitation of f-EPSP amplitude (>150%) upon an increase of stimulus frequency from 0.1 Hz to 1 Hz and 3) depression of evoked f-EPSPs > 70% by superfusion of DCG-IV at the end of each experiment. The slice was replaced if criteria 1 and 2 were unmet. As shown below (Figure 27), superfusion of BRS-015 (100  $\mu$ M) increased f-EPSP amplitude by  $41.5 \pm 10.6\%$  of control ( $n = 4$ ,  $P < 0.05$ , paired *t*-test). This effect was reversible upon wash-out of the compound. Application of the vehicle (DMSO) at a similar concentration as that used to solubilise BRS-015 had no effect. These results show that BRS-015 had a reversible enhancing effect on excitatory synaptic transmission from the dentate gyrus to CA3. Fortuitously, the results also indicated that the solvent concentration used for dissolution of BRS-015 was not responsible for the observed enhancing effect.

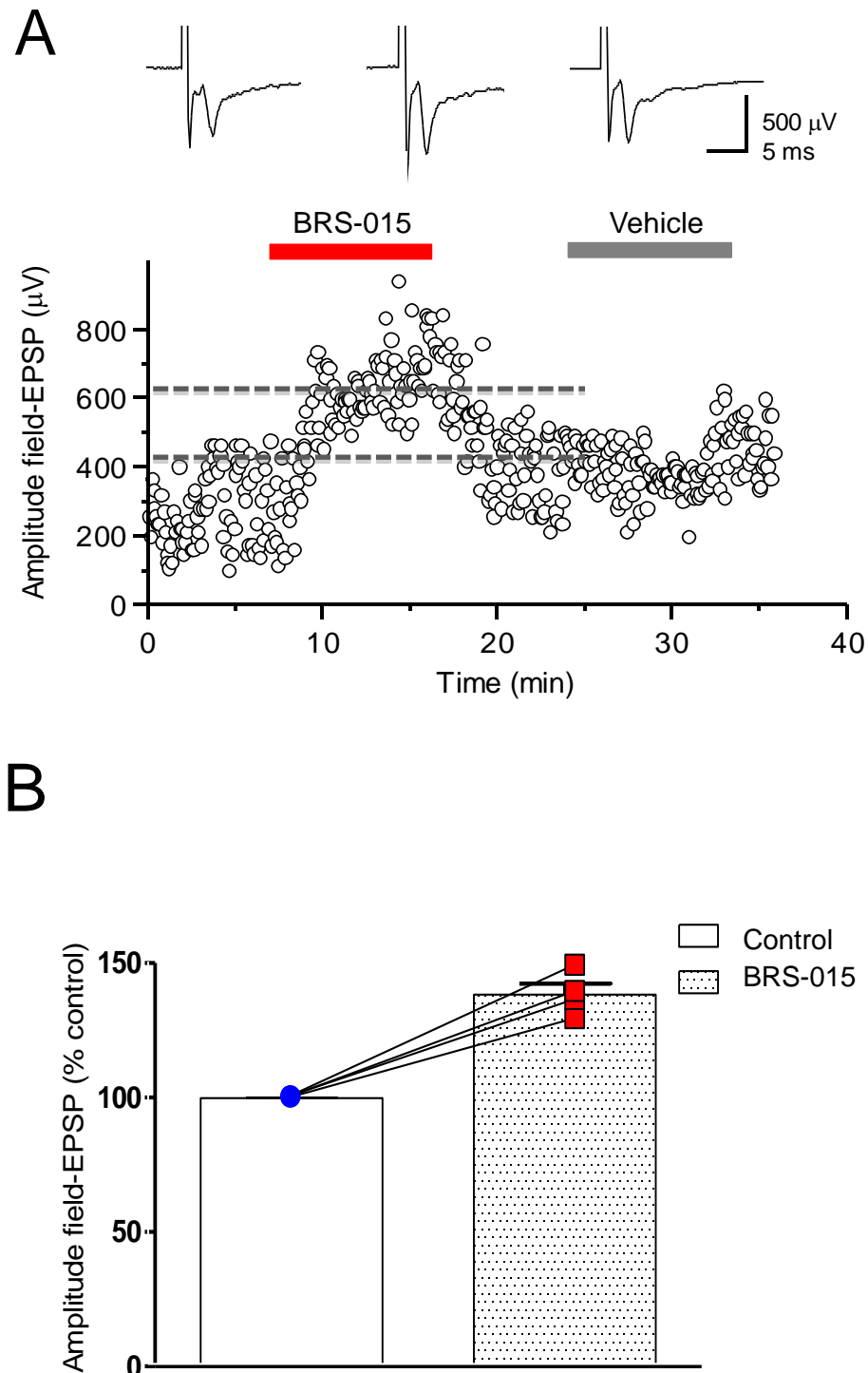


**Figure 27: BRS-015 enhances excitatory synaptic transmission from the dentate gyrus to CA3.** **A:** Plot of f-EPSP amplitude against time showing an increase upon superfusion of BRS-015 (100  $\mu\text{M}$ ) and no change upon superfusion of DMSO (0.1%). Representative example traces (averages of 5 consecutive f-EPSPs) obtained in each condition are shown above the plot (data from one slice). **B:** Summary bar chart from 5 extracellular recordings showing the enhancing effect of BRS-015.

With such a promising result in hand we decided to compare the effect of BRS-015 with the well-know drug piracetam in order to determine the potential of our compound with the most prominent memory enhancing drug. Previous studies had shown the onset of activity with piracetam in the CA1 region in the hippocampus at a concentration of 1 mM (Olpe and Lynch, 1982).

We elected to employ the same protocol to measure mossy fibre f-EPSPs as for the initial screening of BRS-015 in order to obtain a comparative result. Following this initial study, we observed that piracetam at low concentrations (100  $\mu$ M), was essentially inactive and had no effect on basal neurotransmission at mossy fibre synapses. Only superfusion of piracetam at much higher concentrations (500  $\mu$ M) led to a limited increase in f-EPSP amplitude (Figure 28). However, even at this concentration it was essentially inactive as it only increased f-EPSP amplitude by  $9.3 \pm 3.8\%$  of control as shown below ( $n = 3$ ,  $P < 0.05$ , paired  $t$ -test).

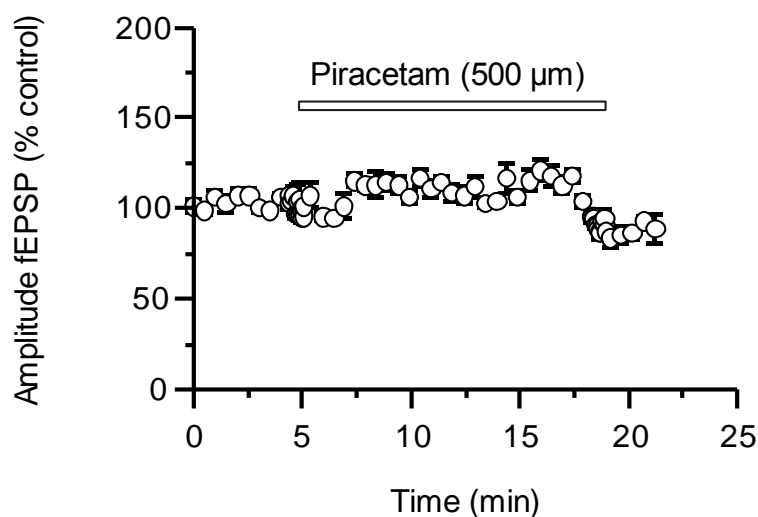
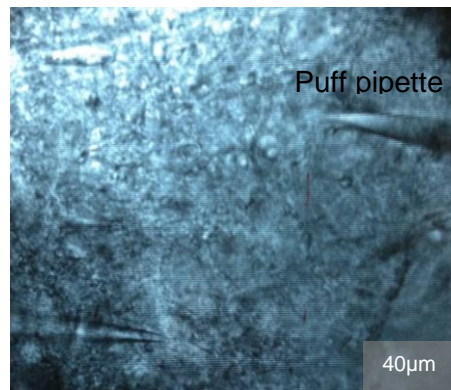


**Figure 28: Piracetam enhances excitatory synaptic transmission from the dentate gyrus to CA3.** Plot of EPSP amplitude against time showing an increase upon superfusion of piracetam (500  $\mu$ M) (summary of 3 extracellular recordings).

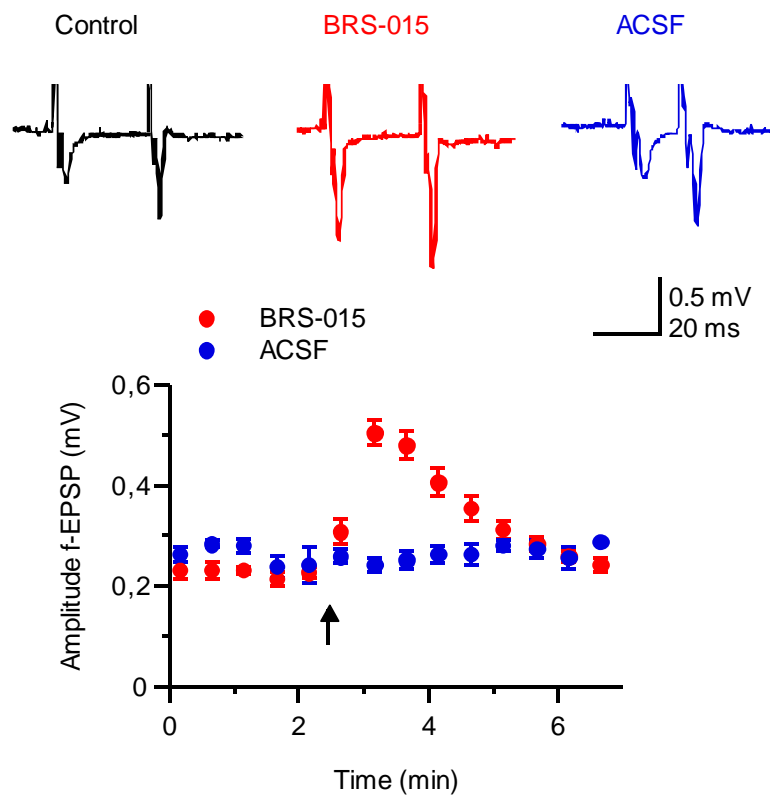
With such an initial promising demonstration that the comparative activity of our compound was better than the current drug used to treat memory disorders, we decided to investigate the mechanism of the action of BRS-015 in more detail to explore its potential.

Due to the fact that bath application of BRS-015 will affect many neurones and synapses within the slice neuronal network, we elected to selectively apply the compound locally at the border between the stratum radiatum and stratum lucidum, in close vicinity (50-200 micrometers) to the electrode used for extracellular recordings. As shown in Figure 29, puff application of BRS-015 (10-30 psi, 10-20 ms; 100 mM in a patch pipette) increased f-EPSP amplitude by  $82.3 \pm 6.6$  % of control ( $n = 4$ ,  $P < 0.001$ , paired  $t$ -test, Figure 29). We also observed that the effect was quickly reversible and was not accompanied by a change in the paired-pulse ratio of evoked synaptic responses (PPR control:  $1.56 \pm 0.13$ , BRS-015:  $1.51 \pm 0.11$ ,  $n = 4$ ;  $P > 0.05$ , Figure 30). To verify that the enhancing effect of BRS-015 was not due to a mechanical artefact, a pipette containing ACSF was introduced in the tissue and positioned at exactly the same location as the BRS-015 containing pipette. We observed that ACSF puffs of similar intensities and durations as those used for BRS-015 puffs had no effect on f-EPSPs amplitude, arguing against mechanical disturbance induced by pressure application.

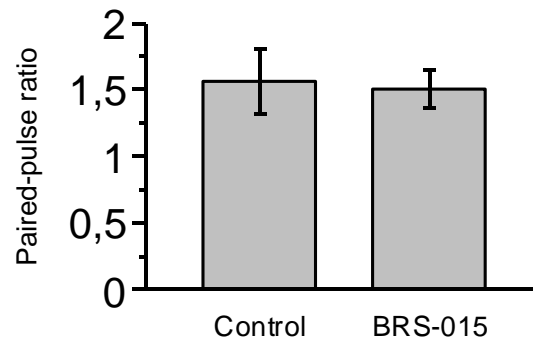
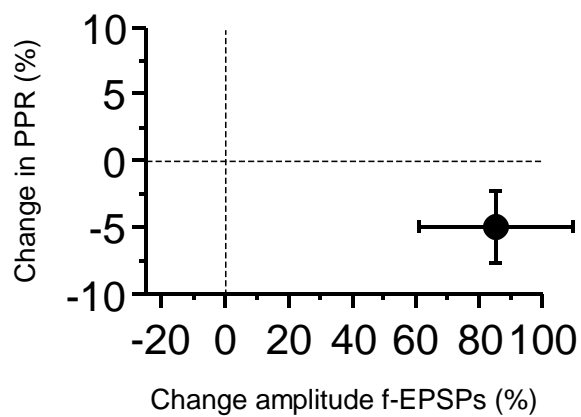
A



B



**Figure 29: Local application of BRS-015 in stratum lucidum increases the amplitude of dentate-evoked f-EPSPs recorded from CA3** **A:** Infrared–DIC image showing a puff pipette (top right) used for local pressure application of BRS-015 (100  $\mu$ M intrapipette, 10 sec, 20 psi) positioned  $\sim$ 150  $\mu$ m away from the recording electrode (bottom left) located in stratum lucidum. **B:** In red: plot of EPSP amplitude against time showing an increase upon local pressure application of BRS-015; in blue: no change occurs following local application of control solution ACSF in the same slice. Data are from 4 extracellular recordings.

**A****B**

**Figure 30: The enhancing effect of BRS-015 is not accompanied by a change in paired-pulse ratio of f-EPSP amplitude. A:** Summary bar chart showing no change in the paired-pulse ratio of f-EPSPs amplitude when BRS-015 was applied locally. **B:** Similar data expressed against the magnitude of f-EPSP facilitation. Data were pooled from 4 extracellular recordings.

In summary, although these preliminary experiments were performed from one animal, the results clearly suggested that BRS-015 has a reversible and powerful enhancing effect on glutamatergic transmission from the dentate gyrus to CA3, possibly by acting directly at mossy fibre synapses. The caveat of the approach, however, is that the concentration of BRS-015 that reaches the synapses is unknown.

## 6.2. Whole-cell patch-clamp recordings

### 6.2.1. Effect of BRS-015 on electrical properties of CA3 pyramidal neurones

Due to the fact that the facilitation of evoked f-EPSPs as shown above could result from increased excitability in CA3 pyramidal neurones (e.g. a change in  $R_{in}$ ), whole-cell recordings were undertaken to examine possible changes in the electrical membrane properties and firing patterns. Current-clamp recordings were performed in CA3 pyramidal cells using a K-gluconate based pipette solution, whilst obviating DC current injection when applying step protocols in current-clamp mode. GABAergic transmission was blocked by adding picrotoxin (50  $\mu$ M) and CGP-52432 (10  $\mu$ M) in the bath. I-V relations were obtained in every cell by delivering a series of hyperpolarising and depolarising current steps (-100 pA – +120 pA) until steady-state firing was reached. Superfusion of BRS-015 (100  $\mu$ M) did not alter the membrane potential (control:  $-69.8 \pm 2.7$  mV, BRS-015:  $-65.4 \pm 3.9$  mV,  $n = 5$ ,  $P > 0.05$ ) or the  $R_{in}$  of CA3 pyramidal neurones (control:  $246.4 \pm 18.9$  M $\Omega$ , BRS-015:  $212.84 \pm 27.6$  M $\Omega$ ,  $n = 5$ ,  $P > 0.05$ ). In addition, BRS-015 had no effect on the mean firing frequency of CA3 pyramidal neurones (control:  $7.4 \pm 1.3$  Hz, BRS-015:  $7.1 \pm 1.1$  Hz,  $n = 5$ ;  $P > 0.05$ ). Finally, rheobase current was not affected by the application of BRS-015 (control: 38 pA, BRS-015: 36 pA,  $n = 5$ ;  $P > 0.05$ ). A summary of these results is presented in Figure 31.

These findings support the notion that BRS-015 has little effect on the intrinsic electrical membrane properties in individual neurones and favor the hypothesis that enhancement of synaptic transmission consecutive to BRS-015 application might result from an action on synaptic conductances or changes in afferent excitability which would then translate into increased glutamate release and/or increased number of active synapses. They also emphasise that the increase in EPSC amplitude is unlikely to result from a network effect, where overall excitability would be enhanced.

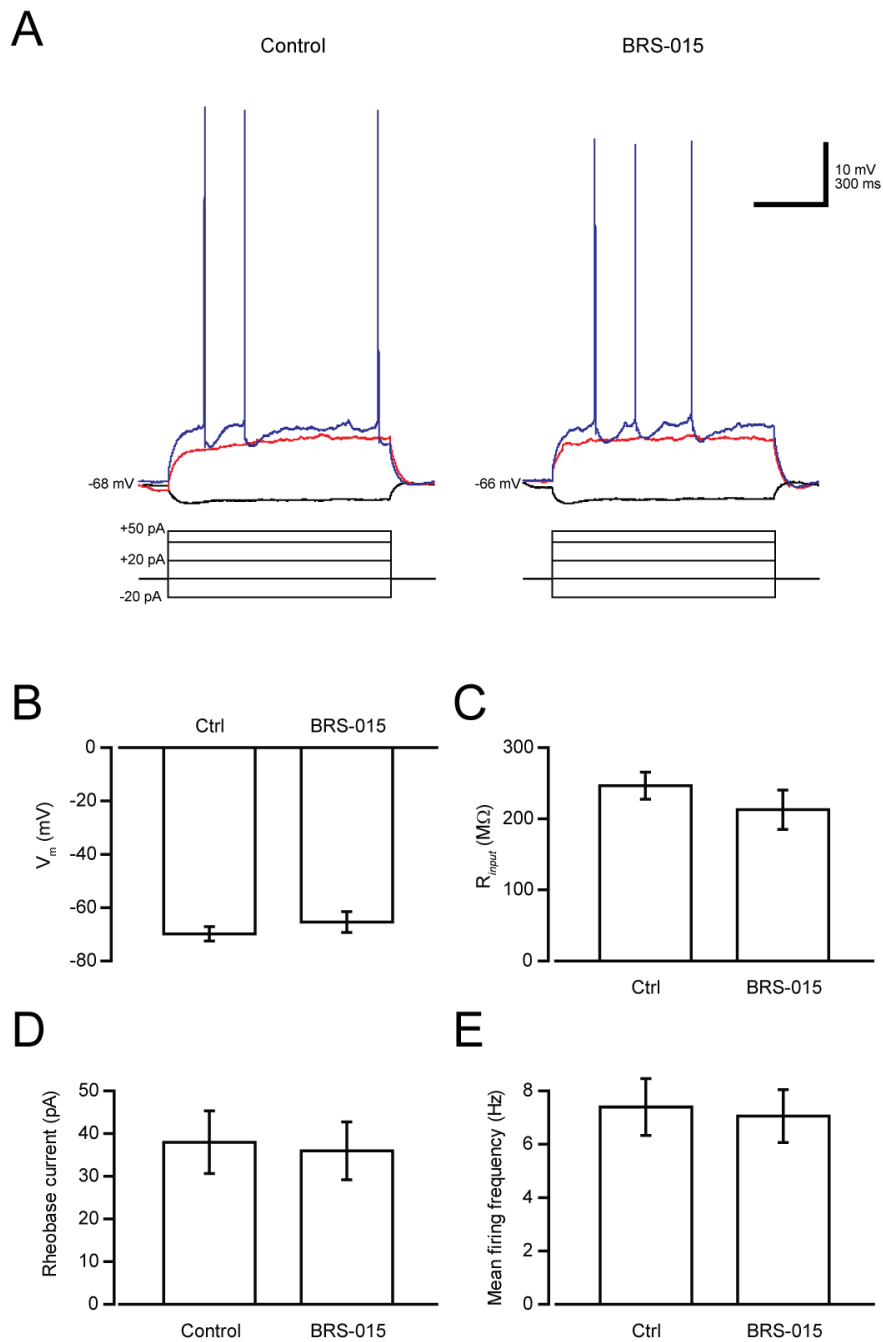


**Figure 31: BRS-015 does not alter the basic electrical membrane properties of CA3 pyramidal neurones:** **A:** Representative traces showing the effect of BRS-015 on sub-threshold and supra-threshold voltage responses. The current injected for sub-threshold voltage deflection is +40 pA and the rheobase current is +50 pA. In the background of BRS-015, the rheobase current of +50 pA remains unchanged, eliciting the same number of action potentials. **B – E:** Summary histograms showing no effect of the superfusion of BRS-015 (100  $\mu$ M) on the membrane potential, input resistance, rheobase current and mean firing frequency of CA3 pyramidal neurones (data pooled from 5 recordings).

### 6.2.2. Effect of BRS-015 on dentate-evoked EPSCs

In this second set of patch clamp recordings we looked at the effects of BRS-015 on dentate-evoked EPSCs recorded in CA3 pyramidal neurones held in voltage-clamp mode at  $V_{holding} = -70$  mV. Glutamatergic responses were recorded in the continuous presence of the GABA<sub>A</sub> receptor antagonist picrotoxin (50  $\mu$ M) and the GABA<sub>B</sub> receptor antagonist CGP-52432 (10  $\mu$ M). Dentate stimuli were delivered at a basal frequency of 0.1 Hz and a 50 ms inter-stimulus interval (20 Hz) was chosen for paired stimuli. As shown in Figure 32, superfusion of BRS-015 (100  $\mu$ M) increased the amplitude of evoked EPSCs by  $77.8 \pm 11.3\%$  of control amplitude ( $n = 5$ ,  $P < 0.003$ , paired  $t$ -test). The holding current measured before and after application of BRS-015 was not significantly different ( $\Delta I_{holding}$ :  $10.9 \pm 8.3$  pA,  $P > 0.1$ , paired  $t$ -test). Interestingly, the potentiating effect of BRS-015 decreased before wash-out. Finally, bath application of the mGluR II agonist DCG-IV (1  $\mu$ M) depressed dentate evoked EPSCs by ( $70.7 \pm 29.3\%$ ,  $n = 4$ ;  $P < 0.05$ ) implying that they were mediated by activation of mossy fibre synapses.

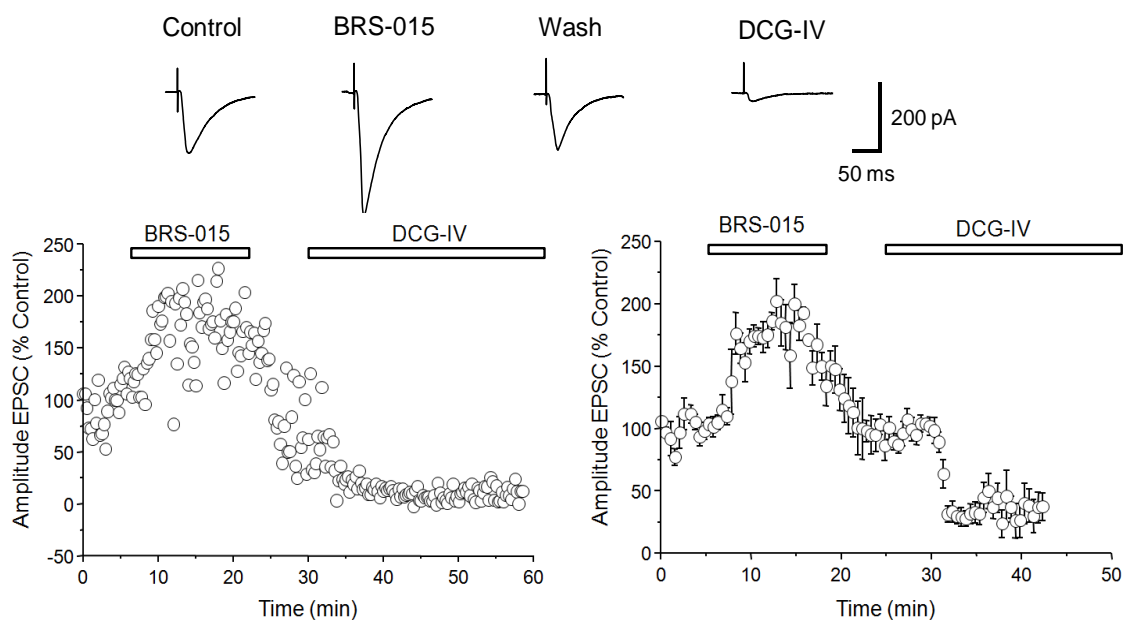


**Figure 32: BRS-015 facilitates evoked mixed AMPA/KA receptor-mediated EPSCs in CA3 pyramidal neurones.** **Left:** Plot of normalised EPSC amplitude against time showing an increase upon superfusion with BRS-015 (100  $\mu$ M) and depression by the group II metabotropic glutamate receptor agonist DCG-IV (1  $\mu$ M). (Data are from one CA3 pyramidal neurone). **Right:** Summary plot based on data from 5 neurones (5 slices) (each point represents the mean  $\pm$  S.E.M).

### 6.2.3. Dose - response relation: $EC_{50}$ .

Several experiments were performed based on a similar design to cover a range of differing concentrations of BRS-015 (Figure 33). Again, a stimulus electrode was implanted in the stratum lucidum and whole-cell voltage-clamp recordings were obtained from visually identified CA3 pyramidal neurones held in voltage-clamp. Bath application of BRS-015 (0.01-0.1  $\mu\text{M}$ ,  $n = 2$ ) had no effect whereas BRS-015 (1  $\mu\text{M}$ ,  $n = 4$ ) reversibly enhanced EPSCs by  $7.1 \pm 6.7\%$ . When testing higher concentrations, BRS-015 was applied at 10 and 100  $\mu\text{M}$  and was shown to enhance evoked EPSCs by  $39.2 \pm 8.4\%$  ( $n = 4$ ) and  $72.9 \pm 4.7\%$  ( $n = 5$ ), respectively. Increasing the concentration of BRS-015 up to 1 mM yielded further facilitation of evoked EPSCs with an initial saturation of the effect depicted as a plateau in the dose-response relation ( $85.1 \pm 4.9\%$  amplitude increase,  $n = 2$ ). Fitting the concentration-facilitation curve with a logistic function yielded an  $EC_{50}$  of 12  $\mu\text{M}$ .

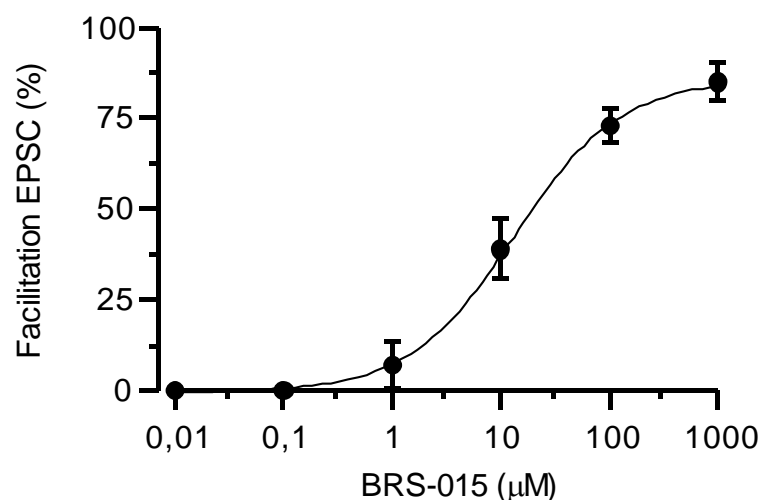


**Figure 33: The effect of BRS-015 on dentate-evoked EPSCs in CA3 pyramidal neurones is concentration-dependent.** Concentration-facilitation curve showing the relation between BRS-015 concentration (logarithmic scale) and the enhancement of EPSC amplitude in CA3 pyramidal neurones. Doses below 1  $\mu\text{M}$  had no effect whereas a higher concentration of 1 mM enhanced EPSCs amplitude by ~80%. Each concentration was tested at least in 3 CA3 pyramidal neurones. Fitting the relationship with a logistic function yields an  $EC_{50}$  of 12  $\mu\text{M}$ .

Although higher concentrations were not tested, these results clearly highlight the dose-dependent effects of BRS-015 on synaptic transmission as shown by the sigmoid relation between dose and enhancement of EPSC amplitude. The compound appeared active at concentrations as low as 1  $\mu\text{M}$  indicating good tissue penetration and high propensity to modulate excitatory synaptic transmission. In summary, BRS-015 has a powerful enhancing and reversible action on excitatory synaptic transmission at mossy fibre – CA3 synapses ( $\text{EC}_{50}$  of 12  $\mu\text{M}$ ) without altering the intrinsic electrical properties in CA3 pyramidal neurones.

### 6.3. Effect of BRS-015 on the paired-pulse ratio and decay-time constant of evoked EPSCs

The evidence presented so far indicated that BRS-015 facilitated mossy fibre-CA3 pyramidal cell transmission and increased the amplitude of mossy fibre evoked-EPSCs by >80% (Figure 34). A possible explanation for such an increase could be that compound BRS-015 increases glutamate release from presynaptic sites. Alternatively, increased glutamate binding to postsynaptic receptors might occur in the presence of BRS-015. Therefore our next step was to analyse changes in the paired-pulse ratio of the amplitude of evoked synaptic responses and to examine differences in the decay-time constant of evoked EPSCs following BRS-015 application. These two measurements were performed to gain insight into changes affecting the release probability and the biophysical properties of postsynaptic receptors respectively.

The ratio of amplitude of two consecutive EPSCs elicited with a 50 ms interval (20 Hz) was compared before and after application of BRS-015 (100  $\mu$ M). The PPR of EPSC amplitude was not significantly affected by BRS-015 (control:  $1.86 \pm 0.34$ , BRS-015:  $1.52 \pm 0.14$ ,  $n = 5$ ;  $P > 0.05$ ). This result could suggest that BRS-015 does not influence glutamate release probability at large mossy fibre – CA3 synapses.

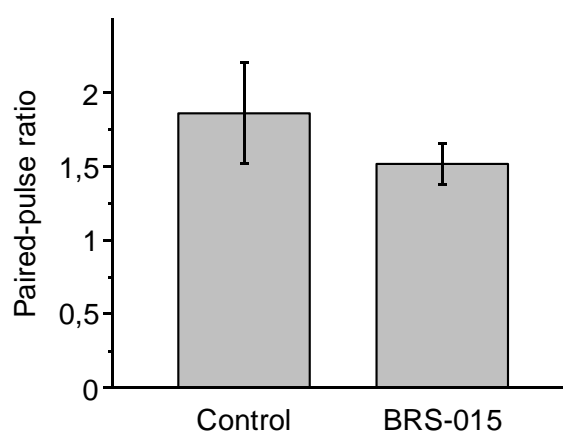


**Figure 34: Lack of effect of BRS-015 on paired-pulse ratio of mossy fibre-evoked EPSCs.** Summary histogram showing a non-significant reduction of the paired-pulse ratio of EPSCs amplitude in the presence of BRS-015 (100  $\mu$ M). Data are presented from 5 CA3 pyramidal neurones;  $P > 0.05$ , paired  $t$ -test.

Compound BRS-015 could also act on glutamate receptors in the postsynaptic membrane, by a mechanism that enhances glutamate receptor affinity and thus glutamate binding. Indeed, glutamate binding to postsynaptic receptors for a longer time could lead to larger EPSCs in pyramidal neurones. Differences in the EPSC decay-time constant could indicate such an increase in affinity. To analyse EPSCs kinetics, consecutive traces were averaged and scaled to their maximum peak amplitude in control conditions and in the presence of BRS-015 (100  $\mu$ M). As shown in Figure 35, EPSCs decays were then fitted with a single exponential function to extract the decay-time constant,  $\tau_m$ .

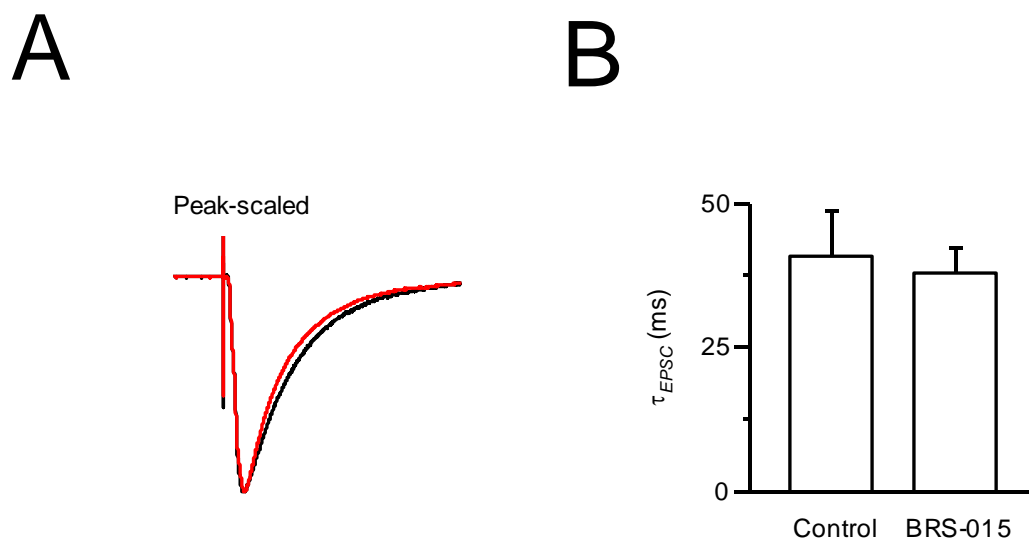


**Figure 35: BRS-015 has no effect on dentate-evoked EPSCs decay-time constant in CA3 pyramidal neurones:** **A:** Superimposed peak-scaled EPSCs (averages on 5 consecutive trials) taken from 1 CA3 pyramidal cell in control condition (black trace) and under superfusion of BRS-015 (100  $\mu$ M) (red trace). **B:** Summary bar plot showing no significant difference in EPSC decay-time constant between control and BRS-015 groups (Data presented are from 5 neurones (5 slices)  $P > 0.05$ , paired  $t$ -test).

Comparing  $\tau_m$  before and after superfusion of BRS-015 did not yield a significant difference ( $\tau_m$  control  $40.8 \pm 7.8$  ms,  $n = 5$ ;  $P < 0.05$ ,  $\tau_m$  **BRS-015:**  $37.9 \pm 4.3$  ms,  $n = 5$ ;  $P < 0.05$ ). Thus it is unlikely that the enhancement of EPSC amplitude induced by BRS-015 resulted from changes in EPSC kinetics, as those observed when glutamate spills over from neighboring synapses or when receptor affinity has increased.

#### **6.4. Effect of BRS-15 on pharmacologically isolated EPSCs**

Electrical stimulation in the dentate gyrus evokes EPSCs in CA3 pyramidal neurones whose components may be pharmacologically distinguished by using appropriate specific glutamate receptor antagonists. Hence, we analysed the effect of BRS-015 on firstly NMDA receptor-mediated EPSCs and secondly, kainate receptor mediated EPSCs and compared the results to those obtained when recording mixed AMPA/kainate EPSCs as shown in the results above.

#### 6.4.1. Effect on NMDA receptor-mediated EPSCs

In order to record NMDA-mediated EPSCs, CA3 pyramidal cells were held in voltage-clamp mode at  $V_{holding} = +40$  mV while GABA<sub>A</sub>, GABA<sub>B</sub>, AMPA and kainate receptors were blocked by bath application of picrotoxin (50  $\mu$ M), CGP 52432 (5  $\mu$ M) and NBQX (20  $\mu$ M), respectively. As shown below in Figure 36 NMDA-EPSCs had the tendency to run-down. However, superfusion of BRS-015 (100  $\mu$ M) had no major effect on their amplitude (decreased by  $4.0 \pm 13.5\%$  of control,  $n = 6$ ;  $P > 0.05$ , paired  $t$ -test). NMDAR-mediated EPSCs were completely abolished with addition of *D*-APV (50  $\mu$ M) in the perfusion solution showing that they were mediated by NMDA receptors. These results show that NMDA receptor-mediated EPSCs are not affected by compound BRS-015.

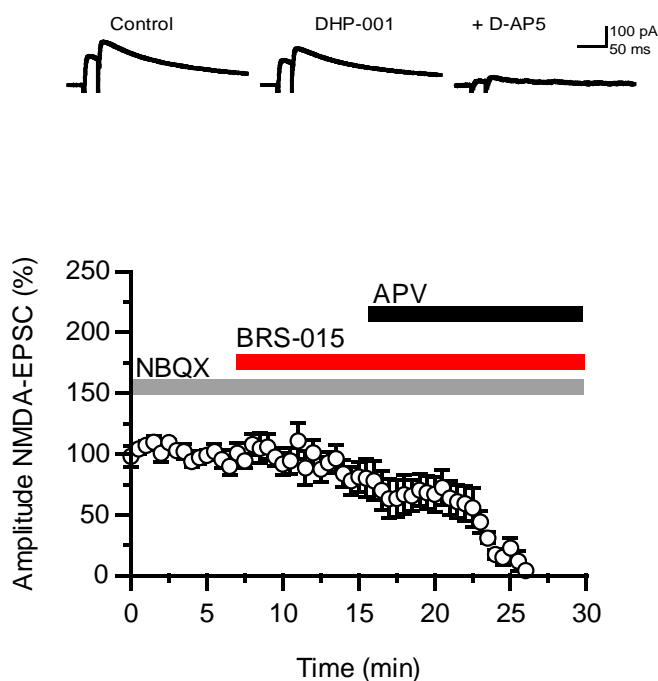


**Figure 36: BRS-015 does not affect NMDA receptor-mediated EPSCs in CA3 pyramidal neurones.** Plot of normalised NMDA receptor-mediated EPSC amplitude against time showing no effect of BRS-015 (100  $\mu$ M) when AMPA and kainate receptors were blocked with NBQX (20  $\mu$ M). Representative NMDA receptor-mediated currents (NMDAR-EPSC, averages of 5 consecutive trials) are shown on top. (Data from 6 CA3 pyramidal neurones.) There was a slight run-down of NMDA receptor mediated EPSC that developed with time.

### 6.5. Effect on kainate receptor-mediated EPSCs

Kainate receptor-mediated EPSCs form a minor component of the evoked response implying that kainate receptors could potentially be modulated by BRS-015. In order to isolate kainate receptor-mediated EPSCs, AMPA receptors were blocked by addition of GYKI-53655 (50  $\mu$ M) in the perfusion solution together with all other antagonists. Again, cells were held in voltage-clamp at -60 mV using a CsCl-containing micropipette. After obtention of a stable baseline, BRS-015 was then added to the bath and the effect on kainate receptor mediated transmission analysed. BRS-015 (100  $\mu$ M) did not affect the amplitude of kainate receptor-mediated EPSCs (decrease of  $2.2 \pm 1.4\%$ ,  $n = 5$ ,  $P > 0.05$ , paired  $t$ -test, Figure 37). The holding current measured before and after application of BRS-015 was not significantly different either ( $\Delta I_{\text{holding}}$ :  $10.9 \pm 8.3$  pA,  $P > 0.1$ , paired  $t$ -test).

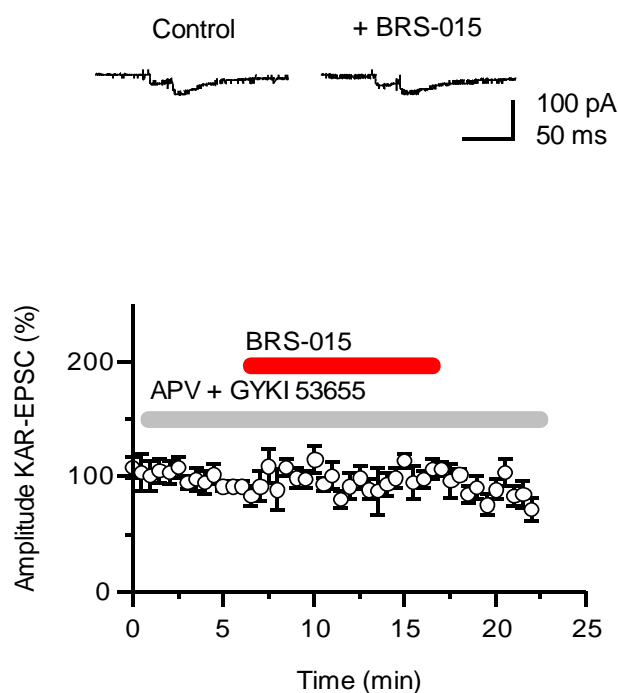


**Figure 37: No effect of BRS-015 on kainate receptor-mediated EPSCs in CA3 pyramidal neurones.** Plot of normalised EPSC amplitude against time showing no effect of BRS-015 (100  $\mu$ M) when NMDA receptors were blocked with *D*-AP5 (50  $\mu$ M) and AMPA receptors blocked with GYKI 53655 (50  $\mu$ M) (Data from 5 CA3 pyramidal neurones). Representative kainate receptor mediated currents (KAR-EPSC, averages of 5 consecutive trials) are shown on top.

The final application of NBQX (20  $\mu$ M) completely abolished evoked EPSCs demonstrating that they were mediated by kainate receptors (not shown). Thus, neither NMDA receptors nor kainate receptors seemed to be directly modulated by compound BRS-015 prompting the possibility that it could act as an AMPA receptor modulator.

## 6.6. Summary of pharmacological manipulations

So far, the cumulative pharmacology experiments seemed to indicate that BRS-015 facilitates glutamatergic neurotransmission by enhancing AMPA receptor function. Using selective glutamate receptor antagonists, we determined that BRS-015 enhanced mixed AMPA/kainate receptor-mediated EPSCs but had no effect on NMDA or kainate receptor-mediated EPSCs studied in isolation. A histogram summarising the results obtained from different pharmacological manipulations is shown below in Figure 38.

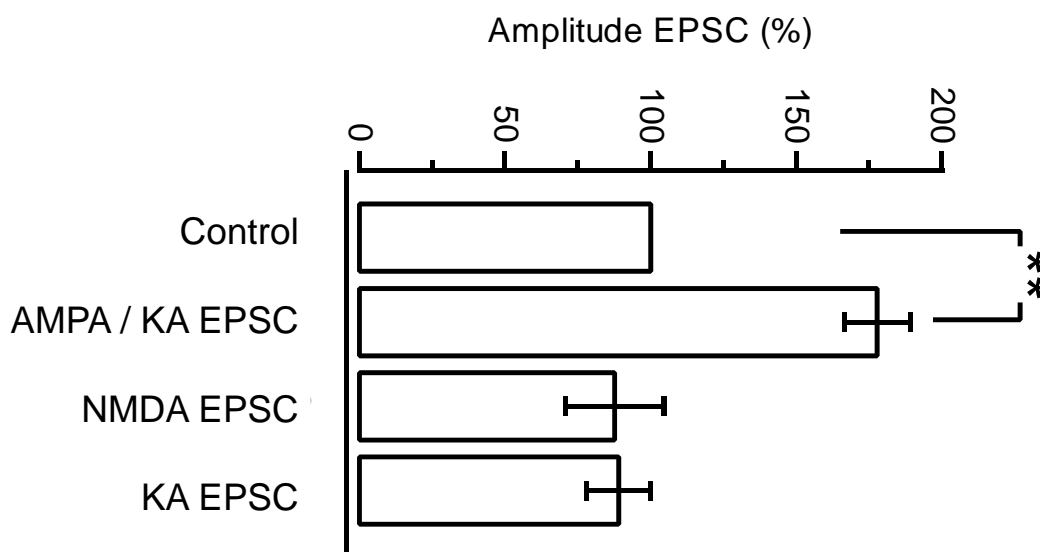


**Figure 38: Bar chart summarising the effect of BRS-015 on pharmacologically isolated EPSCs in CA3 pyramidal neurones.** BRS-015 selectively potentiated mixed AMPA and kainate receptor-mediated EPSCs but had no effect on NMDA or kainate receptor-mediated EPSCs (\*\*,  $P < 0.01$ ; unpaired  $t$ -test).

Whether this selective action on mixed AMPA/KA receptor-mediated EPSCs is a consequence of direct modulation of AMPA receptors by BRS-015 remains to be demonstrated in studies performed in expression systems and in binding studies. Other potential candidate mechanisms would involve direct AMPA receptor subunit phosphorylation and increased cell surface expression of AMPA receptors.

### **6.7. Effect of BRS-015 on glutamate-evoked currents in CA3 pyramidal neurones.**

One potential mechanism by which BRS-015 could modulate AMPA receptor-mediated neurotransmission is by direct binding to AMPA receptors in the postsynaptic membrane. If this was the case, then BRS-015 should enhance glutamate-evoked currents recorded from CA3 pyramidal neurones. To test this hypothesis, *L*-glutamate was puff-applied with a Picospritzer (100 mM intrapipette, puff pressure 5 – 20 psi, puff duration 10 -50 ms; every 60 sec) approximately 50-150  $\mu\text{m}$  away from a patched CA3 pyramidal neurone held with a Cs-Cl electrode at  $V_{\text{holding}} = -70$  mV. GABA receptors were blocked with picrotoxin (50  $\mu\text{M}$ ) and CGP 52432 (5  $\mu\text{M}$ ), and NMDA receptors with *D*-APV (50  $\mu\text{M}$ ). As shown in Figure 39, when pressure-applying glutamate onto the recorded neurone, inward currents were recorded as a reversible increase in  $I_{\text{holding}}$  that lasted 0.8 – 1.2 seconds. Repetitive glutamate application every minute in control conditions elicited inward currents that did not show signs of desensitisation. Superfusion of BRS-015 (100  $\mu\text{M}$ ) increased the amplitude of glutamate-evoked currents by  $51.3 \pm 14.7\%$  ( $n = 5$ ;  $P < 0.05$ , paired *t*-test, Figure 39). This effect was reversible and decreased before wash-out, similar to the effects on electrically-evoked EPSCs. Application of CNQX (50  $\mu\text{M}$ ) at the end of the experiments almost abolished glutamate-evoked currents confirming that they were largely mediated by AMPA and KA receptors.

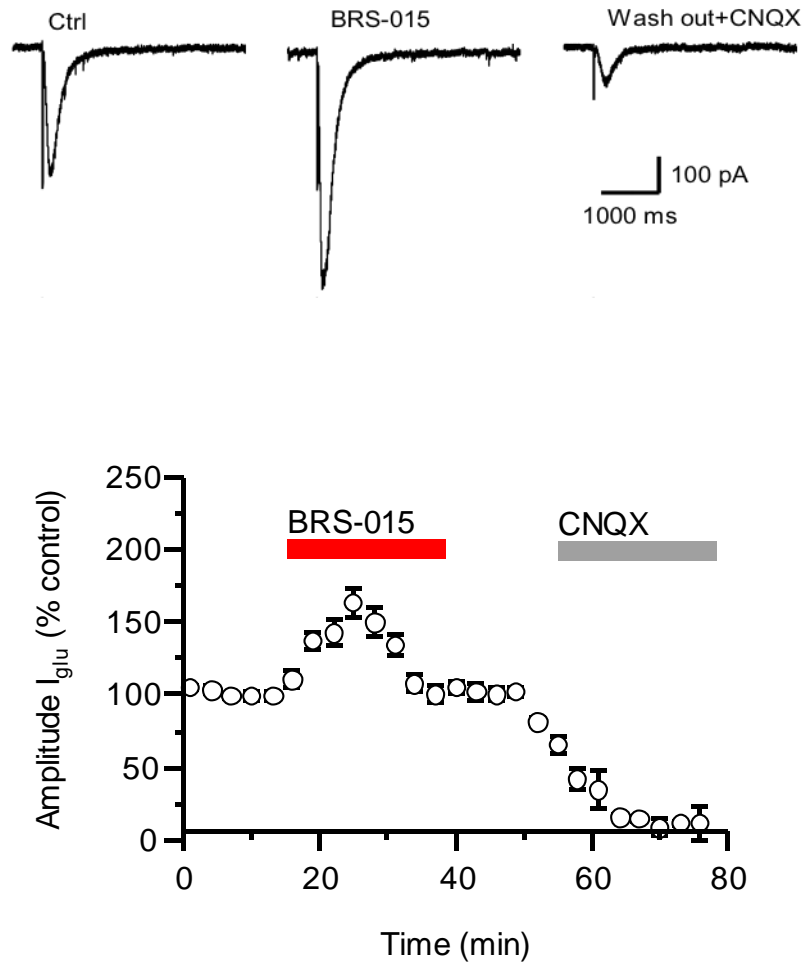


**Figure 39: BRS-015 enhances glutamate-evoked currents in CA3 pyramidal neurones:** Amplitude of puff-evoked glutamate currents plotted against time showing a reversible increase upon superfusion of BRS-015 (100  $\mu$ M). Application of CNQX (50  $\mu$ M) at the end of the experiment demonstrated that glutamate responses were mediated by AMPA and kainate receptors, but also involved other receptors as judged by the residual current. Data presented are from 3 different slices. Traces on top show glutamate currents recorded in the different pharmacological conditions (single traces).

These experiments showed that a postsynaptic cationic conductance mediated by direct activation of AMPA and kainate receptors with exogenous glutamate induced inward currents that were substantially enhanced, thus mimicked the effect of BRS-015 on stimulus-evoked EPSCs in CA3 neurones. Interestingly, the level of facilitation of glutamate-evoked mixed AMPA/KA currents was of the same order of magnitude as that of evoked EPSCs.

## 6.8. Effect of BRS-015 on mossy fibre LTP

In addition to the acute enhancing action of BRS-015 on baseline excitatory synaptic transmission at mossy fibre synapses, we tested the hypothesis that BRS-015 could modulate LTP induction. LTP is a long lasting change in synaptic strength that is expressed when presynaptic afferences are stimulated repetitively at high frequency (e.g. 100 Hz). The classic Hebbian LTP is present at Schaffer collateral synapses in the CA1 region and it is dependent on NMDAR (Harris and Cotman, 1986). Unlike LTP in the CA1 region, the induction of mossy fibre LTP is independent of NMDAR activation. However, recent studies by Rebola indicated an existence of NMDAR-dependant metaplasticity at MF synapses, in which NMDARs act as a switch to generate LTP, which is expressed and maintained by the presence of an increased number of active AMPA receptors at the potentiated synapse (Rebola *et al.*, 2011).

In a first set of experiments, we examined the effect of BRS-015 on NMDA receptor-independent mossy fibre LTP (MF-LTP) in slices superfused with picrotoxin (50  $\mu$ M), CGP-52432 (10 M) and *D*-AP5 (50  $\mu$ M). A bipolar stimulus electrode was placed in the stratum granulosum in the dentate gyrus to activate granule cells and their mossy fibre inputs and a second electrode positioned in the distal part of stratum radiatum, to activate associational-commisural fibres (A/C) acting as a control pathway (Figure 40).

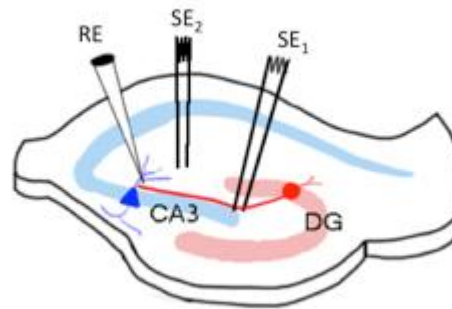


**Figure 40: Drawing of the experimental design.** A stimulus electrode ( $SE_1$ ) was positioned in the hilus at the start of area CA3 stimulating mossy fibre (red) exiting a granule cell in the dentate gyrus (DG) and the recording electrode (RE) in stratum lucidum next to synapses on pyramidal cell dendrites (blue). Second stimulus electrode ( $SE_2$ ) was positioned in the distal part of stratum radiatum, to activate associational-commissural fibres (A/C) acting as a control pathway.

Electrical stimulation was delivered every 10 seconds at one or the other pathways and tetanic stimulation was delivered to the mossy fibre input only. As shown in Figure 41, a subthreshold stimulus burst  $HFS_1$  (100 Hz for 1 sec) delivered in the stratum granulosum caused postsynaptic potentiation of f-EPSPs ( $74.5 \pm 30.6\%$ ,  $n = 4$ ,  $P > 0.05$ ) but their amplitude returned to baseline after 5-7 minutes. This stimulus protocol did not affect f-EPSPs evoked by stimulation of A/C fibres (Figure 42) indicating little cross-contamination between the two pathways. Consecutive application of BRS-015 (100  $\mu$ m) increased stratum granulosum-evoked f-EPSPs by  $81.4 \pm 43.8\%$  ( $n = 4$ ,  $P > 0.05$ ) but had no significant effect on A/C evoked responses (increase of  $8.9 \pm 14.7\%$ ,  $n = 5$ ,  $P > 0.05$ ). In the continuous presence of BRS-015, the strength of the stratum granulosum stimulus was then reset to match the amplitude of f-EPSPs before  $HFS_1$ . After a period of recording of baseline activity, a second stimulus ( $HFS_2$ ) of the same strength as  $HFS_1$  was then applied. The amplitude of f-EPSPs measured 20 minutes after  $HFS_2$  was increased by  $47.8 \pm 10.6\%$  ( $n = 4$ ,  $P < 0.05$ , paired  $t$ -test). Final application of DCG-IV (1  $\mu$ M) depressed stratum-granulosum evoked f-EPSPs by  $82.8 \pm 3.8\%$  ( $n = 4$ ,  $P < 0.01$ , paired  $t$ -test) confirming that they were mediated by mossy fibre synapses (not shown).

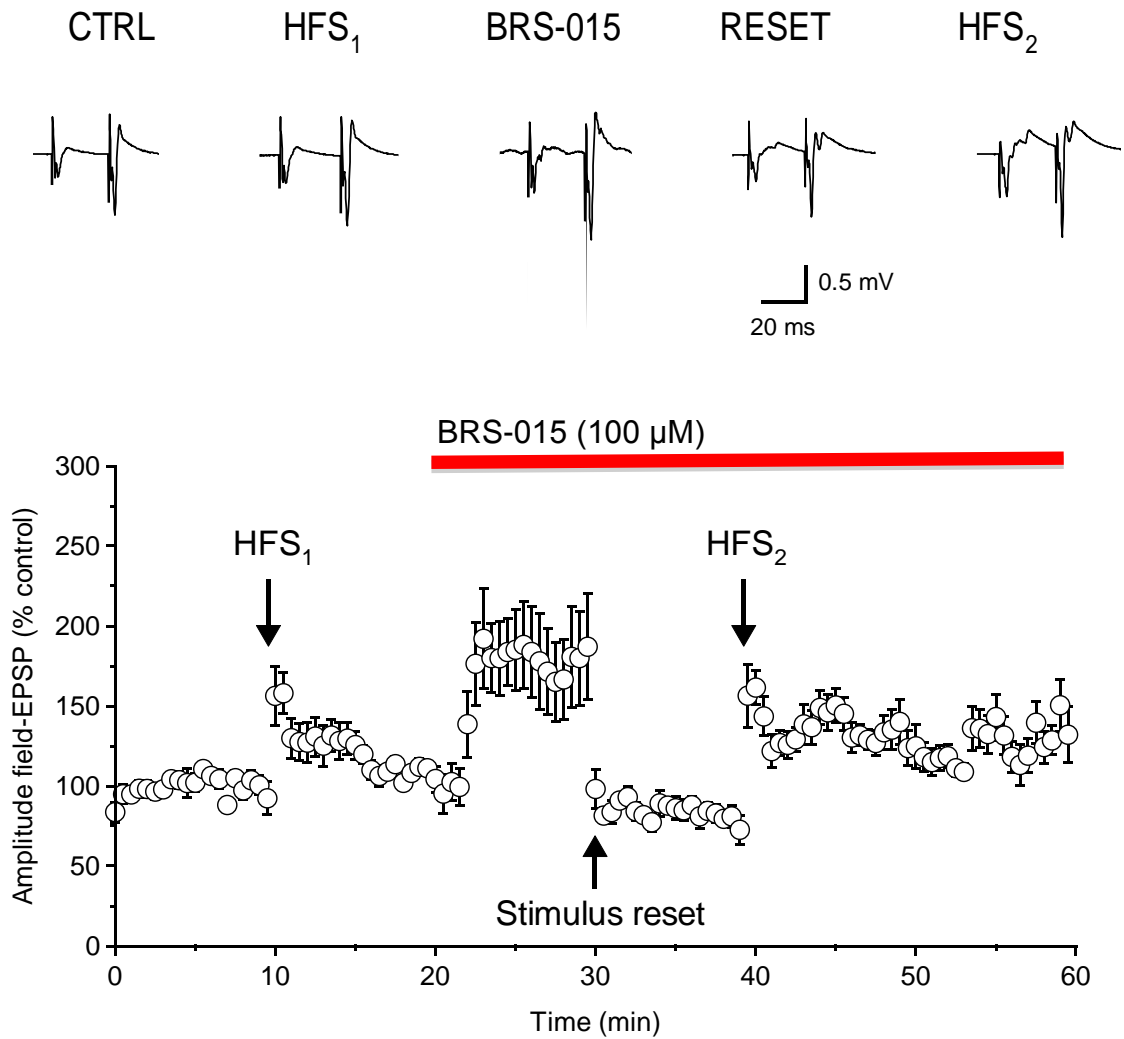


**Figure 41: BRS-015 lowers the threshold for induction of mossy fibre LTP.** Normalised f-EPSP amplitude plotted against time showing that a sub-threshold high-frequency stimulus train (HFS<sub>1</sub>: 100 Hz for 1 second) does not induce LTP in contrast to a second sub-threshold stimulus (HFS<sub>2</sub>) delivered 20 minutes following BRS-015 (100 μM) superfusion, leading to sustained LTP. A stimulus reset was performed when the enhancing effect of BRS-015 on f-EPSP amplitude had reached a maximum. The stimulus strength was then lowered to match the size of f-EPSPs before HFS<sub>1</sub>. Representative paired f-EPSPs (inter-stimulus interval 20 ms) are shown on top (averages of 5 consecutive trials). Data are plotted as mean ± S.E.M and are presented from recordings obtained in 4 slices from 4 animals. Picrotoxin (50 μM), CGP-52432 (10 μM) and *D*-AP5 (50 μM) were included in the perfusion solution.

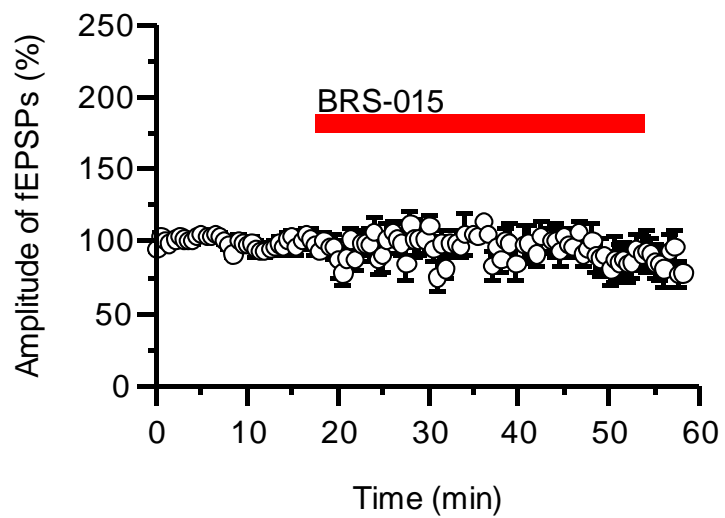
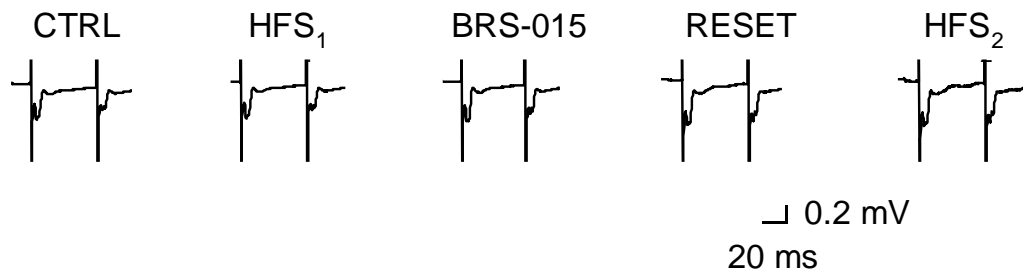


**Figure 42: BRS-015 does not alter basal synaptic transmission at A/C fibre – CA3 synapses.** Data are represented as mean  $\pm$  S.E.M and are from the same experiments as those shown in Figure 41.

It has been shown that NMDA receptors contribute to a form of LTP that is expressed postsynaptically at mossy fibre – CA3 synapses (Rebola *et al.*, 2011). This form of LTP differs from the NMDA receptor independent LTP examined above, the locus of which is presynaptic. Thus, in a second set of experiments, we explored whether the effect of BRS-015 on the induction of MF-LTP differed when NMDARs were left intact and were not blocked. In this case, *D*-AP5 was omitted from the perfusion medium but the same LTP induction paradigm was used. As shown in Figure 43, a subthreshold stimulus burst HFS<sub>1</sub> (100 Hz for 1 sec) delivered in the stratum granulosum again caused postsynaptic potentiation of f-EPSPs ( $55.4 \pm 17.9\%$ ,  $n = 10$ ,  $P > 0.05$ ) but their amplitude returned to baseline. Consecutive application of BRS-015 (100  $\mu$ M) increased stratum granulosum-evoked f-EPSPs by  $24.9 \pm 9.1\%$  ( $n = 7$ ,  $P > 0.05$ ). The amplitude of f-EPSPs measured 20 minutes after HFS<sub>2</sub> was also enhanced by  $79.6 \pm 16.9\%$  ( $n = 7$ ,  $P < 0.05$ , paired *t*-test). Final application of DCG-IV (1  $\mu$ M) depressed f-EPSPs to  $56 \pm 15.4\%$  ( $n = 5$ ,  $P < 0.01$ , paired *t*-test) confirming that they were mediated by mossy fibre synapses.

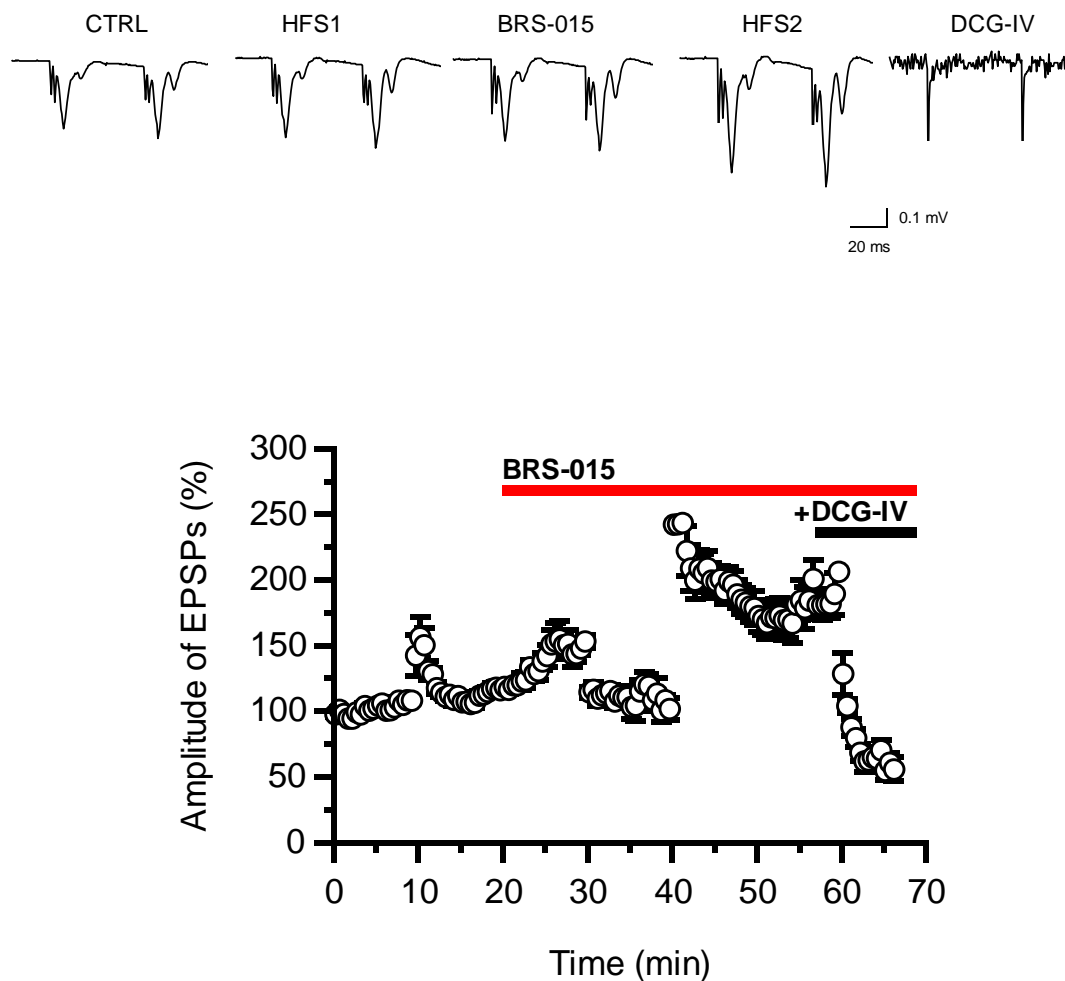


**Figure 43: Effect of BRS-015 on mossy fibre LTP in the absence of NMDA receptor blockade.** Normalised f-EPSP amplitude plotted against time showing that a sub-threshold high-frequency stimulus train (HFS<sub>1</sub>: 100 Hz for 1 second) does not induce LTP in contrast to a second sub-threshold stimulus (HFS<sub>2</sub>) delivered 20 minutes following BRS-015 (100  $\mu$ M) superfusion, leading to sustained LTP. The pronounced depression of evoked responses consecutive to DCG-IV application confirms that they were mediated by mossy fibre synapses. A stimulus reset was performed when the enhancing effect of BRS-015 on f-EPSP amplitude had reached a maximum. The stimulus strength was then lowered to match the size of f-EPSPs before HFS<sub>1</sub>. Representative paired f-EPSPs (inter-stimulus interval 20 ms) are shown on top (averages of 5 consecutive trials). Data are plotted as mean  $\pm$  S.E.M and are presented from recordings obtained in 4 slices. Picrotoxin (50  $\mu$ M) and CGP-52432 (10  $\mu$ M) were included in the perfusion solution.

Comparing the magnitude of LTP measured 15 minutes after when BRS-015 (100  $\mu$ M) was applied in the presence or absence of an NMDA receptor antagonist yielded a non-significant increase of  $22 \pm 16.5\%$  when NMDA receptors were left unblocked (Figure 44, LTP-*D*-AP5:  $44.6 \pm 16.5\%$ ,  $n = 4$ ; LTP- no *D*-AP5,  $66.6 \pm 21.7\%$   $n = 8$ ;  $P > 0.05$ , Wilcoxon Rank Sum test for unpaired data).

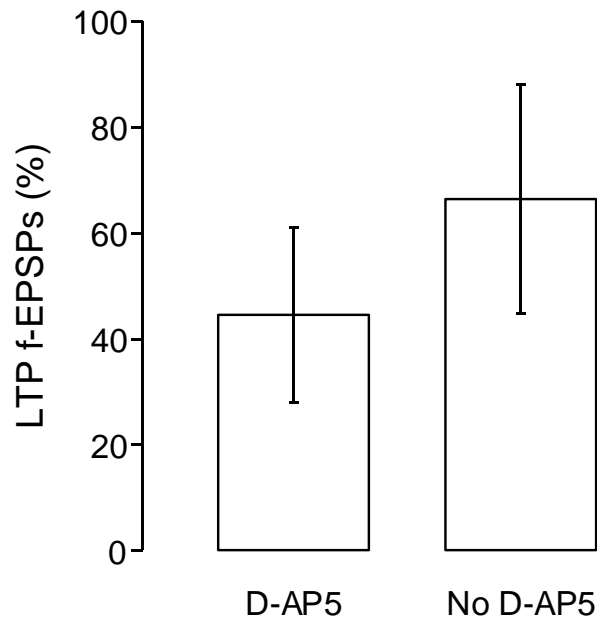


**Figure 44: Comparing the effect of BRS-015 on mossy fibre LTP in the presence or absence of the NMDA receptor antagonist *D*-AP5.** All experiments were performed in the presence of GABA<sub>A</sub> and GABA<sub>B</sub> receptor blockers added to the perfusion solution.

In a third set of experiments, the effect of BRS-015 was analysed when synapses had already been potentiated using a standard high-frequency stimulation induction protocol made of 3 bursts of 100 stimuli at 100 Hz separated by 10 seconds. As shown in Figure 45, this protocol induced a large post-tetanic potentiation of f-EPSPs followed by decay and a period of mossy fibre LTP. When BRS-015 (100  $\mu$ M) was applied during this period of sustained plasticity no effect on f-EPSPs amplitude was observed ( $0.5 \pm 15$  % decrease,  $n = 4$ ;  $P > 0.05$ ).

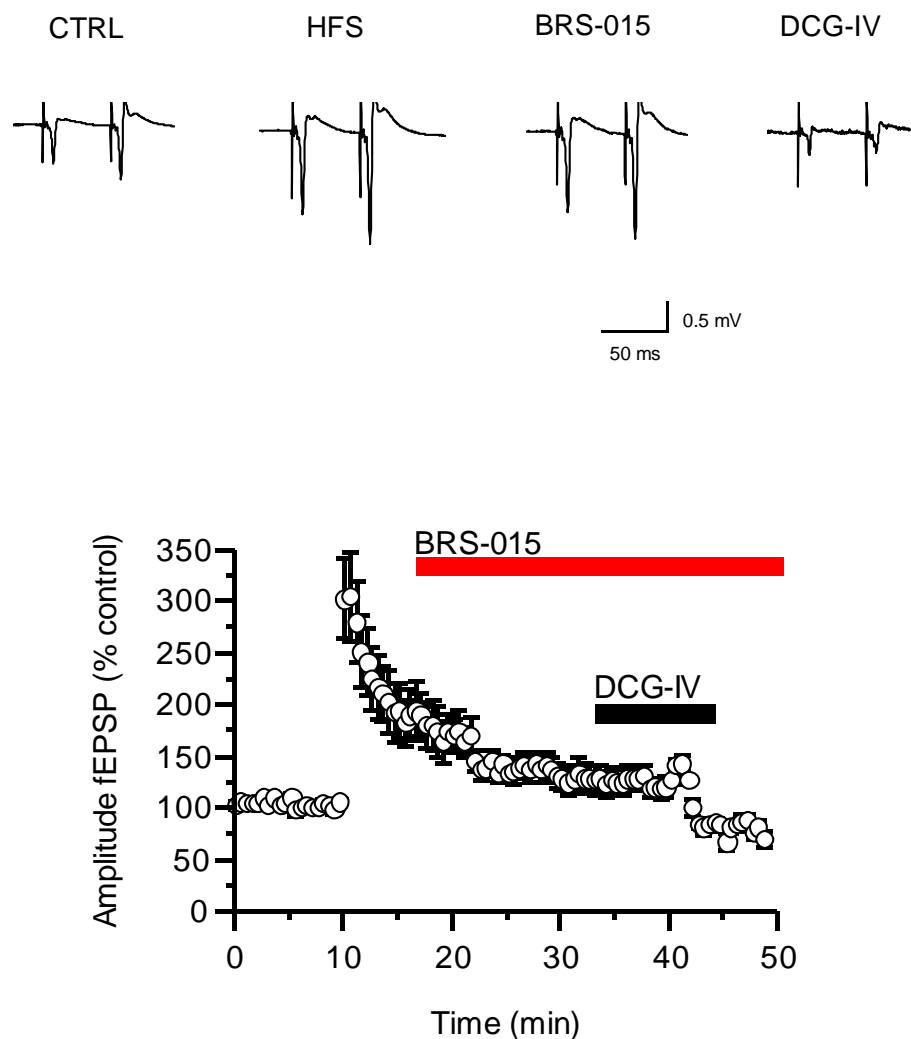


**Figure 45: BRS-015 does not affect synaptic transmission at synapses that undergo mossy fibre LTP.** No effect of BRS-015 during sustained LTP induced by HFS (3 times 100 Hz for 1 sec, every 10 sec) and depression by DCG-IV (1  $\mu$ M).

Taken together, these experiments demonstrated that BRS-015 lowers the threshold for induction of MF-LTP without altering the shorter form of plasticity known as PTP. They also suggested that A/C synapses have a different sensitivity to BRS-015 compared to mossy fibre synapses. Furthermore, they illustrated that the magnitude of plasticity attained when bath-applying the compound had little dependence upon NMDA receptors being available, in line with a mechanism driven by AMPA receptor modulation. Lastly, compound BRS-015 had no effect when applied after mossy fibre synapses underwent LTP. Most likely, saturation of LTP might have prevented further enhancement of f-EPSPs by the compound (ceiling effect).

### **6.9. Effect of single enantiomers of BRS-015 on evoked glutamatergic synaptic transmission from the dentate gyrus to CA3**

From our results, we have shown that BRS-015 is a highly potent small molecule, which causes a large increase in synaptic transmission and potentiation and as such, has good potential for further development. However, despite its activity, a key question remains which relates to its structure. BRS-015 is obtained as a racemate following the intramolecular acylal cyclisation and as such, both the (+)- and (-)-enantiomers were present in our assays. The initial focus of this thesis was directed towards identification of the molecular target and we were therefore unable to separate each enantiomer due to a lack of time, but if BRS-015 or related congeners are to progress towards pre-clinical development, there is a need to determine whether it is the racemate or a single enantiomer that is active and accounts for its enhancing activity.

The literature is replete with drugs that have been supplied to patients as racemic mixtures, only for the deleterious effects of one of the enantiomers to emerge. The most prominent of these is thalidomide, which caused such tragic consequences in unborn infants the 1970's. It was supplied as a single enantiomer for the treatment of morning sickness, but underwent racemisation under physiological conditions, where its supposedly inactive enantiomer led to its notorious effects on limb growth. As such, regulatory agencies have since pushed for single enantiomers as treatments and if BRS-015 or a related compound is to progress towards development as a drug, we therefore need to address this key question and investigate the activity and toxicity of both enantiomers.

There are a number of methods that are available whereby enantiomers can be separated, but due to time restraints, BRS-015 was separated by chiral HPLC of the racemate by Reach Separations who were able to separate ~ 50 mg of each enantiomer from 200 mg of the racemate. With each enantiomer in hand, we looked at the effect of (-)- and (+)-BRS-015 on mossy fibre f-EPSPs at a concentration of 100  $\mu$ M. As can be seen below, superfusion of (-)-BRS-015 (100  $\mu$ M) caused an increase in f-EPSP amplitude by  $73.5 \pm 15.1\%$  of control (Figure 46;  $n = 5$ ,  $P < 0.05$ ), paired  $t$ -test). However, under the same conditions,

superfusion of (+)-BRS-015 (100  $\mu$ M) had no effect on f-EPSP amplitude (Figure 47; increase of  $0.2 \pm 3.2\%$  of control  $n = 5$ ,  $P > 0.05$ , paired  $t$ -test). Final application of DCG-IV (1  $\mu$ M) depressed stratum-granulosum evoked f-EPSPs  $> 70\%$ , confirming that they were mediated by mossy fibre synapses.

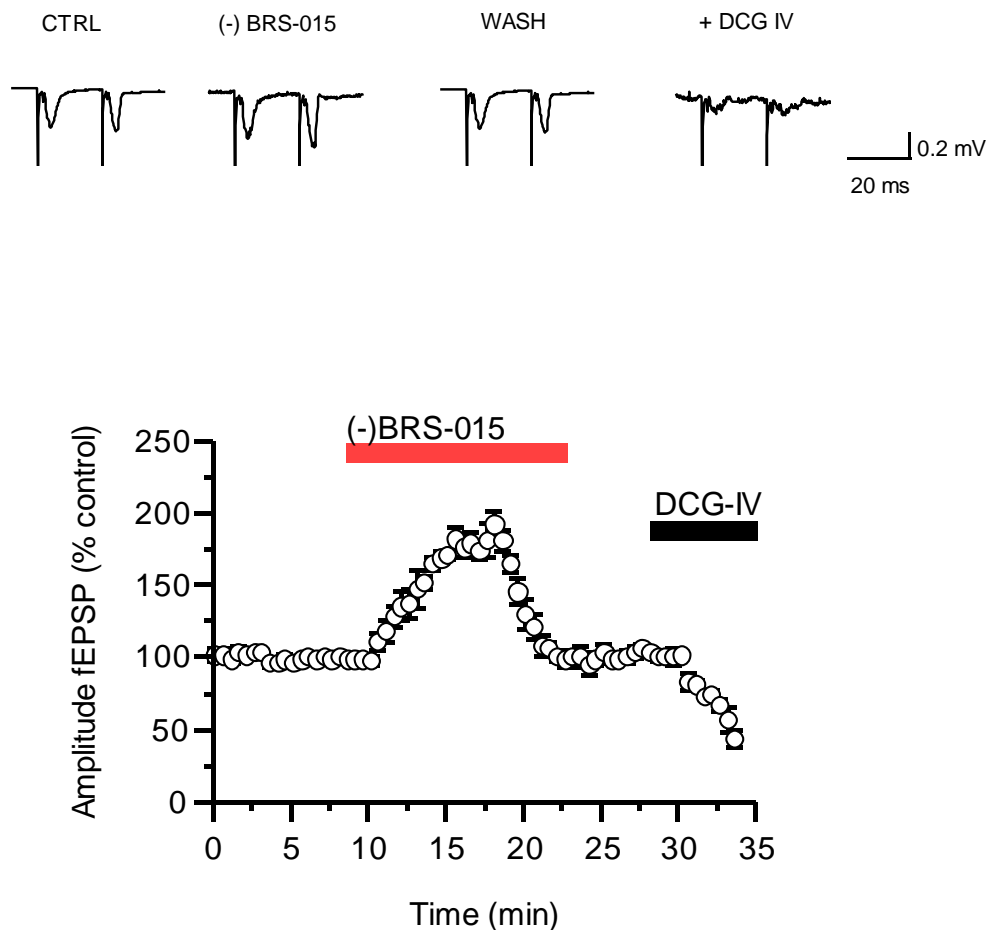


**Figure 46: The effect of (-)-BRS-015 on basal synaptic transmission. A:** Plot of EPSP amplitude against time showing an increase upon superfusion of (-)-BRS-015 (100  $\mu$ M) and depression upon superfusion by DCG-IV (1  $\mu$ M) (data from 5 extracellular recordings). Representative example traces (averages of 5 consecutive f-EPSPs) obtained in each condition are shown above the plot.

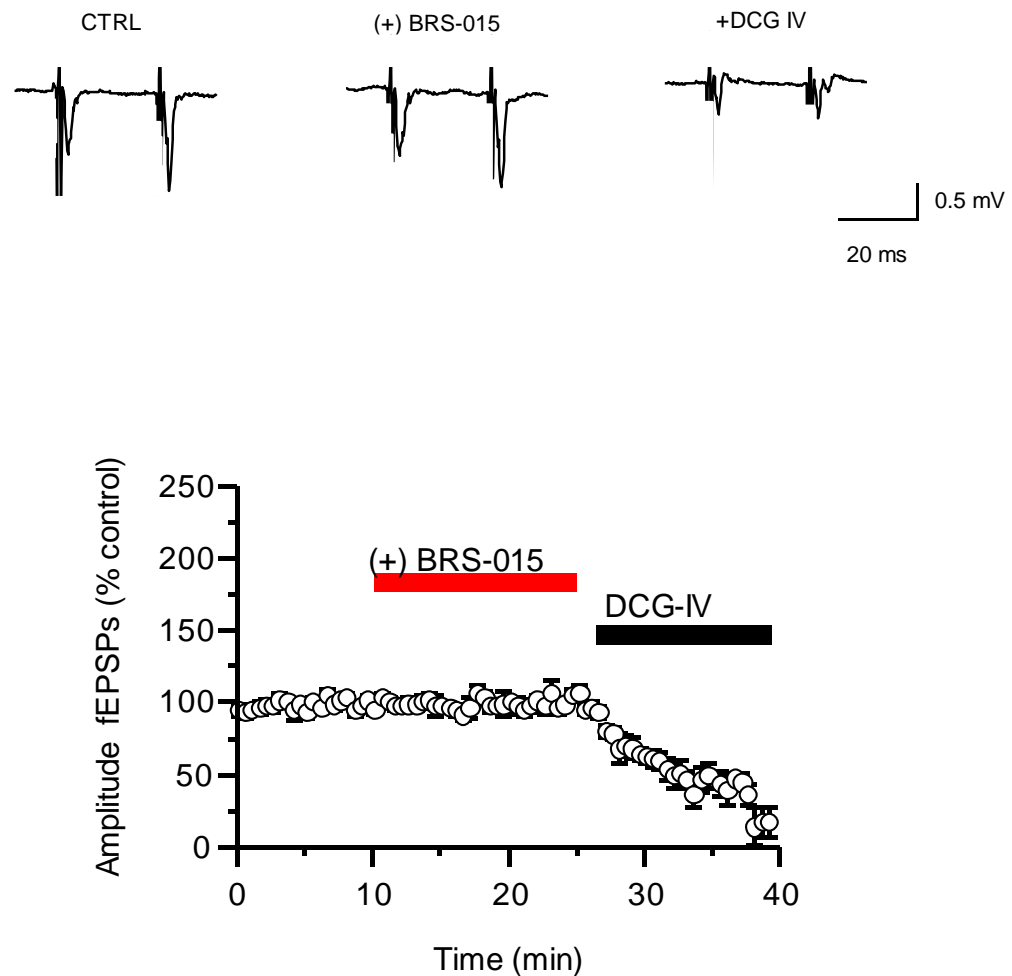


**Figure 47: The effect of (+)-BRS-015 on basal synaptic transmission. A:** Plot of EPSP amplitude against time showing no change upon superfusion of (+)-BRS-015 (100  $\mu$ M) and depression upon superfusion by DCG-IV (1  $\mu$ M) (data from 5 extracellular recordings). Representative example traces (averages of 5 consecutive f-EPSPs) obtained in each condition are shown above the plot.

## **7.0. Toxicity of BRS-015**

## 7.0. Toxicity of BRS-015

As a result of the fact that BRS-015 had displayed significant potential and enhanced EPSPs and fEPSCs to such a great extent, we elected to look at the toxicity profile of the racemate as all studies to date, had been performed on this mixture. The compound was first examined for its effects against CrFK cells (a feline liver cell line), which in our research group had proven useful for the determination of toxic compounds and was carried out at Vetsuisse in Zurich by Mr Christopher Asquith in the Hilton group.

The method used for the assay was the MTT assay, where 3-(4,5-dimethylthiazol-2-yl)-2,5-diphenyltetrazolium bromide (MTT) was used to determine the compounds' toxicity and viability of cells by MTT dye reduction. First 10,000 CRFK cells were eluted with Roswell Park Memorial Institute (RPMI) 1640 medium supplemented with 10% fetal bovine serum 100 M/mL Glutamine and 1% v/v antibiotic antimycotic (Ab/Am) (total volume 200  $\mu$ L) onto 96-well plates and incubated for 24 hours (37 °C, 5% CO<sub>2</sub>). The medium was then removed by vacuum and replaced with the specific dilution (1 nM-1 mM) to test the toxicity (3 x 200  $\mu$ L). BRS-015 was then suspended in 2% DMSO and RPMI 1640 medium supplemented with 10% fetal bovine serum 100 M/mL Glutamine (Gibco) and 1% v/v antibiotic/ antimycotic (Ab/Am) (Gibco) and diluted to the desired concentrations. After 24 hours, the wells were observed and the medium removed. The cells were then suspended in RPMI 1640 phenol red-free medium (180  $\mu$ L) and MTT (3 mg/mL) (20  $\mu$ L) and incubated 4 hours at (37 °C, 5% CO<sub>2</sub>). The medium was then removed by vacuum and the cells were lysed with methanol (200  $\mu$ L) to reveal a bright purple formazan product. The methanol-formazan absorbance was then determined at 570 nm using a BioTek Synergy HT plate reader with KC4 software. Data was expressed as the percentage of viability (normalised to cells with no exposure) of compound-treated wells compared to that of untreated control wells.

The 24-hour assay was designed to rule out any major toxicity issues, which was important as cytotoxic compounds removed at an early stage can prevent false positives and later development of toxic core structures. The MTT assay was used to quantify the level of cell viability, which is a colorimetric assay and

can be used for measuring the viability of living cells. The mitochondrial reductase enzymes reduce the tetrazolium salt, by cleavage of the central core to produce an insoluble formazan, which gives a purple colour. The assay measures the cellular metabolic activity *via* NADPH-dependent cellular oxidoreductase enzymes and the amount of formazan dye is directly proportional to the amount of viable cells (ratio between number of live versus dead cells).

BRS-015 performed well with a high concentration  $CC_{50}$  of 847.0  $\mu$ M. This leaves a wide range potential for dosing and avoids any short-term toxicity issues (Table 6).

Concentration	Absorbance <sup>a</sup>	Cell Count	Viability (%)
Medium	0.0457	10968	100.00
1nM	0.0487	11688	106.56
10nM	0.0517	12408	113.13
100nM	0.0490	11760	107.22
1 $\mu$ M	0.0500	12000	109.41
10 $\mu$ M	0.0484	11616	105.91
100 $\mu$ M	0.0480	11520	105.03
1mM	0.0177	4248	38.73
		$CC_{50} =$	847.0 $\mu$ M

**Table 6: Results of BRS-015 toxicity screening.** <sup>a</sup> Geometric mean, each concentration tested in triplicate after 24 hours, as a difference of the untreated cells.

To further develop BRS-015 and direct it towards lead development, further toxicity analysis was carried out using HepG2 cells, which are a human hepatocellular carcinoma cell line, whose cells are epithelial in morphology, as well as the 3T6 murine cell line, which was derived from a primary mouse embryonic fibroblast cells. Using this assay, cells (3T6 murine fibroblast) were grown to ~80% confluency in a 10-cm dish, before splitting to 96-well plates, 10% of the 10-cm dish per 96-well plate, 50  $\mu$ l per well. One column of 8 wells was left empty (to be a reagent blank in the assay). The cells were then allowed to grow overnight before drug was added to four wells at the starting concentration (typically 200  $\mu$ M) and in subsequent wells down a 1 in 2 dilution

series with the final four wells of cells where no drug was present. This allowed two drugs to be tested per 96-well plate. The cells were left in the presence of drug for 48 hrs. The medium was removed and the cells washed with PBS. The cell number was determined using a CytoTox 96<sup>®</sup> Non-Radioactive Cytotoxicity Assay (Promega) which is used to measure lactate dehydrogenase (LDH) that is released from lysed cells. LDH is a stable cytosolic enzyme that is measured with an enzymatic assay. The addition of the reaction buffer results in a conversion of a tetrazolium salt into a red formazan product that can be measured with a 96-well plate reader. The amount of colour formed is proportional to the number of cells lysed.

Cells were lysed with 50  $\mu$ l/well of single-strength lysis buffer for 45-60 minutes. This was followed by 50  $\mu$ l/well of LDH assay reagent for 30 minutes before terminating the reaction by the addition of 50  $\mu$ l/well stop buffer. The absorbance was read at 490 nm and the absorbance relative to untreated wells (untreated cells = 1.0) was plotted against drug concentration. The LD<sub>50</sub> was determined graphically from the concentration at which the absorbance falls to 50% of the control value.

From this assay, it was shown that BRS-015 was essentially non-toxic (2 mM max tested, n=6) using the 3T6 cell line. In the HepG2 cell line, BRS-015 presented with an LD<sub>50</sub> of 914  $\mu$ M, showing that HepG2 cells are marginally sensitive, with an LD<sub>50</sub> of 0.9 mM, which is a concentration that can be considered to be high.

From these combined assays, we clearly demonstrated that BRS-015 is surprisingly non-toxic to two different species derived cell lines and that due to its activity, it is a highly non-toxic compound that warrants further investigation.

## **8.0. Discussion & Conclusions**

## 8.0. Discussion and Conclusions

The research described in this thesis was based on the synthesis and activity of the novel compound BRS-015, which was discovered during the total synthesis of the natural product clausenamamide. Following its synthesis, analysis of its electrophysiological profile in acute hippocampal slices was carried out in order to try to determine its pertinent biological activity and mode of action.

Despite extensive studies into the effects and biological activities of nootropic drugs in the CA1 region of the hippocampus, the literature is surprisingly silent about their effects in the CA3 region (Kaneko et al., 1997, Moriguchi et al., 2013). Mossy fibre – CA3 pyramidal cell synapses provide a major excitatory input to the hippocampus and as such, are an ideal model with which to study the effects of nootropic drugs. In particular, mossy fibre synapses present a form of LTP whose induction is independent of NMDA receptors, thus narrowing our investigations into the mechanisms by which nootropic drugs might affect the threshold for synaptic plasticity. In addition, the large size of mossy fibre terminals allows direct patch-clamp measurements to be undertaken which enable investigations into presynaptic mechanisms, e.g. an effect of nootropic drugs on presynaptic ion channels or receptors. We therefore used this model as a means to determine the effect of compounds that were discovered during the total synthesis of clausenamamide. Finally, we limited our investigations towards glutamatergic transmission to CA3 pyramidal neurones.

### 8.1. The effect of BRS-015 on dentate – CA3 neurotransmission

Our results clearly demonstrate that our novel compound has a reversible enhancing effect on excitatory synaptic transmission mediated by hippocampal mossy fibre synapses. We analysed the effect of BRS-015 on basal synaptic transmission from the dentate gyrus to CA3 (Figures 27–38) and found that superfusion of BRS-015 had a powerful enhancing effect when compared with piracetam with annual sales of over \$2 billion (Figure 28), on responses elicited by activation of mossy fibre synapses. This effect was reversible and was not due to the effect of the solvent DMSO, as shown by the separate application of DMSO, which clearly had no effect on basal synaptic transmission (Figure 27).

In addition to bath-application, we also used local puff application of BRS-015 in order to deliver the compound near to active synapses made onto the recorded neurones and found that it increased synaptic transmission without altering the ratio of amplitude of paired f-EPSPs (Figures 29, 30).

These findings were validated in single cell experiments where we analysed the effects of BRS-015 on the electrical properties of CA3 pyramidal neurones as well as evoked EPSCs. Whilst it had no effect on the membrane potential, input resistance or firing rate in CA3 pyramidal neurones, superfusion of BRS-015 (100  $\mu$ M) reversibly enhanced the amplitude of evoked EPSCs by around 75%. Furthermore, the effect of BRS-015 on dentate-evoked EPSCs was concentration-dependent with an  $EC_{50}$  of 12  $\mu$ M (Figure 33).

We examined the effect of BRS-015 on synaptic transmission in the continuous presence of AMPA, AMPA/kainate and NMDA receptor antagonists in order to shed light on putative receptor targets (Figure 38). When AMPA receptors were blocked by GYKI-53655, superfusion of BRS-015 had no effect on kainate receptor mediated EPSCs. Similarly, NMDA receptor mediated EPSCs recorded in the presence of the AMPA/kainate antagonist NBQX were not affected by BRS-015. These results strongly suggested that BRS-015 may act as a positive modulator of AMPA receptors, thus enhancing synaptic transmission.

## **8.2. Mechanistic insights into the mode of action of BRS-015**

We demonstrated that BRS-015 does not change the intrinsic electrical membrane properties of CA3 pyramidal cells, namely the membrane potential, the input resistance, or the mean firing rate. These results suggest that the enhancing effect of BRS-015 on evoked EPSCs in CA3 pyramidal neurones is unlikely to result from changes in network excitability and emphasizes the potential of this compound to modulate an excitatory synaptic conductance in pyramidal neurones.

### 8.3. Pre- or postsynaptic mechanism of BRS-015?

Changes in the ratio of amplitudes of two consecutive synaptic responses evoked by a paired-pulse stimulus paradigm (e.g. 50 ms inter-stimulus interval) provide indirect information about whether a drug or compound affects transmitter release *via* a presynaptic mode of action (Zucker, 1989). The present results show that application of BRS-015 (100  $\mu$ M) had no effect on the paired-pulse ratio of evoked EPSCs suggesting that it does not modulate receptors or channels that regulate glutamate release probability (Figure 34). Again, this analysis emphasizes that the enhancing effect of BRS-015 on excitatory synaptic transmission is likely to originate from postsynaptic sites rather than *via* presynaptic modulation of glutamate release at mossy fibre synapses.

Further supporting evidence for direct AMPAR modulation by BRS-015 came from our results on the enhancing effect of BRS-015 on glutamate-induced currents in CA3 pyramidal neurones. Indeed, with NMDA receptors blocked, superfusion of BRS-015 (100  $\mu$ M) reversibly increased the amplitude of glutamate-induced currents by around 50% (Figure 39), in line with postsynaptic modulation of membrane conductance.

Overall, the data presented here are in line with previous studies in which a structural relative of BRS-015 – aniracetam – was found to facilitate glutamatergic transmission in the hippocampus. Aniracetam increased the amplitude of f-EPSPs evoked by stimulation of Schaffer collaterals (Staubli *et al.*, 1990; Xiao *et al.*, 1991) and had no effect on the paired-pulse ratio. Aniracetam was also shown to increase the size of glutamate-induced inward currents (Isaacson and Nicoll, 1991) and, similar to BRS-015, the effect was almost instantaneous and reversible. Piracetam, in contrast, had no effect on glutamate-evoked responses, indicating that not every member of the nootropic drug family possesses a similar enhancing effect on f-EPSPs (Isaacson and Nicoll, 1991, Heise, 1987). In our hands, only superfusion of a very high concentration of piracetam (500  $\mu$ M) gave a slight increase of f-EPSP amplitude of  $9.3 \pm 3.8\%$  (Figure 29;  $n = 3$ ,  $P < 0.03$ ), paired *t*-test) (Olpe and Lynch, 1982).

As shown by Arai and Suzuki (Arai *et al.*, 2004) nootropic drugs can also regulate the kinetics of AMPA receptors. Aniracetam was shown to reduce glutamate receptor desensitisation and slow the decay-time constant of evoked EPSCs (Isaacson and Nicoll, 1991, Ito *et al.*, 1990). Analysis of the corresponding EPSCs decay-time in our experiments revealed that BRS-015 has no effect. However, a more detailed investigation as to whether BRS-015 might alter AMPA receptor desensitization and kinetics would require experiments performed with outside-out patches from pyramidal cells. It was presented by Partin and co-workers that aniracetam can slow AMPARs channel closing machinery and as a consequence, the onset of their desensitization (Partin *et al.*, 1996). Interestingly, the enhancing effect of BRS-015 started to decrease before the wash-out period which could suggest modulatory action on AMPARs and associated desensitization.

#### **8.4. Effect of BRS-015 on synaptic plasticity**

Positive AMPA receptor modulators have frequently been shown to promote long-term potentiation, in addition to their known enhancing effects on various forms of memory in animals and humans *via* several different mechanisms (Arai *et al.*, 2004, Staubli *et al.*, 1990, Staubli *et al.*, 1994, Ingvar *et al.*, 1997).

We examined the effects of BRS-015 on mossy fibre synaptic plasticity and found that *i*) it had no effect on the large post-tetanic potentiation typical of mossy fibre synapses, *ii*) it lowered the threshold for LTP induced with a sub-threshold paradigm and *iii*) BRS-015 had no effect when it was delivered 20 minutes after LTP induction, i.e. when mossy fibre synapses had already been potentiated.

The use of a sub-threshold stimulus paradigm by itself was clearly insufficient to achieve sustained potentiation of postsynaptic responses. Such a limited stimulus therefore served as a sub-threshold LTP induction protocol to study the effect of BRS-015 on mossy fibre LTP. As previously noted by several groups (Arai *et al.*, 2004, Arai and Lynch, 1992), the possibility of generating LTP in the CA1 region under such condition is increased in the presence of an AMPA receptor modulator. In line with these studies, the sub-threshold high-frequency stimulation protocol used in our experiments elicited LTP only when BRS-015

(100  $\mu$ M) was present in the perfusion medium (Figures 41, 43). These results demonstrate that BRS-015 facilitated mossy fibre LTP by lowering its threshold of induction. However, whether this was a consequence of presynaptic modulation, or the result of enhanced AMPA receptor function still remains to be fully elucidated.

Interestingly, in the absence of an NMDA receptor antagonist, the amplitude of f-EPSPs measured 20 minutes after HFS<sub>2</sub> increased to  $179.6 \pm 16.6\%$  of baseline (Figure 44) compared to 132% when *D*-AP5 was included in the perfusion solution. Although circumstantial, this observation is in line with the recent idea that (Rebola *et al.*, 2011) NMDA receptors might drive a 'metaplastic switch' "making mossy fibre synapses competent for generating NMDAR-dependent LTP of AMPA EPSCs". Thus, during LTP induction, BRS-015 could act as a catalyst and 'awake' silent NMDARs at mossy fibre synapses *via* modulation of AMPA receptor activity. Conversely, functional AMPA receptor expression could be induced by NMDAR activation at initially silent synapses (Liao *et al.*, 1995, Durand *et al.*, 1996). This phenomenon might be relevant to LTP induction in the CA1 region where it can trigger the conversion from silent AMPA receptors to functional ones (Nicoll and Malenka, 1995). The facilitatory effect of BRS-015 on mossy fibre LTP could thus result from the interplay between direct AMPA receptor modulation and indirect recruitment of NMDA receptors consecutive to depolarisation and relief of the Mg<sup>2+</sup> block.

The magnitude of LTP that is frequently achieved in CA1 when superfusing compounds of the racetam family is typically between 30-60%, (Malykh and Sadaie, 2010) similar to the effect of BRS-015 (100  $\mu$ M). Interestingly, application of CX546 has been shown to result in an increase in LTP of almost 100% *via* AMPA receptor-mediated depolarisation, which in turn can enhance NMDA receptor activation. Noteworthy is the fact that CX546; analogous to BRS-015, showed no effect on NMDA receptor-mediated currents (Arai *et al.*, 2004). Moreover, aniracetam had no effect on NMDA-receptor mediated EPSCs in CA1 pyramidal neurones but increased the magnitude of post-tetanic potentiation (Isaacson and Nicoll, 1991).

In summary, a secondary consequence of the positive modulation of AMPAR *via* BRS-015 can be linked with the recruitment of voltage-sensitive NMDA receptor activity, providing evidence for an additional mechanism for increasing synaptic strength.

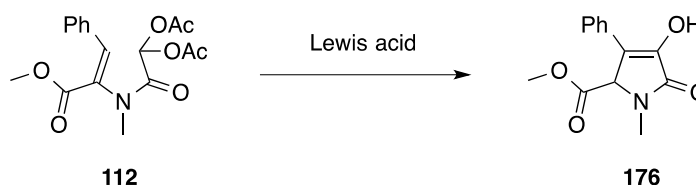
A downstream mechanism of AMPA receptor modulation by BRS-015 would lead to increased calcium levels in the postsynaptic neurone and thus further LTP (Arai *et al.*, 2004). At hippocampal synapses, the strength of synaptic plasticity is determined by the amount of calcium influx during the LTP induction process. Therefore, BRS-015 could modulate the strength of synaptic plasticity by regulating the activity of  $\text{Ca}^{2+}$  dependent protein kinases such as calcium/calmodulin-dependent protein kinase II (CaMKII) (Lisman *et al.*, 2002).

Finally, when applying BRS-015 following the classic LTP induction protocol (3 x 100 Hz during 1 second, every 10 seconds) no further potentiation of evoked f-EPSPs was observed (Figure 45). This result supports the idea that once synapses have been potentiated to their maximum level, no further effect on LTP can be seen. Previous studies have shown that aniracetam interferes with the expression of LTP (Staubli *et al.*, 1990, Staubli *et al.*, 1992, Xiao *et al.*, 1991) and has also been shown to modulate the induction of LTP, dependent on the induction protocol. As such, an approximate 22% increase of control was observed with the application of 5 theta bursts and no effect when 10 theta burst stimuli was used on the induction of LTP (Arai and Lynch, 1992). Such a result indicates that the drug affects the induction of LTP per burst but does not change the ceiling of the maximum degree of LTP that is normally present.

Pleasingly one of the key results regarding the future potential of BRS-015 in the cytotoxicity assays revealed that BRS-015 is essentially non-toxic and so warrants further development to explore its potential.

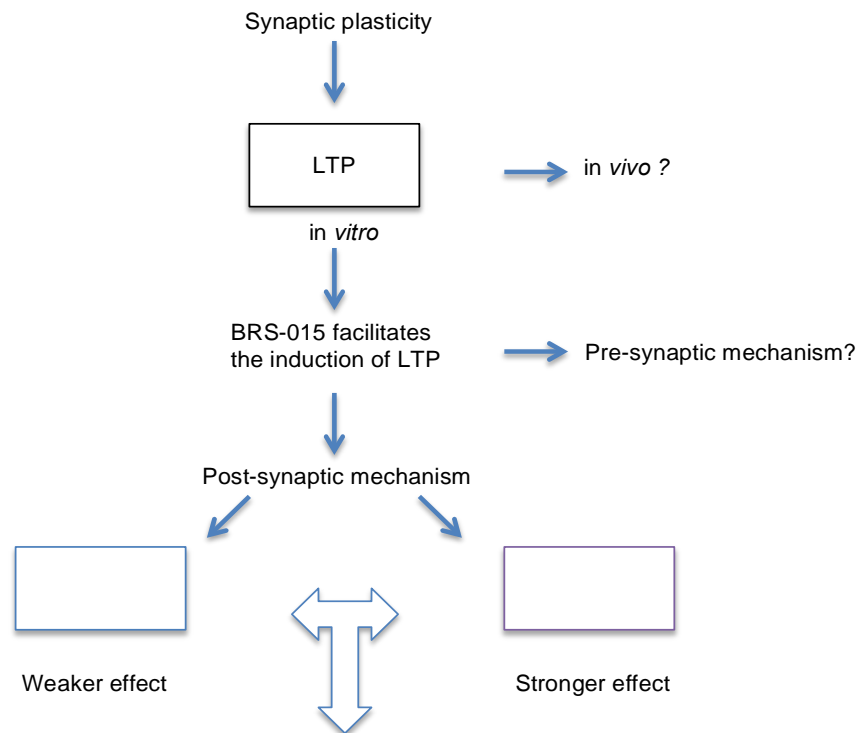
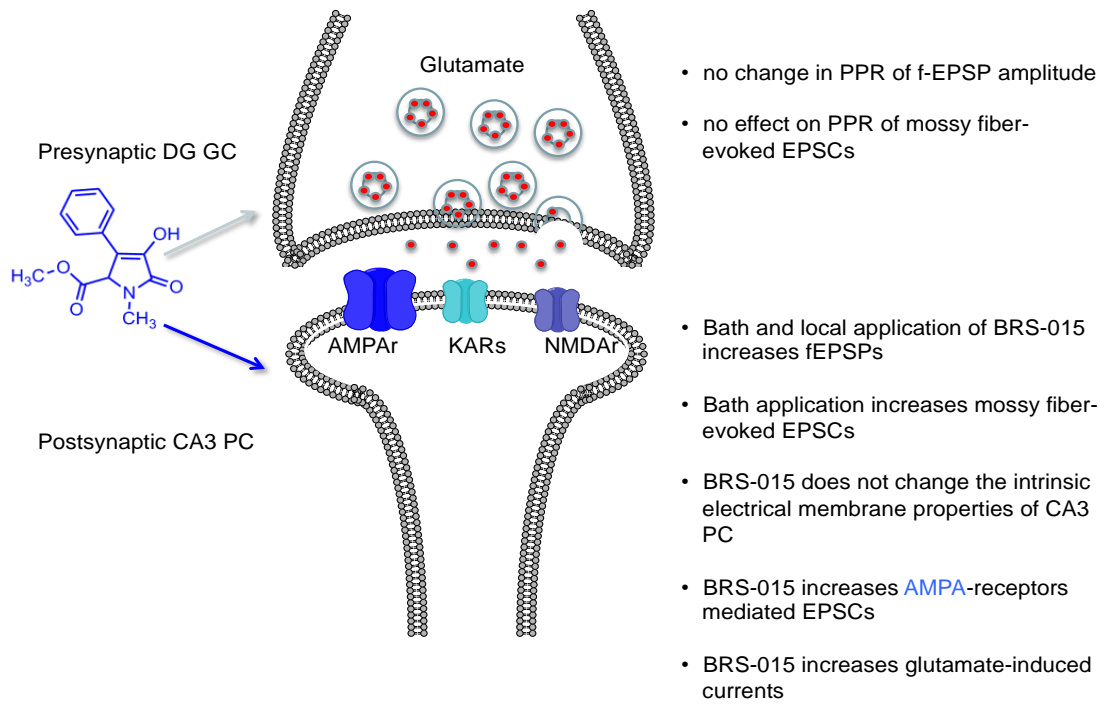
## 9.0. Conclusions

In summary, the present study has clearly shown the intramolecular acylal cyclisation reaction that we have developed has led to the synthesis of compounds related to clausenamide as shown below (Scheme 53). In particular, the mechanistic insights observed in the synthesis of related bicyclic derivatives (Scheme 27) demonstrate that this chemical approach is feasible for a number of related analogues and warrants further investigation.



**Scheme 53: Synthesis of BRS-015**

In addition, the chemistry that we have developed has led to the filing of a patent to protect a novel compound - BRS-015, which we have shown to have a strong and reversible enhancing effect on excitatory synaptic transmission in the CA3 region by a mechanism involving the modulation of AMPA receptor mediated currents. It also facilitated the induction of a long-lasting form of synaptic plasticity in CA3 cells. However, the exact mechanistic pathway by which it has led to such an enhanced transmission remains still to be fully elucidated if BRS-015 or a closely related analogue were to progress towards further development as a memory enhancing compound, its plausible mechanism is presented in Figure 48.



BRS-015 'awakens' silent NMDARs at mossy fibre synapses via modulation of AMPAR activity

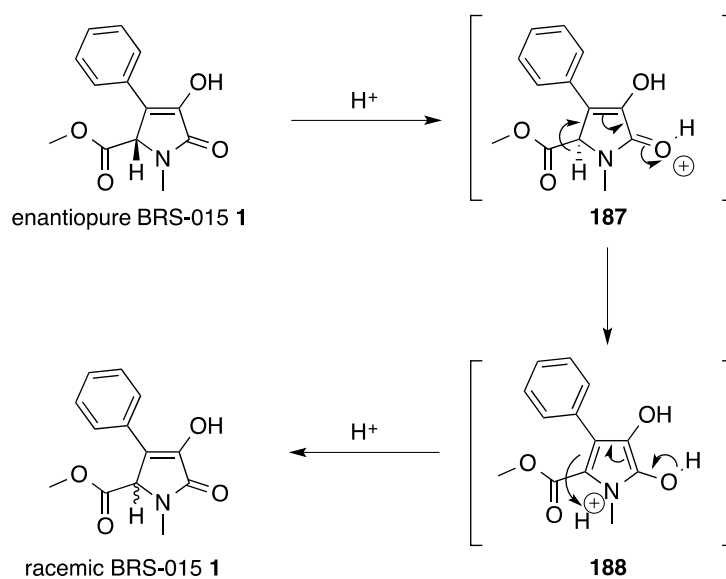
**Figure 48: Schematic diagram showing the possible mechanism by which BRS-015 induces long-lasting enhancement in excitatory synaptic transmission.**

## **10.0. Future Work**

## 10.0. Future Work

The results have clearly shown that the effects of (-)-BRS-015 on mossy fibre f-EPSPs is clearly promising and warrants further investigation as it indicates the selective nature of this small molecule and suggests that the (-)-enantiomer accounts for all of the observed activity. Future work should therefore focus on the (-)-enantiomer and should explore its effects on LTP.

However, despite this result, it clearly does not exclude the possibility that the drug cannot be developed as a racemic mixture, only that we should investigate the potential effects of each enantiomer. One of the challenges associated with the structure of BRS-015 is its vinylogous double bond. The single chiral centre may undergo epimerisation under physiological conditions as shown below (Scheme 54).



**Scheme 54: Potential Racemisation of BRS-015**

Protonation of the carbonyl oxygen can lead to formation of the intermediate pyrrole **188**. However, re-protonation of this intermediate can occur from either face and therefore may lead to racemisation under physiological conditions. We therefore need to examine this under simulated physiological conditions to determine whether this is indeed the case.

In addition to the question of chirality is the need to investigate the activity of related molecules in order to develop a compound that can progress towards further development. Clearly the methyl ester is a sensible starting point for functional group interconversion, but we should also look at the effects on activity of modification of the phenyl ring and the group on the amidic nitrogen. Examples of compounds that we intend to investigate in the future are shown below (Figure 49).

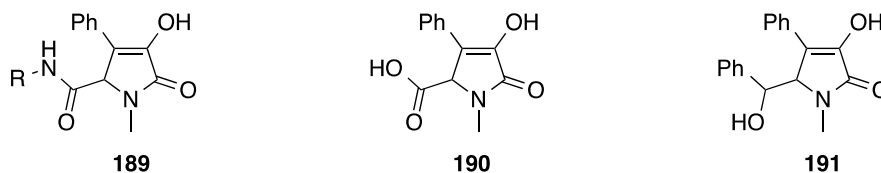


**Figure 49: Potential analogues development of BRS-015**

We also anticipate that the amide and OH groups are crucial for binding and resultant biological activity. Simple methylation of the alcohol will enable us to demonstrate this as shown below (Figure 50).

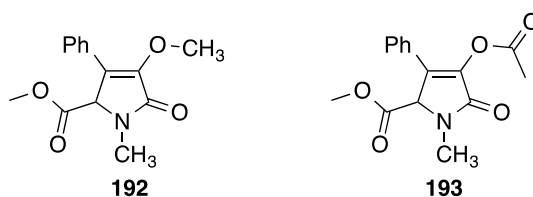


**Figure 50: Alcohol analogues of BRS-015**

In order to guide our future synthetic developments relating to BRS-015, we also need to investigate the *insilico* binding of BRS-015. Therefore future work should also focus on the effects of BRS-015 on various AMPA receptor subunits. Using the published crystal structure of piracetam bound to GluA2, we will carry out docking studies to examine where the molecule binds in the three possible binding pockets as shown by Ahmed and co-workers (Ahmed and Oswald, 2010). Moreover, only AMPA receptors that lack GluA2 are permeable to calcium, which makes the GluA2 subunit a preferred target.

At the cellular level, future mainstream lines of research need to be developed to elucidate the mechanisms of action of BRS-015 and to grasp a better understanding of the biological spectrum of activity of apperanted compounds.

The following processes need to be investigated, all of which can potentiate synaptic strength *via* candidate postsynaptic mechanisms:

- i) Direct binding to AMPA receptors: in this scenario, BRS-015 would bind to a specific AMPA receptor subunit as shown for previous allosteric modulators, e.g. phillantotoxine on GluA2 (Poulsen *et al.*, 2014);
- ii) Indirect modulation *via* protein kinase activation and downstream phosphorylation of AMPA receptor subunits;
- iii) Indirect modulation *via* inhibition of phosphodiesterases: in this model, AMPA receptors would normally function under constitutive phosphorylation and de-phosphorylation activity;
- iv) All of the above, leading to insertion of new AMPA receptors at synapses either by lateral diffusion of *via* intracellular recycling pathways.

Despite the amount of *in vitro* studies required to progress BRS-015 or related congeners towards preclinical development, it is clear that it already has a significant effect. It therefore has good potential for the treatment of memory disorders, implying that future efforts should also be explored *in vivo*. Therefore, future work should focus on classic memory impairment tests such as the Morris water maze, or passive avoidance, novel object recognition tests and paired learning and memory tests, ideally in aged animals (Savonenko *et al.*, 2012). Currently, BRS-015 is under evaluation and further studies by Eli Lilly will be reported in due course. These studies were initiated after the research described in this thesis and will be reported elsewhere.

## 11.0. Experimental

## 11.0. Experimental

### 11.1. General Methods for Synthesis

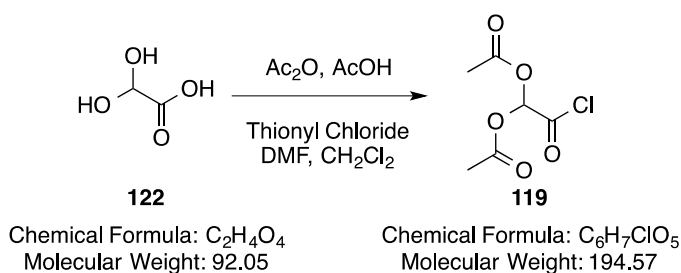
All reactions requiring the use of dry conditions were carried out under an atmosphere of nitrogen and all glassware was pre-dried in an oven (110 °C) and cooled under nitrogen prior to use. Stirring was by internal magnetic follower unless otherwise stated. All reactions were followed by TLC and organic phases extracted were dried with anhydrous magnesium sulfate. Diethyl ether, tetrahydrofuran, dichloromethane, toluene, methanol, acetonitrile and triethylamine were purchased as anhydrous solvents from Sigma-Aldrich chemical company. Purification was carried out by column chromatography using the flash column chromatography technique reported by Still and others (Still *et al*, 1978) or by Biotage automatic purification. The silica gel used was Merck 60 (230-400 mesh). Thin layer chromatographic analysis was carried out using Merck aluminium-backed plates coated with silica gel 60 F<sub>254</sub>. Components were visualised using combinations of ultraviolet light and iodine stain.

Infrared spectra were recorded on a Perkin Elmer 1605 FT-IR spectrophotometer. Melting points were determined using open glass capillaries on a Stuart Scientific SMP3 apparatus and are uncorrected. <sup>1</sup>H NMR and <sup>13</sup>C NMR spectra were recorded on a Bruker AV400, operating at 400 MHz for proton and 101 MHz for carbon, or a Bruker AV500 spectrometer operating at 500 MHz for proton and 126 MHz for carbon.

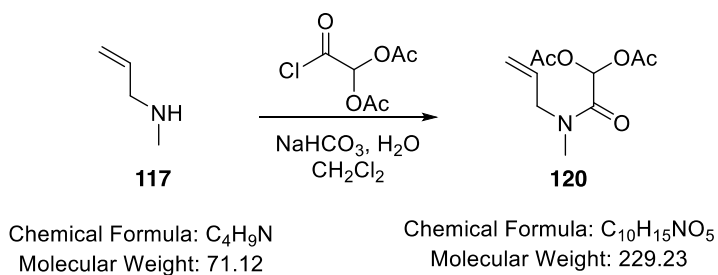
Chemical shifts ( $\delta_{\text{H}}$  and  $\delta_{\text{C}}$ ) are quoted as parts per million downfield from 0. The multiplicity of a <sup>1</sup>H NMR signal is designated by one of the following abbreviations: s = singlet, d = doublet, t = triplet, q = quartet, quin = quintet, sept = septet, br = broad and m = multiplet. Coupling constants (*J*) are expressed in Hertz.

High resolution mass spectra were carried out at School of Pharmacy. Mass spectra were carried out using either an Agilent Micromass Q-TOF premier Tandem Mass Spectrometer from Micromass utilising electrospray. All samples

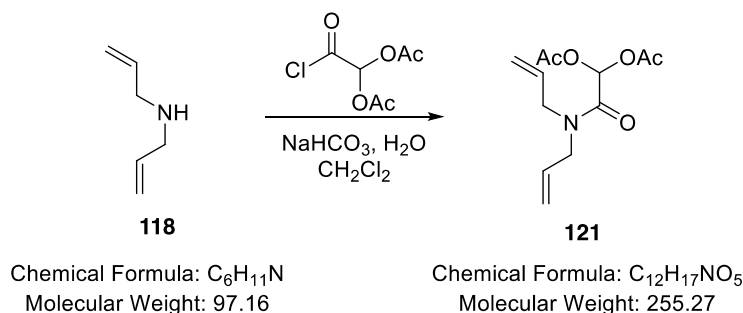
were run under electrospray ionization mode using 50% acetonitrile in water and 0.1% formic acid as solvent.

Diacetoxyacetyl chloride **119**

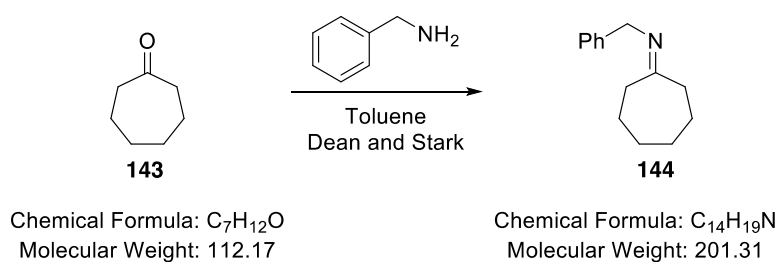
A solution of glyoxylic acid monohydrate **122** (16.0 g, 174 mmol) in acetic anhydride (49.2 mL, 521 mmol) and acetic acid (30.0 mL, 521 mmol) was heated at 150 °C for 3 hours and then allowed to cool to RT over 1 hour. Excess reactants were removed under azeotropic distillation (toluene 2 x 100 mL) under reduced pressure. The residue was taken up in dichloromethane (200 mL) followed by sequential addition of thionyl chloride (25.4 mL, 348 mmol) and dimethylformamide (0.03 mL, 0.35 mmol). The mixture was heated under reflux conditions (50 °C) until formation of diacetoxyacetyl chloride and loss of diacetoxyacetic acid was confirmed by <sup>1</sup>H NMR spectroscopy. Solvent and excess thionyl chloride were removed under reduced pressure and the crude product purified by distillation under reduced pressure (64-65 °C/ 1.0 mmHg) to give diacetoxyacetyl chloride **119** (15.0 g, 77.1 mmol, 45%) as a colourless oil;  $\nu_{\max}/\text{cm}^{-1}$  1763 (C=O), 1376 (CH<sub>3</sub>), 1200 (C-C(O)-C), 718 (C-Cl);  $\delta$  H (500 MHz; CDCl<sub>3</sub>) 6.79 (1 H, s, CH), 2.09 (6 H, s, CH(OC(O)CH<sub>3</sub>)<sub>2</sub>);  $\delta$  C (126 MHz; CDCl<sub>3</sub>) 168.21 (CO), 167.67 (CO), 88.03 (CH(OAc)<sub>2</sub>), 20.48 (CH<sub>3</sub>);  $m/z$  195 (100%, [M+H]<sup>+</sup>): Found [M+H]<sup>+</sup> 195.5805, C<sub>6</sub>H<sub>8</sub>ClO<sub>5</sub> requires 195.5801.

2-(Allyl(methyl)amino)-2-oxoethane-1,1-diyl diacetate **120**

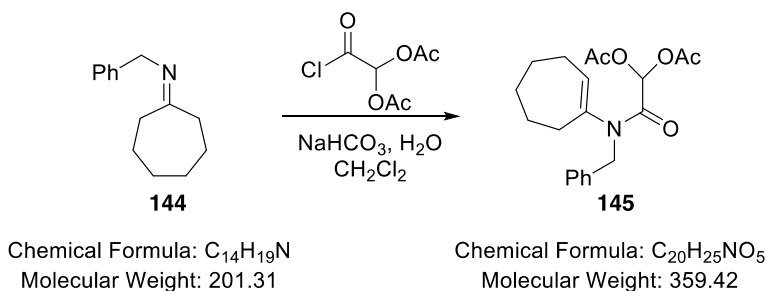
A solution of diacetoxyacetyl chloride **119** (1.24 g, 6.38 mmol) in dichloromethane (5 mL) was added to a rapidly stirred biphasic solution of *N*-allylmethylamine **117** (0.45 g, 6.38 mmol) and sodium bicarbonate (0.54 g, 6.38 mmol) in water (50 mL) and the resulting mixture stirred rapidly for 3 hours. The mixture was separated and the aqueous layer extracted with dichloromethane (50 mL). The combined organic extracts were dried (MgSO<sub>4</sub>), filtered and solvent removed under reduced pressure. The residue was purified by flash column chromatography (1:1 EtOAc-petroleum ether (40-60 °C), R<sub>f</sub> = 0.46) to give amide **120** (1.02 g, 4.43 mmol, 69%) as a pale pink oil as a 1:1 mixture of amide rotamers;  $\nu_{\text{max}}/\text{cm}^{-1}$  (CH<sub>2</sub>Cl<sub>2</sub>) 2595 (NCH<sub>3</sub>), 1717 (C=O), 1646 (N(CH<sub>3</sub>)C=O); <sup>1</sup>H NMR (400 MHz, CDCl<sub>3</sub>)  $\delta$  7.14 (0.5 H, s, C(O)CH), 7.10 (0.5 H, s, C(O)CH), 5.72 (1 H, m, CH<sub>2</sub>=CH-CH<sub>2</sub>-N(CH<sub>3</sub>)), 5.32 - 5.01 (2 H, m, CH<sub>2</sub>=CH-CH<sub>2</sub>-N(CH<sub>3</sub>)), 3.97 (1 H, d, *J*=5.8 Hz, CH<sub>2</sub>=CH-CH<sub>2</sub>-N(CH<sub>3</sub>)), 3.94 - 3.78 (1 H, m, CH<sub>2</sub>=CH-CH<sub>2</sub>-N(CH<sub>3</sub>)), 2.94 (1.5 H, s, NCH<sub>3</sub>), 2.93 (1.5 H, s, NCH<sub>3</sub>), 2.14 (3 H, s, OC(O)CH<sub>3</sub>), 2.11 (3 H, s, OC(O)CH<sub>3</sub>); <sup>13</sup>C NMR (101 MHz, CDCl<sub>3</sub>)  $\delta$  168.95 (OC(O)CH<sub>3</sub>), 168.85 (OC(O)CH<sub>3</sub>), 164.20 (C(O)CH), 163.79 (C(O)CH), 132.01 (CH<sub>2</sub>=CH-CH<sub>2</sub>-N(CH<sub>3</sub>)), 131.83 (CH<sub>2</sub>=CH-CH<sub>2</sub>-N(CH<sub>3</sub>)), 118.16 (CH<sub>2</sub>=CH-CH<sub>2</sub>-N(CH<sub>3</sub>)), 117.85 (CH<sub>2</sub>=CH-CH<sub>2</sub>-N(CH<sub>3</sub>)), 84.07 (C(O)CH), 83.90 (C(O)CH), 51.56 (CH<sub>2</sub>=CH-CH<sub>2</sub>-N(CH<sub>3</sub>)), 50.94 (CH<sub>2</sub>=CH-CH<sub>2</sub>-N(CH<sub>3</sub>)), 34.27 (NCH<sub>3</sub>), 34.05 (NCH<sub>3</sub>), 20.73 (OC(O)CH<sub>3</sub>), 20.70 (OC(O)CH<sub>3</sub>); *m/z* 230 (43%, [M+H]<sup>+</sup>); Found [M+H]<sup>+</sup> 230.1027, C<sub>10</sub>H<sub>16</sub>NO<sub>5</sub> requires 230.1028.

2-(Diallylamino)-2-oxoethane-1,1-diyl diacetate **121**

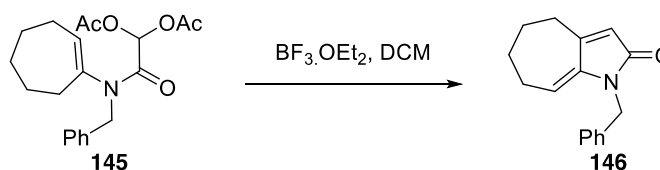
A solution of diacetoxyacetyl chloride **119** (1.58 g, 8.13 mmol) in dichloromethane (10 mL) was added to a rapidly stirred biphasic mixture of diallylamine **118** (0.79 g, 8.13 mmol) in dichloromethane (100 mL) and sodium bicarbonate (0.68 g, 8.13 mmol) in water (50 mL) and the resulting mixture stirred for 3 hours. The mixture was separated, and the aqueous layer extracted with dichloromethane (50 mL). The combined organic extracts were dried (MgSO<sub>4</sub>), filtered and solvent removed under reduced pressure. The residue was purified by flash column chromatography (1:3 EtOAc- petroleum ether (40-60 °C), R<sub>f</sub> = 0.31) to give 2-(diallylamino)-2-oxoethane-1,1-diyl diacetate **121** (1.69 g, 6.63 mmol, 82%) as a pale pink oil;  $\nu_{\text{max}}/\text{cm}^{-1}$  (CH<sub>2</sub>Cl<sub>2</sub>) 1718 (C=O), 1657 N(CH<sub>3</sub>)C=O; <sup>1</sup>H NMR (400 MHz, CDCl<sub>3</sub>)  $\delta$  7.08 (1 H, s, C(O)CH), 5.84 - 5.64 (2 H, m, CH<sub>2</sub>=CH-CH<sub>2</sub>-N, N-CH<sub>2</sub>-CH=CH<sub>2</sub>), 5.24 - 5.09 (4 H, m, CH<sub>2</sub>=CH-CH<sub>2</sub>-N, N-CH<sub>2</sub>-CH=CH<sub>2</sub>), 3.97 (2 H, d, *J* = 5.8 Hz, N-CH<sub>2</sub>-CH=CH<sub>2</sub>), 3.88 (2 H, dt, *J* = 4.9, 1.6 Hz, N-CH<sub>2</sub>-CH=CH<sub>2</sub>), 2.11 (6 H, s, (OC(O)CH<sub>3</sub>)<sub>2</sub>); <sup>13</sup>C NMR (101 MHz, CDCl<sub>3</sub>)  $\delta$  168.73 (OC(O)CH<sub>3</sub>), 164.01 (OC(O)CH<sub>3</sub>), 132.15 (CH<sub>2</sub>=CH-CH<sub>2</sub>-N), 131.86 (N-CH<sub>2</sub>-CH=CH<sub>2</sub>), 118.04 (CH<sub>2</sub>=CH-CH<sub>2</sub>-N), 117.62 (CH<sub>2</sub>=CH-CH<sub>2</sub>-N), 83.83 (C(O)CH), 48.54 (CH<sub>2</sub>=CH-CH<sub>2</sub>-N), 48.52 (N-CH<sub>2</sub>-CH=CH<sub>2</sub>), 20.56 (OC(O)CH<sub>3</sub>); *m/z* 278 (42%, [M+Na]<sup>+</sup>); Found [M+Na]<sup>+</sup> 278.0999, C<sub>12</sub>H<sub>17</sub>NNaO<sub>5</sub> requires 278.1004.

Cycloheptanone imine **144**

A mixture of cycloheptanone **143** (0.72 mL, 6.07 mmol) and benzylamine **129** (0.66 mL, 6.07 mmol) in toluene was heated at reflux in the presence of a Dean Stark trap for 3 hours. Solvent was removed under reduced pressure to give the imine **144** as a colourless oil that was used immediately without further purification.

2-(Benzyl(cycloheptenyl)amino)-2-oxoethane-1,1-diyl diacetate **145**

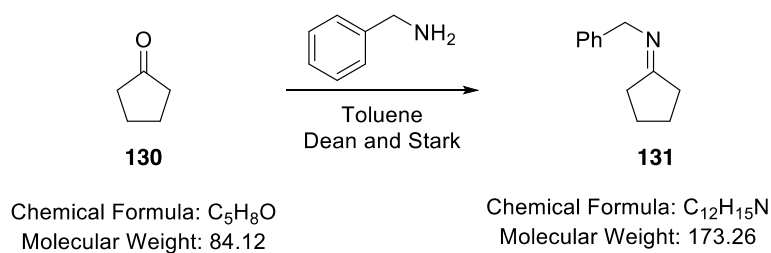
A solution of diacetoxyacetyl chloride **119** (1.28 g, 6.56 mmol) in dichloromethane (10 mL) was added to a rapidly stirred biphasic mixture of cycloheptanone imine **144** (1.20 g, 5.96 mmol) and sodium bicarbonate (1.00 g, 11.9 mmol) in dichloromethane (100 mL) and water (20 mL) and the resulting mixture stirred for 3 hours. The mixture was separated, and the aqueous layer extracted with dichloromethane (50 mL). The combined organic extracts were dried ( $\text{MgSO}_4$ ), filtered and solvent removed under reduced pressure. The residue was purified by flash column chromatography (1:2 EtOAc-petroleum ether (40-60 °C),  $R_f = 0.38$ ) to give 2-(benzyl(cycloheptenyl)amino)-2-oxoethane-1,1-diyl diacetate **145** (0.86 g, 2.38 mmol, 44%) as a colourless oil;  $\nu_{\text{max}}/\text{cm}^{-1}$  ( $\text{CH}_2\text{Cl}_2$ ) 2932 (C-H), 1772 (C=O), 1677 (C=C);  $^1\text{H}$  NMR (400 MHz,  $\text{CDCl}_3$ )  $\delta$  7.30 (5 H, m, CH-Ar), 7.16 (1 H, s, CH-O), 5.53 (1 H, t,  $J$  5.5, CH-C), 5.01 (1H, brs,  $\text{CH}_2$ -Ar), 4.26 (1 H, brs,  $\text{CH}_2$ -Ar), 2.32 (2 H, brs,  $\text{CH}_2$ -C), 2.16 (6 H, s,  $2\times(\text{CH}_3)$ ), 2.01 (2 H, q,  $J$  6.6,  $\text{CH}_2$ -CH), 1.61 (6 H, brm,  $3\times(\text{CH}_2\text{-CH}_2)$ );  $^{13}\text{C}$  NMR (101 MHz,  $\text{CDCl}_3$ )  $\delta$  163.1 (C=O), 140.7 (Cq), 136.6 (Cq), 134.6 (CH-C), 129.0 (CH-Ar), 128.3 (CH-Ar), 127.5 (CH-Ar), 84.2 (CH-O), 49.9 ( $\text{CH}_2$ -Ar), 33.1 ( $\text{CH}_2$ -C), 30.9 ( $\text{CH}_2$ -CH), 26.8 ( $\text{CH}_2\text{-CH}_2$ ), 26.0 ( $\text{CH}_2\text{-CH}_2$ ), 25.8 ( $\text{CH}_2\text{-CH}_2$ ), 20.6 ( $2\times(\text{CH}_3)$ );  $m/z$  360 (26%,  $[\text{M}+\text{H}]^+$ ); Found  $[\text{M}+\text{H}]^+$  360.1802,  $\text{C}_{20}\text{H}_{26}\text{NO}_5$  requires 360.1811.

**1-Benzyl-4,5,6,7-tetrahydrocyclohepta-( $\beta$ )-pyrrol-2(1*H*)-one **146****

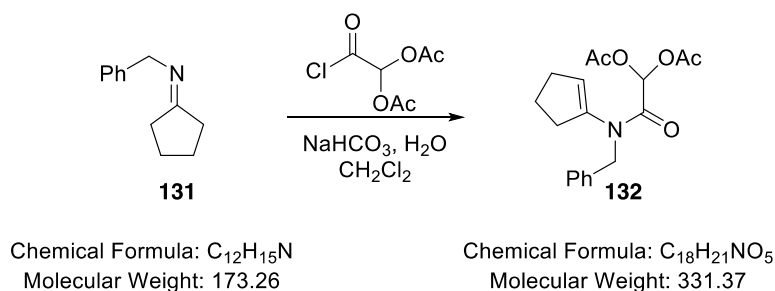
Chemical Formula: C<sub>20</sub>H<sub>25</sub>NO<sub>5</sub>  
Molecular Weight: 359.42

Chemical Formula: C<sub>16</sub>H<sub>17</sub>NO  
Molecular Weight: 239.32

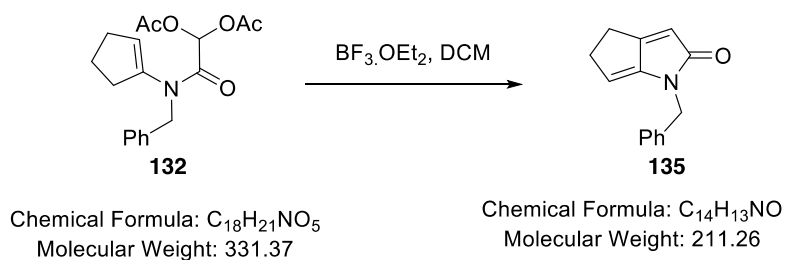
Boron trifluoride diethyl etherate (0.07 mL, 0.56 mmol) was added to the solution of 2-(benzyl(cycloheptenyl)amino)-2-oxoethane-1,1-diyl diacetate **145** (0.100 g, 0.28 mmol) in DCM (10 mL) at 0 °C and the resulting mixture stirred at this temperature for 30 minutes and then at room temperature overnight. The mixture was poured into water (40-50 mL), and extracted with dichloromethane (3 x 30 mL). The combined organic extracts were washed with water (2 x 50 mL), dried (MgSO<sub>4</sub>), filtered and solvent removed under reduced pressure. The residue was purified by flash column chromatography (1:2 EtOAc-petroleum ether (40-60 °C), R<sub>f</sub> = 0.43) to give 1-benzyl-4,5,6,7-tetrahydrocyclohepta-( $\beta$ )-pyrrol-2(1*H*)-one **146** (0.02 g, 0.09 mmol, 31%) as a colourless oil;  $\nu_{\max}/\text{cm}^{-1}$  (CH<sub>2</sub>Cl<sub>2</sub>) 1682 (C=O); <sup>1</sup>H NMR (400 MHz, CDCl<sub>3</sub>)  $\delta$  7.33 - 7.06 (5 H, m, ArH), 5.85 (1 H, s, C(O)CH), 5.49 (1 H, dd, *J* = 8.0, 3.4 Hz, CH), 4.70 (2 H, s, N-CH<sub>2</sub>-Ph), 2.74 - 2.61 (2 H, m, CH<sub>2</sub>), 2.29 (2 H, m, CH<sub>2</sub>), 1.67 (4 H, m, CH<sub>2</sub>); <sup>13</sup>C NMR (101 MHz, CDCl<sub>3</sub>)  $\delta$  169.62 (C=O), 151.71 (C=C(H)C=O), 140.27 (quaternary C), 137.75 (ArCH), 128.55 (ArCH), 127.04 (ArCH), 120.28 (C(O)CH), 116.87 (CH), 42.45 (N-CH<sub>2</sub>-Ph), 29.90 (CH<sub>2</sub>), 28.17 (CH<sub>2</sub>), 27.53 (CH<sub>2</sub>), 24.64 (CH<sub>2</sub>); *m/z* 240 (34%, [M+H]<sup>+</sup>); Found [M+H]<sup>+</sup> 240.1396, C<sub>16</sub>H<sub>18</sub>NO requires 240.1388.

***N*-Cyclopentylidene-1-phenylmethanamine 131**

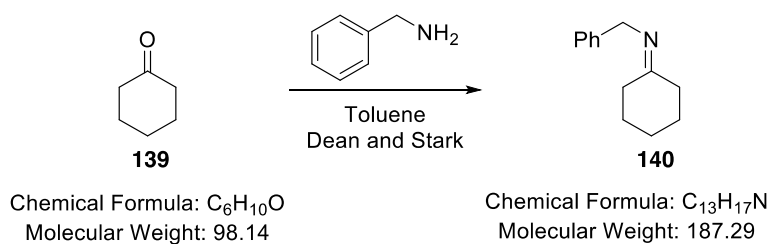
A mixture of cyclopentanone **130** (0.54 mL, 6.07 mmol) and benzylamine **129** (0.66 mL, 6.07 mmol) in toluene (15 mL) was heated at reflux under Dean and Stark water removal conditions for 3 hours. Solvent was removed under reduced pressure to give *N*-cyclopentylidene-1-phenylmethanamine **131** (1.05 g, 6.07 mmol, 100%) as a colourless oil that was used immediately without further purification.

2-(Benzyl(cyclopentenyl)amino)-2-oxoethane-1,1-diyl diacetate **132**

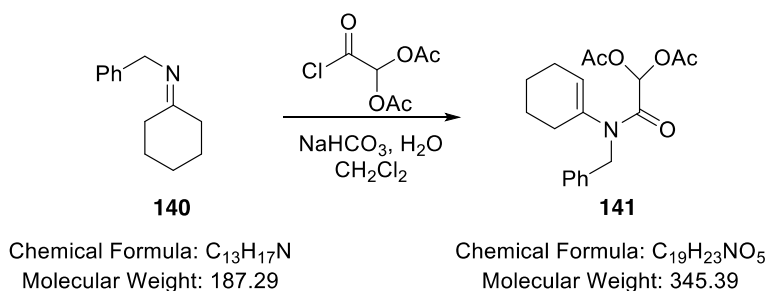
A solution of diacetoxyacetyl chloride **119** (1.18 g, 6.07 mmol) in dichloromethane (10 mL) was added to a rapidly stirred biphasic mixture of *N*-cyclopentylidene-1-phenylmethanamine **131** (1.05 g, 6.07 mmol) and sodium bicarbonate (0.51 g, 6.07 mmol) in DCM (100 mL) and water (50 mL) the resulting mixture stirred for 48 hours. The mixture was separated, and the aqueous layer extracted with dichloromethane (50 mL) and the combined extracts dried (MgSO<sub>4</sub>), filtered and solvent removed under reduced pressure. Purification by flash column chromatography (1:4, EtOAc-petroleum ether (40-60 °C), R<sub>f</sub> = 0.38) gave 2-(benzyl(cyclopentenyl)amino)-2-oxoethane-1,1-diyl diacetate **132** (0.92 g, 2.77 mmol, 46%) as a colourless oil; <sup>1</sup>H NMR (400 MHz, CDCl<sub>3</sub>) δ 7.29 - 7.12 (5 H, m, Ar CH), 7.09 (1 H, s, C(O)CH), 5.39 (1 H, s, C(H)=C), 4.59 (2 H, s, NCH<sub>2</sub>), 2.37 - 2.14 (4 H, m, CH<sub>2</sub>, CH<sub>2</sub>), 2.07 (6 H, s, OC(O)CH<sub>3</sub>), 1.83 (2 H, dd, *J* = 15.1, 7.7 Hz, CH<sub>2</sub>); <sup>13</sup>C NMR (101 MHz, CDCl<sub>3</sub>) δ 168.52 (C=O), 163.43 (NC=O), 136.42 (C(H)=C), 140.36 (C(H)=C), 129.97 (quaternary C), 128.29(ArCH), 128.00 (ArCH), 127.30 (ArCH), 83.93 (C(O)CH), 49.52 (NCH<sub>2</sub>), 32.07(CH<sub>2</sub>), 30.04 (CH<sub>2</sub>), 21.99, (CH<sub>2</sub>), 20.38 (OC(O)CH<sub>3</sub>); *m/z* 331 (100%, [M]<sup>+</sup>); Found [M+H]<sup>+</sup> 332.1489, C<sub>18</sub>H<sub>22</sub>NO<sub>5</sub> requires 332.1498.

1-Benzyl-4,5-dihydrocyclopenta[*b*]pyrrol-2(1*H*)-one **135**

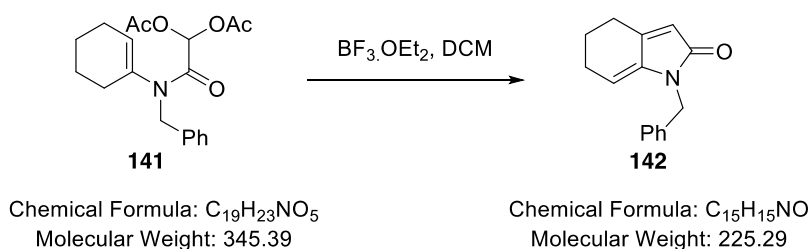
Boron trifluoride diethyl etherate (0.52 mL, 4.22 mmol) was added to a solution of 2-(benzyl(cyclopentenyl)amino)-2-oxoethane-1,1-diyl diacetate **132** (0.28 g, 0.85 mmol) in DCM (3.5 mL) and the resulting solution stirred for 10 minutes and heated at reflux for 6 hours. The mixture was poured into water (40-50 mL), and extracted with DCM (3 x 30 mL) and the combined organic extracts washed with water (2 x 50 mL), dried ( $\text{MgSO}_4$ ), filtered and solvent removed under reduced pressure. The residue was purified by flash column chromatography (1:2, EtOAc-petroleum ether (40-60 °C),  $R_f = 0.47$ ) to give 1-benzyl-4,5-dihydrocyclopenta-( $\beta$ )-pyrrol-2(1*H*)-one **135** (0.12 g, 0.56 mmol, 67%) as a colourless oil;  $\nu_{\text{max}}/\text{cm}^{-1}(\text{CH}_2\text{Cl}_2)$  1692 (C=O);  $^1\text{H NMR}$  (400 MHz,  $\text{CDCl}_3$ )  $\delta$  7.34 - 7.10 (5 H, m, ArCH), 5.76 - 5.57 (1 H, m, C(H)-C=O), 5.33 (1 H, m, C(H)=C), 4.72 (2 H, s, NCH<sub>2</sub>), 2.80 - 2.68 (2 H, m, CH<sub>2</sub>), 2.68 - 2.59 (2 H, m, CH<sub>2</sub>);  $^{13}\text{C NMR}$  (101 MHz,  $\text{CDCl}_3$ )  $\delta$  161.87 (C=O), 146.39 (C=C(H)C=O), 137.28 (quaternary C), 128.60 (ArCH), 127.68 (ArCH), 127.44 (ArCH), 113.36 (C=C(H)C=O), 109.31 (HC=C), 44.34 (N-CH<sub>2</sub>-Ph), 35.07 (CH<sub>2</sub>), 23.89 (CH<sub>2</sub>);  $m/z$  349 (15%,  $[\text{M}+\text{H}]^+$ ); Found  $[\text{M}+\text{H}]^+$  212.1071,  $\text{C}_{14}\text{H}_{14}\text{NO}$  requires 212.1075.

***N*-Cyclohexylidene-1-phenylmethanamine 140**

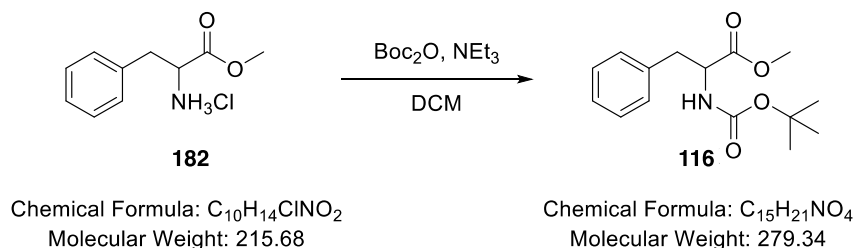
A solution of cyclohexanone **139** (0.63 mL, 6.07 mmol) and benzylamine **129** (0.66 mL, 6.07 mmol) in toluene (15 mL) was heated at reflux under Dean and Stark water removal conditions for 3 hours and solvent removed under reduced pressure to give *N*-cyclohexylidene-1-phenylmethanamine **140** (1.14 g, 6.07 mmol, 100%) as a colourless oil that was used immediately without further purification.

2-(Benzyl(cyclohexenyl)amino)-2-oxoethane-1,1-diyl diacetate **141**

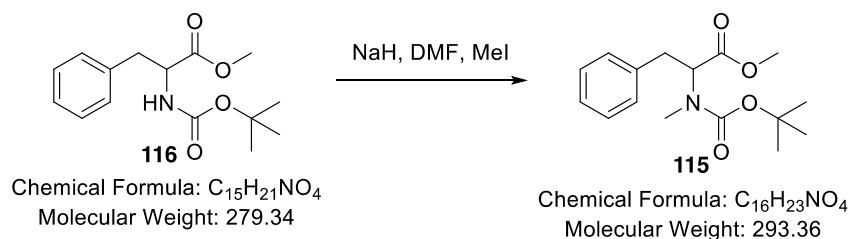
A solution of diacetoxyacetyl chloride **119** (1.18 g, 6.07 mmol) in dichloromethane (10 mL) was added to a rapidly stirred biphasic mixture of *N*-cyclohexylidene-1-phenylmethanamine **140** (1.14 g, 6.07 mmol) and sodium bicarbonate (0.51 g, 6.07 mmol) in dichloromethane (100 mL) and water (100 mL) and the resulting mixture stirred for 48 hours. The mixture was separated, and the aqueous layer extracted with dichloromethane (50 mL). The combined organic extracts were dried ( $\text{MgSO}_4$ ), filtered and solvent removed under reduced pressure. The residue was purified by flash column chromatography (1:3, EtOAc-petroleum ether (40-60 °C),  $R_f = 0.34$ ) to give 2-(benzyl(cyclohexenyl)amino)-2-oxoethane-1,1-diyl diacetate **141** (0.37 g, 1.07 mmol, 18%) as a colourless oil;  $\nu_{\text{max}}/\text{cm}^{-1}$  ( $\text{CH}_2\text{Cl}_2$ ) 1748 (OAc), 1682 (C=O);  $^1\text{H}$  NMR (400 MHz,  $\text{CDCl}_3$ )  $\delta$  7.27 - 7.13 (5 H, m, ArCH), 7.04 (1 H, s, C(O)CH), 5.38 (1 H, t,  $J = 1.6$  Hz, C=CH), 4.56 (2 H, s, NCH<sub>2</sub>), 2.07 (6 H, s, OC(O)CH<sub>3</sub>), 2.05 - 1.99 (2 H, m, CH<sub>2</sub>), 1.94 - 1.84 (2 H, m, CH<sub>2</sub>), 1.64 - 1.51 (2 H, m, CH<sub>2</sub>), 1.50 - 1.37 (2 H, m, CH<sub>2</sub>);  $^{13}\text{C}$  NMR (101 MHz,  $\text{CDCl}_3$ )  $\delta$  168.76 (C=O), 163.51 (NC=O), 136.78 (C(H)=C), 136.36 (quaternary C), 130.14 (ArCH), 128.63 (ArCH), 128.37 (ArCH), 127.44 (C=CH), 84.19 (C(O)CH), 49.78 (NCH<sub>2</sub>), 27.70 (CH<sub>2</sub>), 24.78 (CH<sub>2</sub>), 22.45 (CH<sub>2</sub>), 21.20 (CH<sub>2</sub>), 20.58 (OC(O)CH<sub>3</sub>).  $m/z$  368 (100 %,  $[\text{M}+\text{Na}]^+$ ); Found  $[\text{M}+\text{H}]^+$  346.1646,  $\text{C}_{19}\text{H}_{24}\text{NO}_5$  requires 346.1654.

1-Benzyl-5,6-dihydro-(1*H*)-indol-2(4*H*)-one **142**

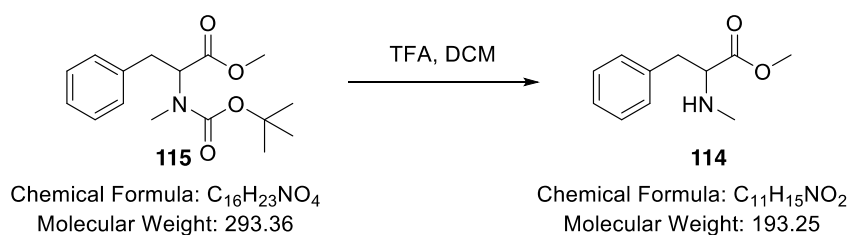
Boron trifluoride diethyl etherate (0.18 mL, 1.46 mmol) was added to a solution of 2-(benzyl(cyclohexenyl)amino)-2-oxoethane-1,1-diyl diacetate **141** (0.10 g, 0.29 mmol) in DCM (3.5 mL) and the resulting mixture stirred for 10 minutes and heated at reflux for 3 hours. The mixture was poured into water (40-50 mL) and extracted with dichloromethane (3 x 30 mL). The combined organic extracts were washed with water (2 x 50 mL), dried (MgSO<sub>4</sub>), filtered and solvent removed under reduced pressure. The residue was purified by flash column chromatography (1:3, EtOAc-petroleum ether (40-60 °C), R<sub>f</sub> = 0.28) to give 1-benzyl-5,6-dihydro-1*H*-indol-2(4*H*)-one **142** (0.03 g, 0.11 mmol, 38%) as a colourless oil;  $\nu_{\text{max}}/\text{cm}^{-1}$  (CH<sub>2</sub>Cl<sub>2</sub>) 1678 (NC=O); <sup>1</sup>H NMR (400 MHz, CDCl<sub>3</sub>)  $\delta$  7.32 - 7.25 (2 H, m, Ar-CH), 7.23 - 7.17 (3 H, m, Ar-CH), 5.80 (1 H, d, *J* = 1.6 Hz, C=CH), 5.50 (1 H, td, *J* = 4.7, 1.7 Hz, HC=C), 4.74 (2 H, s, N-CH<sub>2</sub>-Ph), 2.69 - 2.55 (2 H, m, CH<sub>2</sub>), 2.24 (2 H, m, CH<sub>2</sub>), 1.78 (2 H, m, CH<sub>2</sub>); <sup>13</sup>C NMR (101 MHz, CDCl<sub>3</sub>)  $\delta$  166.4 (C=O), 147.60 (C=C(H)C=O), 128.55 (ArCH), 127.17 (ArCH), 127.10 (ArCH), 115.55 (C=CH), 110.89 (HC=C), 42.60 (N-CH<sub>2</sub>-Ph), 24.36 (CH<sub>2</sub>), 24.23 (CH<sub>2</sub>), 23.44 (CH<sub>2</sub>) missing 2 x quaternary C; *m/z* 248 (38%, [M+Na]<sup>+</sup>), Found [M+H]<sup>+</sup> 226.1237, C<sub>15</sub>H<sub>16</sub>NO requires 226.1232.

Methyl 2-(*tert*-Butoxycarbonylamino)-3-phenylpropanoate **116**

Di-*tert*-butyl dicarbonate (19.4 mL, 83.0 mmol) was added to a solution of *L*-phenylalanine methyl ester hydrochloride **182** (15.0 g, 69.5 mmol) and triethylamine (19.6 mL, 139 mmol) in dichloromethane (200 mL) and the resulting solution stirred at room temperature for 48 hours. Solvent was removed under reduced pressure and the residue partitioned between DCM (100 mL) and a saturated aqueous solution of sodium bicarbonate (50 mL). The combined organic layers were washed with aqueous solution of sodium bicarbonate (50 mL) and dried (MgSO<sub>4</sub>). The residue was purified *via* Biotage (1:2, EtOAc-petroleum ether (40-60 °C), snap 50 g column, R<sub>f</sub> = 0.73) to give methyl 2-(*tert*-butoxycarbonylamino)-3-phenylpropanoate **116** (19.4 g, 69.6 mmol, 100%) as a colourless oil as a mixture of amide rotamers;  $\nu_{\text{max}}/\text{cm}^{-1}$  (CH<sub>2</sub>Cl<sub>2</sub>) 3373 (NH), 2977 (Ar(CH)), 1744 (CO<sub>2</sub>CH<sub>3</sub>), 1667 (NCO<sub>2</sub><sup>t</sup>Bu); <sup>1</sup>H NMR (400 MHz, CDCl<sub>3</sub>)  $\delta$  7.27 (5H, m, ArCH), 7.08 (1H, br s, -NH-), 4.94 (0.6H, s, NHCH), 4.53 (0.4H, s, NHCH), 3.62 (3H, s, COOCH<sub>3</sub>), 3.04 (2H, m, ArCH<sub>2</sub>COOCH<sub>3</sub>), 1.38 (9H, s, HN-COOC(CH<sub>3</sub>)<sub>3</sub>); <sup>13</sup>C NMR (101 MHz, CDCl<sub>3</sub>)  $\delta$  172.55 (COOCH<sub>3</sub>), 155.40 (NC(O)OC(CH<sub>3</sub>)<sub>3</sub>), 136.44 (quaternary C), 129.44 (ArCH), 128.69 (ArCH), 127.27 (ArCH), 76.85 (C(CH<sub>3</sub>)<sub>3</sub>), 54.63 (CH<sub>2</sub>CHC(O)OCH<sub>3</sub>), 51.68 (OCH<sub>3</sub>), 38.46 (CH<sub>2</sub>), 27.18 (C(CH<sub>3</sub>)<sub>3</sub>); *m/z*: 302.1 (100%, [M+Na]<sup>+</sup>); Found [M+Na]<sup>+</sup> 302.1364, C<sub>15</sub>H<sub>21</sub>NNaO<sub>4</sub> requires 302.1368.

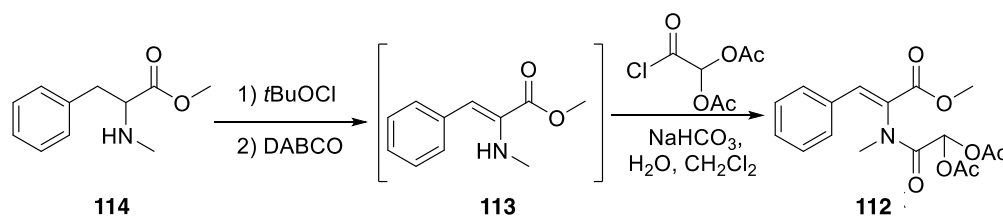
Methyl 2-(*tert*-Butoxycarbonyl(methyl)amino)-3-phenylpropanoate **115**

A suspension of sodium hydride (0.17 g of a 60% in mineral oil, 4.32 mmol) was added to a solution of methyl 2-(*tert*-butoxycarbonylamino)-3-phenylpropanoate **116** (1.09 g, 3.92 mmol) in DMF (15 mL) and the resulting mixture stirred for 4 hours. Iodomethane (0.45 mL, 7.20 mmol) was added to the resulting solution and the mixture stirred for 24 hours at room temperature. The final mixture was quenched by addition of a solution of saturated aqueous ammonium chloride (15 mL) and solvent removed under reduced pressure. The residue was partitioned between water (50 mL) and ethyl acetate (50 mL) and the combined organic extracts washed with brine (100 mL), dried (MgSO<sub>4</sub>), filtered and solvent removed under reduced pressure. The residue was purified *via* Biotage (1:6, EtOAc-petroleum ether (40-60 °C), snap 50 g column, R<sub>f</sub> = 0.50) to give *N*-Boc-*N*-methyl phenylalanine methyl ester **115** (0.82 g, 2.80 mmol, 78%) as a light oil as a 0.6 : 0.4 mixture of amide rotamers;  $\nu_{\max}/\text{cm}^{-1}$  (CH<sub>2</sub>Cl<sub>2</sub>) 2975 (Ar(CH)), 1744 (CO<sub>2</sub>CH<sub>3</sub>), 1669 (NCO<sub>2</sub><sup>t</sup>Bu); <sup>1</sup>H NMR (400 MHz, CDCl<sub>3</sub>)  $\delta$  7.12-7.26 (5 H, m, Ar-H), 4.90 (0.6 H, s, CH), 4.53 (0.4 H, s, CH), 3.70 (3 H, s, COOCH<sub>3</sub>), 3.22 (1 H, m, CH<sub>2</sub>), 2.94 (1 H, m, CH<sub>2</sub>), 2.67 (3 H, s, NCH<sub>3</sub>), 1.30 (9 H, s, C(CH<sub>3</sub>)<sub>3</sub>); <sup>13</sup>C NMR (101 MHz, CDCl<sub>3</sub>)  $\delta$  172.11 (COOCH<sub>3</sub>), 171.82 (COOCH<sub>3</sub>), 156.01 (NCOOC(CH<sub>3</sub>)<sub>3</sub>), 155.16 (NCOOC(CH<sub>3</sub>)<sub>3</sub>), 137.92 (ArCH), 137.61 (ArCH), 129.24 (ArCH), 129.15 (ArCH), 128.74 (ArCH), 128.58 (ArCH), 126.84 (ArCH), 126.78 (ArCH), 80.46 (C(CH<sub>3</sub>)<sub>3</sub>), 80.18 (C(CH<sub>3</sub>)<sub>3</sub>), 61.86 (CH<sub>2</sub>CHC(O)OCH<sub>3</sub>), 59.73 (CH<sub>2</sub>CHC(O)OCH<sub>3</sub>), 52.35 (OCH<sub>3</sub>), 35.75 (CH<sub>2</sub>), 35.26 (CH<sub>2</sub>), 32.75 (CH<sub>3</sub>N), 32.12 (CH<sub>3</sub>N), 28.43 (C(CH<sub>3</sub>)<sub>3</sub>), 28.39 (C(CH<sub>3</sub>)<sub>3</sub>); *m/z*: 293 (26%, M<sup>+</sup>); Found [M+Na]<sup>+</sup> 316.1523, C<sub>16</sub>H<sub>23</sub>NNaO<sub>4</sub> requires 316.1525.

***N*-Methyl phenylalanine methyl ester **114****

Trifluoroacetic acid (1.2 mL, 15.58 mmol) was added to a solution of *N*-Boc-*N*-methyl phenylalanine methyl ester **115** (0.82 g, 2.80 mmol) in DCM (10 mL) at room temperature and the resulting solution stirred for 6 hours. The resulting mixture was quenched with saturated aqueous sodium hydrogen carbonate solution (30 mL). Solvent and excess trifluoroacetic acid were removed under reduced pressure. The residue was partitioned between dichloromethane (50 mL) and saturated aqueous sodium hydrogen carbonate solution (50 mL). The combined organic layers were dried ( $MgSO_4$ ), filtered and solvent removed under reduced pressure to give methyl-2-(methylamino)-3-phenylpropanoate **114** (0.53 g, 2.76 mmol, 99%) as a pale yellow oil; (1:2, EtOAc-petroleum ether (40-60°C),  $R_f = 0.08$ );  $\nu_{max}/cm^{-1}$  ( $CH_2Cl_2$ ) 2975 (Ar(CH)), 1744 ( $CO_2CH_3$ );  $^1H$  NMR (400 MHz,  $CDCl_3$ )  $\delta$  7.15 - 7.29 (5 H, m, Ar-H), 3.64 (3 H, s,  $COOCH_3$ ), 3.44 (1 H, t,  $J = 6.7$  Hz, CH), 2.94 (2 H, d,  $J = 6.7$  Hz,  $CH_2$ ), 2.35 (3 H, s,  $NCH_3$ ), 1.60 (1 H, s, NH);  $^{13}C$  NMR (101 MHz,  $CDCl_3$ )  $\delta$  174.64 ( $COOCH_3$ ), 137.07 (quaternary C), 129.0(ArCH), 128.37 (ArCH), 126.65 (ArCH), 64.69 (CH), 51.66 ( $OCH_3$ ), 39.51 ( $CH_2$ ), 34.62 ( $CH_3N$ );  $m/z$  194.1 (100%,  $[M+H]^+$ ); Found  $[M+H]^+$  194.1183,  $C_{11}H_{16}NO_2$  requires 194.1181.

**(Z)-2-((3-Methoxy-3-oxo-1-phenylprop-1-en-2-yl)(methyl)amino)-2-oxoethane-1,1-diyl diacetate **112****

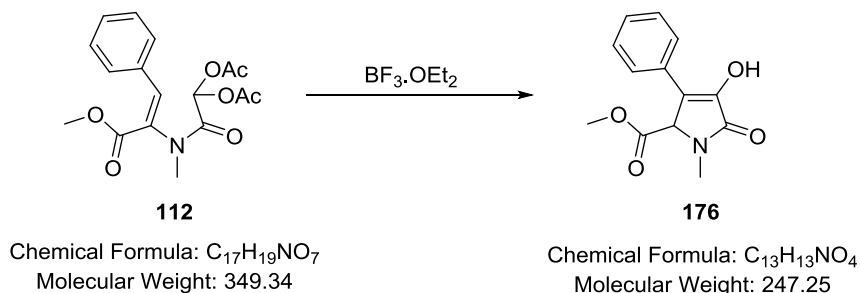


Chemical Formula: C<sub>11</sub>H<sub>15</sub>NO<sub>2</sub>  
Molecular Weight: 193.25

Chemical Formula: C<sub>17</sub>H<sub>19</sub>NO<sub>7</sub>  
Molecular Weight: 349.34

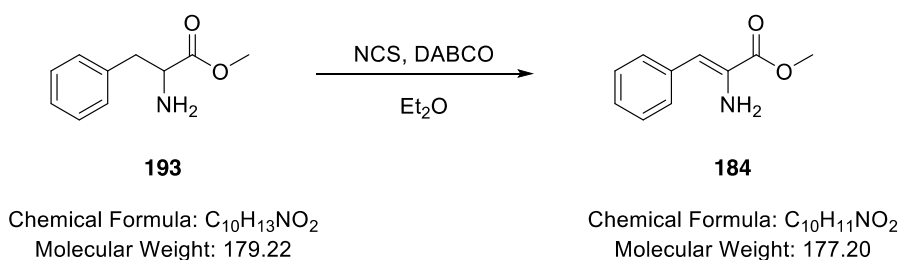
*tert*-Butyl hypochlorite (1.78 g, 16.4 mmol) was added in one portion to a stirred solution of *N*-methyl phenylalanine methyl ester **114** (3.01 g, 15.6 mmol) in diethyl ether (60 mL) in the dark (foil wrapped) and stirred for two hours. DABCO (2.75 g, 24.5 mmol) was added to the resulting mixture and the resulting mixture stirred in the absence of light for 12 hours. The reaction mixture was filtered and the solids washed with a little dry ether (15 mL). Solvent was removed under reduced pressure to give the crude dehydrogenated product **113**. The crude product thus obtained, was taken up in dichloromethane (100 mL) and a solution of sodium hydrogen carbonate (2.62 g, 31.2 mmol) in water (50 mL) was added, followed by rapid addition of a solution of diacetoxyacetyl chloride **119** (1.59 g, 8.19 mmol) in dichloromethane (20 mL). The resulting biphasic mixture was stirred rapidly for 24 hours. The layers were separated and the aqueous phase extracted with dichloromethane (2 x 50 mL). The combined extracts were dried (MgSO<sub>4</sub>), filtered and solvent removed under reduced pressure. Purification by Biotage (1:2, EtOAc-petroleum ether (40-60 °C), snap 50 g column, R<sub>f</sub> = 0.31) gave the title compound **112** (3.82 g, 10.9 mmol, 70%) as a yellow oil;  $\nu_{\max}/\text{cm}^{-1}$  (CH<sub>2</sub>Cl<sub>2</sub>) 3058, 3028, 2952, 1755, 1742 (CO<sub>2</sub>CH<sub>3</sub>), 1693 (C=O); <sup>1</sup>H NMR (400 MHz, CDCl<sub>3</sub>)  $\delta$  7.20-7.40 (5 H, m, Ar-H), 3.89 (1 H, s, HC=COOCH<sub>3</sub>), 3.71 (3 H, s, COOCH<sub>3</sub>), 3.19 (3 H, s, NCH<sub>3</sub>), 2.11 (6 H, s, (CH(OC(O)CH<sub>3</sub>)<sub>2</sub>); <sup>13</sup>C NMR (101 MHz, CDCl<sub>3</sub>)  $\delta$  170.29 (COOCH<sub>3</sub>), 164.94 (NCO(C(O)COCH<sub>3</sub>)<sub>2</sub>), 142.15 (quaternary C), 132.56 (HC=C), 131.39 (Ar-CH), 130.86 (Ar-CH), 129.70 (Ar-CH), 100.21 (HC=C), 83.48 (C(O)CH(OAc)<sub>2</sub>), 52.30 (COOCH<sub>3</sub>), 36.23 (NCH<sub>3</sub>), 20.41 (CH(OC(O)CH<sub>3</sub>)<sub>2</sub>); *m/z* 349 (31%, M<sup>+</sup>), 218 (36), 191 (100), 131 (51); Found [M<sup>+</sup>] 349.11615, C<sub>17</sub>H<sub>19</sub>NO<sub>7</sub> requires 349.11686.

**Methyl 4-hydroxy-1-methyl-5-oxo-3-phenyl-4, 5-dihydro-1H-pyrrole-2-carboxylate 176**

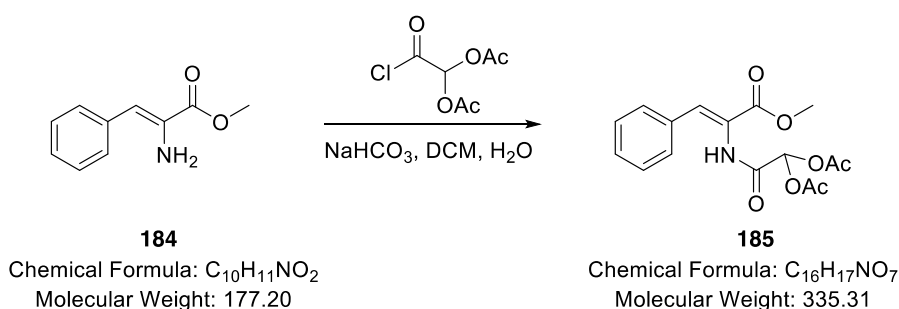


Boron trifluoride diethyl etherate (8.00 mL, 63.1 mmol) was added to amide **112** (1.64 g, 4.69 mmol) at room temperature and the resulting mixture stirred for 36 hours. The mixture was poured into water (40-50 mL) and extracted with dichloromethane (3 x 30 mL). The combined organic extracts were washed with water (2 x 50 mL), dried (MgSO<sub>4</sub>), filtered and solvent removed under reduced pressure. The residue was purified by Biotage (1:2, EtOAc-petroleum ether (40-60 °C), snap 25 g column, R<sub>f</sub> = 0.21) and further purified by recrystallisation (methanol) to give methyl 4-hydroxy-1-methyl-5-oxo-3-phenyl-2,5-dihydro-1H-pyrrole-2-carboxylate **176** (0.856 g, 3.94 mmol, 72%) as a white solid; mp. 219-221 °C;  $\nu_{\text{max}}/\text{cm}^{-1}$  (CH<sub>2</sub>Cl<sub>2</sub>) 3133 (OH), 1741 (COOCH<sub>3</sub>), 1687 (C=O), 1206 (NCH<sub>3</sub>); <sup>1</sup>H NMR (400 MHz, CDCl<sub>3</sub>)  $\delta$  7.72 - 7.66 (2 H, m, Ar-H), 7.27 - 7.36 (2 H, m, Ar-H), 7.17- 7.24 (1 H, m, Ar-H), 6.42 (1 H, s, OH), 4.92(1 H, s, CHCO<sub>2</sub>CH<sub>3</sub>), 3.63 (3 H, s, CO<sub>2</sub>CH<sub>3</sub>), 3.01 (3 H, s, NCH<sub>3</sub>); <sup>13</sup>C NMR (101 MHz, CDCl<sub>3</sub>)  $\delta$  168.93 (CO<sub>2</sub>CH<sub>3</sub>), 167.75 (NCO), 143.45 (C(OH)=C(Ph)), 130.78 (quaternary C), 128.59 (Ar-CH), 127.90 (Ar-CH), 126.85 (Ar-CH), 116.98 (C(OH)=C(Ph)), 63.28 (CH(COOCH<sub>3</sub>)), 53.01 (OCH<sub>3</sub>), 28.61 (NCH<sub>3</sub>); *m/z* 246 (100%, M-H<sup>+</sup>), 217.9 (43%); Found [M+H<sup>+</sup>] 248.0931, C<sub>13</sub>H<sub>14</sub>NO<sub>4</sub> requires 248.0923.

BF <sub>3</sub> ·Et <sub>2</sub> O(eq.)	Solvent	Boiling point[°C]	Yield	Time [hrs]
2	DCM	40 °C	58%	12 (reflux)
2	DCE	60 °C	62%	6 (reflux)
20	neat	126 °C	70%	3 (reflux)
20	neat	-	72%	36 (r. t.)

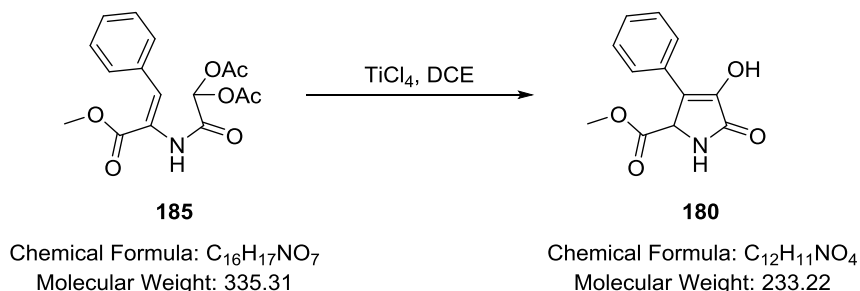
**(Z)-Methyl 2-amino-3-phenylacrylate 184**

*N*-Chlorosuccinimide (8.06 g, 60.4 mmol) was added portionwise over two hours to a stirred solution of phenylalanine methyl ester **193** (10.8 g, 60.4 mmol). The resulting mixture was stirred for 2 hours in the dark (foil wrapped). Solvent was removed in the dark and the residue taken up in petroleum spirit (150 mL), filtered and solvent removed under reduced pressure. The residue was taken up in diethyl ether (150 mL) and DABCO (8.13 g, 72.4 mmol) added and the resulting mixture stirred in the absence of light for 12 hours. The mixture was filtered and solvent removed under reduced pressure. The residue was purified by flash column chromatography (1:5, EtOAc -petroleum spirit 40-60 °C,  $R_f = 0.53$ ) to give the amine **184** as a yellow semi-solid (2.80 g, 15.80 mmol, 26%);  $\nu_{\max}/\text{cm}^{-1}$  (CH<sub>2</sub>Cl<sub>2</sub>) 3367 (NH<sub>2</sub>), 2951 (C=CH), 1710 (CO<sub>2</sub>CH<sub>3</sub>); <sup>1</sup>H NMR (400 MHz, CDCl<sub>3</sub>)  $\delta$  7.12 - 7.26 (5 H, m, Ar-H), 6.43 (1 H, s, CH=C), 4.18 (2 H, s, NH<sub>2</sub>), 3.81 (3 H, s, COOCH<sub>3</sub>); <sup>13</sup>C NMR (101 MHz, CDCl<sub>3</sub>)  $\delta$  166.38 (C=O), 136.71 (quaternary C), 132.35 (CH=C), 129.10 (ArCH), 128.15 (ArCH), 127.24 (ArCH), 109.67 (CH=C), 52.87 (OCH<sub>3</sub>). Due to the unstable nature of this compound further data was not obtained.

**(Z)-2-((3-Methoxy-3-oxo-1-phenylprop-1-en-2-yl)amino)-2-oxoethane-1,1-diyl diacetate 185**

A solution of sodium hydrogen carbonate (2.44 g, 29.0 mmol) in water (100 mL) was added to a solution of amine (5.14 g, 29.0 mmol) in DCM (150 mL), followed by addition of a solution of diacetoxyacetyl chloride **119** (5.64 g, 29.0 mmol) in DCM (50 mL). The resulting biphasic mixture was stirred for 12 hours. The layers were separated and the aqueous phase extracted with dichloromethane (2 x 50 mL). The combined extracts were dried (MgSO<sub>4</sub>), filtered and solvent removed under reduced pressure. Purification by flash column chromatography (1:2, EtOAc -petroleum spirit (40-60 °C), R<sub>f</sub> = 0.22) gave the title compound **185** as a colourless oil (7.21 g, 21.5 mmol, 74%);  $\nu_{\max}/\text{cm}^{-1}$  (CH<sub>2</sub>Cl<sub>2</sub>) 3446 (NH), 1746.6 (CO<sub>2</sub>CH<sub>3</sub>), 1693, 1434, 1224; <sup>1</sup>H NMR (400 MHz, CDCl<sub>3</sub>)  $\delta$  8.08 (1 H, s, NH), 7.42-7.45 (2 H, m, Ar-H), 7.38 (1 H, s, CH(OAc)<sub>2</sub>), 7.30-7.34 (3 H, m, Ar-H), 6.91 (1 H, s, HC=C), 3.74 (3 H, s, OCH<sub>3</sub>), 2.11 (6 H, s, (CH(OC(O)CH<sub>3</sub>)<sub>2</sub>); <sup>13</sup>C NMR (101 MHz, CDCl<sub>3</sub>)  $\delta$  168.48 (COOCH<sub>3</sub>), 165.11 (CH<sub>3</sub>NCO(COCOCH<sub>3</sub>)<sub>2</sub>), 133.92 (quaternary C), 133.04 (HC=C), 131.39 (Ar-CH), 129.78 (Ar-CH), 128.44 (Ar-CH), 122.81 (HC=C), 85.10 (C(O)CH(OAc)<sub>2</sub>), 53.03 (COOCH<sub>3</sub>), 20.51 (CH(OC(O)CH<sub>3</sub>)<sub>2</sub>); *m/z* 358.1 (100%, [M+Na]<sup>+</sup>); Found [M+Na]<sup>+</sup> 358.0914, C<sub>16</sub>H<sub>17</sub>NNaO<sub>7</sub> requires 358.0903.

**Methyl 4-hydroxy-5-oxo-3-phenyl-2,5-dihydro-1H-pyrrole-2-carboxylate**  
**180**



Titanium tetrachloride (3.29  $\mu\text{L}$ , 0.03 mmol) was added to a solution of amide **185** (0.01 g, 0.03 mmol) in 1,2-dichloroethane (0.15 mL) and the resulting mixture heated at reflux for 2 hours. The resulting brown solution was concentrated under reduced pressure and the residue taken up in DCM (10 mL) poured into water (40-50 mL) and extracted with dichloromethane (3 x 30 mL). The combined organic extracts were washed with water (2 x 50 mL), dried ( $\text{MgSO}_4$ ), filtered and solvent was removed under reduced pressure. The product was purified by recrystallisation (ethyl acetate/ petroleum spirit) to give methyl 4-hydroxy-5-oxo-3-phenyl-2,5-dihydro-1H-pyrrole-2-carboxylate **180** (3.60 mg, 0.02 mmol, 52%) as a pale yellow solid;  $\nu_{\text{max}}/\text{cm}^{-1}$  ( $\text{CH}_2\text{Cl}_2$ ) 3133.4 (OH), 1741.34 ( $\text{COOCH}_3$ ), 1687.5 ( $\text{C}=\text{O}$ );  $^1\text{H}$  NMR (400 MHz,  $\text{CDCl}_3$ ) 7.73 - 7.77 (2 H, s, Ar-H), 7.39-7.45 (2 H, s, Ar-H), 7.30-7.35 (1 H, s, Ar-H), 6.60 (1 H, s, OH), 6.34 (1 H, br. s, NH), 5.17 (1 H, d,  $J$  1.0,  $\text{CH}(\text{CO}_2\text{CH}_3)$ ), 3.70 (3 H, s,  $\text{OCH}_3$ );  $^{13}\text{C}$  NMR (101 MHz,  $\text{CDCl}_3$ )  $\delta$  168.37 ( $\text{C}=\text{O}$ ), 165.07 ( $\text{CH}(\text{COOCH}_3)$ ), 140.82 ( $\text{C}(\text{OH})=\text{C}(\text{Ph})$ ), 130.01 (quaternary C), 129.87 (Ar-CH), 128.92 (Ar-CH), 128.76 (Ar-CH), 116.48 ( $\text{C}(\text{OH})=\text{C}(\text{Ph})$ ), 61.66 ( $\text{CH}(\text{COOCH}_3)$ ), 53.62 ( $\text{OCH}_3$ ); Found  $[\text{M}+\text{Na}]^+$  256.0595,  $\text{C}_{12}\text{H}_{11}\text{NO}_4\text{Na}$  requires 256.0586.

## 12.0. References

## 12.0. References

### References

- ABELL, P. I. & LENNON, D. J. J. 1965. Stereochemistry of the Decarboxylation of Some 1,1,2-Cycloalkanetricarboxylic Acids<sup>1</sup>. *The Journal of Organic Chemistry*, 30, 1206-1208.
- ACSADY, L., KAMONDI, A., SIK, A., FREUND, T. & BUZSAKI, G. 1998. GABAergic cells are the major postsynaptic targets of mossy fibers in the rat hippocampus. *J Neurosci*, 18, 3386-403.
- ADEBAJO, A. C., IWALEWA, E. O., OBUOTOR, E. M., IBIKUNLE, G. F., OMISORE, N. O., ADEWUNMI, C. O., OBAPARUSI, O. O., KLAES, M., ADETOGUN, G. E., SCHMIDT, T. J. & VERSPOHL, E. J. 2009. Pharmacological properties of the extract and some isolated compounds of *Clausena lansium* stem bark: anti-trichomonal, antidiabetic, anti-inflammatory, hepatoprotective and antioxidant effects. *J Ethnopharmacol*, 122, 10-9.
- AHMED, A. H. & OSWALD, R. E. 2010. Piracetam defines a new binding site for allosteric modulators of alpha-amino-3-hydroxy-5-methyl-4-isoxazole-propionic acid (AMPA) receptors. *J Med Chem*, 53, 2197-203.
- AKHONDZADEH, S., TAJDAR, H., MOHAMMADI, M. R., MOHAMMADI, M., NOUROOZINEJAD, G. H., SHABSTARI, O. L. & GHELICHNIA, H. A. 2008. A double-blind placebo controlled trial of piracetam added to risperidone in patients with autistic disorder. *Child Psychiatry Hum Dev*, 39, 237-45.

- ALLE, H., KUBOTA, H. & GEIGER, J. R. 2011. Sparse but highly efficient Kv3 outpace BKCa channels in action potential repolarization at hippocampal mossy fiber boutons. *J Neurosci*, 31, 8001-12.
- AMARAL, D. G., ISHIZUKA, N. & CLAIBORNE, B. 1990. Neurons, numbers and the hippocampal network. *Prog Brain Res*, 83, 1-11.
- AMARAL, D. G., SCHARFMAN, H. E. & LAVENEX, P. 2007. The dentate gyrus: fundamental neuroanatomical organization (dentate gyrus for dummies). *Prog Brain Res*, 163, 3-22.
- AMARAL, D. G. & WITTER, M. P. 1989. The three-dimensional organization of the hippocampal formation: a review of anatomical data. *Neuroscience*, 31, 571-91.
- ANDERSEN P, M. R., AMARAL DJ, BLISS TV, O'KEEFE J 2007a.
- ANDERSEN P, M. R., AMARAL DJ, BLISS TV, O'KEEFE J 2007b. *The Hippocampus Book*, New York, Oxford University Press.
- ARAI, A. & LYNCH, G. 1992. Factors regulating the magnitude of long-term potentiation induced by theta pattern stimulation. *Brain Res*, 598, 173-84.
- ARAI, A. C., XIA, Y. F. & SUZUKI, E. 2004. Modulation of AMPA receptor kinetics differentially influences synaptic plasticity in the hippocampus. *Neuroscience*, 123, 1011-24.
- ASCHER, P. & NOWAK, L. 1988. The role of divalent cations in the N-methyl-D-aspartate responses of mouse central neurones in culture. *J Physiol*, 399, 247-66.

- AUSTIN, J. E. & BUCKMASTER, P. S. 2004. Recurrent excitation of granule cells with basal dendrites and low interneuron density and inhibitory postsynaptic current frequency in the dentate gyrus of macaque monkeys. *J Comp Neurol*, 476, 205-18.
- BARBERIS, A., SACHIDHANANDAM, S. & MULLE, C. 2008. GluR6/KA2 kainate receptors mediate slow-deactivating currents. *J Neurosci*, 28, 6402-6.
- BARNES, S. J., OPITZ, T., MERKENS, M., KELLY, T., VON DER BRELIE, C., KRUEPPEL, R. & BECK, H. 2010. Stable mossy fiber long-term potentiation requires calcium influx at the granule cell soma, protein synthesis, and microtubule-dependent axonal transport. *J Neurosci*, 30, 12996-3004.
- BATYSHEVA, T. T., BAGIR, L. V., KOSTENKO, E. V., ARTEMOVA, I. Y., VDOVICHENKO, T. V., GANZHULA, P. A., ZHURAVLEVA, E. Y., ISMAILOV, A. M., LISENKER, L. N., NESTEROVA, O. V., OTCHESKAYA, O. V., ROTOR, L. D., KHOZOVA, A. A. & BOIKO, A. N. 2009. Experience of the out-patient use of memotropil in the treatment of cognitive disorders in patients with chronic progressive cerebrovascular disorders. *Neurosci Behav Physiol*, 39, 193-7.
- BEKKERS, J. M. & STEVENS, C. F. 1989. NMDA and non-NMDA receptors are co-localized at individual excitatory synapses in cultured rat hippocampus. *Nature*, 341, 230-3.
- BELLOCCHIO, E. E., REIMER, R. J., FREMEAU, R. T., JR. & EDWARDS, R. H. 2000. Uptake of glutamate into synaptic vesicles by an inorganic phosphate transporter. *Science*, 289, 957-60.

- BENOITON, N. L., DEMAYO, R. E., MOORE, G. J. & COGGINS, J. R. 1971. A modified synthesis of -N-carbobenzoxy-L-lysine and the preparation and analysis of mixtures of -N-methyllysines. *Can J Biochem*, 49, 1292-5.
- BERG, L. K., LARSSON, M., MORLAND, C. & GUNDERSEN, V. 2013. Pre- and postsynaptic localization of NMDA receptor subunits at hippocampal mossy fibre synapses. *Neuroscience*, 230, 139-50.
- BERGERSEN, L., RUIZ, A., BJAALIE, J. G., KULLMANN, D. M. & GUNDERSEN, V. 2003. GABA and GABAA receptors at hippocampal mossy fibre synapses. *Eur J Neurosci*, 18, 931-41.
- BISCHOFBERGER, J., ENGEL, D., LI, L., GEIGER, J. R. & JONAS, P. 2006. Patch-clamp recording from mossy fiber terminals in hippocampal slices. *Nat Protoc*, 1, 2075-81.
- BISCHOFBERGER, J., GEIGER, J. R. & JONAS, P. 2002. Timing and efficacy of Ca<sup>2+</sup> channel activation in hippocampal mossy fiber boutons. *J Neurosci*, 22, 10593-602.
- BLACKSTAD, T. W., BRINK, K., HEM, J. & JEUNE, B. 1970. Distribution of hippocampal mossy fibers in the rat. An experimental study with silver impregnation methods. *J Comp Neurol*, 138, 433-49.
- BLISS, T. V. & COLLINGRIDGE, G. L. 2013. Expression of NMDA receptor-dependent LTP in the hippocampus: bridging the divide. *Mol Brain*, 6, 5.
- BLISS, T. V., COLLINGRIDGE, G. L. & MORRIS, R. G. 2014. Synaptic plasticity in health and disease: introduction and overview. *Philos Trans R Soc Lond B Biol Sci*, 369, 20130129.

- BORTOLOTTI, Z. A., NISTICO, R., MORE, J. C., JANE, D. E. & COLLINGRIDGE, G. L. 2005. Kainate receptors and mossy fiber LTP. *Neurotoxicology*, 26, 769-77.
- CAJAL, R. Y. 1909. *Histologie du systeme nerveux de l'homme et des vertebres*
- CHOPIN, P. & BRILEY, M. 1992. Effects of four non-cholinergic cognitive enhancers in comparison with tacrine and galanthamine on scopolamine-induced amnesia in rats. *Psychopharmacology (Berl)*, 106, 26-30.
- CLAIBORNE, B. J., AMARAL, D. G. & COWAN, W. M. 1986. A light and electron microscopic analysis of the mossy fibers of the rat dentate gyrus. *J Comp Neurol*, 246, 435-58.
- CLAIBORNE, B. J., AMARAL, D. G. & COWAN, W. M. 1990. Quantitative, three-dimensional analysis of granule cell dendrites in the rat dentate gyrus. *J Comp Neurol*, 302, 206-19.
- COLE, K. S. & CURTIS, H. J. 1939. ELECTRIC IMPEDANCE OF THE SQUID GIANT AXON DURING ACTIVITY. *J Gen Physiol*, 22, 649-70.
- COPANI, A., GENAZZANI, A. A., ALEPPO, G., CASABONA, G., CANONICO, P. L., SCAPAGNINI, U. & NICOLETTI, F. 1992. Nootropic drugs positively modulate alpha-amino-3-hydroxy-5-methyl-4-isoxazolepropionic acid-sensitive glutamate receptors in neuronal cultures. *J Neurochem*, 58, 1199-204.
- CORSELLIS, J. A. & BRUTON, C. J. 1983. Neuropathology of status epilepticus in humans. *Adv Neurol*, 34, 129-39.

- CROISILE, B., TRILLET, M., FONDARAI, J., LAURENT, B., MAUGUIERE, F. & BILLARDON, M. 1993. Long-term and high-dose piracetam treatment of Alzheimer's disease. *Neurology*, 43, 301-5.
- CULL-CANDY, S., KELLY, L. & FARRANT, M. 2006. Regulation of Ca<sup>2+</sup>-permeable AMPA receptors: synaptic plasticity and beyond. *Curr Opin Neurobiol*, 16, 288-97.
- DAI, X. & HUANG, P. 2012. A Short and Flexible Synthetic Approach to the Naturally Occurring Racemic Neoclausenamide and Its Analogs. *Chinese Journal of Chemistry*, 30, 1953-1956.
- DENG, W., AIMONE, J. B. & GAGE, F. H. 2010. New neurons and new memories: how does adult hippocampal neurogenesis affect learning and memory? *Nat Rev Neurosci*, 11, 339-50.
- DERRICK, B. E., WEINBERGER, S. B. & MARTINEZ, J. L., JR. 1991. Opioid receptors are involved in an NMDA receptor-independent mechanism of LTP induction at hippocampal mossy fiber-CA3 synapses. *Brain Res Bull*, 27, 219-23.
- DONEVAN, S. D. & ROGAWSKI, M. A. 1993. GYKI 52466, a 2,3-benzodiazepine, is a highly selective, noncompetitive antagonist of AMPA/kainate receptor responses. *Neuron*, 10, 51-9.
- DURAND, G. M., KOVALCHUK, Y. & KONNERTH, A. 1996. Long-term potentiation and functional synapse induction in developing hippocampus. *Nature*, 381, 71-5.
- EDWARDS, F. A., KONNERTH, A., SAKMANN, B. & TAKAHASHI, T. 1989. A thin slice preparation for patch clamp recordings from neurones of the mammalian central nervous system. *Pflugers Arch*, 414, 600-12.

- ENGEL, D. & JONAS, P. 2005. Presynaptic action potential amplification by voltage-gated Na<sup>+</sup> channels in hippocampal mossy fiber boutons. *Neuron*, 45, 405-17.
- ERKER, G., RIEDEL, M., KOCH, S., JOEDICKE, T. & WUERTHWEIN, E.-U. 1995. Preparation of Stable Primary Enamines: 1-Aminobutadienes by Allyl Grignard Addition to Aryl Cyanides Followed by Controlled Hydrolysis. *The Journal of Organic Chemistry*, 60, 5284-5290.
- FEDI, M., REUTENS, D., DUBEAU, F., ANDERMANN, E., D'AGOSTINO, D. & ANDERMANN, F. 2001. Long-term efficacy and safety of piracetam in the treatment of progressive myoclonus epilepsy. *Arch Neurol*, 58, 781-6.
- FENG, Z., LI, X., ZHENG, G. & HUANG, L. 2009. Synthesis and activity in enhancing long-term potentiation (LTP) of clausenamide stereoisomers. *Bioorg Med Chem Lett*, 19, 2112-5.
- FOSTER, A. C., MENA, E. E., MONAGHAN, D. T. & COTMAN, C. W. 1981. Synaptic localization of kainic acid binding sites. *Nature*, 289, 73-5.
- FROESTL, W., MUHS, A. & PFEIFER, A. 2012. Cognitive enhancers (nootropics). Part 1: drugs interacting with receptors. *J Alzheimers Dis*, 32, 793-887.
- GAINOTTI, G., BENEDETTI, N., CALTAGIRONE, C. & NOCENTINI, U. 1986. Cognitive improvement in clinical trials with nootropic drugs: when can it be expected and how to clarify its meaning. *Clin Neuropharmacol*, 9 Suppl 3, S65-9.
- GARENGEOT, D. 1742. *Splanchnologie ou l'anatomie des visceres*, Paris, C. Osmond.

- GEIGER, J. R. & JONAS, P. 2000. Dynamic control of presynaptic Ca(2+) inflow by fast-inactivating K(+) channels in hippocampal mossy fiber boutons. *Neuron*, 28, 927-39.
- GIELEN, M., SIEGLER RETCHLESS, B., MONY, L., JOHNSON, J. W. & PAOLETTI, P. 2009. Mechanism of differential control of NMDA receptor activity by NR2 subunits. *Nature*, 459, 703-7.
- GIURGEA, C. E., GREINDL, M. G. & PREAT, S. 1983. Nootropic drugs and aging. *Acta Psychiatr Belg*, 83, 349-58.
- GOLA, M. & ROMEY, G. 1970. Reponses anormales a des courants sous-liminaire de certaines membranes somatiques (neurones géants d'*Helix pomatia*). *Pflügers Archiv*, 327, 105-131.
- GUSEV, E. I., BOIKO, A. N., KOL'IAK, E. V., KARALKIN, A. V., KAMCHATOV, P. R. & MARTYNOV, M. 2008. [The impact of microcirculation dysfunction on the clinical presentations of multiple sclerosis in patients above 45 years and the possible ways of correction of the vascular pathology]. *Zh Nevrol Psikhiatr Im S S Korsakova*, 108, 25-31.
- GUTIERREZ, R. 2000. Seizures induce simultaneous GABAergic and glutamatergic transmission in the dentate gyrus-CA3 system. *J Neurophysiol*, 84, 3088-90.
- HAKKARAINEN, H. & HAKAMIES, L. 1978. Piracetam in the treatment of post-concussional syndrome. A double-blind study. *Eur Neurol*, 17, 50-5.

- HAMILL, O. P., MARTY, A., NEHER, E., SAKMANN, B. & SIGWORTH, F. J. 1981. Improved patch-clamp techniques for high-resolution current recording from cells and cell-free membrane patches. *Pflugers Arch*, 391, 85-100.
- HARRIS, E. W. & COTMAN, C. W. 1986. Long-term potentiation of guinea pig mossy fiber responses is not blocked by N-methyl D-aspartate antagonists. *Neurosci Lett*, 70, 132-7.
- HARTWIG, W. & BORN, L. 1987. Diastereoselective and enantioselective total synthesis of the hepatoprotective agent clausenamide. *The Journal of Organic Chemistry*, 52, 4352-4358.
- HE, M., ROMMEL, M. & BODE, J. W. 2012. Formal Synthesis of (±)-Clausenamide by NHC-Catalyzed  $\gamma$ -Lactam Formation. *Heterocycles*, 86, 1689-1696.
- HEBB, D. 1949. *The organization of behavior*, New York, Wiley & Sons.
- HEISE, G. A. 1987. Facilitation of memory and cognition by drugs. *Trends Pharmacol Sci.*, 8, 65.
- HENZE, D. A., URBAN, N. N. & BARRIONUEVO, G. 2000. The multifarious hippocampal mossy fiber pathway: a review. *Neuroscience*, 98, 407-27.
- HOLINSKI, S., CLAUS, B., ALAARAJ, N., DOHMEN, P. M., KIRILOVA, K., NEUMANN, K., UEBELHACK, R. & KONERTZ, W. 2008. Cerebroprotective effect of piracetam in patients undergoing coronary bypass surgery. *Med Sci Monit*, 14, Pi53-7.

- HOLINSKI, S., CLAUS, B., ALAARAJ, N., DOHMEN, P. M., NEUMANN, K., UEBELHACK, R. & KONERTZ, W. 2011. Cerebroprotective effect of piracetam in patients undergoing open heart surgery. *Ann Thorac Cardiovasc Surg*, 17, 137-42.
- [HTTP://WWW.ALZHEIMERS.ORG.UK](http://www.alzheimers.org.uk). Available:  
<http://www.alzheimers.org.uk> [Accessed].
- HUANG, Y. Y., LI, X. C. & KANDEL, E. R. 1994. cAMP contributes to mossy fiber LTP by initiating both a covalently mediated early phase and macromolecular synthesis-dependent late phase. *Cell*, 79, 69-79.
- HUETTNER, J. E. 2003. Spine-tingling excitement from glutamate receptors. *Sci STKE*, 2003, pe53.
- HUGANIR, R. L. & NICOLL, R. A. 2013. AMPARs and synaptic plasticity: the last 25 years. *Neuron*, 80, 704-17.
- HUTT, A. J. & VALENTOVÁ, J. 2003. The Chiral Switch: The Development of Single Enantiomer Drugs from Racemates. *Acta Facultatis Pharmaceuticae Universitatis Comeniana*, 50, 7-23.
- INGVAR, M., AMBROS-INGERSON, J., DAVIS, M., GRANGER, R., KESSLER, M., ROGERS, G. A., SCHEHR, R. S. & LYNCH, G. 1997. Enhancement by an ampakine of memory encoding in humans. *Exp Neurol*, 146, 553-9.
- ISAACSON, J. S. & NICOLL, R. A. 1991. Aniracetam reduces glutamate receptor desensitization and slows the decay of fast excitatory synaptic currents in the hippocampus. *Proc Natl Acad Sci U S A*, 88, 10936-40.

- ISHIZUKA, N., COWAN, W. M. & AMARAL, D. G. 1995. A quantitative analysis of the dendritic organization of pyramidal cells in the rat hippocampus. *J Comp Neurol*, 362, 17-45.
- ISHIZUKA, N., WEBER, J. & AMARAL, D. G. 1990. Organization of intrahippocampal projections originating from CA3 pyramidal cells in the rat. *J Comp Neurol*, 295, 580-623.
- ITO, I., TANABE, S., KOHDA, A. & SUGIYAMA, H. 1990. Allosteric potentiation of quisqualate receptors by a nootropic drug aniracetam. *J Physiol*, 424, 533-43.
- JUNG, M. W. & MCNAUGHTON, B. L. 1993. Spatial selectivity of unit activity in the hippocampal granular layer. *Hippocampus*, 3, 165-82.
- KAMIYA, H. & OZAWA, S. 2000. Kainate receptor-mediated presynaptic inhibition at the mouse hippocampal mossy fibre synapse. *J Physiol*, 523 Pt 3, 653-65.
- KAMIYA, H., SHINOZAKI, H. & YAMAMOTO, C. 1996. Activation of metabotropic glutamate receptor type 2/3 suppresses transmission at rat hippocampal mossy fibre synapses. *J Physiol*, 493 ( Pt 2), 447-55.
- KANEKO, S., MAEDA, T. & SATOH, M. 1997. Cognitive enhancers and hippocampal long-term potentiation in vitro. *Behav Brain Res*, 83, 45-9.
- KAPUR, A., YECKEL, M. F., GRAY, R. & JOHNSTON, D. 1998. L-Type calcium channels are required for one form of hippocampal mossy fiber LTP. *J Neurophysiol*, 79, 2181-90.

- KEINANEN, K., WISDEN, W., SOMMER, B., WERNER, P., HERB, A., VERDOORN, T. A., SAKMANN, B. & SEEBURG, P. H. 1990. A family of AMPA-selective glutamate receptors. *Science*, 249, 556-60.
- KEW, J. N., KOESTER, A., MOREAU, J. L., JENCK, F., OUAGAZZAL, A. M., MUTEL, V., RICHARDS, J. G., TRUBE, G., FISCHER, G., MONTKOWSKI, A., HUNDT, W., REINSCHIED, R. K., PAULY-EVERS, M., KEMP, J. A. & BLUETHMANN, H. 2000. Functional consequences of reduction in NMDA receptor glycine affinity in mice carrying targeted point mutations in the glycine binding site. *J Neurosci*, 20, 4037-49.
- KIM, J. H. & SCIALLI, A. R. 2011. Thalidomide: The Tragedy of Birth Defects and the Effective Treatment of Disease. *Toxicological Sciences*, 122, 1-6.
- KISELEVA, T. N., LAGUTINA IU, M. & KRAVCHUK, E. A. 2005. [Effect of fezam on ocular dynamics in patients with senile macular degeneration]. *Vestn Oftalmol*, 121, 26-8.
- KOHARA, K., PIGNATELLI, M., RIVEST, A. J., JUNG, H. Y., KITAMURA, T., SUH, J., FRANK, D., KAJIKAWA, K., MISE, N., OBATA, Y., WICKERSHAM, I. R. & TONEGAWA, S. 2014. Cell type-specific genetic and optogenetic tools reveal hippocampal CA2 circuits. *Nat Neurosci*, 17, 269-79.
- KULLMANN, D. M. 2001. Presynaptic kainate receptors in the hippocampus: slowly emerging from obscurity. *Neuron*, 32, 561-4.
- KULLMANN, D. M. 2007. *The hippocampus book* Oxford; New York, Oxford University Press.

- KUMAR, J., SCHUCK, P. & MAYER, M. L. 2011. Structure and assembly mechanism for heteromeric kainate receptors. *Neuron*, 71, 319-31.
- LAURI, S. E., BORTOLOTTI, Z. A., NISTICO, R., BLEAKMAN, D., ORNSTEIN, P. L., LODGE, D., ISAAC, J. T. & COLLINGRIDGE, G. L. 2003. A role for Ca<sup>2+</sup> stores in kainate receptor-dependent synaptic facilitation and LTP at mossy fiber synapses in the hippocampus. *Neuron*, 39, 327-41.
- LEI, S., PELKEY, K. A., TOPOLNIK, L., CONGAR, P., LACAILLE, J. C. & MCBAIN, C. J. 2003. Depolarization-induced long-term depression at hippocampal mossy fiber-CA3 pyramidal neuron synapses. *J Neurosci*, 23, 9786-95.
- LENEGRE, A., CHERMAT, R., AVRIL, I., STERU, L. & PORSOLT, R. D. 1988. Specificity of piracetam's anti-amnesic activity in three models of amnesia in the mouse. *Pharmacol Biochem Behav*, 29, 625-9.
- LERMA, J. 2003. Roles and rules of kainate receptors in synaptic transmission. *Nat Rev Neurosci*, 4, 481-95.
- LERMA, J. & MARQUES, J. M. 2013. Kainate receptors in health and disease. *Neuron*, 80, 292-311.
- LI, L., BISCHOFBERGER, J. & JONAS, P. 2007. Differential gating and recruitment of P/Q-, N-, and R-type Ca<sup>2+</sup> channels in hippocampal mossy fiber boutons. *J Neurosci*, 27, 13420-9.
- LI, X., ZHU, C., LI, C., WU, K., HUANG, D. & HUANG, L. 2010. Synthesis of N-substituted Clausenamide analogues. *Eur J Med Chem*, 45, 5531-8.

- LIANG, Y., YUAN, L. L., JOHNSTON, D. & GRAY, R. 2002. Calcium signaling at single mossy fiber presynaptic terminals in the rat hippocampus. *J Neurophysiol*, 87, 1132-7.
- LIAO, D., HESSLER, N. A. & MALINOW, R. 1995. Activation of postsynaptically silent synapses during pairing-induced LTP in CA1 region of hippocampal slice. *Nature*, 375, 400-4.
- LISMAN, J., SCHULMAN, H. & CLINE, H. 2002. The molecular basis of CaMKII function in synaptic and behavioural memory. *Nat Rev Neurosci*, 3, 175-90.
- LIU, D., YU, X. & HUANG, L. 2013. Novel Concise Synthesis of (-)-Clausenamide. *Chinese Journal of Chemistry*, 31, 344-348.
- LIU, S. & ZHANG, J. 1998. [Difference between the effects of (-) clausenamide and (+) clausenamide on the synaptic transmission in the dentate gyrus of anesthetized rats]. *Yao Xue Xue Bao*, 33, 254-8.
- LIU, S. J. & CULL-CANDY, S. G. 2002. Activity-dependent change in AMPA receptor properties in cerebellar stellate cells. *J Neurosci*, 22, 3881-9.
- LIU, S. L., ZHAO, M. R. & ZHANG, J. T. 1999. Effects of (-), (+)-clausenamide on anisodine-induced acetylcholine decrease and associated memory deficits in the mouse brain. *Acta Pharm. Sin.*, 33, 259-263.
- LU, S. P. & LEWIN, A. H. 1998. Enamine/imine tautomerism in  $\alpha,\beta$ -unsaturated- $\alpha$ -amino acids. *Tetrahedron*, 54, 15097-15104.

- LUKYANETZ, E. A., SHKRYL, V. M. & KOSTYUK, P. G. 2002. Selective blockade of N-type calcium channels by levetiracetam. *Epilepsia*, 43, 9-18.
- MALENKA, R. C. & BEAR, M. F. 2004. LTP and LTD: an embarrassment of riches. *Neuron*, 44, 5-21.
- MALYKH, A. G. & SADAIE, M. R. 2010. Piracetam and piracetam-like drugs: from basic science to novel clinical applications to CNS disorders. *Drugs*, 70, 287-312.
- MARCHAL, C. & MULLE, C. 2004. Postnatal maturation of mossy fibre excitatory transmission in mouse CA3 pyramidal cells: a potential role for kainate receptors. *J Physiol*, 561, 27-37.
- MARISCO, P. C., CARVALHO, F. B., ROSA, M. M., GIRARDI, B. A., GUTIERRES, J. M., JAQUES, J. A., SALLA, A. P., PIMENTEL, V. C., SCHETINGER, M. R., LEAL, D. B., MELLO, C. F. & RUBIN, M. A. 2013. Piracetam prevents scopolamine-induced memory impairment and decrease of NTPDase, 5'-nucleotidase and adenosine deaminase activities. *Neurochem Res*, 38, 1704-14.
- MARQUES, F., SOUSA, J., SOUSA, N. & PALHA, J. 2013. Blood-brain-barriers in aging and in Alzheimer's disease. *Molecular Neurodegeneration*, 8, 38.
- MAYER, M. L. 2005. Crystal structures of the GluR5 and GluR6 ligand binding cores: molecular mechanisms underlying kainate receptor selectivity. *Neuron*, 45, 539-52.

- MAYER, M. L., WESTBROOK, G. L. & GUTHRIE, P. B. 1984. Voltage-dependent block by Mg<sup>2+</sup> of NMDA responses in spinal cord neurones. *Nature*, 309, 261-3.
- MCBAIN, C. & DINGLELINE, R. 1992. Dual-component miniature excitatory synaptic currents in rat hippocampal CA3 pyramidal neurons. *J Neurophysiol*, 68, 16-27.
- MORIGUCHI, S., TANAKA, T., NARAHASHI, T. & FUKUNAGA, K. 2013. Novel nootropic drug sunifiram enhances hippocampal synaptic efficacy via glycine-binding site of N-methyl-D-aspartate receptor. *Hippocampus*, 23, 942-51.
- MUSSO, H. 1968. Selektive Synthesen der endo- und exo-Norcaran-carbonsäuren-(7). *Chemische Berichte*, 101, 3710-3720.
- NAVARRO, S. A., SERAFIM, K. G., MIZOKAMI, S. S., HOHMANN, M. S., CASAGRANDE, R. & VERRI, W. A., JR. 2013. Analgesic activity of piracetam: effect on cytokine production and oxidative stress. *Pharmacol Biochem Behav*, 105, 183-92.
- NEHER, E. & SAKMANN, B. 1976. Single-channel currents recorded from membrane of denervated frog muscle fibres. *Nature*, 260, 799-802.
- NEHER, E. & SAKMANN, B. 1992. The patch clamp technique. *Sci Am*, 266, 44-51.
- NICOLL, R. A. & MALENKA, R. C. 1995. Contrasting properties of two forms of long-term potentiation in the hippocampus. *Nature*, 377, 115-8.

- NICOLL, R. A. & SCHMITZ, D. 2005. Synaptic plasticity at hippocampal mossy fibre synapses. *Nat Rev Neurosci*, 6, 863-76.
- NING, N., HU, J. F., SUN, J. D., HAN, N., ZHANG, J. T. & CHEN, N. H. 2012a. (-)Clausenamide facilitates synaptic transmission at hippocampal Schaffer collateral-CA1 synapses. *Eur J Pharmacol*, 682, 50-5.
- NING, N., SUN, J., DU, G., HAN, N., ZHANG, J. & CHEN, N. 2012b. (+)-epi-Clausenamide, but not (-)-epi-clausenamide, showed more potential than (-)-clausenamide on facilitating synaptic transmission in CA1 region of hippocampal synapses. *Neurosci Lett*, 523, 99-103.
- NOWAK, L., BREGESTOVSKI, P., ASCHER, P., HERBET, A. & PROCHIANTZ, A. 1984. Magnesium gates glutamate-activated channels in mouse central neurones. *Nature*, 307, 462-5.
- OH-NISHI, A., SAJI, M., SATOH, S. Z., OGATA, M. & SUZUKI, N. 2009. Late phase of long-term potentiation induced by co-application of N-methyl-d-aspartic acid and the antagonist of NR2B-containing N-methyl-d-aspartic acid receptors in rat hippocampus. *Neuroscience*, 159, 127-35.
- OLPE, H. R. & LYNCH, G. S. 1982. The action of piracetam on the electrical activity of the hippocampal slice preparation: a field potential analysis. *Eur J Pharmacol*, 80, 415-9.
- PAOLETTI, P., BELLONE, C. & ZHOU, Q. 2013. NMDA receptor subunit diversity: impact on receptor properties, synaptic plasticity and disease. *Nat Rev Neurosci*, 14, 383-400.
- PAOLETTI, P. & NEYTON, J. 2007. NMDA receptor subunits: function and pharmacology. *Curr Opin Pharmacol*, 7, 39-47.

- PARTIN, K. M., FLECK, M. W. & MAYER, M. L. 1996. AMPA receptor flip/flop mutants affecting deactivation, desensitization, and modulation by cyclothiazide, aniracetam, and thiocyanate. *J Neurosci*, 16, 6634-47.
- PERNIA-ANDRADE, A. J. & JONAS, P. 2014. Theta-gamma-modulated synaptic currents in hippocampal granule cells in vivo define a mechanism for network oscillations. *Neuron*, 81, 140-52.
- PIERCEY, M. F., VOGELSANG, G. D., FRANKLIN, S. R. & TANG, A. H. 1987. Reversal of scopolamine-induced amnesia and alterations in energy metabolism by the nootropic piracetam: implications regarding identification of brain structures involved in consolidation of memory traces. *Brain Res*, 424, 1-9.
- POULSEN, M. H., LUCAS, S., STROMGAARD, K. & KRISTENSEN, A. S. 2014. Evaluation of PhTX-74 as subtype-selective inhibitor of GluA2-containing AMPA receptors. *Mol Pharmacol*, 85, 261-8.
- REBOLA, N., CARTA, M., LANORE, F., BLANCHET, C. & MULLE, C. 2011. NMDA receptor-dependent metaplasticity at hippocampal mossy fiber synapses. *Nat Neurosci*, 14, 691-3.
- ROLLENHAGEN, A. & LUBKE, J. H. 2010. The mossy fiber bouton: the "common" or the "unique" synapse? *Front Synaptic Neurosci*, 2, 2.
- ROZOV, A. & BURNASHEV, N. 1999. Polyamine-dependent facilitation of postsynaptic AMPA receptors counteracts paired-pulse depression. *Nature*, 401, 594-8.

- RUIZ, A., CAMPANAC, E., SCOTT, R. S., RUSAKOV, D. A. & KULLMANN, D. M. 2010. Presynaptic GABAA receptors enhance transmission and LTP induction at hippocampal mossy fiber synapses. *Nat Neurosci*, 13, 431-8.
- RUIZ, A. J. & KULLMANN, D. M. 2012. Ionotropic receptors at hippocampal mossy fibers: roles in axonal excitability, synaptic transmission, and plasticity. *Front Neural Circuits*, 6, 112.
- SACHIDHANANDAM, S., BLANCHET, C., JEANTET, Y., CHO, Y. H. & MULLE, C. 2009. Kainate receptors act as conditional amplifiers of spike transmission at hippocampal mossy fiber synapses. *J Neurosci*, 29, 5000-8.
- SAFIULINA, V. F., FATTORINI, G., CONTI, F. & CHERUBINI, E. 2006. GABAergic signaling at mossy fiber synapses in neonatal rat hippocampus. *J Neurosci*, 26, 597-608.
- SALIN, P. A., SCANZIANI, M., MALENKA, R. C. & NICOLL, R. A. 1996. Distinct short-term plasticity at two excitatory synapses in the hippocampus. *Proc Natl Acad Sci U S A*, 93, 13304-9.
- SANDLER, R. & SMITH, A. D. 1991. Coexistence of GABA and glutamate in mossy fiber terminals of the primate hippocampus: an ultrastructural study. *J Comp Neurol*, 303, 177-92.
- SAVONENKO, A. V., MELNIKOVA, T., HIATT, A., LI, T., WORLEY, P. F., TRONCOSO, J. C., WONG, P. C. & PRICE, D. L. 2012. Alzheimer's Therapeutics: Translation of Preclinical Science to Clinical Drug Development. *Neuropsychopharmacology*, 37, 261-277.

- SAVTCHOUK, I. & LIU, S. J. 2011. Remodeling of synaptic AMPA receptor subtype alters the probability and pattern of action potential firing. *J Neurosci*, 31, 501-11.
- SCHINDLER, U. 1989. Pre-clinical evaluation of cognition enhancing drugs. *Prog Neuropsychopharmacol Biol Psychiatry*, 13 Suppl, S99-115.
- SCHMITZ, D., FRERKING, M. & NICOLL, R. A. 2000. Synaptic activation of presynaptic kainate receptors on hippocampal mossy fiber synapses. *Neuron*, 27, 327-38.
- SCHMITZ, D., MELLOR, J., BREUSTEDT, J. & NICOLL, R. A. 2003. Presynaptic kainate receptors impart an associative property to hippocampal mossy fiber long-term potentiation. *Nat Neurosci*, 6, 1058-63.
- SCHMITZ, D., MELLOR, J. & NICOLL, R. A. 2001. Presynaptic kainate receptor mediation of frequency facilitation at hippocampal mossy fiber synapses. *Science*, 291, 1972-6.
- SCHWARZER, C. & SPERK, G. 1995. Hippocampal granule cells express glutamic acid decarboxylase-67 after limbic seizures in the rat. *Neuroscience*, 69, 705-9.
- SCOTT, R. & RUSAKOV, D. A. 2006. Main determinants of presynaptic Ca<sup>2+</sup> dynamics at individual mossy fiber-CA3 pyramidal cell synapses. *J Neurosci*, 26, 7071-81.

- SHIGEMOTO, R., KINOSHITA, A., WADA, E., NOMURA, S., OHISHI, H., TAKADA, M., FLOR, P. J., NEKI, A., ABE, T., NAKANISHI, S. & MIZUNO, N. 1997. Differential presynaptic localization of metabotropic glutamate receptor subtypes in the rat hippocampus. *J Neurosci*, 17, 7503-22.
- STAUBLI, U., AMBROS-INGERSON, J. & LYNCH, G. 1992. Receptor changes and LTP: an analysis using aniracetam, a drug that reversibly modifies glutamate (AMPA) receptors. *Hippocampus*, 2, 49-57.
- STAUBLI, U., KESSLER, M. & LYNCH, G. 1990. Aniracetam has proportionally smaller effects on synapses expressing long-term potentiation: Evidence that receptor changes subserve LTP. *Psychobiology*, 18, 377-381.
- STAUBLI, U., ROGERS, G. & LYNCH, G. 1994. Facilitation of glutamate receptors enhances memory. *Proc Natl Acad Sci U S A*, 91, 777-81.
- STEWART, O. & SCOVILLE, S. A. 1976. Cells of origin of entorhinal cortical afferents to the hippocampus and fascia dentata of the rat. *J Comp Neurol*, 169, 347-70.
- STORM-MATHISEN, J., LEKNES, A. K., BORE, A. T., VAALAND, J. L., EDMINSON, P., HAUG, F. M. & OTTERSEN, O. P. 1983. First visualization of glutamate and GABA in neurones by immunocytochemistry. *Nature*, 301, 517-20.
- SWANSON, G. T. 2009. Targeting AMPA and kainate receptors in neurological disease: therapies on the horizon? *Neuropsychopharmacology*, 34, 249-50.

- SZABADICS, J. & SOLTESZ, I. 2009. Functional specificity of mossy fiber innervation of GABAergic cells in the hippocampus. *J Neurosci*, 29, 4239-51.
- TAKAMORI, S., RHEE, J. S., ROSENMUND, C. & JAHN, R. 2000. Identification of a vesicular glutamate transporter that defines a glutamatergic phenotype in neurons. *Nature*, 407, 189-94.
- TANG, K. & ZHANG, J. T. 2002. The effects of (-)clausenamide on functional recovery in transient focal cerebral ischemia. *Neurol Res*, 24, 473-8.
- TELLITU, I. & DOMÍNGUEZ, E. 2012. The Application of [Bis(trifluoroacetoxy)iodo]benzene (PIFA) in the Synthesis of Nitrogen-Containing Heterocycles. *Synlett*, 23, 2165-2175.
- TONG, G., MALENKA, R. C. & NICOLL, R. A. 1996. Long-term potentiation in cultures of single hippocampal granule cells: a presynaptic form of plasticity. *Neuron*, 16, 1147-57.
- TONG, S., WANG, D. X., ZHAO, L., ZHU, J. & WANG, M. X. 2012. Enantioselective synthesis of 4-hydroxytetrahydropyridine derivatives by intramolecular addition of tertiary enamides to aldehydes. *Angew Chem Int Ed Engl*, 51, 4417-20.
- TOTH, K. & MCBAIN, C. J. 1998. Afferent-specific innervation of two distinct AMPA receptor subtypes on single hippocampal interneurons. *Nat Neurosci*, 1, 572-8.
- TOTH, K., SUARES, G., LAWRENCE, J. J., PHILIPS-TANSEY, E. & MCBAIN, C. J. 2000. Differential mechanisms of transmission at three types of mossy fiber synapse. *J Neurosci*, 20, 8279-89.

- UCHIGASHIMA, M., FUKAYA, M., WATANABE, M. & KAMIYA, H. 2007. Evidence against GABA release from glutamatergic mossy fiber terminals in the developing hippocampus. *J Neurosci*, 27, 8088-100.
- UEBELHACK, R., VOHS, K., ZYTOWSKI, M., SCHEWE, H. J., KOCH, C. & KONERTZ, W. 2003. Effect of piracetam on cognitive performance in patients undergoing bypass surgery. *Pharmacopsychiatry*, 36, 89-93.
- VALENCIA, A., SAPP, E., KIMM, J. S., MCCLORY, H., REEVES, P. B., ALEXANDER, J., ANSONG, K. A., MASSO, N., FROSCHE, M. P., KEGEL, K. B., LI, X. & DIFIGLIA, M. 2013. Elevated NADPH oxidase activity contributes to oxidative stress and cell death in Huntington's disease. *Hum Mol Genet*, 22, 1112-31.
- VAN DE GLIND, E. M. M., VAN ENST, W. A., VAN MUNSTER, B. C., OLDE RIKKERT, M. G. M., SCHELTENS, P., SCHOLTEN, R. J. P. M. & HOOFT, L. 2013. Pharmacological Treatment of Dementia: A Scoping Review of Systematic Reviews. *Dementia and Geriatric Cognitive Disorders*, 36, 211-228.
- VERLOES, R., SCOTTO, A. M., GOBERT, J. & WULFERT, E. 1988. Effects of nootropic drugs in a scopolamine-induced amnesia model in mice. *Psychopharmacology (Berl)*, 95, 226-30.
- VERRI, M., PASTORIS, O., DOSSENA, M., AQUILANI, R., GUERRIERO, F., CUZZONI, G., VENTURINI, L., RICEVUTI, G. & BONGIORNO, A. I. 2012. Mitochondrial alterations, oxidative stress and neuroinflammation in Alzheimer's disease. *Int J Immunopathol Pharmacol*, 25, 345-53.
- VIGNES, M. & COLLINGRIDGE, G. L. 1997. The synaptic activation of kainate receptors. *Nature*, 388, 179-82.

- VOGT, K. E. & NICOLL, R. A. 1999. Glutamate and  $\gamma$ -aminobutyric acid mediate a heterosynaptic depression at mossy fiber synapses in the hippocampus. *Proceedings of the National Academy of Sciences*, 96, 1118-1122.
- W. CAPPI, M., W. FLOOD, R., M. ROBERTS, S., SKIDMORE, J., M. WILLIAMSON, N., CHEN, W.-P., LIAO, Y.-W. & A. SMITH, J. 1998. New procedures for the Julia-Colonna asymmetric epoxidation: synthesis of (+)-clausenamide. *Chemical Communications*, 1159-1160.
- WALKER, M. C., RUIZ, A. & KULLMANN, D. M. 2001. Monosynaptic GABAergic signaling from dentate to CA3 with a pharmacological and physiological profile typical of mossy fiber synapses. *Neuron*, 29, 703-15.
- WALKER, M. C., RUIZ, A. & KULLMANN, D. M. 2002. Do mossy fibers release GABA? *Epilepsia*, 43 Suppl 5, 196-202.
- WANG, J.-Q. & TIAN, W.-S. 1996. An asymmetric total synthesis of (+)-(3R,4S,5R,7S)-neoclausenamide. *Journal of the Chemical Society, Perkin Transactions 1*, 209-212.
- WANG, Y., YAO, Q. Q. & WANG, M. Z. 2010. High performance liquid chromatographic separation of clausenamide enantiomers with chiral-AGP stationary phase. *Chinese Chemical Letters*, 21, 860-863.
- WEST, M. J., SLOMIANKA, L. & GUNDERSEN, H. J. 1991. Unbiased stereological estimation of the total number of neurons in the subdivisions of the rat hippocampus using the optical fractionator. *Anat Rec*, 231, 482-97.

- WIERA, G., WOZNIAK, G., BAJOR, M., KACZMAREK, L. & MOZRZYMAS, J. W. 2013. Maintenance of long-term potentiation in hippocampal mossy fiber-CA3 pathway requires fine-tuned MMP-9 proteolytic activity. *Hippocampus*, 23, 529-43.
- XIAO, P., STAUBLI, U., KESSLER, M. & LYNCH, G. 1991. Selective effects of aniracetam across receptor types and forms of synaptic facilitation in hippocampus. *Hippocampus*, 1, 373-380.
- XU, L., LIU, S. L. & ZHANG, J. T. 2005. (-)-Clausenamamide potentiates synaptic transmission in the dentate gyrus of rats. *Chirality*, 17, 239-44.
- YAKURA, T., MATSUMURA, Y. & IKEDA, M. 1991. Formal Total Synthesis of Clausenamamide. *Synlett*, 1991, 343-344.
- YANG, L., WANG, D. X., ZHENG, Q. Y., PAN, J., HUANG, Z. T. & WANG, M. X. 2009. Highly efficient and concise synthesis of both antipodes of SB204900, clausenamamide, neoclausenamamide, homoclausenamamide and zeta-clausenamamide. Implication of biosynthetic pathways of Clausena alkaloids. *Org Biomol Chem*, 7, 2628-34.
- YECKEL, M. F., KAPUR, A. & JOHNSTON, D. 1999. Multiple forms of LTP in hippocampal CA3 neurons use a common postsynaptic mechanism. *Nat Neurosci*, 2, 625-33.
- YOSHINO, M., SAWADA, S., YAMAMOTO, C. & KAMIYA, H. 1996. A metabotropic glutamate receptor agonist DCG-IV suppresses synaptic transmission at mossy fiber pathway of the guinea pig hippocampus. *Neurosci Lett*, 207, 70-2.

- 
- ZALUTSKY, R. A. & NICOLL, R. A. 1990. Comparison of two forms of long-term potentiation in single hippocampal neurons. *Science*, 248, 1619-24.
- ZHANG, L., ZHOU, Y. & YU, X. 2012. Suzuki–Miyaura Coupling Based Enantioselective Synthesis of (+)-epi- Clausenamides and the Enantiomer of Its 3-Deoxy Analogue. *Synlett*, 2012, 1217-1220.
- ZHU, C. Y., DENG, X. M., SUN, X. L., ZHENG, J. C. & TANG, Y. 2008. Highly enantioselective synthesis of isoxazoline N-oxides. *Chem Commun (Camb)*, 738-40.
- ZUCKER, R. S. 1989. Short-term synaptic plasticity. *Annu Rev Neurosci*, 12, 13-31.